Università degli Studi di Napoli Federico II
DEPARTMENT OF CHEMICAL, MATERIALS AND PRODUCTION ENGINEERING
(DICMAPI)
PHD IN INDUSTRIAL PRODUCTS AND PROCESSES ENGINEERING
XXXV CYCLE

LONG-LASTING ANASTOMOSIS ON-A-CHIP

Endogenous extracellular matrix as a key element for modeling stable and perfusable vascular network through a microfluidic device

Supervisor
Prof. Dr. P.A. Netti

Coordinator
Prof. Dr. A. D'Anna

Advisors
Francesco Urciuolo, PhD
Giorgia Imparato, PhD

PhD Student **Francesco Del Giudice**

2019/2023

Acronyms

3D: three-dimensional

AF: Area Fraction

bFGF: basic fibroblast growth factor

CFD: computational fluid dynamics

CLS: capillary-like structure

EC: endothelial cell

ECFC: endothelial colony-forming cell

ECM: extracellular matrix

FITC: fluorescein isothiocyanate

GOC: gut-on-chip

HDF: human dermal fibroblast

HIEC: human intestinal epithelial cell

hLF: human lung fibroblast

hMVEC: human microvascular endothelial cell

HUVEC: human umbilical vein endothelial cell

ISEMF: intestinal sub-epithelial myofibroblast

MP: multiphoton

µTP: microtissue precursor

NHLF: normal human lung fibroblast

PDMS: polydimethylsiloxane

PMA: phorbol-12-myristate-13-acetate

PMMA: polymethyl methacrylate

PV-µTP: pre-vascularized microtissue precursor

PVD: pre-vascularized dermis

rMVEC: rat microvascular endothelial cell

SHG: second harmonic generation

SMC: smooth muscle cell

UEA I: Ulex Europaeus Agglutinin I (specific HUVEC dye)

VEGF: vascular endothelial growth factor

Abstract

Since tissue engineering has been developed, it represents one of the main strategies that bioengineering has to obtain *in vitro* substitutes for wounded tissues in human body, replicating the physiological environment with low risk of rejection after *in vivo* implantation. One of the main issues regarding tissue engineering is represented by nutrients diffusion during biological construct formation, which is insufficient in preventing necrosis of tissues in the scale of millimeters before *in vivo* application. The easiest way to increase the exchange of nutrients and metabolites in *in vitro* 3D cultures is providing a dynamic culture, which can be obtained in bioreactors or with a microfluidic approach. The custom design of a microfluidic device and the controlled use of cell media flows – with systems such as syringe pumps or hydrostatic pressure - can reduce the negative effects of scarce diffusion inside the extracellular matrix (ECM). Another solution to the problem may be vascularization, which consists in the process of formation of blood vessels. The presence of a perfusable network may switch the mechanism of molecule transport from diffusive to convective, leading to nutrients and oxygen convection through vessels *lumen* and exchange through the endothelial walls, reducing the impact of diffusion coefficient. The formation of a mature capillary network inside a biological construct may also better resemble the biological environment, and can provide a deeper understanding of physiological phenomena in a 3D model *in vitro*. Microfluidics can be used for inducing capillary formation inside a biological construct; a phenomenon which needs fine control over parameters such as flow rate, pressure and gradients for biochemical and mechanical stimulation of different cells, that microfluidic devices can guarantee. Once vascularization is obtained, the biological tissue may be implanted *in vivo* with a reduced time of adaptation to human body, or the vascular network may be kept perfusable by using the microfluidic device. Basically, an organ-on-chip can be obtained as a platform to investigate and

analyze a circulatory system *in vitro*. Usually, *in vitro* vascular networks are generated by two distinct approaches: by endothelial-lined channels, or by self-assembled networks. The former strategy relies on the formation of a cavity network, which may be obtained in hydrogels or in synthetic materials, or in a polydimethylsiloxane (PDMS) device realized with soft-lithography techniques. Endothelial cells (ECs) are seeded inside the cavities and attach to the walls, with or without the presence of adhesion molecules coatings: these techniques guarantee high control over the geometry and the size of obtained vessels, but the vascular model clearly differs from the *in vivo* vasculature, since the formation of a real network is technically impossible. The latter strategy is based on the vasculogenesis phenomenon – the *de novo* vessel formation – which normally happens during embryogenesis *in vivo*. It has been demonstrated that seeding ECs inside a hydrogel in the presence of fibroblasts induces the self-assembly of ECs into vessel-like structure because of different growth factors secreted by fibroblasts: the architecture of such networks better resemble *in vivo* vasculature conformation, while the control over the network geometry is lost and the perfusability of the vessel network may be difficult to achieve or control. Geometrical cues also play a critical role in the endothelial behaviour *in vitro*.

In this context, the aim of the presented project regards the formation of a perfusable, mature and long-lasting capillary network in a bio-engineered construct featured by endogenous extracellular matrix (ECM) inside a custom-designed microfluidic platform. By controlling parameters such as flow rate – thus velocity profiles and shear rate – the microfluidic platform aims to allow the perfusability of vascular vessels and, consequently, the transport of nutrients inside the stromal tissue, in a long-lasting manner.

Briefly, the microfluidic device that will be designed and produced in this project will consist of two parts: two channels for the inlet and outlet and the control of flows, and one chamber for the introduction of a biohybrid that closely resembles physiological tissues. The biological construct will be a stromal tissue equivalent, whose most important features are the 3D structure and the endogenous ECM. At first, the integration of a macroscopic pre-vascularized bioengineered equivalent (disk of 1 mm in height and up to 1 cm in diameter) on-chip will be described. Afterwards, pre-vascularized micro-tissue units will be introduced into a different microfluidic platform to obtain tissue assembly and the long-lasting anastomosis on-chip.

The approach in this project will rely on the combination of the two described strategies: the designed microfluidic device will feature channels, which will be lined with ECs, in direct communication to the tissue chamber through a series of interpillar pores. The channel-chamber interface will match with the lateral surface of the tissue itself, which will undergo endothelial lining as the channel walls of the chip. Controlling transendothelial flow at the communication pores, shear stress on the lining ECs, VEGF

gradients – from the inlet or directly secreted by fibroblasts in the tissue – and flow rates, endothelial sprouts will depart from the channel-chamber interface and anastomose to the pre-vascular network inside the stromal tissue.

The combination of tissue engineering and microfluidics may lead to prolonging the maturation of capillaries inside the tissue, thus determining a long-lasting vascularization on-chip model. This organ-on-chip configuration is increasingly relevant because of the different applications it is suitable for: building a small-scale version of functional human tissues and organs has shown to be a potential alternative to animal tests with a high throughput, a model for a deeper understanding of patho-physiological cell behaviours and a step forward towards personalized medicine, with the use of patient-derived cells to engineer the *in vitro* biological construct. Furthermore, the obtained platform may be used for the study of pathological angiogenesis phenomena correlated with tumors, as the biological construct inside the device can be engineered with tumor-related cells.

1. State-of-the-art

1.1 Vascular system, vasculogenesis and angiogenesis

The vascular system, also called circulatory system, is an organ system that allows the circulation of blood and the transport of nutrients, oxygen, carbon dioxide, hormones, and blood cells in human body to provide nourishment, stabilize temperature and pH, and maintain homeostasis. Most of the tissues and organs constituting human body depend on vascularization for their sustenance and to correctly fulfil their functions. Vascular system of living organisms – animal or human – are constituted by arteries, capillaries and veins, which differ in diameter, structure and localization in the body. Through vascular system, cellular functions such as growth and development, absorption of nutrients, and removal of metabolic waste products – homeostasis – are ensured. In order to achieve balance of functions, vessels and structural elements involved must show a certain degree of homology in cellular structure and composition, and maintain differences in cellular properties. For example, blood vessels in the heart and in the nephron of the kidney share similarities in structure, but their functions are different: while heart vessels mainly convey oxygen to heart muscles, nephron blood vessels selectively filter blood constituents [7].

From a histological point of view, vascular system elements are mainly constituted by a common organization - except for some complex niches – in which three distinct regions can be defined: *tunica intima*, *tunica media* and *tunica adventitia*. *Tunica intima* is the inner and thinner layer, consisting of a single-layer of endothelial cells (ECs) which adhere on a basement membrane – or basal lamina. A fibro-elastic connective tissue underneath endothelial layer determines ECs stability and flexibility. Endothelium is a key component on both macro- and micro-scales. An endothelial monolayer with tight junctions generates a dynamic barrier which acts as a selectively permeable barrier between circulating blood and surrounding tissues [8].

Tunica intima is mainly involved in thrombolysis and coagulation processes, inflammatory and immunological phenomena. *Tunica media* predominantly consists of smooth muscle cells and elastin fibers, which are mainly organized in larger arteries and allows for flexibility functions, and an external elastic lamina as structural support. *Tunica adventitia* is the outermost layer, mainly constituted by fibro-elastic connective tissue, lymphatic and nerve plexi along with the vasa vasorum.

Vascular system develops as an arterial tree, which connects to capillary system and to the venous tree. Oxygenated blood from the lungs is ejected from the left ventricle of the heart into a large network of arteries, which can be histologically divided into two distinct types: elastic and muscular. Elastic (or conducting) arteries move large volumes

of blood, usually in heart. This type of arteries, such as the aorta, is constituted by several layers of perforated elastic membrane and their main function is to accommodate large changes in blood volume such as those typically associated with ejection from the left ventricle of a beating heart. The highly elastic nature of the walls of these blood vessels provides an important function to the smaller blood vessels found distally in the arterial vascular tree: they switch from an oscillating blood flow regime to a more homogeneous movement of blood away from the heart. However, despite this important function, arteries in the body are mainly muscular (or distributing). The function of muscular arteries is to rapidly distribute blood to all organs and tissues. While the walls of these arteries are predominantly muscular in nature, histological studies show that these arteries contain discontinuous elastic fibers within the large layer of smooth muscle cells. The continuous bifurcation of arteries leads to blood flow within the smallest blood vessels of the arterial tree, resulting in blood flow reduction, which is necessary to prevent damage to the capillaries - the fragile vessels that connect the arterial vascular tree to the venous system. The capillaries also regulate the microcirculation by altering the tone of the smooth muscle in the arteriolar wall [9]. Capillary histological sections lack of smooth muscle. Rather, the capillary consists of a single layer of endothelial cells (about 0.25 mm thick), a basement membrane, and a population of pericytes or `Rouget' cells that varies in distribution within vascular beds. The total surface area generated by the capillaries in the body is approximately 1000 m^2 - the size of a tennis court. This surface area represents the exchange surface for diffusion of the majority of nutrients, solutes, and water are to surrounding tissues. Several types of capillaries can be distinguished: continuous, fenestrated, and discontinuous. The continuous capillary is the most ubiquitous type found in the body. These capillaries have a continuous endothelial and basement cell membrane layer and are found in many organs such as the heart, lung, kidneys, and brain. The fenestrated capillary is usually less commonly found and is instead present in endocrine organs and in the glomeruli of the kidney. Anatomically stable cylindrical pores or fenestrae between 75 and 100 Å in diameter perforate these capillaries, which restricts the passage of proteins but allows for the relative free passage of solutes and water. Discontinuous capillaries or sinusoids are found only in highly specialized tissues such as the liver and blood-forming organs such as the bone marrow and spleen. The large pores between endothelial cells in these capillaries (1500 ± 2500 Å) allow for the exchange of cellular constituents between the blood and tissue. The return of blood to the heart via the venous system begins with its movement into the postcapillary venules, which coalesce to form larger veins. The transition from capillary to vein is marked by the gradual re-appearance of smooth muscle cells in the tunica media of the vessel wall and a layer of collagen and elastic fibers in the adventitia. The size of the veins varies between 1 and 10 mm in diameter and some veins such as those located in the lower limbs of the body contain uni-directional semi-lunar valves that prevent blood from pooling in the extremities. Both small- and medium-sized veins acquire a greater

level of smooth muscle cells in their tunica media while large veins have an increased amount of connective tissue in this layer.

1.2 Vasculogenesis and angiogenesis

The formation and maintenance of our vascular system is of crucial importance both during development and throughout our adult lives. Blood vessels formation during early embryogenesis starts with angiogenic cell coalescence, which determines the formation of hollow cannules. Early capillary-like networks at embryonal stage develop from angioblasts that differentiate into endothelial cells (ECs); this process is known as vasculogenesis - defined as the *de novo* formation of vascular vessel network - which also occurs during adulthood through recruitment of ECs from bone marrow. During development, and following the formation of a primary network, expansion and sprouting occurs from existing vessels by a process known as angiogenesis. Angiogenic phenomena can be divided in two different types: sprouting angiogenesis and intussusceptive angiogenesis. In the former case, vascular vessels form by growth, proliferation, alignment, tube formation and, finally, anastomosis with surrounding vessels occurs, while the latter can be defined as the splitting of a vessel in two or more smaller vessels. The basic steps of sprouting angiogenesis include enzymatic degradation of capillary basement membrane, ECs proliferation, directed migration of ECs, tubulogenesis (EC tube formation), vessel fusion, vessel pruning, and pericyte stabilization (Figure 1.2.1, A). Usually, sprouting angiogenesis phenomena develop in hypoxia conditions, when oxygen sensors detect low concentrations of O_2 and trigger the signals cascade for new vessels formation, in which Vascular Endothelial Growth Factor – A (VEGF-A) plays a critical role. In particular, an endothelial tip cell guides the developing capillary sprout through the ECM toward an angiogenic stimulus such a VEGF-A[10][11]. Long, thin cellular protrusions on tip cells - called *filopodia* - secrete large amounts of proteolytic enzymes, which digest a pathway through the ECM for the developing sprout. The filopodia of tip cells are rich in VEGF-A receptors (VEGFR2), which let them “sense” VEGF-A concentration gradients and causing their alignment to it. A tip cell needs a sufficient number of anchored filopodia in order to determine contraction of actin filaments, which is necessary to pull the tip cell towards VEGF stimulus. Simultaneously, endothelial stalk cells proliferate behind tip cells causing capillary sprout elongation. Vacuoles form and coalesce, forming a lumen within a series of stalk cell. Usually, two or more capillary sprouts converge at the source of VEGF-A secretion, so that the tip cells fuse together creating a continuous lumen through which oxygenated blood can flow [12]. When oxygen supply returns normal in the local tissue, VEGF-A levels can diminish to near normal, due to recruitment success [13][14].

Maturation and stabilization of the capillary requires recruitment of pericytes, deposition of ECM, physiological shear stress and other mechanical signals [8].

As described above, angiogenic sprouting is vital for delivery of nutrients and gas exchange to ischemic regions, but it also plays a critical role in tissue remodeling, regeneration and in solid tumor growth [15]. Biochemical gradients are essential in angiogenic phenomena, both in physiological and pathological environment [16]. Vascular Endothelial Growth Factor (VEGF) is the most important growth factor in the angiogenesis phenomenon, usually for hypoxia conditions, and is secreted by several cell types: fibroblasts, monocytes, macrophages and lymphocytes, which determine recruitment of ECs from neighbouring vessels. Biochemical signals do not represent the only triggers for sprouting angiogenesis processes: it has been demonstrated that the combination of fluid forces and VEGF gradients is necessary to induce endothelial sprouts in a hydrogel *in vitro* [17][18][19]. Interstitial flow determines a mechanical stimulation over the cells forming the vessels, which translates in the passage from a quiescent state to an active state, thus proliferating and inducing sprouting formation [20].

On the other hand, intussusceptive angiogenesis is obtained by formation of new blood vessels with a splitting process, due to interstitial tissues invasion inside existing vessels. A transluminal tissue pillar forms and expands, thus resulting in the formation of two smaller vessels. Intussusceptive angiogenesis is also called *splitting angiogenesis* because the vessel wall extends into the lumen causing a single vessel to split in two [12]. This type of angiogenesis is reportedly faster and more efficient compared to sprouting angiogenesis because, at least in the first steps, it only requires reorganization of existing endothelial cells and does not depend on immediate endothelial proliferation or migration. Even if intussusceptive angiogenesis can occur during adult life, its critical role is played during vascular development in embryos where growth is fast and resources are limited [8].

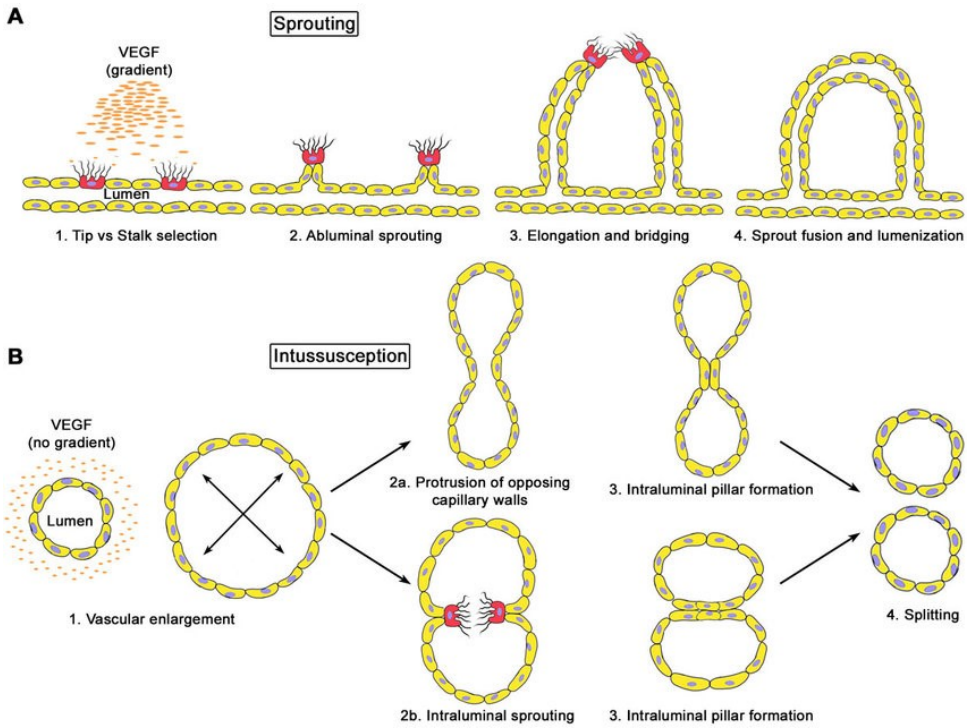

Figure 1.2.1: Graphical representation of sprouting and intussusception mechanisms. (A) Schematization of sprouting angiogenesis mechanisms, with tip-stalk selection, abluminal sprouting, elongation and bridging, and sprout fusion and lumenization. (B) Intussusceptive angiogenesis starting from vascular enlargement, followed by protrusion of opposite endothelial walls – or intraluminal sprouting, intraluminal pillar formation and splitting.

1.3 Stromal tissue

In order to opportunely frame the context of vascular system formation, a description of stromal tissue reveals to be fundamental. In general, a distinction between stroma and parenchyma was introduced in the anatomical science in order to better understand the role and the functions of different components of human body. While parenchyma (from Greek "*parenkhein"*, meaning *"beside", "to pour in"* whereas *énkhuma* means *"content of a vessel*") is used to define the functional part of an organ, comprising the cells that operate the specific roles for which the organ is responsible for, the stroma (from Greek "*stroma*", "*layer*, *bed covering*") can be described as the part of a tissue or organ with a structural or connective role: stromal cells and tissues support and give structure to organs, glands, or other tissues in the body. The stroma is mostly made up of connective tissue, blood vessels, lymphatic vessels, and nerves [21]. It provides nutrients to the tissue or organ and removes waste and extra fluid. The stroma may also be involved in the body's immune response and in

the growth and spread of cancer cells. In particular, changes in the stroma drive invasion and metastasis, the hallmarks of malignancy [22].

Stromal tissue presents a highly ordered structuration (Figure 1.3.1) and its remodeling represents an important factor in both physiological and pathological phenomena such as angiogenesis of vessel structures and migration dynamics of cancer cells, in particular the key cell–matrix interactions such as motility, cell spreading, f-actin alignment, focal adhesion, and cadherin expression are mainly determined by the collagen fiber morphology to a larger extent than the initial cell type [23][21].

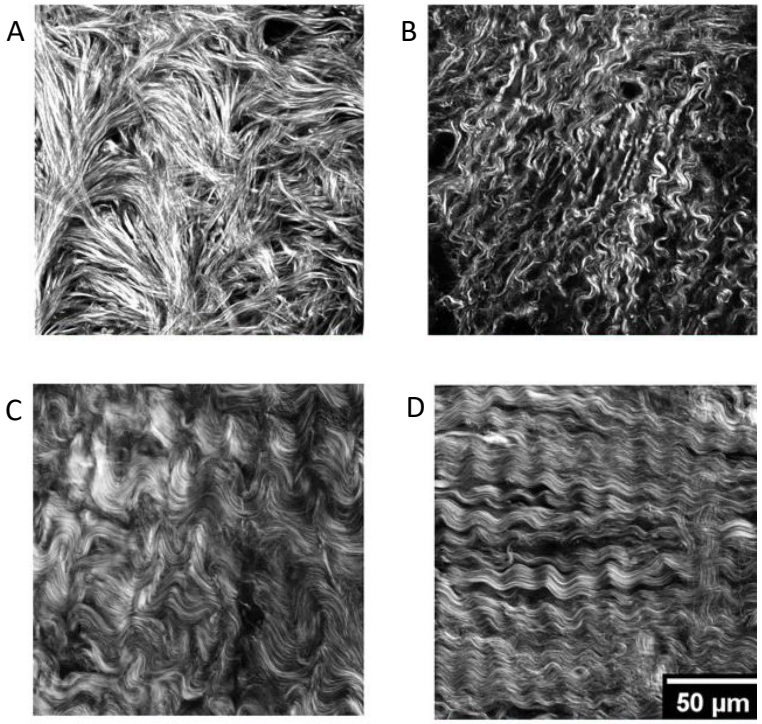

Figure 1.3.1: (A-D) Second harmonic generation (SHG) images of collagen fibers constituting human ovarian stroma. (A) Normal stromal tissue; (B) High-risk for tumor stromal tissue; (C) Benign tumor stromal tissue; (D) High grade tumor stromal tissue. Clear differences in collagen fibers assemblies are shown, which influence cell behaviour (Alkmin et al., 2020).

Given the remodeling of stromal tissue *in vivo*, replicating such dynamic modifications *in vitro* represents a non-trivial challenge to address the development of *in vitro* 3D stromal models that fully recapitulate *in vivo*, in particular regarding the formation of vasculature. The above-described features of stroma are fundamental in the development of vessel networks, both *in vitro* and *in vivo*, since stroma structuration

acts as a scaffold for the vascular system to properly form and develop inside every district of human body. Stroma supports not only parenchyma, but also vascular vessels in order to completely determine transport of nutrients and removal of metabolites. Stroma remodeling represents an important feature for both *in vitro* and *in vivo* formation of vasculature, due to the dynamicity of stroma-vasculature system, their cross-talk and co-operation for both physiological and pathological behaviour of cells.

1.4 *In vitro* vascularization strategies

Vascularization is seen as the key element for the development and the enhancement of *in vitro* tissue models and biological 3D constructs, as it allows not only oxygen, nutrients and waste exchange, but also provides for inductive biochemical exchange and structural template for growth, which are crucial cues for large-scale and more reproducible tissue organization [24][25][26][27]. Several biological equivalents have been developed for *in vitro* applications: organoids, engineered tissues, cell-loaded hydrogels revealed to be the most increasingly investigated for their similarity to their physiological counterparts and for their mechanical properties [28][29][30][31].

One of the key limitations - shared by all of the above-mentioned biological equivalents - in using organoid-based or tissue engineering approaches to generate functional tissue is that, upon reaching a certain size, organoids cease to proliferate and develop a necrotic core [32], the latter also shown by engineered tissues [28][33][34]. This crucial issue was firstly faced by tissue engineers, which addressed vascular networks as the missing element for *in vitro* tissue development and physiological behaviour. Generating vascularized constructs still represents a long-lasting goal in the context of tissue engineering [35][36], also shared by other 3D constructs approaches such as organoids. Indeed, it has long been realized that, with the exception of a few avascular tissues, any attempts at generating larger scale tissue constructs without a perfusable vascular network would be limited to a length scale of approximately 150 μm imposed by the natural diffusion limit of oxygen and nutrients in tissue [24][37].

Different strategies have been developed to obtain *in vitro* vascularization of organoids, engineered tissues and cell-loaded hydrogels [38][39][40][41]. Here a list of the most relevant will be presented, in order to understand the technologies involved, the achievements and the improvements needed[42], [43].

- *Bioprinting*: it can be defined as a layer-by-layer deposition of hydrogels loaded with different cell types [44][45][46][47]. It has generally been explored in studies aiming at generating large-scale tissue constructs, and has been most frequently performed by either filament deposition or droplet-based approaches. Fused filament fabrication (FFF) or fused deposition modeling

(FDM) involves the extrusion of a cell-loaded gel in the form of a thin filament and its deposition in a pre-programmed, controlled manner to form a designed pattern. Considering vascularization of *in vitro* tissue applications, FDM has been used to deposit ECs interleaved or in combination with other cell types. Kinoshita et al. developed an efficient strategy to obtain multilayered, branched structures of vascular tissue models using fluidic channels for *in situ* hydrogel formation. An aqueous solution of RGD-alginate loaded with smooth muscle cells (SMCs) was injected inside agarose channels, obtaining a several hundred micrometers thick layer. Later, ECs were seeded on hydrogel channel walls and cultured for 7 days to obtain hierarchically organized, multilayered vascular tissues [48].

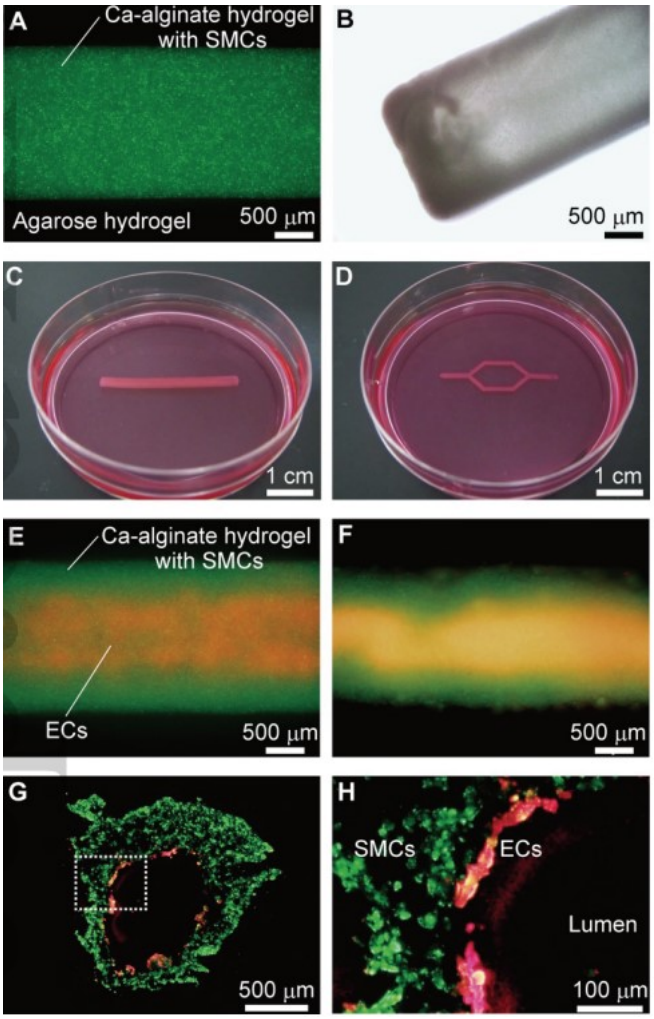

Figure 1.4.1: (A-D) Fabrication of vascular tissues using green fluorescently-labeled SMCs and the recovery from hydrogel channels. (A) Fluorescence imaging of the tubular alginate hydrogel with

SMCs fabricated within the agarose hydrogel channels. (B) Optical microscope image of a fabricated vascular tissue with an outer diameter of 2 mm. (C, D). Two different configurations of vascular tissues with the outer diameters of 2 and 1 mm, respectively. These linear and branched shapes corresponded to the agarose hydrogel channel structures. (E-H) Fluorescence images of the multilayered vascular tissues composed of HUVECs and SMCs. (E, F) Fluorescence images showing the green-labeled SMCs and red-labeled ECs (E) After 10 hours of static culture and washing with medium and (F) after 7 days of perfusion culture. (G, H) Cross-section of the vascular tissue. Lumen inside tubular ECs configuration is clearly visible. Image (H) represents a magnification view of the rectangular region in image (G).

Another bioprinting technique was exploited by Leong et al. to fabricate coaxial tubules consisting of an ECs core and adipose cells in the external hydrogel layer, resulting in a pre-vascularized functional adipose tissue which anastomosed with the host vasculature in a mouse model [49]. Briefly, the research group developed an interfacial polyelectrolyte complexation (IPC) fiber assembly technique to generate an aligned endothelial vessel network. Patterned constructs of ECs with adipocytes and hepatocytes anastomosed with the host, developing a vascularized tissue. To create an organized network of endothelial vessels within the hydrogel, we first investigated the processes of cell alignment and self-assembly to form tubes within the fibers. The assembly of IPC fibers was obtained with the complexation of water-soluble chitin and rat methylated collagen with sodium alginate. Gel extrusion methods, despite their relative versatility, are not suitable for developing intertwined and highly branched network topology occurring *in vivo* due to their continuous mode of filament deposition. Another limitation of the approach is that the minimal diameter of vessels achievable is determined by the diameter of the nozzle used for extrusion;

- *Digital micro mirror patterning*: Stereolithography-based additive manufacturing based on light-mediated cross-linking of photosensitized polymers (photopolymerization) has been widespread used in medical and biological research field due to its fundamental feature of enabling truly arbitrary 3D geometries with high resolution. In order to create pre-vascularized tissues with more complex architecture at higher resolution, approaches based on photopolymerization of cell-laden gel liquid precursors by digital micro-mirror (DMD) devices have been explored. Polymerization is selectively induced in regions exposed to UV of other wavelength illumination in a 2D pattern generated by the projection of an image bitmap via a micro-fabricated mirror array. Complex layer-by-layer 3D structures can be formed by consequent illumination of serial projected patterns, interleaved by cycles of washing out of the unexposed, unpolymerized liquid gel precursor. An important example can

be seen in Zhu et al. work, based on a two-step illumination process of two different cell-laden photosensitive gels: the first was loaded with HUVECs and illuminated with a complex geometrical patterned mirror, the second was loaded with HepG2 cells and illuminated using a complementary mirror. The result was a complex microarchitecture of vessel network inside a hydrogel, which mimicked a vascularized tissue (Figure 1.4.2).

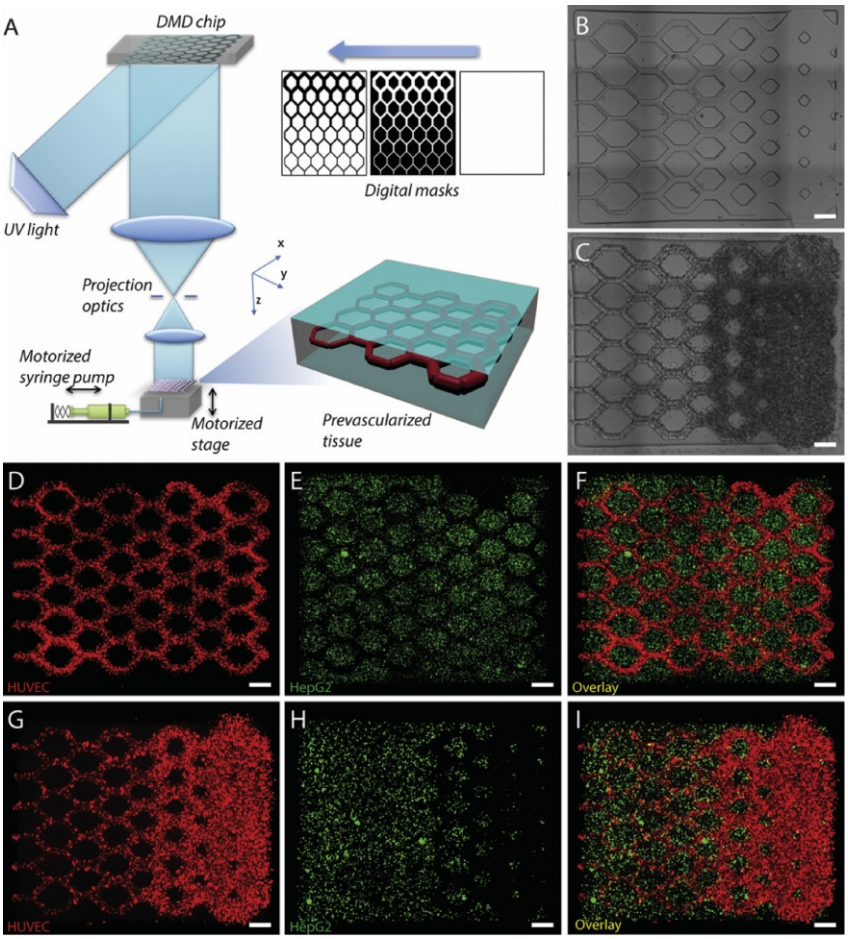

Figure 1.4.2: 3D bioprinting of the prevascularized tissue constructs. (A) Schematization of operating principle of bioprinting platform. (B) Bioprinted construct without cells and developing a gradient of width in channels. (C) Bioprinted construct with HUVECs and 10T1/2 (50:1) encapsulated inside channels. (D to F) Fluorescent images showing the bioprinting of heterogeneous cell-laden tissue constructs within uniform channel width. HUVECs (red) are encapsulated in the channels and HepG2 (green) are encapsulated in the surrounding area. (G to I) Fluorescent images showing the bioprinting of heterogeneous cell-laden tissue constructs with gradient channel widths. Scale bars are 250 mm (Leong et al.).

- *Direct 2-photon fabrication*: Two-photon stereo-lithography, based on non-linear two-photon absorption, determines selective photopolymerization of sub-micron volumes of gels, generating complex 3D microstructures in a single processing step. One of the earliest studies showing the potential of this approach was conducted by Ovsianikov et al. [50] and consisted in the fabrication of micro-compartments for bacterial colonies by *in situ* two-photon cross-linking of gelatin: this work first demonstrated the possibility of generating arbitrary spatial arrangements at the micrometer scale to allow interactions between defined cell populations. Since it presents as a particularly dimensionally flexible and accurate technique, two-photon stereolithography has been increasingly employed in cell biology and bioengineering, including in recent attempts to directly fabricate perfusable networks. In pioneering work on direct 2-photon fabrication of tubular structures, branching vessels with internal diameters under 20 μm was obtained by Meyer et al. in a recent study. While this study did not demonstrate the perfusability of the generated networks, it opened the way for similar approaches based on the flexible and versatile design-on-demand capabilities of this technique. In one strategy making use of these 3D design capabilities, micro-pores were created in the walls of a branched network of relatively large (circa 1 mm) polyacrylate vessels, thereby enabling the successful lining of the main vessels with human dermal microvascular endothelial cells, as well as the migration of cells and medium exchange across the vessel walls at precisely defined spatial locations. While 2-photon-based photopolymerization methods appear to achieve unprecedented resolution, their limited throughput, limited choice of biocompatible photoiniators and considerable infrastructural cost have precluded their wider adoption.

- *Sacrificial networks*: To create complex 3D networks, approaches based on removing, rather than adding material, have also been explored. Indeed, a number of studies have been based on the idea that a sacrificial filament network can be embedded in a cell-containing matrix which, upon removal, leaves behind perfusable channels which can then be seeded with endothelial cells to form a vascular network with defined topology. One study based on this approach was performed by Miller et al., who printed an interconnected 3D network of cylindrical-shaped carbohydrate glass and encapsulated it inside ECM with cells. After dissolving the network with cell culture medium, an interconnected network of cavities was formed inside the ECM and ECs were seeded inside, obtaining a perfusable vascular network [51]. The current limitations of most sacrificial network approaches regard challenges of dimensional accuracy and precision, as well as of complete and homogenous

removal of the sacrificial material, in particular for increasingly small and complex geometries. This may indeed account for the limits in achieved vessel dimensions of 150 µm, obtained by Miller et al., which are still an order of magnitude larger than the average capillary size.

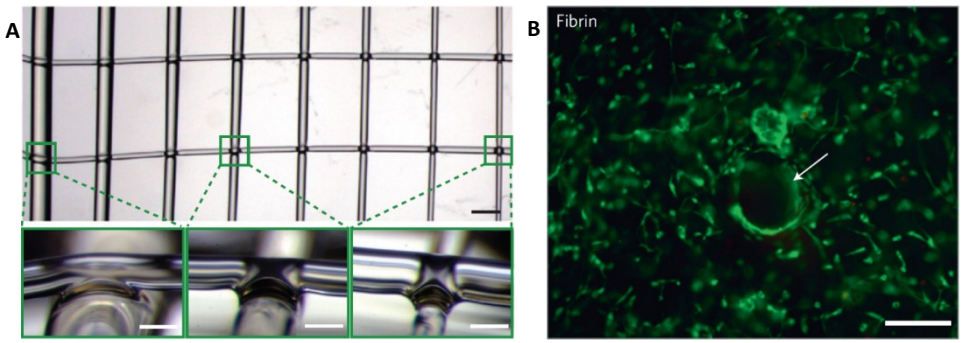

Figure 1.4.3: (A) Top view with different magnification of architectural design printed in carbohydrate glass (scale bar, 1 mm). Melt fusions between filaments are shown in side-view (scale bars, 200 µm). (B) Cross-section image of unlabeled HUVECs (10^6 mL^{-1}) and 10T1/2 (10^6 mL^{-1}) co-cultures encapsulated uniformly in the interstitial space of a fibrin gel (10 mg mL^{-1}). Perfusable networks after two days in culture were stained with a fluorescent live/dead assay (green, Calcein AM; red, Ethidium Homodimer). Lumen in cylindrical channels is highlighted with white arrow. Scale bar, 200 µm.

- *Subtracting fabrication by laser ablation*: existing microfabrication techniques utilizing stereolithography are not limited to photo-patterning of biochemical cues, direct 3D printing or direct laser writing of photopolymerizable materials. Indeed, elegant optical approaches for generating freeform channels *in situ* within cellularized hydrogel materials have also been demonstrated based on laser photo-ablation. Applegate et al. worked on photo-ablation induced by multiphoton absorption of light, which allows for the generation of voids as small as 5µm in diameter. Silk fibroin has been reported as an especially suitable material for this technique due to its large multi-photon cross-section, allowing initiation of multiphoton absorption at low laser power thresholds, thereby reducing self-focusing of the laser beam and other non-linear optical effects. This material supports cell growth and allows cells to penetrate deep inside the structure, and its clarity determines a ∼10× improvement on multiphoton absorption depth over other materials [52]. Collagen type I and PEG-based matrices were also tested with this technique, obtaining high resolution hollow channels inside hydrogels which can be endothelialized. In order to take full advantage of this method, the chosen hydrogel material must have an

appropriate multi-photon cross-section corresponding to the laser wavelength used for fabrication, which substantially limits the choice of available hydrogels.

- *Spontaneous vascularization*: Since the approaches described above cause a lack of responsiveness of vascular structures to dynamic changes in the environment, such as changes in oxygen consumption, tissue patterning, and growth, the presence of mechanisms of active vascular remodeling is compromised. Spontaneous vascularization, a process consisting in the formation of vascular vessels by ECs self-assembly in presence of naturally-secreted growth factors by particular co-cultured cell types in a remodeling ECM, was firstly investigated by Gage and Fischer. An important study was developed by Nashimoto et al., who standardized co-culture spheroids of ECs and human lung fibroblasts (hLF) to generate 600µm-diameter spheroids which, in a microfluidic device with hydrogel endothelialized channels, developed a perfusable vessel network by self-assembly of ECs and angiogenic sprouting (Figure 1.4.4). The spontaneous vascularization was caused by the signaling role played by hLF, which determined – by normal secretion of growth factor such as VEGF – the formation of angiogenic sprouts from side hydrogel to the central spheroid. This study suggests that interactions between vasculature and target tissue *in vitro*, as *in vivo*, are bidirectional, with inductive roles for both [53].

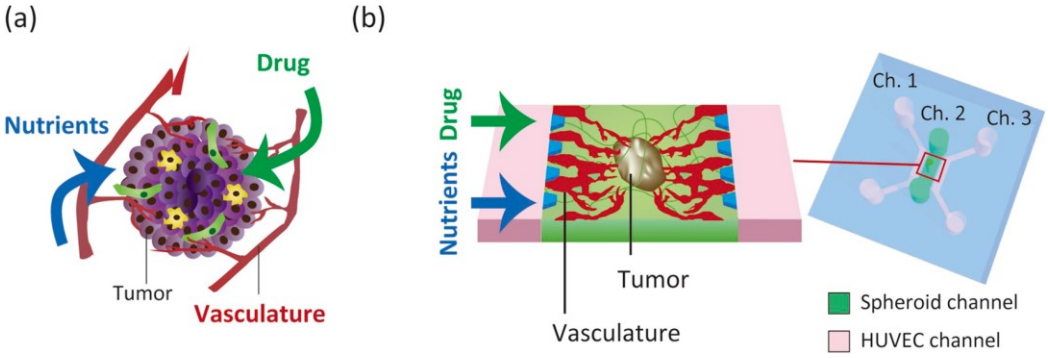

Figure 1.4.4: Schematization of co-culture hLF-HUVECs spheroid (a) and spontaneous vascularization of a spheroid inside an endothelialized hydrogel (b). (Nashimoto et al., 2017)

The approaches described above show clear advantages such as control over vascular network topology and morphology, together with immediate functionality. However, the pre-determination of the obtained vascular structures with the majority of these fabrication processes determines a failure in the response capability to dynamic changes in the environment [54]. In addition, for printing techniques, further development of biocompatible hydrogel materials composition is required to limit swelling and deformation of printed structures in aqueous media after fabrication [37]. Similar issues arise with photo-induced removal of material, where a gel block is subjected to a focused laser light. Since thicker samples must be processed to generate larger vascular networks, objectives with long working distance are required, which normally have low-numerical aperture and thus lead to low spatial resolutions [54]. For both photo-ablation and photo-degradation techniques another limitation which will have to be overcome in order to increase throughput is the high power and/or long illumination times needed, rendering the technique less practical.

Spontaneous vascularization – only achievable in the proper conditions - reveals to be the easiest – yet closer to physiological – way to obtain a perfusable vascular network in a close-to-*in vivo* ECM environment, because of the presence of mechanisms of active vascular remodeling, which appears to be a critical element of any tissue development model system [14], [55], [56][57][58][59].

Another important element emerged in the analysis conducted above regarding engineered tissues and vasculature *in vitro* is exchange of nutrients, which is strictly connected to vascularization process [60]. Before vasculature development inside *in vitro* biological constructs can assure vessels to express their functionality, nutrients and metabolites transport has to be obtained in a different way: dynamic culture seems to be the most used, functional way – yet less medium-consuming – to reach the target of temporarily perfusing the engineered tissues at early stages of vasculature formation.

An important issue emerged in the analysis is the absence of a proper dynamic culture condition, which represents a critical aspect of endothelial vessels development: in-flow represents an important parameter for endothelial vessel sustenance [61], determining maturation of the structure. In order to guarantee proper dynamic flow conditions, a microfluidic approach can be adopted. Next paragraph will focus on the basic principles of microfluidics, materials and techniques involved for device fabrication, and several applications in the vascularization field.

1.5 Microfluidics

Microfluidics is defined as the study and manipulation of fluids at the submillimeter length scale, involving volumes between 10^{-6} and 10^{-18} L inside miniaturized devices. Phenomena that dominate liquids at this scale are different from those that dominate at the macroscale: for instance, gravity at microscale has reduced effects compared to its dominance at the macroscale, while surface tension and capillary forces play a critical role at the microscale. Microfluidics emerged from the convergence of technologies and principles of several pre-existing research branches, such as chemistry, physics, biology, materials science, fluid dynamics, and microelectronics [62].

Microfluidics characteristic small dimensions determine a plethora of advantages, including low fluid volumes, high spatial resolution and massive parallel operation, which lead to low sample substance, portable technologies and multi-tasking operations. In addition, high temporal resolution, low energy consumption and high sensitivity are crucial features of microfluidics, thus resulting suitable in a variety of research fields, including separation of molecules or cells, lab-on-a-chip, micro-reactors and biological model platforms [63].

Through microfluidic approach, control over parameters such as flow rate, velocity, shear stress, spatio-temporal gradients and geometrical cues can be achieved. Laminar flow conditions can be easily established, obtaining non-mixing fluid interfaces, and avoiding phenomena correlated to turbulent regimes. Typically, microfluidic systems are designed with a characteristic dimension length in the order of tens - hundreds of micrometers. Advantages of these microsystems are ease of fabrication, low reagent consumption, parallel and rapid processing ability and large-scale integration. Microfluidic devices can be designed for several applications, some being real-time PCR, immunoassays, whole blood sample preparations, two-dimensional chromatographic separations, dynamic cell culture [64] and organ on-chip platforms [65].

1.5.1 Microfluidic devices materials

One of the fundamental steps in microfluidic studies is selecting the optimum material for the device application and the fabrication process. Since, on a microscale surface, the material properties have an amplified effect, the platform material is likely to affect the properties of synthesized nanomaterials. Specifically, unique phenomena emerge in

capillary microfluidics due to shorter retention times, laminar flows, enhanced heat and mass transfer, and large surface-to-volume ratios [66]. Unlike for macroscale channels, the wetting and contact angles of an aqueous solution on the chip materials are of fundamental importance [67]. Other essential properties that must be considered when choosing the material – depending on the application - are durability, ease of fabrication, transparency, biocompatibility, chemical compatibility with the implied reagents, meeting the temperature and pressure conditions needed for the reaction, and the potential of the surface functionalization.

Suitable materials for microfluidic devices fabrication can be divided in several categories based on chemical and mechanical properties: typically employed substrates include glass, silicon, metals, polymers and ceramics, but the diversity and quality of materials are continuously increasing. Each material present benefits and drawbacks, depending on its destination use.

Various kinds of materials attempt to match these properties and can be used for the manufacturing of microfluidic devices. Typical substrates include glass, silicon, metals, polymers, and ceramics, but the diversity and quality of materials are continuously increasing. Each material has both advantages and disadvantages, depending on its destination use [68].

- *Metals*: a class of materials whose properties make them suitable for some applications and fabrication processes. Regarding workability, they result cheap, widely accessible, easy to machine; considering applications such as microreactors production, they can resist to high heat loads, high pressure, and toxic chemicals (except strong acids). Besides, their resistance to robust handling is convenient for cleaning operations. The most commonly used metals for microfluidic devices fabrication are aluminum, copper, and iron, or alloys with other metals in order to fine-tune their chemical and mechanical properties. Microfluidic devices made of metals have been demonstrated useful in nanomaterial synthesis, as size-tunable methacrylic nanoparticles were obtained in a stainless-steel multi-lamination micromixer. Figure 1.4.1.1 shows the schematization of the stainless-steel micromixer [69].

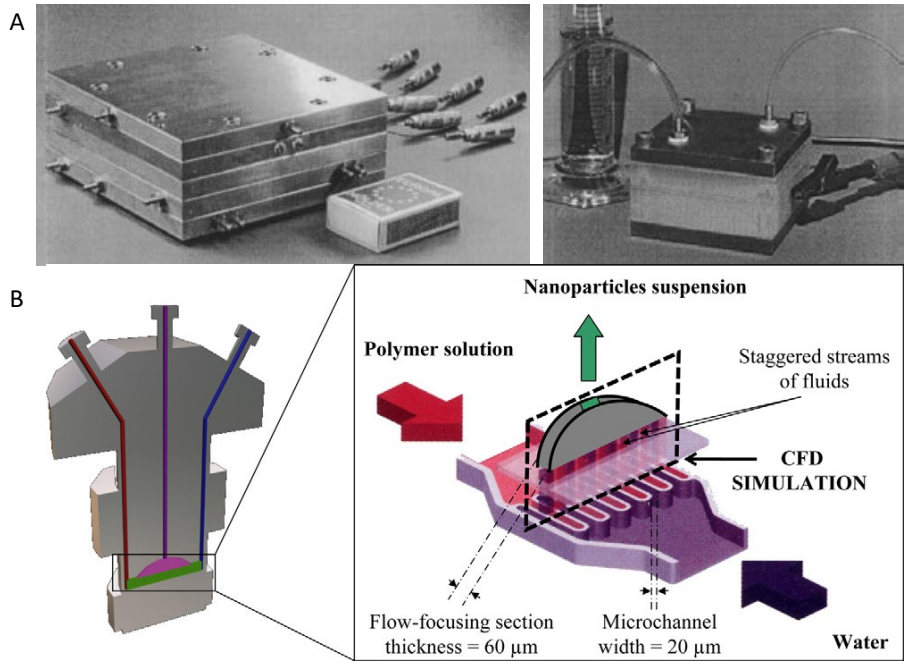

Figure 1.5.1.1: (A) Images of micromixer platform. (B) Overview of stainless-steel micromixer inner microstructure, used for nanoprecipitation. Bally et al., 2012

- *Silicon*: a material with ready availability, chemical compatibility, and thermostability, features that make it suitable for several microfluidic applications. Workability of silicon relies on ease of fabrication and design flexibility, while semiconducting properties, and the possibility of surface modifications determined silicon success for microfluidic platforms for decades. Several disadvantages must be considered when including this material in practical applications, the most evident being opacity, which do not allow direct optical detection in both visible and ultraviolet spectra. Modifications to include transparent portions of material reveal to be necessary if *in situ* imaging is required. Another drawback regards its mechanical properties: fragility and high Young modulus result in disadvantages in incorporating active components, i.e., valves and pumps, which are fundamental for some applications. As an expensive material, it can be difficult to purchase. Nonetheless, silicon microfluidic platforms find use in biological applications, such as point-of-care medical diagnostics and organ-on-chip devices for drug toxicity screening [70]. For example, Chandrasekaran et al. presented a hybrid integrated silicon microfluidic platform for fluorescence-based bio-detection as a micro-opto-electro-mechanical system (MOEM), combining silicon and Pyrex (Figure 1.5.1.2) [71];

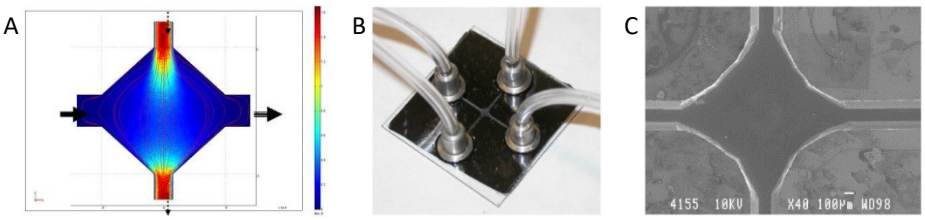

Figure 1.4.1.2: (A) FEM simulation of flow behavior in the M-Zone. (B) Microfluidic chip after packaging. (C) Mixing zone of the microfluidic channel inside silicon-based device. Chandrasekaran et al., 2007

- *Glass*: an interesting material for several microfluidic applications, due to its chemical inertia, thermostability, electrical insulating properties, rigidity, biocompatibility, along with ease of surface functionalization [72]. These properties, along with higher resolution at the micrometer scale that is achieved in glass microcapillary reactors compared with other materials, make glass a suitable material for microreactors – even with extreme reaction conditions in terms of high temperature, high pressure and corrosive solvents - and for the better-controlled synthesis of emulsions and polymeric nanoparticles. Compared to silicon, glass is characterized by excellent optical transparency, a lower price, and the possibility of integrating active components, including valves, pumps of other materials (e.g., silicon, polymers, and hydrogel), but also glass components can be integrated in the form of ultra-thin glass sheets. Due to its transparency, glass can be used for optical detection, which is fundamental in some applications, including live-monitoring dynamic cell culture. Additionally, glass thermal and chemical stability allows for the effective cleaning of the device, either by heating the chip or washing it with chemicals, enhancing its reusability, thus resulting as a cost-limiting material. Glass microfluidic devices usually are composed of soda-lime glass, borosilicate glass or fused quartz. Drawbacks emerge regarding microfabrication of glass, which is hard to manufacture due to its fragility, thus determining costs increasing, as preparation in cleanrooms is sometimes necessary. Figure 1.5.1.3 shows an interesting example of direct laser writing of sub-50 nm fluidic channels in glass for DNA analysis application [73].

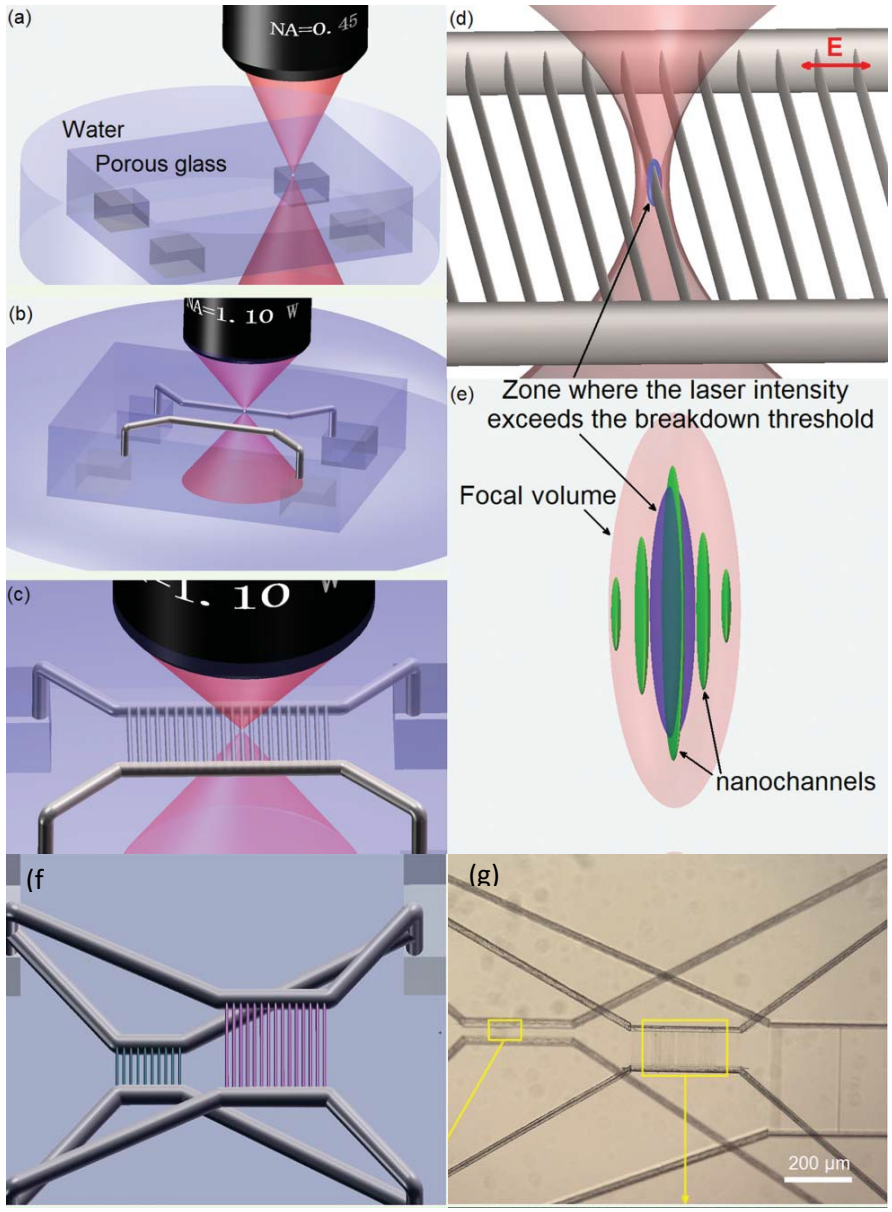

Figure 1.5.1.3: (a–c) Schematization of the design of fabrication method for 3D integrated nanochannels by femtosecond laser direct writing realization. (d) Schematic view of the laser writing of nanochannels. The polarization direction of femtosecond laser is indicated by the red arrow. (e) Schematic illustration of the physical operating principle behind the realization of narrow channel width far beyond the optical diffraction limit. When the laser intensity is decreased to some extent, only the central nanochannel could be induced while other nanograting-like channels vanish. (f) Schematization of pattern design and (g) top-view optical image of the fabricated 3D nanofluidic channels chip for DNA analysis. Liao et al., 2013.

- *Ceramics*: properties that make ceramics suitable for microfluidic devices are a unique surface chemistry, good resistance to corrosive environments, and good thermostability. Nevertheless, ceramics present some limitations in dimensional stability, porosity, and brittleness, thus rendering difficult to integrate this type of material into a complete microchip. Malecha et al. fabricated a monolithic microwave-microfluidic sensor made with low temperature co-fired ceramic (LTCC) technology, consisting of several steps: conductive layers made of silver were deposited using a standard screen-printing method through a 325-mesh steel screen. The registration orifices,

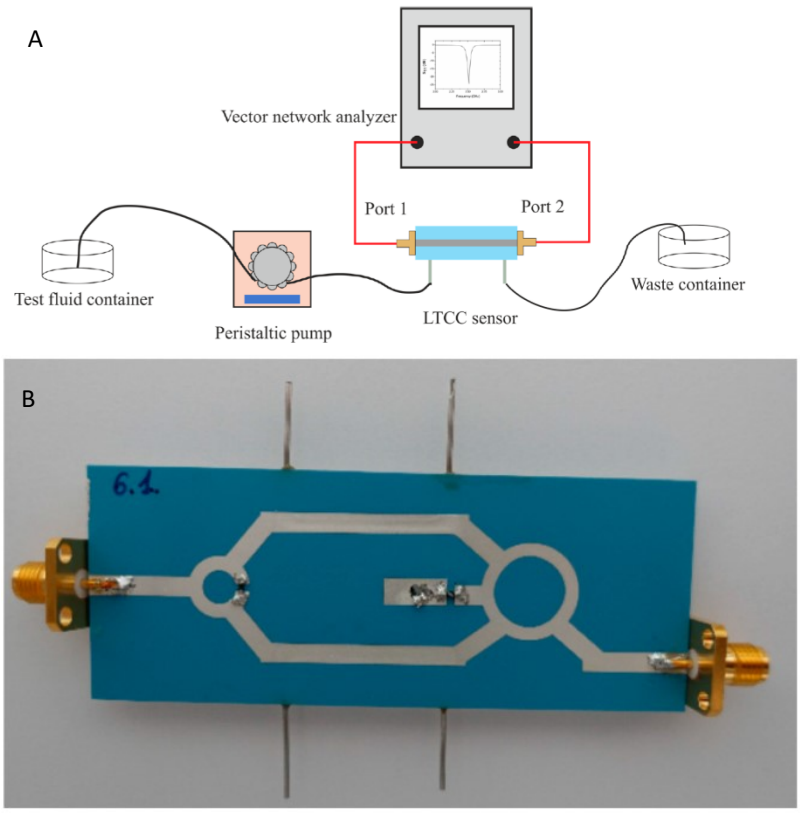

Figure 1.5.1.4: (A) Schematization of experimental set-up and (B) image of a fabricated co-fired ceramic coupler-based sensor. Malecha et al., 2019.

vias, microchannels and other shapes were cut in a green LTCC material using a UV laser. After laser micromachining and screen-printing, the LTCC tapes were stacked and laminated using an isostatic press. The resulting laminates were co-fired in a box furnace at 875 °C. Figure 1.5.1.4 show a schematic representation of experimental set-up and an image of the fabricated device [74].

- *Polymers*: as in various research fields, this material class has gradually substituted silicon and glass for the fabrication of microfluidic devices, since they show a plethora of interesting features and benefits. In comparison to the previously-mentioned materials, polymers are drastically less expensive and rely on easier and lower-cost manufacturing techniques. Polymer versatility can be employed in a variety of applications, comprising nanoparticle synthesis and separation applications. Transparency or semitransparency are important features for application where optical accessibility is needed (live-monitoring of chemical reactions, cell morphology or migration assays). The most common polymers utilized for microfluidic device fabrication include: polydimethylsiloxane (PDMS), polymethylmethacrylate (PMMA), fluorinated polymers, copolymers (COPs/COCs), thiol-ene polymers (TEs), epoxy resins and hydrogels [68].

  A focus must be taken into account for one of the most common materials of this class: PDMS, an elastomer with excellent properties regarding microfluidic devices applications. PDMS is easy to mold and cheap, thus representing a resource for rapid prototyping. Its optical transparency, together with gas permeability, biocompatibility and low autofluorescence makes it one of the best choices for the design of microchips for biological applications, including dynamic cell culture [75][76]. In addition, hydrophobicity and compliance properties are widely considered as interesting features for bio-related research, such as cell screening and biochemical assays [64]. As a drawback, some of these properties can turn into negative effects, especially in organic synthesis. The porosity of PDMS makes it an adsorptive material, in which many molecules can diffuse (organic solvents such as hexane, toluene and chloroform), leading also to undesired swelling of the platform. Another issue may arise from water evaporation through channel walls, which could lead to a variation in solutes concentration. To overcome the problems regarding these specific applications, some other polymeric materials are being investigated for microfluidic fabrication, depending on the desired properties and final use. Kim et al. developed a PDMS microfluidic platform for 3D cell culture and cell-based assays, exploiting PDMS features such as biocompatibility, optical clarity and ease of fabrication, together with ease of coupling with external valves, pumps or connectors for flow control (Figure 1.5.1.5) [77].

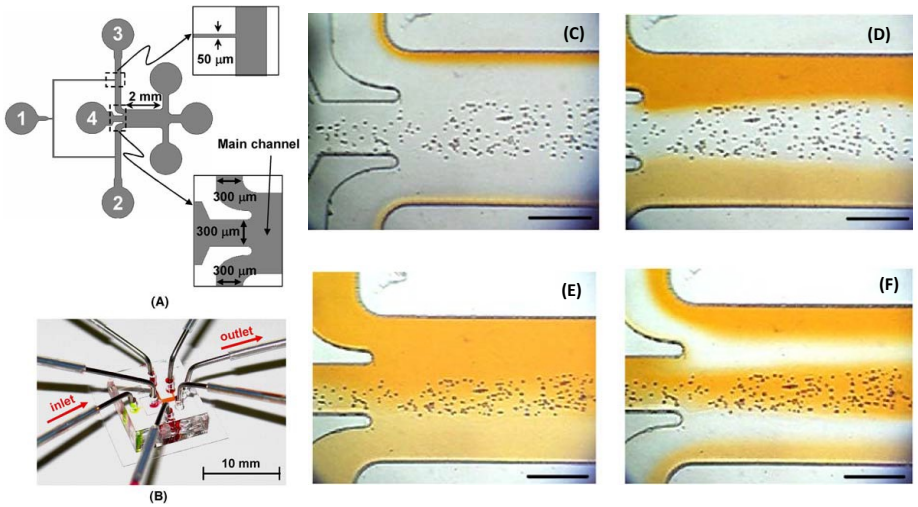

Figure 1.5.1.5: Design schematization (A) and image (B) of PDMS microfluidic platform for cell assays. Pictures of 3-D cell immobilization. All scale bars are 300 µm. (C-F) The mixture of Puramatrix and HepG2 at different flow conditions highlight fine control over flow parameters obtainable with microfluidic platforms. Kim et al., 2006

Another widely used material for the manufacturing of microchips is PMMA, an amorphous thermoplastic with a slightly higher solvent compatibility than PDMS and absence of small-molecule absorption. Its optical transparency, good mechanical properties and surface modifiability makes it interesting for organ-on-a-chip platforms and micro-physiological sets-up [68].

An important category of polymers in microfluidic field is perfluorinated polymers, with the most commonly used being perfluoro-alkoxy alkane (Teflon PFA), fluorinated ethylene-propylene (Teflon FEP), and polytetrafluoroethylene (PTFE). They show thermo-processability, chemical inertia, compatibility with organic solvents, and excellent antifouling properties. PTFE can present optical transparency and a moderate permeability to gases, and its flexibility is sufficient to produce diaphragm valves. These materials have been used in cell cultures, high-precision assays, super-clean tools, valves and pumps.

Cyclo-olefin polymers and copolymers (COPs/COCs) have recently attracted considerable research interest in microfluidics due to their favorable properties, such as optical transparency in the visible and near-UV spectrum, enhanced chemical resistance, low water absorptivity (<0.01%), good electrical insulating properties, long-term stability of surface treatments, and an extremely low level of impurities. These thermoplastics are useful for synthesis devices in which aggressive solvents are employed, being able to withstand acids (e.g., hydrogen chloride, sulfuric acid, and nitric acid); bases (e.g., sodium hydroxide and ammonia); and polar solvents (e.g., ethanol and acetone) [68].

TEs are a family of macromolecular compounds consisting of two monomers, each with at least two -thiol or -allyl (or -ene) groups. These materials could represent a better alternative to other polymers, as they have a significantly higher solvent resistance than PDMS, PMMA, and COCs. TEs also present enhanced optical transparency in the visible spectrum, but the UV transmittance is composition-dependent.

Epoxy resins are another class of polymer materials used for microfluidic device fabrication, emerging for their enhanced stability at high temperatures, chemical resistance, transparency, and very high resolution for patterning, due to their thermosetting property, even though they are mostly used as a component in glass or silicon chips. However, the most striking disadvantage of these materials is their high cost [78].

Hydrogels are an increasingly used class of materials regarding microfluidic approach for their highly porous tridimensional networks formed by hydrophilic polymer chains that allow the diffusion of small molecules and bioparticles [79]. Other advantageous properties of hydrogels include their biocompatibility, low or no cytotoxicity, biodegradability, controllable pore size, high permeability, and aqueous nature [37]. This last feature results in an important opportunity for applications that rely on the resembling of ECM, having intrinsic critical features to mimic natural mechanical and structural cues for cell adhesion, proliferation, and differentiation. These characteristics make hydrogels ideal for encapsulating cells for 3D culture in tissue engineering research [80]–[82]; for the delivery of solutions, cells, and other substances; and for sensors and actuators. However, hydrogels are less frequently used as the primary fabrication material, because maintaining the device integrity is quite challenging due to their poor mechanical properties which can limit their use in the long term. Nonetheless, these materials can be employed in building microfluidic component functionalities, such as semipermeable barriers and smart valves, within a chip made of a more rigid material [83].

Since 2007, paper-based microfluidics has been explored as an alternative to expensive materials for microfluidic applications [84]. Paper-based systems benefit from simplicity, accessibility, significant low costs, high porosity, high physical absorption, ease of manipulation and sterilization, potential for chemical or biological modifications, similarity to the native ECM, bio-affinity, biocompatibility, light weights, and the ability to operate without supporting equipment [85]. What makes paper so interesting is the surface tension of a fluid and its contact angle with cellulose fibers. Hence, the paper's fluid flow is influenced mostly by the cohesive and adhesive forces that produce capillary action in the cellulose matrix. Some researchers treat the pressure force in the analogy with electric circuits, comparing it to the electric voltage source that pushes fluid through the network. Moreover, this phenomenon allows the

precise guiding of fluids by hydrophobically modifying certain regions in the matrix. The special behavior of paper and its advantageous properties make this material suitable for a variety of applications. Paper-based systems are attractive for rapid point-of-care diagnostic testing and medical screening in the developing world [86], being mostly used together with a colorimetric or an electrochemical readout for detecting target biomolecules [87]. Besides, paper microfluidic systems can be directly and in situ operated, even in the absence of technical infrastructure and trained experts, making these devices a promising solution for field analysis or testing at home. However, paper-based systems are limited by their poor mechanical strength in a wet state and thickness requirements for achieving transparency. In addition, passive pumping may cause certain challenges concerning the precise design of the fluid circuit's hydrodynamic resistance. The materials previously mentioned can also be combined into hybrid devices to exploit their advantages in a synergic manner [88]. In this respect, approaches that can be taken include placing soft films between hard chips in sandwich-like structures to form diaphragm valves, incorporating channels with substrates patterned with metal electrodes, combining several materials to adjust the channel permeability in specific regions, or implanting photocurable materials to obtain structures manufactured *in situ*. One example of a composite microfluidic device was proposed by Koijc et al. [89]. They created a cost-effective chip that combined polyvinyl chloride (PVC) foils and Ceram Tapes. Their proposed device presented good optical, mechanical, and thermal characteristics and excellent resistance to high flow rates. Moreover, it benefited from the fact that each layer could be created and tested separately before lamination. Hence, high reliability and reproducibility could be achieved. Another strategy was approached by Gao et al. [90], who combined gas-permeable PDMS with Norland Optical Adhesive 81 (NOA81), a photocurable gas-impermeable polymer, to enable the local control of oxygen tension in microfluidic cell cultures. This hybrid device allowed researchers to establish hypoxic zones of precise dimensions and geometry inside microfluidic cell culture chambers. Chen et al. took yet another approach, investigating microfluidic devices based on a glass–PDMS–glass sandwich configuration [91]. The main advantage of such devices is the possibility to dismount and reuse them in various applications. Their proposed sandwich configuration could exceedingly increase the sealing strength of reversibly adhered devices, being also able to withstand high pressures.

	Cost	Easy to manufacture	Rigidity	Oxygen permeability	Optical accessibility	Chemical modifiability	Biocompatibility
Metals	Low	Yes	High	No	No	Moderate	Yes
Glass	Medium	No	High	No	Yes	Moderate	Yes
Silicon	Medium-High	No	High	No	No	Moderate	Yes
Ceramics	Medium	Yes	High	Moderate	No	Moderate	Moderate
Elastomers	Low	Yes	Low	High	Yes (possible autofluorescence)	Moderate	Yes
Thermo-plastics	Medium	Moderate	Low-Medium	Variable	Yes	Moderate	Yes
Resins	Medium	Yes	Low-Medium	No	Yes	Moderate	Yes
Hydrogels	Low-Medium	Moderate	Low	High	Yes	Excellent	Yes

Table 1.5.1.1: Resuming table of the most important features for the choice of microfluidic platforms materials. Parameters such as chemical modifiability, biocompatibility and oxygen permeability can be ignored in some applications, while other such as rigidity and cost strictly depend on the specific material. Further studies must be taken into account for material choice.

1.5.2 Microfluidic devices fabrication methods

After the choice of the right material for the purposed application, next step of the design process of a microfluidic platform is the evaluation of the fabrication methods, in order to determine the most reliable regarding different parameters, such as time consumption, cost, resolution and precision. It is important to underline that different techniques can be combined in order to produce the designed device. Following, a classification of microfluidic devices fabrication techniques is presented, based on the operating principle of machines and methods applied. It is possible to divide the fabrication techniques into: chemical processes, mechanical processes, laser-based processes and other.

- *Chemical processes*: fabrication methods that imply chemical reactions in order to obtain the designed pattern for microfluidic platform. These processes can be divided in additive – such as inkjet 3D printing [92] – and subtractive – like wet- or dry-etching. The most commonly used chemical techniques are wet-etching, dry-etching and electrochemical discharge machining, which are subtractive techniques regarding materials. Wet-etching features rapid processing rates and the possibility of simultaneously manufacture a large

quantity of wafers. As drawbacks, this technique employs aggressive chemicals for material removal, as the etchant of choice is usually hydrofluoric acid, known as a dangerous substance: this represents a limitation of this fabrication technique, as highly corrosive etchants possess significant safety and environmental hazards. Another disadvantage is the isotropic profile of the etched channels. By contrast, dry-etching techniques, also known as reactive ion-etching, overcome some of the wet etching fabrication challenges (Figure 1.5.2.1) [93]. It is possible to generate anisotropic, precise microscale channel profiles due to the directionality of the ion bombardment. Dry-etching is recommended for transparent substrates but drawbacks reveal to be the slower etching rates compared to wet-etching and poor selectivity relative to the mask. Electrochemical discharge machining is a rather non-conventional fabrication process that uses an electrochemically generated spark on a tool surface. The spark is created by applying a voltage between two electrodes (one counter electrode and one tool electrode) immersed in an electrolyte. The high temperature of the spark removes the undesired material either thermally or chemically. The process can be applied to non-conductive materials, such as ceramics and glass [94].

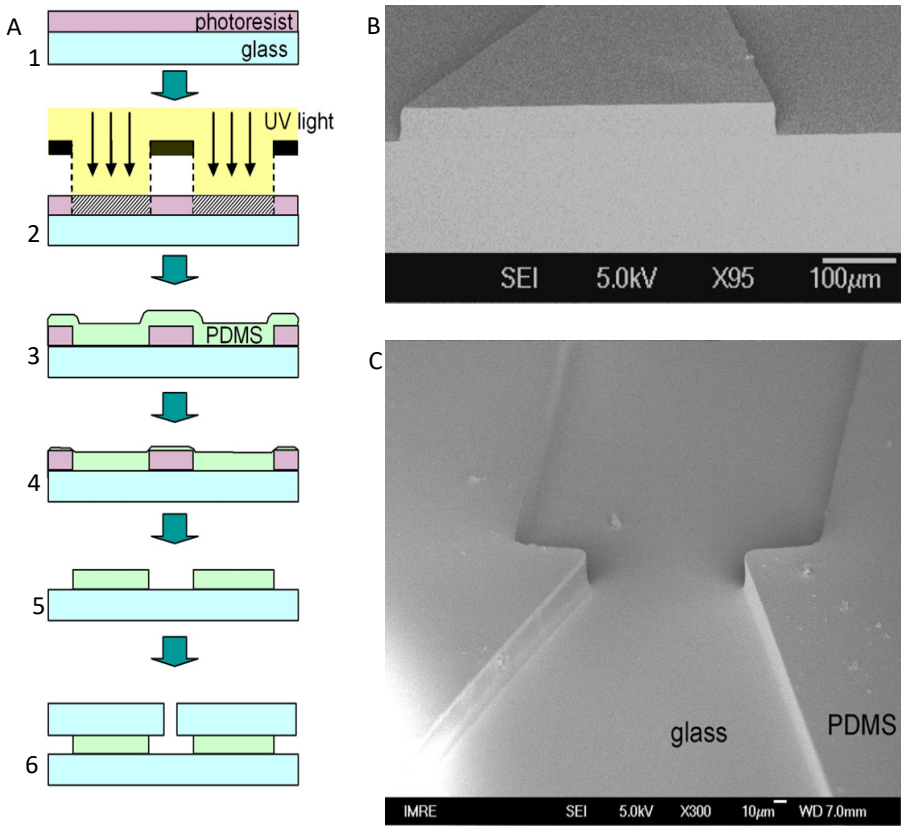

Figure 1.5.2.1: (A) Schematization of dry etching process steps on PDMS-glass hybrid microfluidic platform. 1) Spin photoresist; 2) Expose photoresist through chrome mask; 3) Develop photoresist and spin on PDMS, then cure at 70°C; 4) Blanket reactive ion etching (RIE) etch until PDMS is thin enough to be lifted off; 5) Lift PDMS off and dissolve photoresist in acetone; 6) Bond PDMS to glass. (B-C) Scanning Electron Microscopy (SEM) images of etched PDMS. Oh et al., 2008

- *Mechanical processes*: Micromachining was one of the first known methods for fabricating microfluidic devices, as it was borrowed from the pre-existing field of semiconductors. Mechanical processes must allow the production of crack-free surfaces while preserving good dimensional accuracy and surface roughness. Such techniques are suitable for processing silicon and glass, but they can also be used for polymer-based devices to generate the replication master. Methods such as mechanical cutting, abrasive jet machining, and ultrasonic machining benefit from low cost, high degrees of flexibility, and the possibility to be used together with other processes for creating complex 3D structures. On the other hand, the main limitation of mechanical fabrication processes is their reduced precision and productivity compared to lithographic methods. Micro-milling employs a high-precision computer numerical controlled motion system for removing bulk materials. Removal of material

from the workpiece determines the fabrication of a specific micropattern. This technique's advantages are its ease of use, effectiveness, precision, and low-cost production, being suitable for creating complex 3D structures. Additionally found in the literature as "blasting", abrasive air-jet machining relies on the injection of abrasive particles through a nozzle to be mixed with the air at high speed and very high pressure. Material removal is obtained by the kinetic energy of the particles colliding with the workpiece surface. Similar to abrasive air-jet machining, abrasive water-jet machining is a non-traditional fabrication method that allows the production of complex 2D parts with tight accuracy. The high viscosity of water, compared to air, provides better jet characteristics than in abrasive air-jet machining. Ultrasonic machining also involves abrasion of a substrate through vibration. The working principle is based on creating microcracks on brittle materials, e.g., glass, silicon, and ceramics, thus fabrication the design pattern. Xurography represents the patterning of an adhesive film through the use of a razor blade. It was adapted as a low-cost technique for microfluidic chip fabrication, because it allows the production of robust, inexpensive devices in a short time (several minutes) and without requiring a cleanroom facility. Injection molding is a common method for processing polymers for various objects of daily use. Due to its high-throughput, cost efficiency, and precision, this method has also attracted interest in microfluidics fabrication. Often found in the literature as micro-injection molding, this process consists of transferring pre-polymerized pellets of a thermoplastic from a hopper into a heated barrel. After the material melts, it is injected under pressure inside a heated mold cavity. The pressure is maintained for a given time, while the temperature is decreased below the polymer glass transition temperature. The solidified material is released from the mold. Despite its advantages in terms of costs and method simplicity, the main limitations of micro-injection molding are material restrictions (only thermoplastics) and mold issues (expensive fabrication and limited resolution). Similar to injection molding, hot embossing is based on melting thermoplastics and shaping them into molds by means of pressure and heat [95]. However, instead of injecting the polymer into a cavity, the material is poured and pressed against the mold in such a way that the desired features are transferred from the cast to the softened polymer. This difference allows stress reduction in the processed material. Moreover, more delicate designs can be obtained due to less shrinkage of the cast. However, the limitation of using only thermoplastics is also valid for this method.

Micro-milling, which relies on rotating tips with different diameter that can be used to remove material from a substrate and obtain the designed shape;

Micromilling is an alternative method that has the potential to address some of the challenges in microfabrication. Micromilling is a fabrication method that

generates microscale patterns by means of rotating tips that remove bulk material from a substrate. Despite many other methods have been studied and analyzed previously for microfluidics applications, micromilling is less considered by microfluidic researchers. Nonetheless, arisen interest towards this technique have been caused by several recent works regarding microfluidic devices. Micromilling is a subtractive manufacturing process – which means that material is removed from, and not added to, a substrate - that uses rotating cutting tools to fabricate the designed hollow geometries inside a starting stock piece, commonly referred to as the *workpiece*. The basic milling machine, or mill, consists of: a *worktable* for positioning the workpiece; a cutting tool (usually named *endmill*), and an overhead spindle for securing and rotating the cutting tip. Milling, which was first introduced in research in 1818, has been profoundly developed, and now represents an important tool for fabrication facilities (Figure 1.5.2.2, A). The positions of the worktable (*X* and *Y*-axis) and spindle (*Z*-axis) can be manually adjusted or, in modern equipment, controlled with *computer numerical control (CNC)* that automates the process, thereby improving repeatability and precision, reducing error and adding advanced capabilities (*e.g.*, the direct conversion of computer-aided design (CAD) models to finished pieces). Milling machines with CNC capability (*i.e.*, CNC mills) can be purchased with a wide range of technical specifications, thus operating at different levels of stage precision, spindle speeds, and automation. Modern CNC mills present a resolution in the order of micrometers, and can manufact also in the meter range. The wide availability of cutting tool shapes, materials, and sizes makes mill one of the most eligible tools regarding versatility, to fabricating many types and size of patterns in many different materials. The most interesting aspect of using a CNC mill is the ability to fabricate the designed pattern directly from a 3D CAD model, making it easier and faster to convert design concepts to working devices. Latest advances in technical features have improved precision and resolution down to the micron scale, leading to fabrication of increasingly more intricate geometries with microscale resolution. Micromilling can be useful to obtain microfluidic devices in two ways: (1) manufacturing a master which replicates the negative of the needed pattern, followed by a second fabrication step (*e.g.*, replica molding, embossing, or injection molding) or (2) direct fabrication of patterns and geometries needed for the application. The direct fabrication of polymer-based piece can be performed in 30 minutes, thus representing a major choice for both rapid prototyping and large-scale fabrication of microfluidic platforms. In addition, comprehensive reviews are available on multi-functional machine tools for metal cutting. Even if a gap exists in the study of non-traditional materials to mill - especially for the fabrication of microfluidic devices – and important

database of information regarding microfluidic platform fabrication is available in reviews and manuals.

In order to achieve high quality of manufacturing, thus fully exploiting micromilling features, proper setup of milling steps is crucial. In particular, workpiece fastening and tool alignment represent the two most influential factors on quality [96]. For workpiece setup, the most common and adequate techniques to fasten polymer sheets are vacuum and adhesive tape [97].

Surface roughness and resolution are important factor for qualitatively evaluating microfluidic devices, particularly for biological applications that require live imaging, or that utilize surface interactions (*e.g.*, microfluidic ELISAs with substrate-bound antibodies), where roughness can negatively influence results and experimental plans. Each tip with different diameter has a working spindle rate, which determines best milling conditions for each material: from the balance between time-consumption, permissible surface roughness for the application, and resolution needed, it is possible to regulate spindle rate without problems.

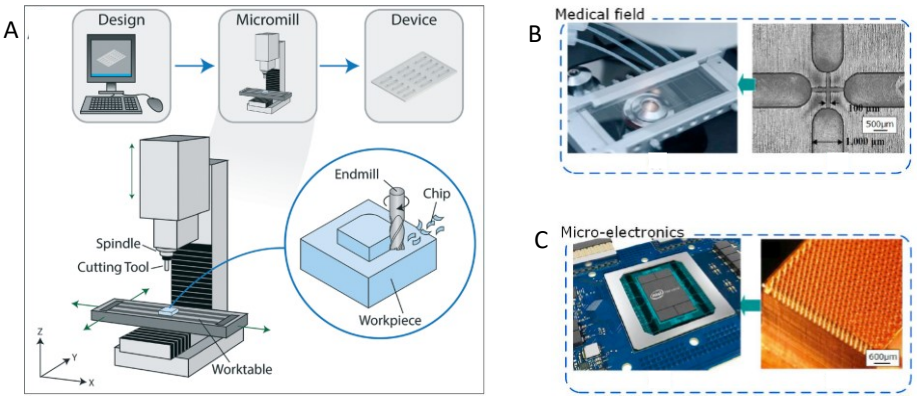

Figure 1.5.2.2: (A) Schematization of micro-milling hardware set-up and approach. (Niculescu et al., 2021). (B, C) Examples of micro-milling based micropatterned devices for different application (Chen et al., 2021).

Another focus must consider soft-lithography, usually addressed in the literature as “replica molding”. Based on the processing of elastomeric polymers and patterning of surfaces using PDMS stamps, soft-lithography implies several steps—namely, fabricating the original hard master, pouring unpolymerized elastomer on top of the master, degassing for air removal, heat-curing, and peeling off the polymer. In this way, a cast-molded stamp (replica) from a flexible material is generated and further used for printing, molding, and embossing micro- and nanostructures. The main advantages of this method are the obtaining of high-resolution replicas, the lower costs and more rapid

production than the old photolithography method, the possibility to generate complex patterns for 3D flows and pneumatic control lines by a layer-by-layer approach, and the ability to produce designs of high flexibility and high optical transmittance. Concerning the limitations of the method, they are mostly related to the replica mold. Specifically, as the materials involved are soft, pattern deformation may occur, especially when removing the cast from the mold. In some applications, soft replicas may undergo swelling, generating modifications to the previously patterned geometry: in order to overcome this limitation, control over humidity and the substitution of the chip with brand-new fabricated ones may represent the best strategy, given the low cost and time consumption of the technique. Another issue is that soft lithography is a semi-cleanroom process, implying costly photolithography techniques to realize the hard master [98][99]. Nonetheless, hard master can be fabricated using one of the existing techniques, thus replica molding represents a versatile approach. Figure 1.5.2.3 shows a schematization of the steps of replica molding technique starting from the fabrication of the hard master with photolithography, but several techniques may be involved in the first step.

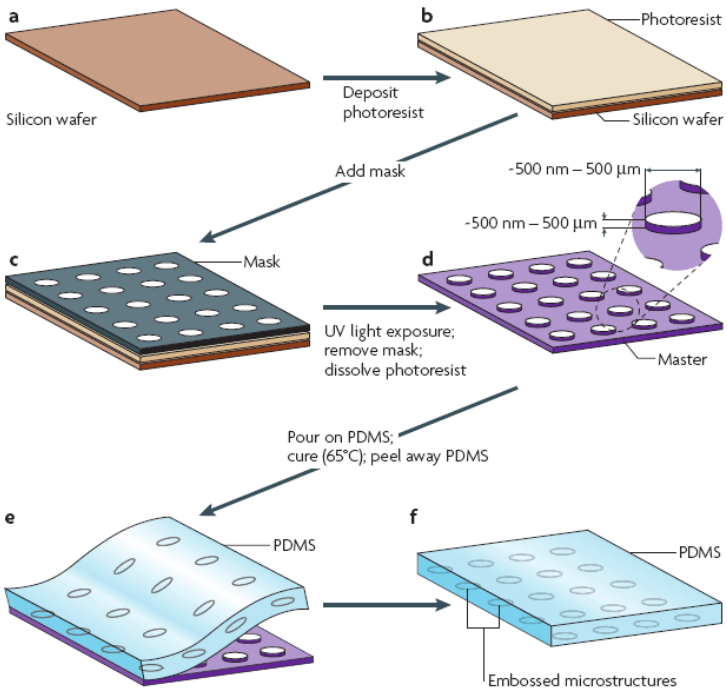

Figure 1.5.2.3: Schematization of the steps for replica molding approach based on photolithography for master fabrication. Several techniques (micro-milling, 3D printing) can be used instead of photolithography for the hard master production, according to material, resolution, cost and time consumption choice. (a-d) Photolithography steps for hard master

fabrication, featuring the negative of the needed pattern. (e, f) Replica molding with poured unpolymerized elastomer (PDMS) and removal after curing. The patterned slab is ready to be bonded to PDMS layer or glass and used for microfluidic application.

- *Laser-based processes*: Generally, lasers are expensive tools, but compared to cleanroom facility costs, they are considered a more accessible fabrication technique. Moreover, laser ablation supports the generation of microfluidic patterns on various materials in a rapid and flexible manner, without the hazards associated with chemical fabrication methods. As a working principle, lasers optically amplify light via the stimulated emission of electromagnetic radiation. A microstructure is created due to the thermal degradation effect, engraving the working material surface. In more detail, short-duration laser pulses of controlled wavelengths break the chemical bonds from polymer molecules, while the associated rapid increase in temperature and pressure result in the ejection of decomposed polymer fragments. Hence, a photo-ablated cavity is produced. The drawbacks of this method are related to the weak reproducibility caused by poor control of the laser focusing, undesirable surface effects, limited throughput, and product quality variations between different types of lasers [94].
  Stereolithography is a classic 3D polymer structure-producing technique that fits under the umbrella of laser-based fabrication processes. This method is ideal for generating very fine features in a short time. Liquid photopolymer resins are printed layer-on-layer and crosslinked with a focused laser or LED light source. UV light is commonly used, but longer wavelengths can also be employed, depending on the photo-initiator type.
  Two-photon polymerization is a technique through which structures are formed by curing arbitrary spots within the material. Two-photon polymerization uses ultrashort laser pulses focused on a liquid resin volume to produce photopolymerization by two-photon absorption. The main disadvantage of two-photon polymerization is that voxels are cured one by one, consuming much time if the exposure area or the number of layers increases.
  An increasingly used lased technique for microfabrication of microfluidic platforms is stereolithography: in particular, 3D printing belongs to the class of photopolymerization techniques and features high resolution, short time-consumption and can rely on the use of biocompatible resins. As other techniques, it can be used to obtain microfluidic device masters which can then be used for indirect fabrication by means of replica molding. Different studies have focused on Ultra Violet (UV) 3D printing. 3D printers can build geometrically intricate microfluidic devices directly from CAD data. Chips are built from photopolymer resins which are liquid chemicals that can solidify by

curing obtained with light exposure. The object is built with a layer-by-layer procedure, starting from the first layer directly attached to a stage (Figure 1.5.2.4, A). The source of UV light is usually positioned in the lower side of the transparent-bottom reservoir that contains the resin, and the process usually develops in minutes. This technique is particularly interesting for rapid prototyping, since the time from design to fabrication is short. A critical parameter that characterizes 3D printers are UV light source wavelength, from which depends the choice of the resin. Other parameters which determine devices quality in terms of mechanical properties, precision of pattern replicating and surface roughness are: exposure time, which consists in the time of UV illumination of each layer, and post-processing, which relies on the use of organic solvents (isopropanol or ethanol) to remove the excess of unpolymerized resin, thus increasing surface finish. Some applications need polish as a surface treatment. Sommonte et al. utilized UV 3D printing to fabricate innovative microfluidic platforms for lysozyme-loaded liposomes (Figure 1.5.2.4, B-C) [100].

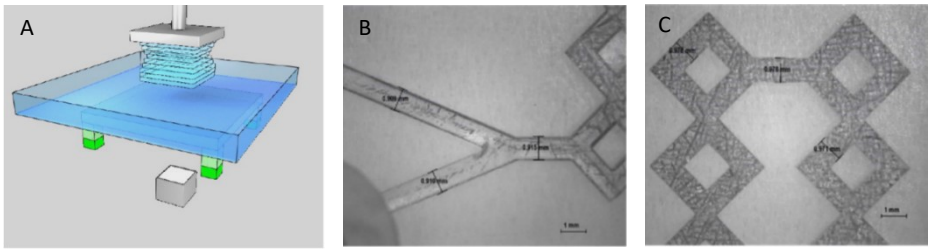

Figure 1.5.2.4: (A) Representation of layer-by-layer procedure of UV 3D printing: CAD file is divided in several slices that are exposed to UV light for the chosen exposure time. (B-C) Micrographs of printed inlet (B) and microchannels (C) (Sommonte et al., 2022).

- *Other processes*: Three-Dimensional printing

  Three-dimensional printing is a relatively new, yet successful approach to forming microfluidic channels. It ensures a precise application of materials to create a great variety of chip designs, especially for applications requiring complicated microfluidic structures. The advantages that 3D printing brings have been exploited through several manufacturing technologies, such as fused deposition modeling, inkjet printing, multi-jet printing, and suspended liquid subtractive lithography. However, some aspects limit the broad implementation of 3D printing in microfluidics manufacturing. The most important are the low z-resolution of printing systems, the limited variety of transparent materials, the need for extremely smooth surface finishes, and limitations in the precision fabrication of the hollow and void sections.

Fused deposition modeling, also found in the literature as freeform filament fabrication or extrusion-based additive manufacturing, is one of the most widespread 3D printing technologies [101]. Fused deposition modeling is based on the melting of a thermoplastic filament, followed by its extrusion through a nozzle and solidification by cooling. The method is simple, effective, and affordable, allowing for multi-material printing. However, some challenges must also be considered when deciding whether fused deposition modeling is suitable for specific microfluidic chips. The printed structures are more susceptible to compressive stress fractures due to inadequate fusion between adjacent layers. Besides, the extruding filament sizes can be larger than the size of the microfluidic channels. Multi-jet modeling, commercially known as PolyJet, is a promising 3D printing technology [68]. Instead of a filament, a photosensitive resin is ejected as a droplet from the printing head and subsequently photo-cured by a light source attached to the inkjet printhead. Multi-jet modeling ensures high accuracy, being also able to build multi-material microfluidic platforms. Inkjet printing was originally used to deposit colored inks, but it recently attracted interest for depositing materials such as metals, ceramics, polymers, and even tissues. In this respect, inkjet printing is seen as a low-cost rapid alternative for chip production. Other advantages of this fabrication method are simplicity, high precision, and high spatial resolution.

As a hybrid technique, replica molding is the most important to highlight, due to its versatility. It consists on the fabrication of a microfluidic device by means of pouring on top of a previously manufactured master – with one of the existing techniques available – a liquid polymer which is then cured (usually PDMS). After curing, the polymer is peeled from the master and, after preparation for inlets and outlets, ready to be bonded to a substrate and utilized for the application for which it was designed.

- *Hybrid Technologies*: Hybrid technologies appeared as a solution to overcome the challenges and limitations of each stand-alone fabrication method. For instance, Alapan et al. combined 3D printing with micromachined laser lamination in order to obtain intricate transparent microfluidic devices [102]. In this way, they eliminated the need for expensive and time-consuming cleanrooms while improving the design precision of the lamination process. Another hybrid technology was proposed by Kojic et al., who integrated the benefits of xurography and thermal lamination into a 3D prototyping printing process [89]. Their fabrication method enabled rapid and robust manufacturing, with the potential of scaling-up the process by parallelizing the whole procedure. Photolithography and thermal curing were brought together by Chen et al. to create a low-cost, pump-free, capillary flow-driven microfluidic

chip. The researchers obtained a two-positron emission tomography (PET)-layered device, with one of the layers containing microchannels formed by a UV-curable TE.

Process	Additive	Subtractive
Chemical	Silicon surface micromachining Lithography Inkjet 3D printing UV 3D printing Direct writing Two-dimensional virtual hydrophilic Channels	Electro-chemical discharge machining Wet etching Dry etching
Mechanical	Injection molding Hot embossing	Micro-milling Micro-grinding Micro-abrasive air-jet machining Micro-abrasive water jet machining Ultrasonic machining Xurography
Laser-based	Selective laser sintering Stereolithography Two-photon polymerization	Photothermal process Ultra-short pulse process Absorbent material process Photochemical modification process Laser direct machining
Other	Forming process Soft lithography Layer-to-layer manufacturing Layer-on-layer manufacturing	Focused ion beam

	Fused deposition modeling 2.5-Dimensional printing	

Table 1.5.2.1: Classification of microfluidic platforms fabrication techniques, based on the operating principle class and the mode of manufacturing materials.

1.6 Vascularization on-chip models

As seen in the previous paragraphs, vascularization processes depend on several parameters, which must be controlled in *in vitro* applications in order to obtain reliable platforms for different uses, some being drug-testing platforms and vasculature study models for patho-physiological phenomena investigation [103][79][104][105]. While on one hand, *in vivo* vascularization models cannot be used as models for vascularization phenomena studies, on the other hand *in vitro* two- and three-dimensional (2D and 3D) cell models are not able to reproduce the complex spatial organization, the homotypic and heterotypic cell interactions that regulate the organ functions and, especially, the dynamic flow conditions generated by blood flow and their effects on cell behaviour [70][106]. To overcome these limitations, microfluidic principles have been applied to reproduce the biological phenomena which depend on tissue microarchitecture and perfusion [82], in order to obtain organ-on-chip, and in general *in vitro* 3D biological environment which can be analyzed and investigated on microfluidic platforms [107][108]. The integration of microfluidics, microfabrication, tissue engineering and biomaterials research makes this new technology capable of providing the basis for preclinical assays with greater predictive power and developing therapeutics for personalized medicine [109]. These systems are microfluidic platforms composed of optically clear plastic, glass, or flexible polymers, such as PDMS, which contain continuously perfused hollow microchannels in which living cells are cultured to recreate *in vitro* structures and functions of tissues and organs. Several types of organ-on-a-chip platforms have been developed [42]: the simplest systems, composed of a single microfluidic channel containing mono-cultured cells that simulate the functions of a tissue or organ, and more complex systems, compartmentalized chips or membrane chips-based systems, thus recreating interfaces between different tissues, such as an endothelial barrier, to investigate specific organ responses, including recruitment of circulating immune cells, by the drugs, toxins, or other environmental disturbances [109][110].

As vasculature is an organ whose main function is to provide nutrients and metabolites transport to every district of human body through blood flow, a strict correlation exists between vascular network and parameters regarding fluidodynamics, such as flow rate, shear stress, flow velocity and pressure, parameters that can be controlled using a microfluidic approach, and in particular considering organ-on-chip strategies. For this

reason, several microfluidic platforms have been developed with the common goal of constituting an *in vitro* vasculature model on-a-chip, which lead to important discoveries, thus adding knowledge to this non-totally understood organ [111].

Since cellular behaviour drastically changes from a 2D homotypic culture to a 3D heterotypic microenvironment, it is important to firstly underline the crucial aspect of geometrical control over 3D space inside microfluidic devices. Huang et al. in 2009 developed a microfluidic platform for co-culture of two different cell types inside to different adjacent hydrogels, in order to evaluate interface heterotypic and paracrine signaling interactions between two different cell populations in a 3D environment, closer to *in vivo* tissues than 2D cultures. By means of stereolithography and replica molding techniques [112], the group was able to fabricate a microfluidic device with fine control over patterned channels, which were separated by precisely spaced hexagonal posts: specifically, three parallel channels communicated by inter-pillar pores of 100 micrometers, which revealed to be fundamental, together with pillar angle and surface hydrophobicity, for liquid hydrogel confinement inside a single channel, that depended on surface wettability, thus surface tension (Figure 1.6.1). Such fine control over dimensions and geometry of pattern represents a step forward in the field of 3D cell culture, due to the possibility to control, on the micrometer scale, gel interfaces and cell behaviour. Different configurations of gels (Collagen type I without cells – Matrigel without cells, collagen loaded with MDA-MB-231 cells – Matrigel or fibrin) were used to highlight the role of gel interfaces inside microfluidic device. Despite Huang et al. group was not focused on vascularization processes, I decided to highlight their work because of the example they provide regarding how important the precise control of geometrical cues is in the field of biology on-chip. Since endothelium represents an important interface between the lumen of vascular vessels and the outside ECM – even with the presence of other layers surrounding endothelium – Huang et al. study on the control of interfaces may represent one of the most interesting approaches to study interface phenomena that occur during angiogenesis and vascular vessel maturation *in vitro* [113].

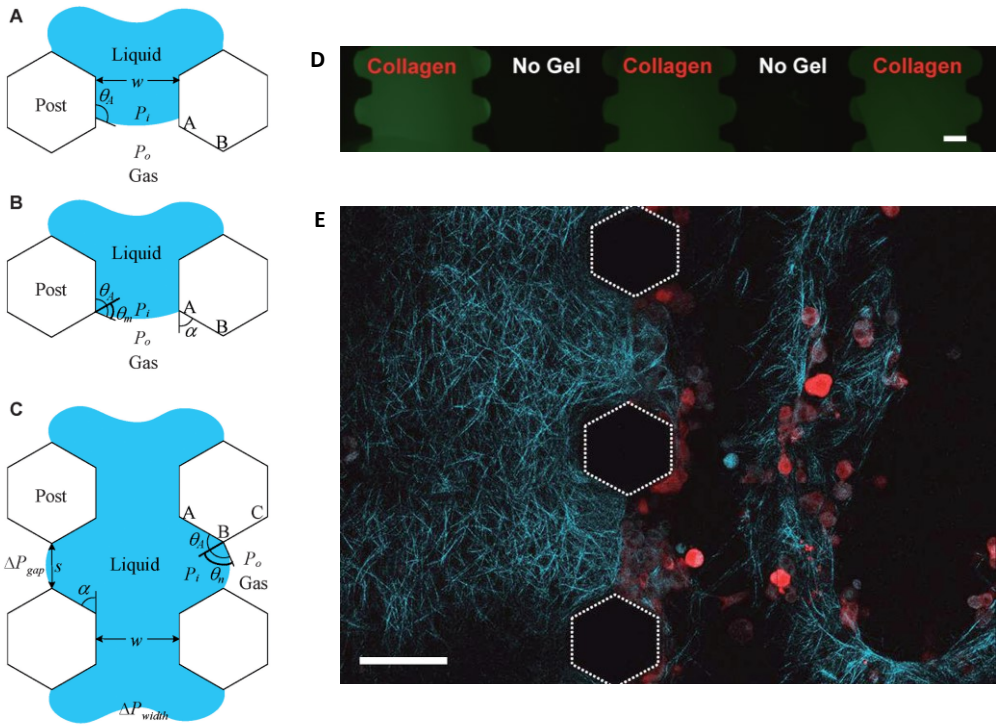

Figure 1.6.1: (A-C) Schematization of gel entrapment inside a single channel by means of surface tension. The correct design of the geometry, considering channel width, angle of the walls of hexagonal pillars, inter-pillar distance and device height, together with physical properties of materials involved (liquid hydrogel and device material) such as surface tension and wettability, determine the proper interface formation. (D, E) Fluorescent images of FITC-labeled collagen correctly entrapped in channels (D), and DS-red-labeled MDA-MB-231 cells were suspended in type I collagen and placed adjacent to another layer of collagen gel (E). Collagen without cells and cell-laden collagen interface is clearly visible, and precisely controlled. Scale bars are 100 µm. Huang et al., 2008

Once highlighted the role of interface control inside microfluidic platforms for 3D cell cultures, I will describe an important study performed by Vickerman, Kamm et al. in 2008, focused on the use of a microfluidic platform for the study on ECs behaviour inside a 3D microenvironment which spatially and chemically reproduced the physiological ECM. The designed device presented two microfluidic channels for cell medium injection that were separated by a central cage for gel entrapment, featuring pillars as mechanical support for the successively loaded hydrogels. Fabrication of the microfluidic device was performed by means of PDMS casting and glass bonding together with the scaffold: this configuration resulted in the formation of two separated channels, which only communicated through the cell-laden hydrogel in the central cage. The microfluidic system described above was used to study capillary morphogenesis; in particular, this approach was the first *in vitro* angiogenesis model based on a microfluidic system which coupled microfabricated technology with the basic concepts

of traditional 3D *in vitro* angiogenesis models and that was geared towards promoting and studying capillary morphogenesis in response to the relevant biochemical and biophysical features present *in vivo*. After device assembly, human micro-vascular endothelial cells (HMVECs) were seeded on collagen interface from medium channel, obtaining a monolayer of ECs perpendicular to the bottom of the chip. It was possible to control flow inside the device, together with chemical gradients of signals such as VEGF or sphingosine-1-phospate (S1P). The presence of a cocktail of growth factors – VEGF, basic fibroblast growth factor (bFGF) and phorbol-12-myristate-13-acetate (PMA) – was crucial for the assembly of HMVECs in tubular-like shapes from collagen interface to bulk hydrogel after 4 days of culture (Figure 1.6.2). Some fluorescent beads can be observed flowing all the way across the gel cage and others collect at necked-down regions in the vascular structure [114].

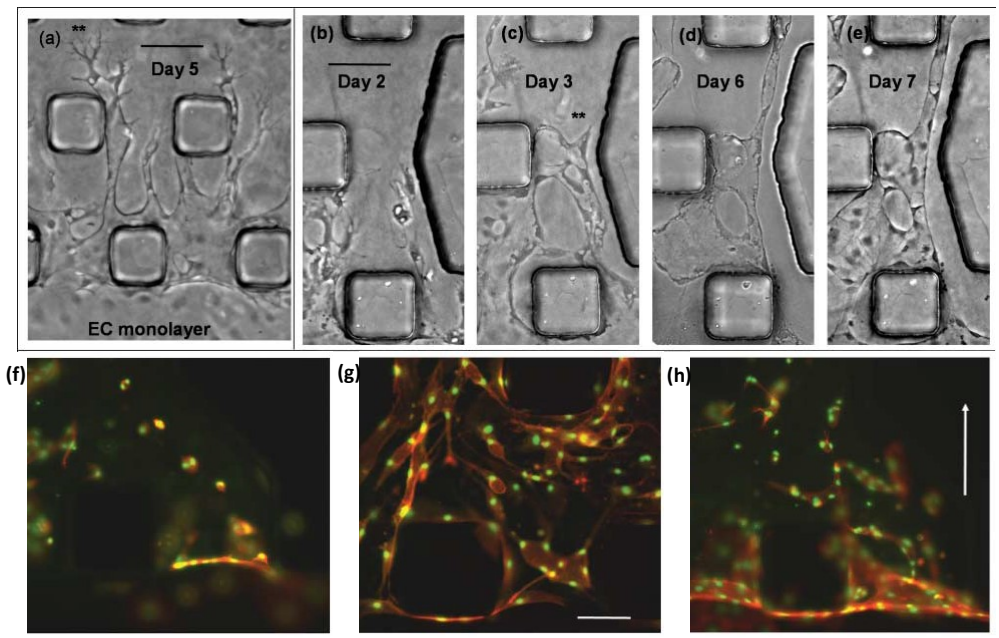

Figure 1.6.2: (a-e) Optical images of HMEVCs inside collagen type I entrapped in the central cage of microfluidic system at several days of culture (day 2 to 7). (f-h) Fluorescent images of HMVECs inside collagen type I hydrogel in different culture conditions, at day 4: (f) HMVECs cultured with fully complemented medium show a non-properly tubular assembly; (g) HMVECs cultured with fully complemented medium plus a cocktail of growth factors (VEGF, bFGF and PMA) form tubular capillary structures inside the gel; (h) HMVECs under dynamic culture with interstitial flow generated with complete medium both present a tubular-like assembly inside the hydrogel and a monolayer assembly at gel interface. Scale bar is 125 µm. Vickerman et al., 2008

The developed microfluidic system was for the first time capable of mimicking many of biochemical complexities present *in vivo* on a single *in vitro* platform. The combination

of 3D scaffolds and microfluidic patterns permitted the control of the fluidic environment, thus obtaining a more similar to *in vivo* 3D microarchitecture and high-quality imaging capabilities for dynamic studies. With this platform Vickerman et al. introduced control over: (1) interstitial flow through the matrix, (2) gradients in non-reactive solutes, (3) properties of cell culture scaffold, and (4) simultaneously monitor cells in real-time. The platform was able to study capillary morphogenesis steps and confocal imaging determines, together with fluorescent particles, the presence of a lumen after 6 days (Figure 1.6.2). From this study emerged that: exogenous gradient of biochemical factors such as VEGF, S1P, PMA and bFGF seem fundamental for angiogenic sprouts formation inside *in vitro* collagen hydrogels; a lumen is clearly visible inside capillary tubules after 7 days of culture; microfluidic device approach shows its potentiality in the study of vasculature *in vitro*.

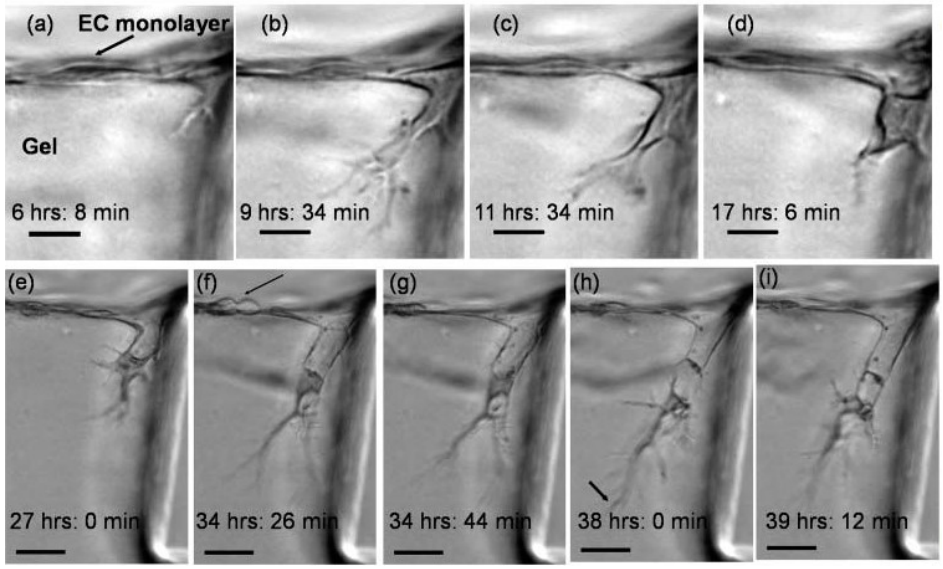

Figure 1.6.3: (a-i) Angiogenic sprout evolution in time (up to 40 hours) inside a collagen type I gel, in a VEGF-rich environment and in the presence of S1P gradient. (Vickerman et al., 2008)

Another important study was developed in the same research group by Sudo, Kamm et al. in 2009, focusing on the role of co-culture inside an *in vitro* vascularization model. The microfluidic platform used was similar to the above-mentioned one, thus presenting two parallel channels and a central gel cage separating the communicating channels. After collagen was injected inside the cage, two different cell types were seeded in the two channels: rat hepatocytes and rat micro-vascular endothelial cells (rMVECs) to obtain a heterotypic 3D culture of the same species. By dynamically changing the culture conditions (Figure 1., E), maintaining in some conditions a fluid

velocity of 27 – 35 µm/min (equal to 1600 – 2100 µm/s, close to physiological velocity inside human capillaries [7][115]) the group was able to obtain a tissue-like assembly of rat hepatocytes, together with angiogenic sprouts formation by rMVECs which lasted 5 days (from day 8 to 13 of co-culture) (Figure 1.6.3) [116].

A different application of the microfluidic platform was obtained by culturing hMVECs or rMVECs alone under static conditions. rMVECs did not self-assembly as capillary sprouts, but migrated inside the gel as a sheet-like formation; hMVECs alone were able to form tubules and tip cells at the top of the sprout were present to close the lumen (Figure 1.6.4, C-D), thus resulting in a better angiogenesis characterization with human cells rather than rat cells (Figure 1.6.4, A-B).

Several results emerge from this study: the condition of dynamic flow is important, thus not necessary for the formation of angiogenic sprouts inside *in vitro* tissue-like environment, since the platform shows angiogenic sprouts even in static conditions – thus with gradients of exogenous biochemical stimuli; fluid flow and gradient of biochemical stimuli represent both important factors for the formation of angiogenic sprouts: focusing on the goal of achieving vascularization of 3D tissue *in vitro*, microfluidic platforms together with dynamic culture and biochemical signals may represent the key element for the correct, close-to-physiological, stimulation of ECs.

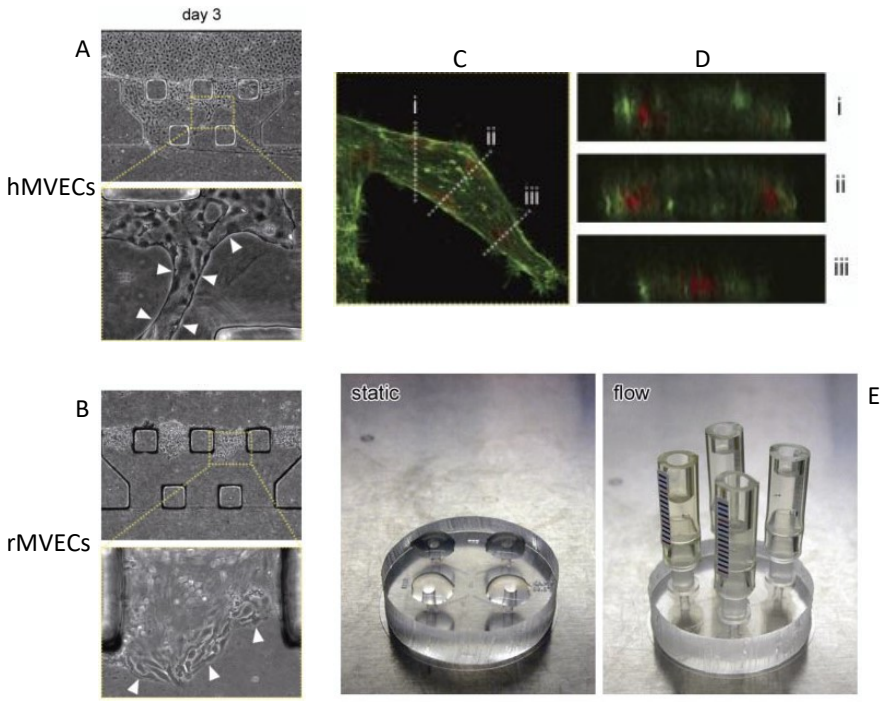

Figure 1.6.4: (A-B) Optical image of hMVECs (A) and rMVECs (B) at day 3 of static culture from collagen-channel interface. hMVECs assembly as tubules, while rMVECs with a sheet-like configuration. (C-D) Fluorescent images of hMVECs angiogenic sprout. Cross-section images showed that hMVECs formed capillary-like structures with lumens (i, ii), whereas the tip cells formed no lumen (iii). (E) Images of static

and dynamic culture sets-up. Flow was obtained by means of hydrostatic pressure, with a difference in volumes in the reservoirs.

In order to further investigate the parameters that influence vascularization on-chip, I will show the results of Song, Munn et al. in 2011, who obtained important achievements regarding the study of the role of mechanical and biochemical stimuli: the group was the first to hypothesize that vascularization processes, particularly sprouting angiogenesis, could be obtained with a combination of mechanical and biochemical stimuli, because *in vivo* sprouting angiogenesis rely on the presence of VEGF in a dynamic environment, characterized by blood flow that exerts forces on vessel walls. The experimental set-up relied on a microfluidic platform constituted by three adjacent channels, communicating by inter-posts openings. Channels height was 50 µm and channels width was 150 µm. The central channel was filled with collagen gel, while the two lateral channels were seeded with HUVECs, in order to obtain an ECs monolayer at the side wall of collagen gel interface with the channels. In particular, they demonstrated that, in the presence of VEGF gradients, physiological shear stress of 3 dyn/cm^2 on an ECs layer attenuated sprouting formation, while in the presence of a sub-physiological shear stress of 0.1 dyn/cm – necessary for maintaining VEGF gradients – sprouts were formed (Figure 1.6.5, A-B). Another important result regards the role of interstitial flow in the angiogenesis phenomena: interstitial flow, both with and without VEGF gradients, stimulated angiogenic sprouts to form, and the sprouts moving in the opposite direction with respect to the interstitial flow presented a higher number of filopodia (Figure 1.6.5). In conclusion, both interstitial flow – a mechanical stimulus similar to plasma extravasation *in vivo* – and VEGF gradient – a biochemical stimulus – enhance angiogenic sprouts formation, while the presence of a continuous physiological shear stress attenuates angiogenic sprouts, as it resembles the shear stress exerted by blood flow in normal conditions, thus without the need of the formation of angiogenic sprouts towards another region of the tissue [20].

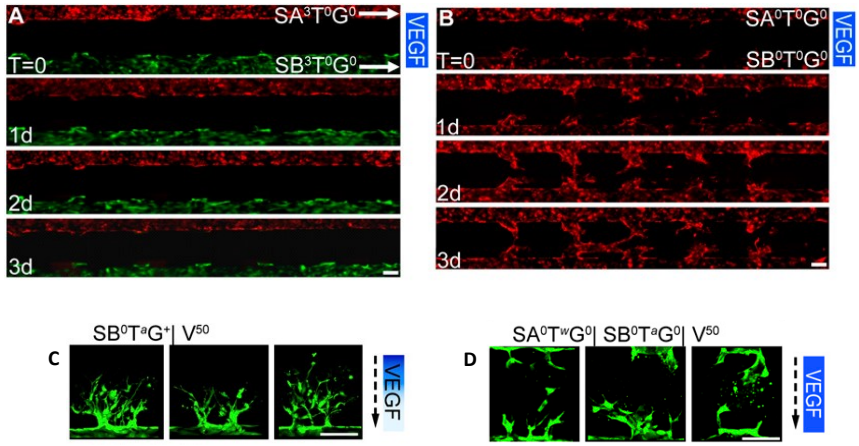

Figure 1.6.5: (A) Fluorescent images, from day 0 to day 3, of HUVECs seeded in the lateral channels, with collagen in the middle channel. $SA^3T^0G^0$ and $SB^3T^0G^0$ mean that shear stress of 3 dyn/cm^2 is present in channels A and B, with no transverse flow and no VEGF gradients: this configuration leads to attenuation of angiogenic sprouts. (B) Fluorescent images, from day 0 to day 3, of HUVECs seeded in the lateral channels, with collagen in the middle channel: $SA^0T^0G^0$ and $SB^0T^0G^0$ mean that no shear stress, transverse flow and VEGF gradients are present, thus static culture condition is represented. Angiogenic sprouts are visible inside the collagen gel. (C-D) Fluorescent images of HUVECs in the presence of VEGF gradient and interstitial flow (C) and without VEGF gradient and with interstitial flow (D): sprouts develop in the opposite direction of interstitial flow in the direction of positive VEGF gradient (C) and with no preferential directionality in the absence of VEGF gradient, thus with more filopodia in the opposite direction of interstitial flow. Scale bar is 100 µm (Song, Munn et al., 2011).

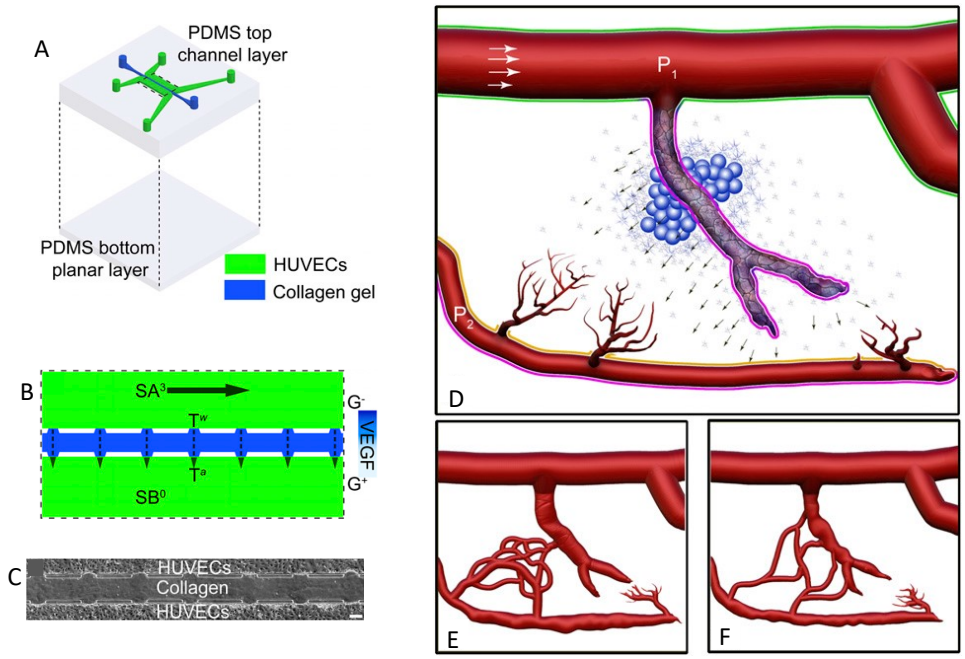

Figure 1.6.6: Microfluidic device with localized 3D ECM for fluid force-mediated angiogenic sprouting and morphogenesis. (A) Multilayer fabrication of the PDMS microfluidic device featuring localized region of collagen gel (blue). The top PDMS layer contains the channel features (50 μm in height) and the bottom layer provides a planar surface. (B) Close-up view of boxed area in A showing seven apertures that allow connection of the two HUVEC channels (green) through the collagen barrier (blue). Each HUVEC channel has independent input and outlet ports, allowing strict control over flow in both channels (SA and SB) and across the collagen matrix (T). (C) Optical micrograph of the three channels, the lateral ones with HUVECs seeded and the central one with collagen gel. (D-F) Representation of the hypothesis regarding the explanation of the phenomena observed during experiments: a damaged tissue is schematized in (D), with hypoxic cells (blue) residing in an ischemic region that secrete VEGF (small blue dots). The damaged, occluded vessel within this region lacks shear stress, but fills with VEGF, and its ECs sense a negative VEGF gradient. This vessel dilates (walls outlined in pink) and becomes leaky in response (arrows; note that P1 > P2). Proximal ECs in the other occluded vessel (lower) see a positive VEGF gradient across the vessel wall (orange outline), whereas those in the opposite wall see a negative gradient (pink outline). The former sprout, whereas the latter dilate. Morphogenesis of non-damaged, well-perfused vessels is inhibited by shear stress (green outline). (E-F) Interstitial flow supports efficient revascularization. If no fluid forces were involved with mediating revascularization and instead relied solely on VEGF and other chemical factors, then many self-connections would be made between the sprouting vessels, leading to inefficient reperfusion (F). However, interstitial flow originating from the leaky and dilated central vessel serves as an important cue that guides the sprouts toward this higher-pressure vessel to ensure more uniform revascularization of the central region supports efficient revascularization. However, interstitial flow originating from the leaky and dilated central vessel serves as an important cue that guides the sprouts toward this higher-pressure vessel to ensure more uniform revascularization of the central region (F). Scale bars are 100 μm (Song, Munn et al., 2011).

Vasculature on-chip, in order to fulfil its function of transporting nutrients and metabolites, must be endowed with an inner lumen, which connects to different regions of the *in vitro* tissue [117]. The previously described models, which represent important studies for the development of this research field, only present a partial lumen that ends with a tip cell closing the vessels, thus not allowing the perfusability of the entire network. For this reason, I will present the results of the study performed by Moya, Hughes et al. in 2013, who developed a microfluidic platform for the vascularization of a cell-laden hydrogel with a highly-branched vascular network that reaches the totality of the hydrogel volume. In particular, the microfluidic device featured a series of 12 daisy-chain shaped chambers, with two fluidic channels connected to each chamber. Two inlets and two outlets consented control over medium flow through a hydrostatic pressure system, with reservoirs presenting different height of media. Fibrin gel loaded with normal human lung fibroblasts (NHLF) and endothelial colony-forming cells (ECFCs) was injected to fill the chambers without leaking inside the channels, due to the proper design of the geometrical pattern of the device. Each chamber connected to the two adjacent channels through a 50 μm communication pore, with the gel interface determining continuity with channels walls. The device was cultured for several days, and between day 14 and day 21 formed a perfusable capillary network inside the cell-laden fibrin gel, in the presence of growth factors secreted by NHLF and of additional,

exogenous growth factors such as VEGF and bFGF. The capillary network was shown to anastomose to the fluidic channels by means of fluorescent microparticles flow, and leakage of endothelial walls was tested using 150 kDa FITC-dextran [118] (Figures 1.6.7 and 1.6.8). From this study several information emerge: the role of stromal cells is fundamental in the vascularization process *in vitro*, due to the biochemical stimuli secreted and the microenvironment they constitute; the presence of a gel that can be remodeled by cells is important for the dynamic changing in vessel architecture; the presence of flow determine a mechanical stimulus for ECs assembly into capillary networks.

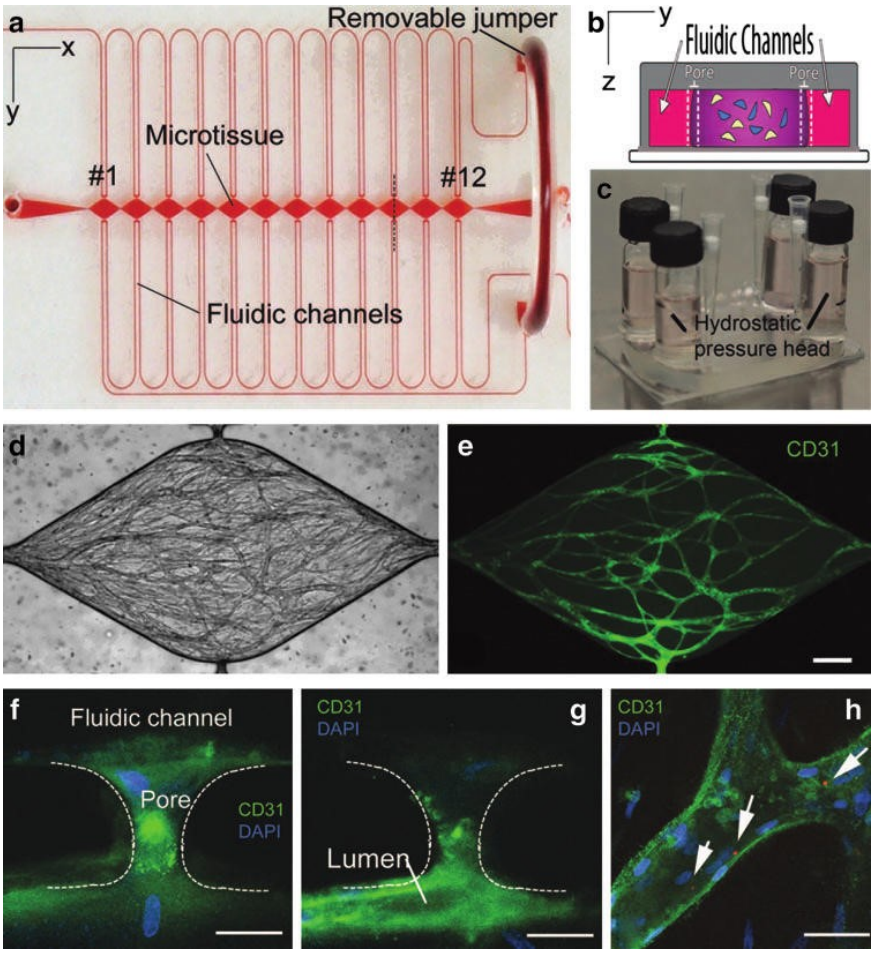

Figure 1.6.7: (a) Image of Moya, Hughes et al. microfluidic platform featuring 12 daisy-chain chambers and two fluidic channels. (b) Schematization of a cross-section of the device: the central chamber is loaded with endothelial cells and stromal cells embedded in a fibrin matrix. (c) Hydrostatic pressure head system for dynamic culture. (d-e) Bright-field image (d) and corresponding fluorescent image (e) of the perfusable capillary network formed between day 14 and 21 of culture. Scale bar is 200 µm. (f-g) Capillary structures enter the communication pores and anastomose with the microfluidic channel (panels f, g and h, scale bar

is 50 µm). Fluorescent red microspheres (1 µm in diameter) introduced into the high-pressure fluid stream were visualized with confocal microscopy (white arrows) confirming perfusability of vessels. (Moya, Hughes et al., 2013).

An update of the previously mentioned study was presented by the same group in the work of Huang, Hughes et al. in 2016. The modification of the previous approach consisted in the EC lining of the two fluidic channels, which presented angiogenic sprouts towards the hydrogel chamber and connection to the capillary network, precedingly formed *via* vasculogenesis in order to obtain a tighter connection between vasculature inside the hydrogel and the fluidic channels.

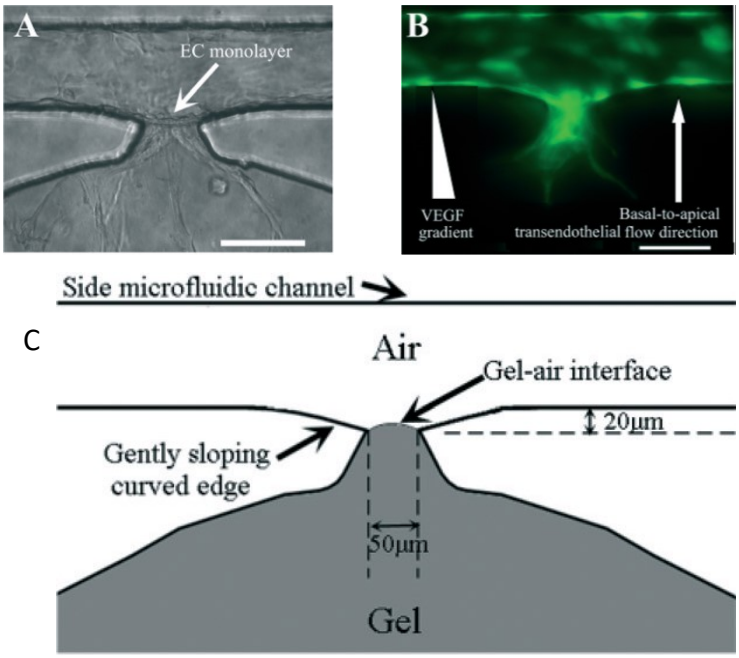

Figure 1.6.8: Bright-field (A) and fluorescent image (B) of channel-gel communication pore: optical micrograph shows EC monolayer at channel-gel interface formed by flow inside channel and physiological shear stress; fluorescent image of FITC-labeled ECs shows the tendency of sprouts formation in presence of both VEGF gradient and basal-to-apical transendothelial flow. Scale bars are 100 µm. (C) Schematization of the principle by which the liquid gel is loaded in the chamber and entrapped without leakage inside the channel: the fine geometry control obtained by stereolithography and replica molding allows for the formation of a 50 µm pore and a sloping curved edge that determine the formation of a meniscus of gel, thus gel-channel interface continues the channel wall. (Huang, Hughes et al., 2016).

The new experimental set-up determined the formation of vascular fragments *via* vasculogenesis inside the NHLF-laden fibrin gel after 2 days of culture. EC mononalyer inside the channel and onto gel-channel interface was obtained by the presence of a

continuous flow, which exerted a shear stress on the endothelial layer, thus causing the elongation of the ECs. Finally, under transendothelial flow and in the presence of VEGF gradients, the vessels inside the gel and the endothelial layer started to communicate and anastomose after 12 days of culture. Perfusability of the network was tested introducing 70 kDa FITC-dextran in the top channel: after 15 minutes the test was stopped and the images showed that the vessels were perfused and no appreciable leakage was present. 70 kDa dextran is a molecule that closely resembles size and molecular weight of human serum albumin (HSA), the most abundant protein constituting human plasma [17]. Despite the interesting results shown, no information regarding vasculature perfusion and maturity lasting are reported, probably due to the lack of a stromal tissue with a supporting role for endothelial cells.

Another recent study that obtained anastomosis of capillary structures to fluidic channels was performed by van Duinen et al. in 2018. The group utilized a high throughput microfluidic platform to obtain an in vitro model of angiogenic sprouting and vessel anastomosis inside a collagen gel. Basically, the microfluidic device used consisted of three channels, whose walls did not develop in the entire height of chip, but they consisted of phase guides that were able to confine the liquid gel during its injection, determining the formation of a meniscus of gel that corresponded to the interface between adjacent channels. After the two side channels endothelialization, a flow was activated by means of a rocker platform that allowed for continuously fresh medium to nourish the cells and for ECs adherence and elongation for the formation of a monolayer at the gel interface. Gradients of growth factors (VEGF, S1P and PMA) were obtained filling only one of the two side channels with growth factors-enriched medium. Angiogenic sprouts started to invade the central channel, consisting of collagen hydrogel, in the direction of positive growth factors gradient. After day 9 of culture, anastomosis between the two side channels occurred by means of connection of the endothelialized channels through the angiogenic sprouts: this phenomenon was accompanied by a network remodeling, thus resulting in the pruning of the angiogenic sprouts that did not anastomose to the side channel, and the thickening of the anastomosed sprouts [119] (Figure 1.6.9 and 1.6.10).

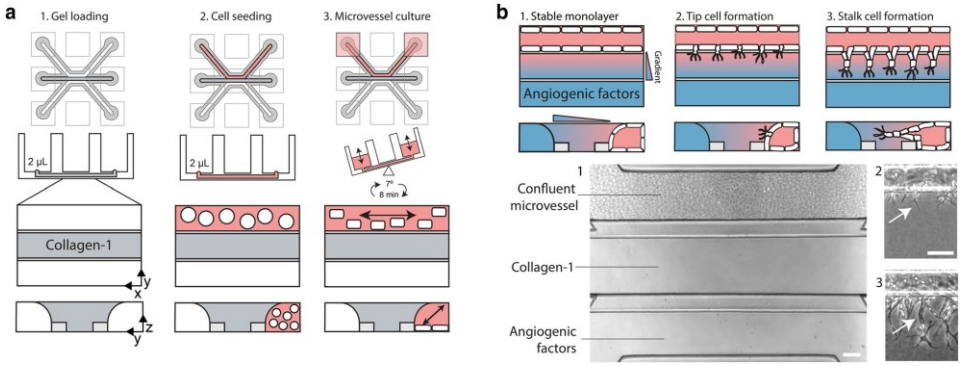

Figure 1.6.9: Graphic representation of the steps for in vitro vascularization utilizing a microfluidic device and a rocker platform: (a) Top- and side-views of gel loading (a.1), cell seeding (a.2) and microvessel culture (a.3) with the rocker platform and the focus on phase guides, gel meniscus an ECs elongation in side channels. (b) Schematization of culture configuration. Pink-to-blue shade represent VEGF, PMA and S1P positive gradient. Formation of ECs monolayer (b.1), tip cell formation (b.2) and stalk cell formation (b.3) are both schematize (upper right) and shown in bright-field micrographs (bottom right). Study by van Duinen et al., 2018.

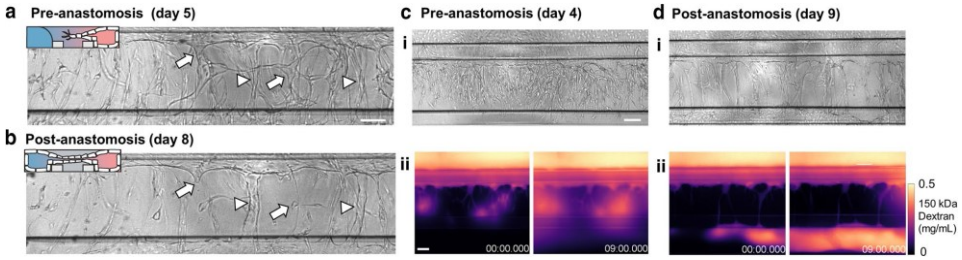

Figure 1.6.10: Pre- and post-anastomosis bright-field and fluorescent micrographs of the microfluidic device: (a) and (c) show the microarchitecture of vessels before anastomosis occurred, while (b) and (d) represent the corresponding post-anastomosis networks: it is visible the thickening of the anastomosed sprouts (arrowheads) and the pruning of non-anastomosed sprouts (arrows). (c.i) and (c.ii) show 150 kDa dextran permeability test of pre- and post-anastomosis, respectively. Study by van Duinen et al., 2018.

This important study shows that VEGF fundamental, thus not sufficient for angiogenesis phenomena triggering. The lack of co-culture of ECs with other cell types represents a drawback of this model, that cannot be utilized as a vasculature *in vitro* model, which may have also a stromal counterpart.

Seiler et al. in 2020 developed a vascularized gut-on-chip model utilizing patient-derived small intestinal myofibroblasts and human intestinal epithelial cells (HIECs) that can represent a step forward for its translational relevance and for vasculature surrounding environment understanding (Figures 1.6.11 and 1.6.12). Briefly, fibrin gel was loaded with patient-derived intestinal sub-epithelial myofibroblasts (ISEMFs) to replicate a niche of cells inside human small intestine inside a microfluidic device (Figure 1.6.11);

ECs were also seeded inside the gel, and self-assembly of ECs into tubular formations occurred due to the presence of the myofibroblasts that secreted the necessary biochemical signals. After activating interstitial flow, the ECs formed a vessel network from channel to channel after 7 days, that lasted until day 10 of culture [120].

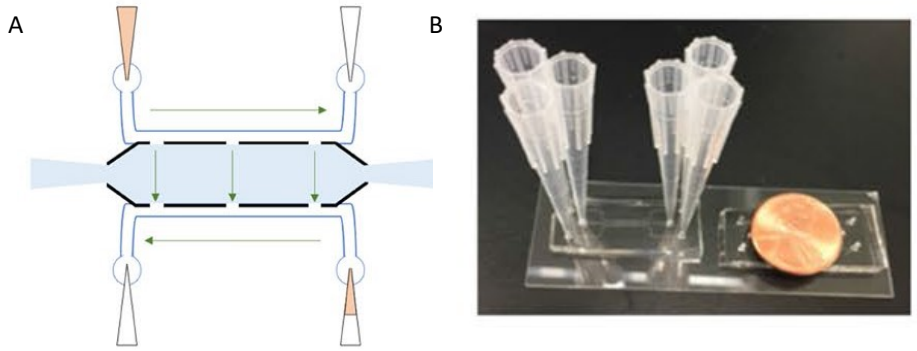

Figure 1.6.11: Schematization (A) and image (B) of microfluidic platform fabricated by means of stereolithography and replica molding. Communication pores between channels and chamber have a 100 µm width. Seiler et al., 2020.

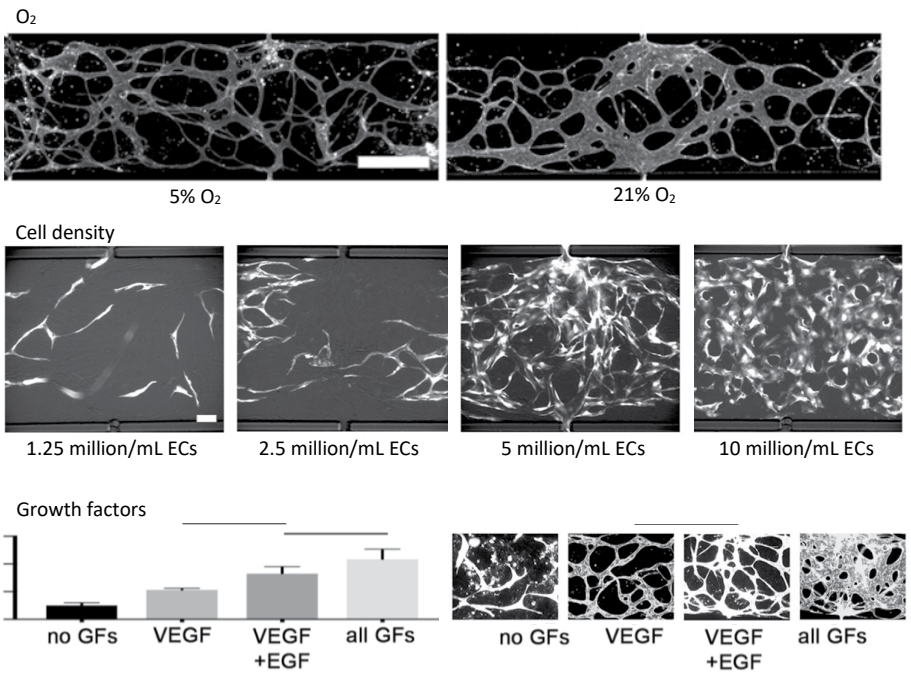

Figure 1.6.12: Images collagen chamber with ISEMFS-HUVECs co-culture: first row shows vasculature at different O_2 concentration: 5%, physiological concentration for capillaries, accompanies the formation of

capillary structures with mean diameter of 20.5 ± 2.4 µm, while at 21% - concentration "sensed" by large arteries *in vivo* – present a mean diameter of 98 ± 16.9 µm, thus demonstrating the influence of O_2 on vessel lumen size. Second row reports a study regarding cell density, thus determining the different loading cell densities, each sequential density being double to the one prior (Fig. 3B). Of note, ISEMFs are large cells relative to ECs, and while the final ISEMF to EC ratio was approximately 1:1 with regard to pelleted cell volume, the numerical ratio was approximately 1:3. Using higher ratios of ISEMFs to ECs was associated with rapid fibrin degradation and vessel collapse (not shown). As such, reported densities (Fig. 3B) are relative to ECs, with final EC concentrations of 1.25, 2.5, 5, or 10 million cells/mL of fibrin. The highest cell density (10 million ECs/mL) tended to yield obscured, enlarged vessel morphology. The lowest cell density (1.25 million ECs/mL) did not generate perfused vessels. There were several cases of perfused vessel formation at 2.5 million ECs/mL, and consistent success with 5 million ECs/mL. Thus, cell density and cell ratios are physiologically relevant factors to keep consistent across experimental conditions. Third row shows the effects of different growth factors, alone or combined. The results show that a rich cocktail of growth factors enhance perfusable network formation, but it is interesting to note that VEGF, combined with epidermal growth factor (EGF), generated higher number of vessel branches and endpoints with respect to VEGF alone, suggesting that VEGF is not considerable as the only actor in the vascularization process.

The model described above was used to obtain a vascularized gut-on-chip model with patient-derived ISEMFs and HIECs. As such, to construct a more complex and translational model of GOC, the group modified the microfluidic device design as shown in Figure 1.6.13. Briefly, a layer-by-layer device with the channels separated by a microporous membrane was fabricated. The lower channel was used to culture vasculature, as described above, and patient-derived HIECs were cultured on the apical side of the membrane in the upper channel, as a monolayer (Figure 1.6.13, A). In this system, polarized HIEC growth was demonstrated by apical mucin (MUC2) secretion from differentiated goblet cells (Figure 1.6.13 B, C). In summary, the group showed that perfused vasculature can be co-cultured in the sub-epithelial channel of a gut-on-chip platform, establishing a model as a "proof of principle" for the co-culture of more complex *in vitro* vascularization on-chip.

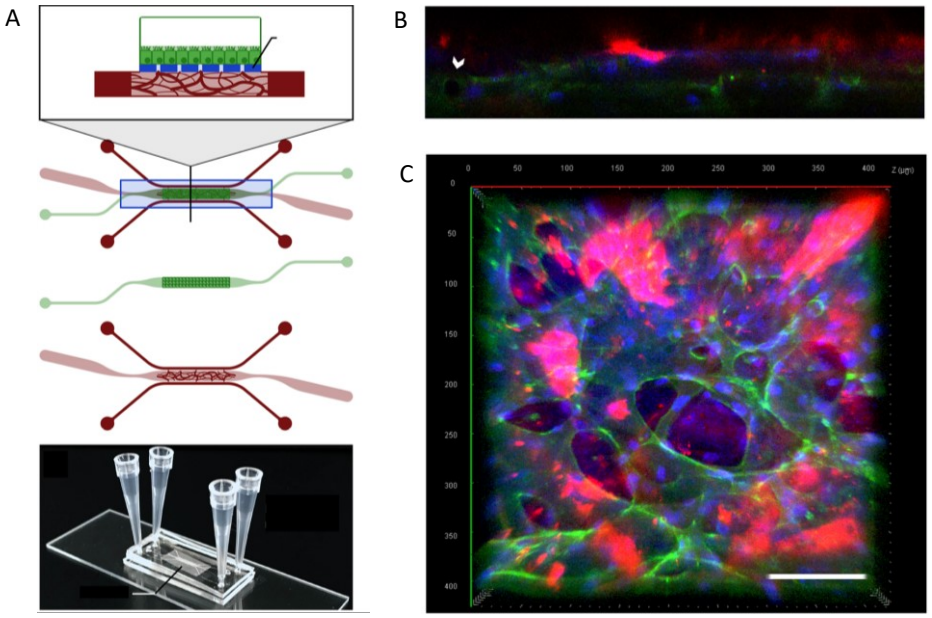

Figure 1.6.13: (A) Schematization of gut-on-chip model with epithelium and vasculature, in side-view, top-view, top-exploded view and image of fabricated device: isolation of luminal flow (upper chamber) and systemic circulation (perfused vasculature) is allowed with this configuration. (B) Confocal Z-stack image shows epithelium above vasculature. Ileal epithelium has apical secretion of mucin (MUC2, red), and DAPI nuclear counterstain (blue) indicates basolateral nuclear localization, indicative of epithelial polarity when cultured as a monolayer in the upper chamber, with vasculature (indicated by CD31, green) in the lower chamber. Arrow indicates vessel lumen. (C) Top-down view of gut-on-chip. Magnification: 20×, scale bar: 100 µm. Seiler et al., 2020.

Despite the group does not mention lasting of vessel network – they only refer to stabilization of formed network by removal of FGF, whose presence stimulates aggressive fibrin digestion by fibroblasts – this application represents a preliminary step towards the study of vascularized tissues on-chip that try to replicate a human organ.

Finally, a study performed by Nashimoto et al. in 2020 focused on the study of an organoid tumor model inside a microfluidic platform to assess vascularization processes linked to tumoral environment [121]. The idea consisted in the formation of an organoid with MCF7 tumoral cells, human lung fibroblasts (hLFs) and HUVECs with a standard approach for organoid formation. After 2 days, HUVECs assembled establishing a vascular-like organization, due to the presence of fibroblast-secreted growth factors and biochemical instructions. The microfluidic platform used consisted of three parallel channels, with the central one allowing fibrin/collagen gel injection and organoid

accommodation, while the side ones used for HUVECs seeding on the gel vertical walls. Dynamic culture determined the angiogenic phenomena to occur, with sprouts reaching organoids at day 7 of culture. Anastomosis with pre-formed vascular tubules determined the formation of a perfusable vessel network from channels to organoid. The perfusion was only obtained in a tri-culture condition (stromal, tumoral and endothelial cells to form the microenvironment of organoid), maybe due to the tumoral ability to recruit endothelial cells for vascularization of tumor [118]. In particular, perfusion was only maintained for 4 days, maybe for a lack of maturity of the vessels, that can be assessed with the presence of laminin and collagen fibers surrounding vessel walls, together with col-localization of ECs and fibroblasts. While the latter is reported in the study (Figure 1.6.14), it appears clear that organoids do not resemble the complex, hierarchically organized 3D ECM that characterizes in vivo stromal tissue, thus acting with a mechanically supporting role on vessel walls for vascular system maturation and maintenance.

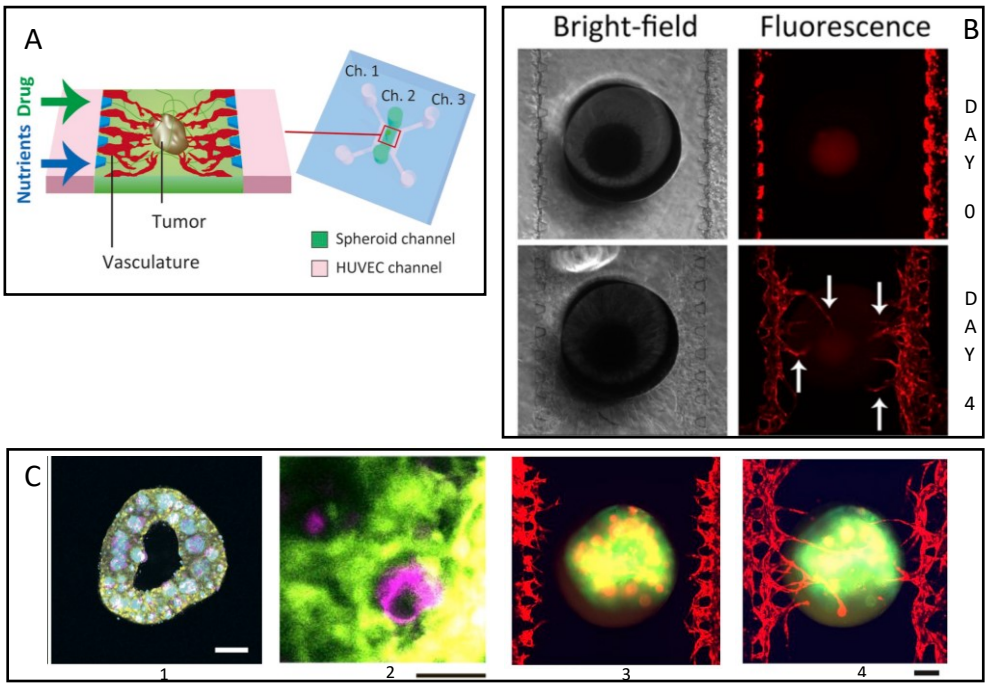

Figure 1.6.14: (A) Schematization of microfluidic approach for *in vitro* vascularization of tumor organoids: the central channel is loaded with a mixture of collagen and fibrin gel, with an organoid included inside, while the side channels are used for ECs seeding and culture media flow. (B) Bright field and fluorescent images of tumor organoid-on-chip at day 0 and day 4 of culture: angiogenic sprouts are highlighted by white arrows. (C) 1) Organoid immunofluorescence showing fibroblast-ECs co-localization (blue and pink, respectively) and MCF7 tumor cells in the interstitial space (green). Scale bar is 200 µm. 2) Immunofluorescence image: lumen of pre-vascular tubular formation inside organoid. Scale bar is 50 µm. 3) and 4) Fluorescent images of vascularized tumor organoid-on-chip, day 2 (left) and 7 (right) of culture.

Image (4) shows anastomosis between pre-network and angiogenic sprouts occurring inside the organoid. Scale bar is 200 µm (Nashimoto et al., 2020).

1.7 Conclusions, limitations of current studies and purposes

Several *in vitro* vascularization models have been presented, with different approaches – tissue engineering, organoids, angiogenesis models, microfluidic platforms – and a plethora of parameters have been pointed out in order to determine which ones represent the most relevant regarding the formation of a stable, long-lasting vasculature in a reliable, easy to fabricate and repeatable platform.

The first important parameter to be considered is flow [122]. The vascular system's main function is connected to the transport of oxygen and nutrients, together with the removal of metabolites from every district of the human body. It relies on blood flow controlling intraluminal flow inside *in vitro* vascular networks appears to be fundamental to maintaining tissue homeostasis– *e.g.* without overcoming the specific physiological levels of velocity limit (500 – 1500 µm/s for blood in human capillaries), shear stress (100 – 500 s^{-1}) [123] and shear stress (0.5 – 1 N/m^2)[115]. For this reason, the above-mentioned and briefly described *in vitro* vascularization strategies of section 1.4, even representing important steps forward in the study of ECs behavior, cannot be purposed as crucial vascularization models for the study of dynamics, drug testing and other applications like tumoral angiogenesis, due to their lack of physiological perfusion flow and of a fully-developed ECM.

Focusing on the *in vitro* vascularization on-chip models presented in section 1.6, it is important to highlight that the winning point of these strategies towards the development of a functional vascular network *in vitro* is represented by the microfluidic approach, which allows for the fine control over parameters – flow rate and thus velocities and shear stress, gradients and small volumes – that are strictly connected to vascular system functionality *in vivo*. Several achievements have been obtained with the application of microfluidic strategies, such as the possibility to investigate angiogenesis phenomena, the control over intraluminal flow, and the potential of testing systemic drugs and therapies in a 3D physio-pathological environment.

Despite the extended research being carried out to investigate the crucial phenomena underlying vasculogenesis, angiogenesis, anastomosis and systemic drug administration, the existing *in vitro* vascularization models lack important physiological features, such as vessel maturity and long-lasting, together with the absence of a well-structured ECM surrounding the vessels, with highly-organized collagen fibers – as shown in section 1.3 regarding stromal tissue that surrounds vascular networks – which

closely replicate *in vivo* physiological and pathological stromal environment. Although these models represent an important advancement if compared to *in vitro* 2D models, however, the use of simplified models – *e.g.*, animal-derived hydrogels, or organoids – to resemble the *in vivo* ECM does not allow for fully reproduction of the microstructure, dynamic mechanical properties, and biochemical functionalities of *in vivo* stromal tissue and the remodeling of vasculature and ECM.

In order to better replicate *in vivo* physio-pathological ECM surrounding vascular networks, since it reveals to be a crucial aspect for sustaining vasculature through time, engineering of the stromal environment must be taken into account [124], [125]. The formation of an endogenous, stable, hierarchically structured ECM consisting of organized, cell-produced collagen fibers and laminin, with cell-secreted biochemical stimuli can represent a step forward for the long-lasting vasculature-on-chip models, with several advantages:

- the prolonging of shelf-life of tissue engineering constructs for *in vivo* transplantation;
- the establishment of platforms for the investigation of long-term phenomena regarding vascular networks – *e.g.* ECM and vessel remodeling through time – and the surrounding microenvironment;
- the potential formation of patient-derived bioengineered constructs with long-lasting perfusable networks for personalized medicine research, and the study of tumor-related pathological vascularization phenomena, with biological long-term response.

The following chapters will describe the purposes I investigated and applied in order to obtain a long-lasting vascularization on-chip device with a perfusable capillary network supported by an endogenous, structured 3D engineered ECM, with a focus on *in vitro* stromal engineered tissue production, the design and fabrication of a microfluidic platform for investigation of vessel anastomotic phenomena in a long-term dynamic culture platform, and the results deriving from their combination. Furthermore, the obtained capillary network will be analyzed in order to determine its structural maturity, presence of lumen and perfusability, which are major features of a long-lasting *in vitro* vasculature.

2 *In vitro* stromal 3D model on-chip

2.1 Introduction

As emerged during the state of art exposition, the presence of an endogenous 3D ECM, with physiologically expressed and presented biochemical stimuli and fibers structuration that closely mimics *in vivo* stromal tissue, reveals to be crucial for the development of a long-lasting vasculature for angiogenesis and subsequent anastomosis phenomena investigation *in vitro*. For these reasons, the engineering of a 3D model of stromal tissue featuring well-structured cell-produced collagen fibers and patient-derived cells may represent a step forward in the study of vasculature formation and development *in vitro*. Based on a protocol developed by my research group, I was able to produce stromal tissue equivalents of 1 mm thickness and of different diameters, with or without a pre-vascular network, as a dermis equivalent tissue.

In order to obtain control over parameters that influence endothelial cells' tubular formations *in vitro* – such as fluid velocities inside the lumina, flow rate and presence of growth factors – a microfluidic approach was chosen.

The microfluidic platform design – shown in Figure 2.1.1 – was developed considering several parameters:

- The presence of a tissue chamber and two media channels for endothelialization, two cell media sources and the possibility to control the flow from different inlets and outlets, simulating the presence of an arterial part and a vein part with capillaries connecting the two parts;
- the generation of correct tissue-channels interfaces for angiogenic sprouts development and anastomosis to vasculature inside the tissue equivalent;
- dimensioning (*i.e.*, chip height, channel cross-section) that allows for a correct transport of nutrients and waste removal, together with the possibility for tissue equivalent to perfectly fit in the platform, and generating the conditions for angiogenic sprouts to develop;
- optical accessibility;
- inlets and outlets spacing for connectors positioning;
- open-chamber design for stromal tissue equivalent positioning;
- membrane for chamber closing after tissue positioning.

As a result of the above-listed cues, the pattern shown in Figure 2.1.1, A was designed: a round-shape central chamber for the positioning of a disk-shaped 3D stromal tissue equivalent, open towards two side channels to determine the formation of the desired interfaces for angiogenic sprouts development. Moreover, the channels allow for both endothelial lining on internal walls and media flow. This configuration presents critical geometrical points at the chamber-channels interfaces, thus resulting in the deciding feature for the choice of the fabrication technique. Based on the design of the micropattern needed for the angiogenesis and anastomosis phenomena induction, the fabrication approach was chosen. A combination of UV 3D printing for master production and replica molding for device fabrication allows for a fast and precise chip manufacturing. Following the steps of punching, bonding to glass coverslips and autoclaving were necessary for the use of the microfluidic platforms for 3D cell culture. This organ-on-chip approach, consisting in a 3D stromal tissue equivalent with heterotypic human cells, endogenous ECM and control over dynamic culture parameters, can determine the development of a microfluidic platform for the investigation of vascular network formation *in vitro*.

The experimental strategy to obtain a microfluidic platform for long-lasting vasculature on-chip relies on the combination of different approaches with the exploiting of different *in vitro* vascularization phenomena: first, a pre-vascular network is formed inside a 3D stromal tissue equivalent *via* vasculogenesis, as human dermal fibroblasts (HDF) present in the matrix secrete endogenous growth factors and signals that determine HUVEC self-assembly in a tubular-like shape, with lumens inside [126][4]. After pre-vascularization is achieved, correct positioning of the 3D stromal equivalent inside the microfluidic device chamber is crucial for the generation of functional interface, consisting of the lateral surface of the dermis in direct communication with the adjacent channels. In this way, after the seeding of endothelial cells into the channels, the 3D stromal equivalent lateral surfaces act as sources of angiogenic sprouts from channels towards the endogenous ECM. In this way the endothelial sprouts are able to anastomose with the capillary network inside the tissue model (Figure 2.1.2). Dynamic culture conditions were designed to rely on a pumpless system, generating a dynamic flow by means of hydrostatic pressure [17]: reservoirs with different cell medium ΔV (Δh) determine a transverse ΔP inside the tissue chamber, thus resulting in a dynamic stimulation on endothelial layers inside the channels and on tissue equivalent. The geometry with two channels, together with the possibility to independently control the flow in the two channels with different volumes of cell medium, determines the possibility to obtain two different longitudinal ΔP inside the channels, and, on the other hand, to determine a transverse ΔP inside the chamber. Longitudinal ΔP inside the channels generates a shear stress on EC monolayers that translates in EC elongation in the direction of flow, resulting in a confluent, tight monolayer resembling a vascular wall; on the other hand, transverse ΔP determines an

interstitial flow inside tissue ECM for the transport of nutrients inside the tissue at first stages of culture, and a transendothelial flow which stimulates the endothelium at tissue-channel interface, and, consequently, the angiogenic sprouts which can connect to the pre-vascular network inside the tissue.

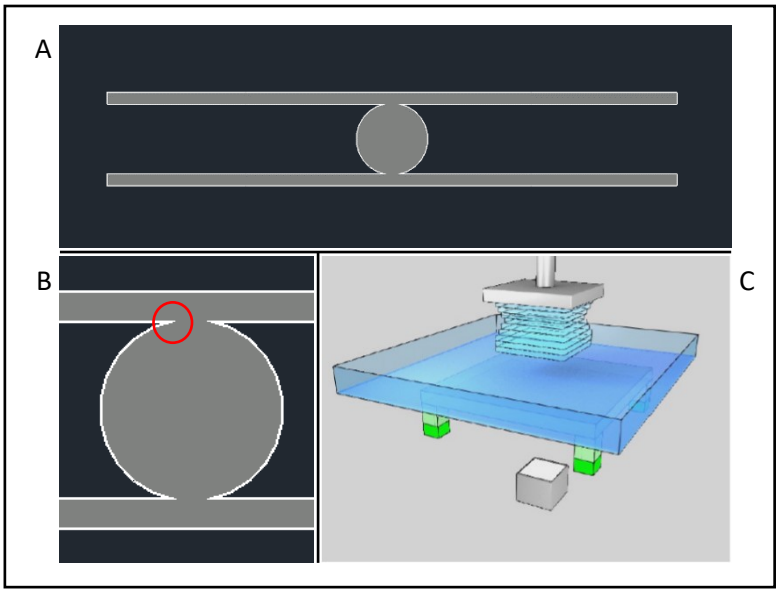

Figure 2.1.1: (A) Schematic representation of microfluidic device design for stromal 3D model vascularization-on-chip, top view. The central chamber allows for tissue equivalent positioning, while the two parallel channels determine tissue nutrition and media flow. (B) Schematization of central part of designed device: geometrical critical point of designed pattern – highlighted with red circle – is shown. (C) UV 3D printing layer-by-layer fabrication allows for fabrication of geometrical complexities.

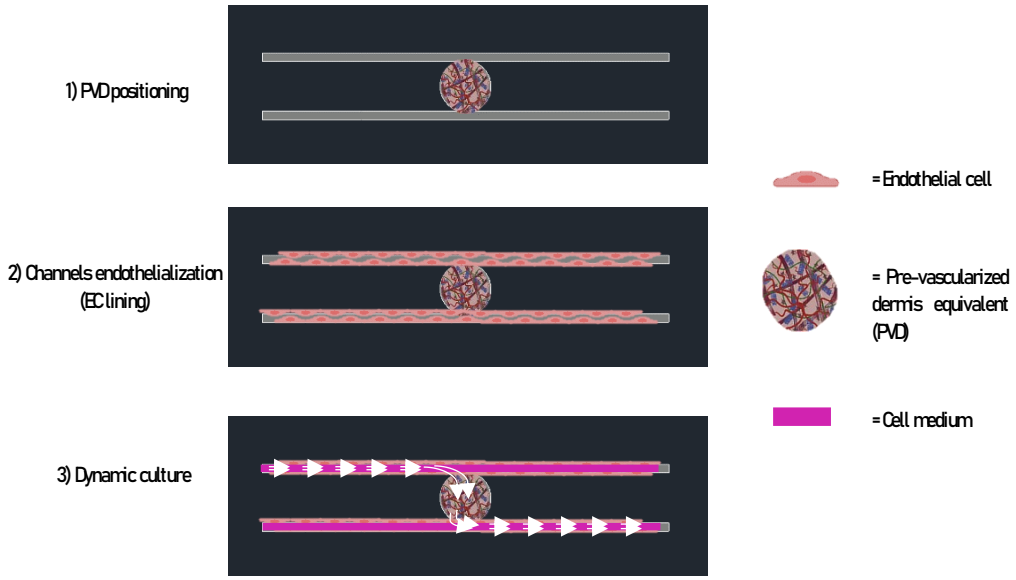

Figure 2.1.2: Schematic representation of vascularization strategy: a microfluidic platform was designed in order to correctly fit a 3D stromal tissue equivalent and to endothelialize its lateral surfaces, which are directly exposed to fluidic channels: endothelial lining of channels walls also determines the adhesion of the endothelial layer at 3D stromal tissue edge, thus generating a continuous endothelial monolayer inside the channel and on tissue-channel interface. Dynamic culture from fluidic channels, the presence of endogenous growth factors inside the chamber and designed geometrical cues act as mechano-chemical stimuli for cells for capillary network development on-chip and its anastomosis to fluidic channels.

2.2 Materials and methods

2.2.1 HDFs source

Cells were extracted from human tissue biopsies surplus obtained by "Azienda Ospedaliera di Rilievo Nazionale e di Alta Specializzazione (AORN) A. Cardarelli/Santobono/Pausillipon at Urology and Biotechnology Centre - AORN" according to the project "Realization of human skin equivalent in vitro" after approval of ethical committee.

2.2.2 HDFs extraction

All the solutions used during the extraction procedure were at 4°C. Human biopsies were washed in PBS1X+antibiotics (1% penicillin/streptomycin- Microgem L0022-100- or 50 µg/mL gentamicin- SIGMA G1397), PBS1X+antimycotic (1% Amphotericin-SIGMA

A2942-) and PBS1X. Fat from the bottom side was removed as much as possible with a scalpel and the tissue was washed again in PBS1X. The skin biopsy was cut into stripes of about 3mm width and incubated in Dispase (GIBCO 0698) solution 1.8 U/mL overnight for 14 hours.

Epidermis and dermis were separated with tweezers and then washed in PBS1X. The dermal pieces were cut in smaller pieces and put in 2,5 mg/mL collagenase A solution (ROCHE 11088793001) for 40 minutes at 37°C. The collagenase was stopped with FBS and then removed. All the pieces were suspended in a little volume of complete MEM and positioned on a petri dish in order to allow the migration of fibroblasts on the surface of the petri.

2.2.3 Cell culture

Human dermal fibroblasts (HDFs) were extracted from healthy foreskin or breast biopsies and cultured in enriched MEM: MEM (Microtech L0440-500) with 20% of FBS (Sigma Aldrich), 2% of Non-Essential Aminoacids (EuroClone ECB3054D), 1% of L-Glutamine (Lonza 17-605E) and 1% of penicillin/streptomycin (Microtech L0022-100), until passage 10/12.

HUVECs (GIBCO C0035C) were purchased by Life Technologies Italia and cultured in enriched VascuLife VEGF Complete Kit (Cell Systems LL-0003) until passage 4.

All cells were cultured at 37°C and 5% CO_2.

2.2.4 Micro-scaffold production

Gelatin porous microbeads (GPMs) were prepared according to a modified double emulsion protocol (O/W/O) [127]. Gelatin droplets containing micro-droplets of toluene were produced through the addition of excess toluene (30 mL) which formed a double emulsion (O/W/O). After cooling below 5 °C, 20 mL of ethanol were added to extract toluene and stabilize GPMs. The resulting microspheres were washed with acetone for toluene removal and then dried overnight at room temperature. GPMs were selectively separated by using commercial sieves (Sieves IG/3-EXP, Retsch, Germany), collecting GPMs with 75-150 µm diameter range and discarding the remaining ones. GPMs have been stabilized using chemical treatment with 4% glyceraldehyde (GAL), to make them stable in an aqueous environment at body temperature. GPMs were dispersed into an acetone/water solution containing different amounts of GAL and mixed at 4°C for 24 hours. The obtained crosslinked GPMs were washed with acetone and dried at room temperature. In order to use GPMs in cell culture, the microbeads were sterilized in absolute ethanol for 24 hours and washed three times in Phosphate Buffered Saline 1X

Solution (PBS) (Sigma) to remove exceeding ethanol. GAL at 4% w/w of the microbeads was used to perform all the experiments.

2.2.5 Micro-tissue precursors (µTPs) production

HDFs were seeded on top of the beads at a density of about 11 HDFs/bead. Cells were cultured into spinner flask bioreactor (Integra) in continuous agitation (30 rpm) after 6 hours of intermitting stirring regime in order to promote cell seeding (30 minutes at 0 rpm, 5 minutes at 30 rpm). The culture medium was enriched MEM plus Ascorbic Acid (2-O-α-D-Glucopyranosiyl-L-Ascorbic-Acid TCI; Cf: 0.5mM). µTPs were cultured for 9 – 10 days before the phase of assembly in order to guarantee the initial collagen synthesis.

2.2.6 Engineered 3D stromal tissue equivalent

As described by Urciuolo et al. [128][129], µTPs suspension was transferred from the spinner flask to a 50 mL Falcon centrifuge tube and, after settling, transferred by pipetting into the maturation chamber to allow their molding in disc-shaped construct (1 mm in thickness, 5 or 8 mm in diameter) (Figure 2.2.6.1). During the filling procedure, the maturation chamber was accommodated onto a custom-made device connected with a vacuum pump in order to accelerate the process and to guarantee the absence of air bubbles in the maturation space. The assembling chamber was a sandwich-like structure with an interposed silicon mold with empty spaces (disc shape: 1 mm in thickness, 5 or 8 mm in diameter) for the µTPs housing. The silicon mold was delimited on both the top and bottom sides by two stainless steel rigid grids characterized by a porous mesh (18 µm) which was able to retain the µTPs and to guarantee the passage of nutrients and waste products. Two polytetrafluoroethylene (PTFE) rings were placed on the grids on both sides of the system and were fastened to each other by means of stainless-steel screws, which close the system. The assembling chamber was placed on the bottom of a spinner flask (Bellco biotechnology code 1967- 00050) and completely surrounded by culture medium. The spinner was operated at 60 rpm. The culture medium was enriched MEM plus Ascorbic Acid. After 4-5 weeks of culture the assembling chamber was opened and stromal tissue constructs, which can be defined as dermis equivalent, were collected [130].

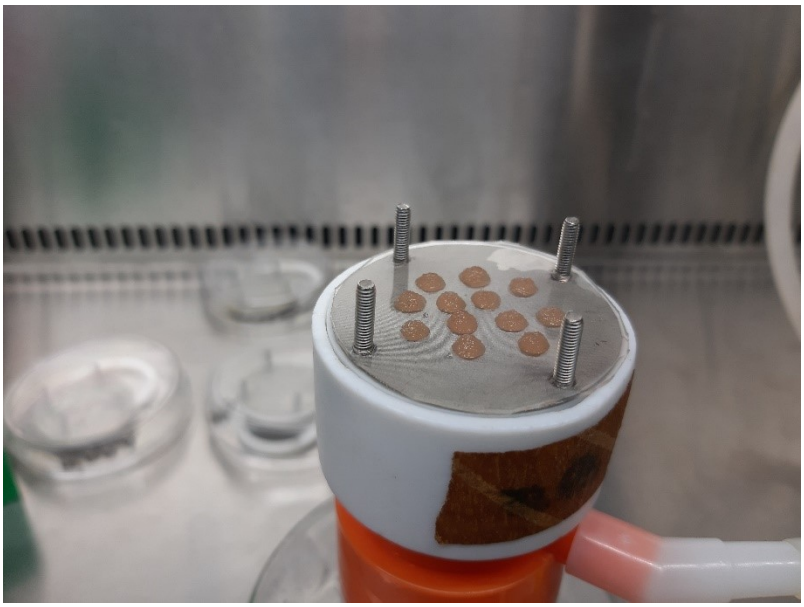

Figure 2.2.6.1: Image of µTPs positioned into the maturation chamber to allow their molding in disc-shaped construct.

2.2.7 Pre-vascularized dermis (PVD) equivalent model production

Endothelial cells seeding and culture was performed into low attachment multiwell in order to avoid cells adhesion onto substrate surface and to allow cells adhesion on the dermis equivalent. HUVECs P4 were seeded as a drop on a surface of the sample, at high density of about 10.000 – 15.000 cells/mm^2. Cells were suspended in 5 – 10 µL of medium, depending on the size of the stromal tissue construct disks, in order to avoid drop falling. After HUVECs seeding, the sample was left at 37°C for 2 hours enabling endothelial cells adhesion and, afterwards, complete medium was added up to completely cover the sample. During the first 2 hours, the sample was monitored to avoid drying and eventually a drop of medium was added on the surface. Complete VascuLife was used for cell seeding and adhesion, while from the following day complete MEM and VascuLife were used in 2:1 ratio. Samples were cultured for at least 1 week before on-chip positioning.

2.2.8 Microfluidic device for PVD

In order to obtain microfluidic devices, the first step was the design of the pattern, followed by a CFD simulation for the correct dimensioning of the device channels and chamber. Last step was the fabrication of devices.

2.2.8.1 Device design

CAD software (open-source AutoCAD, Autodesk) was used for the design of the PVD configuration, suitable for PVD positioning and which may induce anastomotic phenomena. The central cylindrical chamber diameter was 2.5 mm, while height was 1 mm, and connected to two parallel channels through two openings measuring 1 mm, which generated a PVD – channel interface of 1 mm x 1 mm. Channels size was 10 mm (length) x 0.4 mm (width) x 1 mm (height), and each inlet and outlet diameter was 1.5 mm. Some experiments were performed with the introduction of supplementary inlets for HUVECs loading, while other experiments were performed with a slight modification to channels shape, from linear to curved configuration for technical reasons (connectors introduction). Since PVD positioning phase could not be performed using a pipette-driven approach, top side of the chamber was designed to be open and a 2 mm x 2 mm x 0.250 mm PDMS membrane (realized with spin coater, 500 rpm for 30 seconds) was used to close the chamber and ensure continuous flow without leakage.

2.2.8.2 CFD simulation

To define the experimental setup, the three-dimensional velocity distribution, the oxygen profile and pressure gradients of the anastomosis-on-chip platforms were evaluated before *in vitro* trial by using the COMSOL Multiphysics version 5.3a (build 280) in order to define the velocity and the oxygen concentration profile during the perfusion culture [131][132][133]. The simulations were carried out as previously described [134] by modifying several parameters. Briefly, the devices were divided into two different domains, a fluid domain labeled with "f" inside the lateral channels, which identified the regions filled with culture medium, and tissue domain, labeled with "PVD", which identified the central tissue chamber filled with PVD. PVD properties were manually set up considering previous knowledge of the research group [135], while *Free and Porous Media Flow* and *Transport of Diluted Species in Porous Media* modules were coupled in steady state conditions; the first physics implements Navier-Stokes equation for the free fluid phase and Brinkman extended Darcy's equation for the porous matrix, while the second physics implements the mass balance equation:

- Navier-Stokes equation

$$\begin{cases} \rho \boldsymbol{u} \cdot \nabla \boldsymbol{u} = \nabla \cdot [-pI + \mu(\nabla \boldsymbol{u} + (\nabla \boldsymbol{u})^T)] + \boldsymbol{F} \\ \rho \cdot \nabla \boldsymbol{u} = 0 \end{cases}$$

- Brinkman equation

$$\begin{cases} \frac{\rho}{\varepsilon_p}\boldsymbol{u}\cdot\nabla\frac{\boldsymbol{u}}{\varepsilon_p} = \nabla\cdot\left[-pI+\frac{\mu}{\varepsilon_p}(\nabla\boldsymbol{u}+(\nabla\boldsymbol{u})^T)-\frac{2}{3}\frac{\mu}{\varepsilon_p}(\nabla\cdot\boldsymbol{u})I\right]-\left(\mu\kappa^{-1}+\beta_F|\boldsymbol{u}|+\frac{Q_{br}}{\varepsilon_p^2}\right)\boldsymbol{u}+\boldsymbol{F} \\ \rho\,\nabla\cdot\boldsymbol{u} = Q_{br} \end{cases}$$

- Mass balance

$$\begin{cases} \nabla\cdot\boldsymbol{\Gamma_i}+\boldsymbol{u}\cdot\nabla c_i = R_i+S_i \\ \boldsymbol{N}_i = \boldsymbol{\Gamma_i}+\boldsymbol{u}c_i = -\mathcal{D}_{e,i}\nabla c_i+\boldsymbol{u}c_i \end{cases}$$

Concerning the boundary conditions, no slip condition was adopted at the walls, equality for velocity and pressure was imposed at the Navier-Stokes (u, v, w, p)/ Brinkman (u_2, v_2, w_2, p_2) interfaces. Imposing for O_2 concentration in the culture medium (0.22 mol/m^3), the diffusion coefficient (D) (10^{-9} m^2/s), cell density (ρ) ($0.2\cdot10^{14}$ cell/m^3) it is possible to assess O_2 consumption by cells at the given dynamic culture conditions: the imposed ΔP, which guarantees that velocity maintains below the limit of physiological velocity inside human capillaries, allowed for oxygenation of the totality of chip volume, thus guaranteeing cell viability during the experimental campaign.

2.2.8.3 Device fabrication

A .stl extension file was obtained and sent to a UV 3D printer (Max UV, Asiga) and several parameters such as exposure time, slicing thickness and post-processing UV time frame were set in order to optimize surface finish, master stiffness and fabrication time (Table 2.2.1). The UV-polymerizing resin used for master fabrication was a commercial product (Ortho, Freeprint®) and the printed masters were post-processed with two ultrasonication steps in propan-2-ol (isopropyl alcohol, IPA) and with a 30 minutes UV step for further polymerization. After master drying for 24 hours, PDMS (Sylgard 184, Mascherpa) was poured on top of the masters in order to obtain several devices for replica molding. PDMS base and curing agent were mixed using a weight ratio 10:1 and were poured on the PMMA master. Then, the PMMA master with the blend was degassed under vacuum for 1 hour to remove the air bubbles and cured in an oven for 2 hours at 80°C. Then, the PDMS layer was softly detached from the PMMA master and inlets and outlet holes were obtained by inserting inside the fabricated cylindrical guides a biopsy punch (DifaCooper) with a 1.5 mm diameter for inlets and outlets. After punching, the PDMS layer was bonded on a glass coverslip (Menzel-Glaser 24 x 60 mm

1,5) by oxygen plasma treatment for 1 min at 50 W in an oxygen plasma oven (Plasma Femto, Diener). After the treatment, the device was placed in an oven and maintained at 80°C for 24 hours with the metal weights to ensure that the bonding was maintained.

Printing parameters (385 nm UV 3D printer)	Exposure time (time/slice)	Slice thickness	Post-processing	UV post-treatment
Device PVD (negative master)	3.14 s	50 µm	3 min ultrasonication in IPA (2x)	30 minutes

Table 2.2.1: Printing parameters of for the fabrication of negative masters for PVD device.

2.2.9 Channels endothelialization

After PVD positioning, channels were coated with laminin 10 µg/mL (Laminin from Engelbreth-Holm-Swarm murine sarcoma basement membrane, Sigma-Aldrich) and devices were incubated at 37°C in a humidified atmosphere with 5% CO_2 for 30 minutes. After laminin removing by medium dilution, Human Umbilical Vein Endothelial Cells (HUVECs, Lonza) were seeded in both channels at a high density of 10000 – 15000 cells / mm^2. The devices were incubated for a minimum time of 3 hours, alternating vertical and horizontal positioning for cell adherence on each side of the channels, and avoiding channels drying by adding a drop of medium at the free inlets when necessary. Optical microscope was used to monitor HUVECs adhesion, and also a control of HUVECs in a petri dish was used to check cell adhesion. Once HUVECs adhered, devices were connected to syringe pumps (ElveFlow) for dynamic culture and flow was started at different flow rates (10, 5.4 and 1.8 µL/min) depending on device channels cross-section area, in order to maintain velocity inside channels below physiological limit.

2.2.10 Immunofluorescence on the whole sample

Samples were fixed in 4% Paraformaldehyde (P61148-500g Sigma Aldrich) for 30 minutes at RT and washed in PBS1X. They were permeabilized using 0,1% Triton (Triton® X-100 T9284-100ML Sigma) in PBS1X for 5minutes at RT, washed three times with PBS1X and blocked in 1% BSA (A9418-100G Sigma) for 1 hour at RT. Some samples were stained with coincubation of Rhodamine Ulex Europaeus Agglutinin I (UEA I Vector Laboratories RL-1062) and primary Anti-Laminin antibody produced in rabbit (Sigma-Aldrich) and secondary Cy5 for endothelium and laminin marking respectively, while other samples were stained only with UEA I at a final concentration of 20 µg/mL in blocking solution, in order to mark the endothelium, overnight (ON) at 4°C in the dark. Next morning,

samples were washed with PBS1X. The nuclei of all the cells were stained with Sytox Green (Invitrogen S7020) for 20 minutes at RT.

2.2.11 Second harmonic generation signal

For second harmonic generation (SHG) imaging samples were investigated by confocal microscopy (TCS SP5 II Leica) combined with a MPM where the NIR femtosecond laser beam was derived from a tunable compact mode-locked titanium: sapphire laser (Chamaleon Compact OPO-Vis, Coherent). Two-photon excited fluorescence was used to induce SHG and obtain high-resolution images of unstained collagen structures. The samples were observed by using λ_{ex} = 840 nm (two photons) and λ_{em}=415-425 nm. The SHG images were acquired with a resolution of 12 bit, 512x512 pixel by using a 25X water immersion objective (HCX IRAPO L 25.0X0.95 Water, n.a. 0.95).

2.2.12 Quantitative Capillary-like structures (CLS) analysis

Whole samples were investigated by Confocal Leica TCS SP5 II performing 5 z-stacks in different random points of different µTPs. Samples were observed using λ_{ex} = 543 nm/ λ_{em}=550-560 nm to detect Rhodamine, λ_{ex}=488 nm/ λ_{em}=500-530 nm to detect Sytox Green and λ_{ex}=633 nm/ λ_{em}= 650-680 nm for Cy5 (Laminin). The stacks were acquired with a resolution of 12 bit, 512x512 pixels by using a 25X water immersion objective (HCX IRAPO L 25.0X0.95 Water, n.a. 0.95). Each stack was composed by 16 sequential images with a z-slice-space of 1,98 µm.

2.2.13 Statistics

Experiments were performed in triplicate. Data are expressed as mean ± SD. Differences between groups were determined using the statistic test ANOVA Tukey HSD test. Significance between groups was established for *p* value < 0.01 or *p* value < 0,05.

2.3 Results and discussion

2.3.1 Engineered 3D stromal tissue (dermis equivalent) characterization

In order to determine the features of the produced 3D stromal tissue equivalent, several techniques have been involved for characterization. The first characteristic to be assessed was collagen production by HDF cells, which represents a signal of active, proliferative cells in an endogenous environment (Figure 2.3.1.1). Once assessed the presence of well-structured endogenous collagen fibers, the stromal tissue can undergo the pre-vascularization process, necessary for the first step of the chosen strategy.

Figure 2.3.1.2 shows fluorescent images of pre-vascularized dermis equivalent (PVD) with HUVECs labeled in red with specific immunofluorescence agent (UEA I), nuclei in green (Sytox) and collagen fibers in grey by means of two-photon SHG. Figures 2.3.1.2 C and D show vascular capillary like structure (CLS) at different depth, highlighting the 3D development of vasculature inside stromal tissue equivalent *via* vasculogenesis.

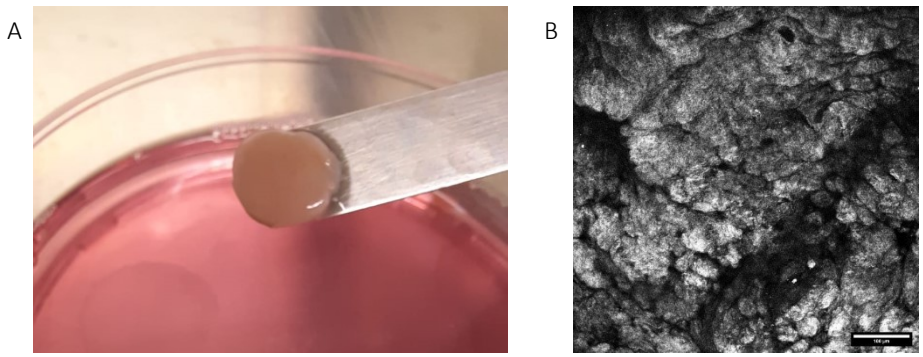

Figure 2.3.1.1: (A) Image of 10 mm diameter engineered 3D stromal tissue, obtained by means of HDF culture within porous gelatin beads and assembly of microtissue precursors. (B) SHG confocal micrograph obtained by means of two-photon excitation, which determine the imaging of collagen fibers. Well-structured endogenous collagen fibers, produced by HDF during assembly process, are clearly visible. Scale bar is 100 µm.

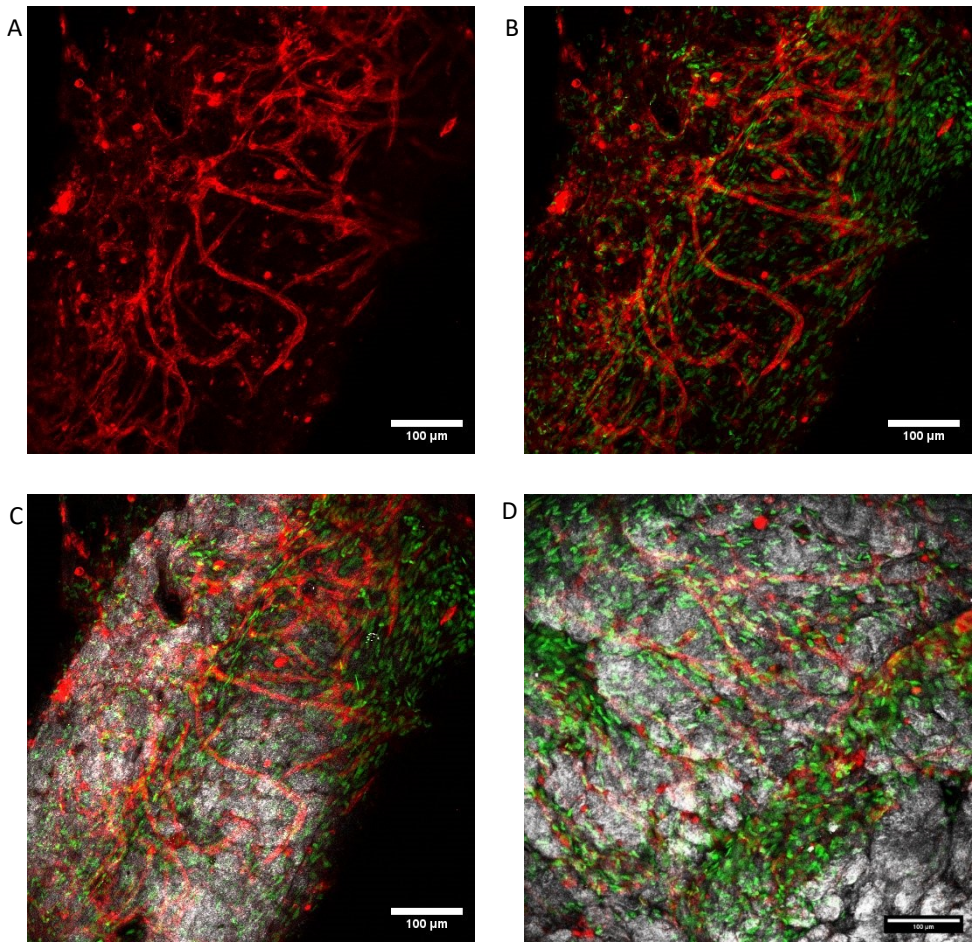

Figure 2.3.1.2: (A) Confocal image of HUVECs forming a pre-vascular network at day 7 of seeding. The capillary network results highly interconnected without adding exogenous molecules other than the ECs medium kit presents. (B) Confocal image overlapping red (HUVECs) and green (HDF and HUVECs nuclei) signals. Capillary tubules show tight junctions between HUVECs and no space between cells can be assessed. (C) Confocal image overlapping red (HUVECs), green (HDF and HUVECs nuclei) and SHG (collagen fibers) signals from a z-stack. (D) Confocal image overlapping red (HUVECs), green (HDF and HUVECs nuclei) and SHG (collagen fibers) signals from a z-stack, at different depth with respect to (C), highlighting the 3D development of capillary-like structure (CLS) inside stromal tissue equivalent. Scale bars are 100 µm.

2.3.3 Microfluidic device design and fabrication

The microfluidic section of this project started from the design of the geometry, as previously described. CFD simulations determined modifications to the initial design in order to allow for O_2 physiological consumption inside the tissue chamber: the definitive

dimensions of the microfluidic chip are reported in Figure 2.3.3.1. The central cylindrical chamber diameter was 2.5 mm, while height was 1 mm, thus accommodating the produced PVD properly. Two parallel channels present two communication pores measuring 1 mm, which generate a PVD – channel interface of 1 mm x 1 mm. Channels size was 10 mm (length) x 0.4 mm (width) x 1 mm (height), and each inlet and outlet diameter was 1.5 mm. The total volume suitable for 3D cell culture (inside the channels and inside the 3D stromal equivalent) of microfluidic device is 12.908 mm^3, (4 mm^3 each channel, 4.909 mm^3 the tissue chamber) which correspond to 12.908 µL.

Since PVD positioning phase could not be performed using a pipette-driven approach, top side of the chamber was designed to be open and a 2 mm x 2 mm x 0.250 mm PDMS membrane (realized with spin coater, 500 rpm for 30 seconds) was used to close the chamber and ensure continuous flow without leakage.

The first step of chip fabrication was UV 3D printing, as previously described. In order to obtain a negative hard master of the designed pattern, with cylindrical guides for inlets and outlets subsequent punching and without the formation of a meniscus of PDMS prepolymer, a tray-like mold was designed and printed, and totally filled with PDMS prepolymer with a precise volume of 3 mL. after PDMS curing at 80° C for 1 hour, the slab was ready to be punched for opening inlets and outlets. The curves introduced inside the channels designed were due to the need of spacing inlets and outlets for connectors introducing (Figure 2.3.3.2).

The first step of design considered the geometrical cues: the correct tissue-channel interface was the leading step of the pattern design, which led to the geometry represented in Figure 2.3.3.1, A. This geometrical configuration, based on literature models study and custom-designed on the 3D stromal tissue I was able to produce, led to next step of the design process: the choice of the fabrication technique. Since the presented geometry features a critical point in the four cusps between tissue chamber and adjacent channels, the ideal technique must be suitable for the manufacturing of this particular configuration. After an investigation regarding several techniques, the ideal fabrication strategy was considered: a 2-step technique, based on a negative master fabrication by means of UV 3D printing, followed by replica molding with PDMS.

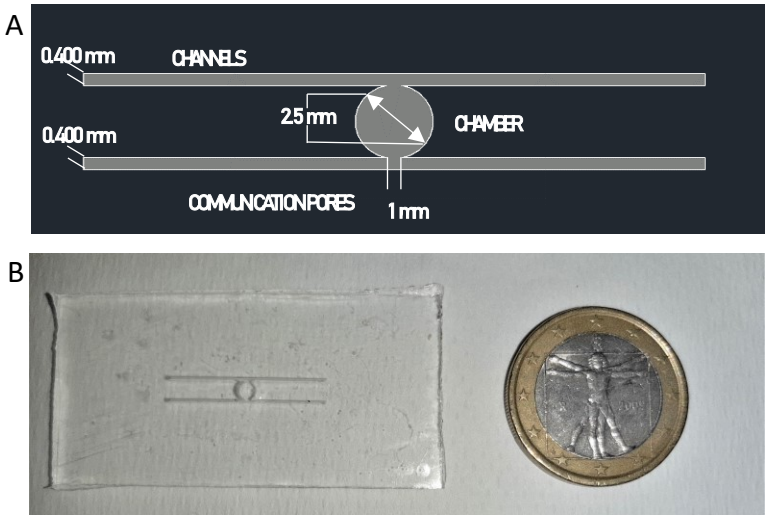

Figure 2.3.3.1: (A) Schematization of microfluidic device for PVD dynamic culture, top-view. Size of the critical geometrical features (channel width, chamber diameter and communication pores) are reported. (B) Image of a PDMS slab obtained by replica molding: pattern is visible in the center.

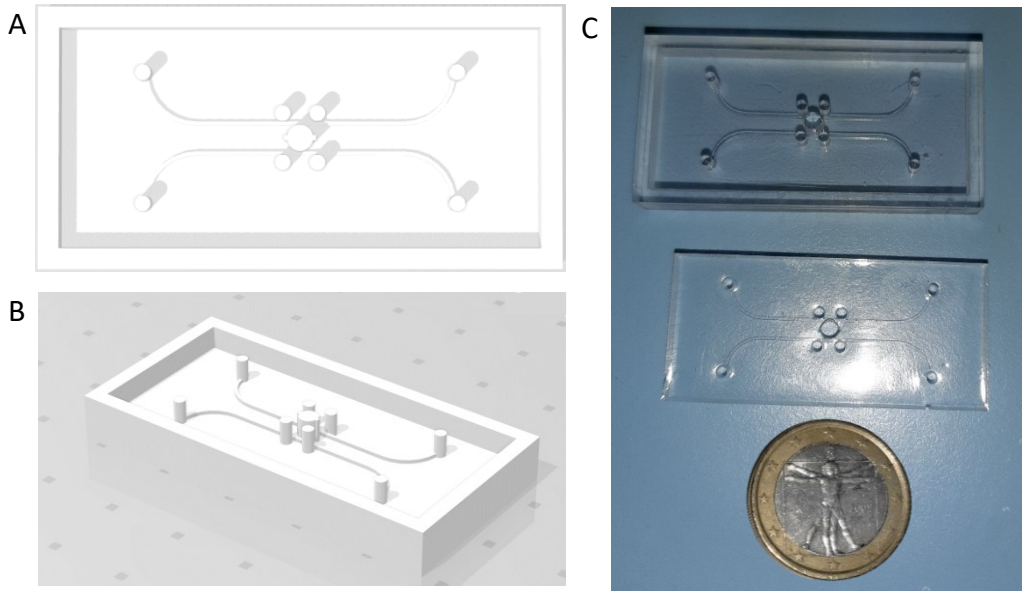

Figure 2.3.3.2: Final configuration of microfluidic device for PVD dynamic culture. Top-view (A) and 45 degrees-view (B) of designed tray mold for replica molding of PVD microfluidic device (.stl file). The 8 cylinders are guides for inlets and outlets for medium flow and ECs seeding inside channels. (C) 3D printed negative master and PDMS positive replica of the microfluidic device.

2.3.4 PVD positioning inside microfluidic device

In order to obtain the best conditions for vascularization processes to occur on-chip, the correct positioning of the pre-vascularized dermis equivalent (PVD) is crucial: the side wall of the PVD must perfectly fit the chamber, in order to constitute a prolonging of the channel walls, without leakage of fluids from the side of the PVD towards the chamber, but only allowing interstitial flow to perfuse the ECM, thus generating a mechanical stimulus to both HDFs, ECM and HUVECs and transporting nutrients and removing metabolites in the first days of dynamic culture.

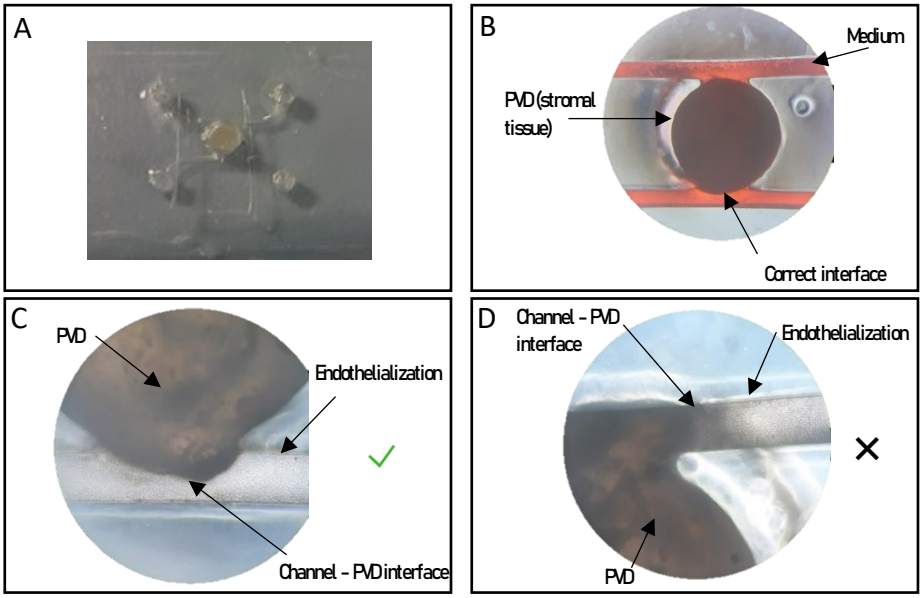

Figure 2.3.4.1: (A) PVD positioned inside a microfluidic device with PDMS membrane on top. (B) Optical microscope 10x image of PVD positioned inside the chamber. Correct PVD – channel interfaces are clearly visible. (C) Magnification of a correct interface generated by PVD positioning and its endothelialization. (D) Magnification of an incorrect PVD – channel interface due to stromal tissue penetration inside the channel, determining clogging of channel, resulting in only partial channel endothelialization and no flow.

2.3.5 Channels endothelialization (EC lining)

After PVD positioning inside the microfluidic chamber, endothelialization of channels was performed in order to obtain two endothelial-lined channels that communicate with the PVD chamber, determining the transport of nutrients to the pre-vascularized stromal tissue and to act as a source of endothelial angiogenic sprouts towards the PVD.

Endothelialization process was performed by means of a pipette-driven approach: HUVECs were centrifuged and, after supernatant removal, a small volume of cells (8 µL/channel) were withdrawn and gently injected in the channels, allowing for completely covering of channel walls. Results of endothelialization after 3 days of dynamic culture are presented in Figure 2.3.5.1. Endotheliaization of channels after 7 days of culture shows partial "invasion" of HUVECs inside non-prevascularized tissue as a result of dynamic culture and endogenous growth factors inside stromal tissue. This result allows for further investigation of the *in vitro* model with a microfluidic approach.

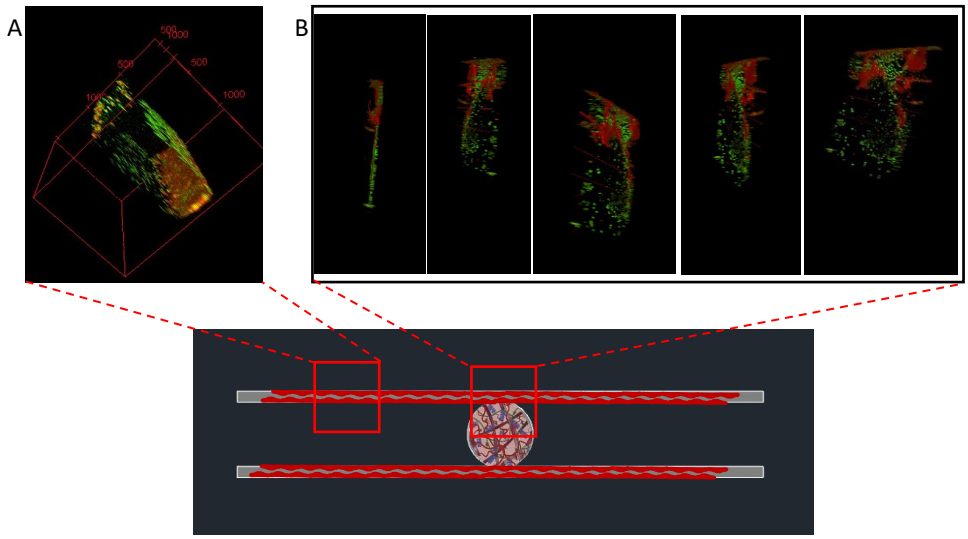

Figure 2.3.5.1: 3D reconstruction of endothelialized microfluidic channels obtained by a confocal z-stack acquisition. HUVECs are labeled in red, nuclei in green. (A) Endothelialized channel after 3 days on dynamic culture: a monolayer of ECs is visible, but endothelial layer on vertical walls is not perfectly confluent. (B) 3D reconstructions from confocal z-stack of PVD – channel interface with HUVECs that partially "invade" the non-prevascularized stromal tissue inside the chamber after 7 days of dynamic culture, from different angles. Red signal highlights HUVECs at high density at the interface, and a partial angiogenic sprout formation inside the chamber, while green signals represent HDF and HUVECs nuclei.

2.3.6 Dynamic culture system

Several dynamic culture systems have been investigated in order to optimize the microfluidic control over parameters such as flow rate and velocities, considering the range of velocities and shear stress that ECs undergo *in vivo*. In particular, human blood velocities inside capillaries range between 500 and 1500 µm/s and shear stress normally exerted by blood over capillary endothelial walls range between 100 and 500 s^{-1}. The

approach I will present relied on a pumpless system to obtain dynamic culture inside the microfluidic device.

In order to obtain both longitudinal and transverse ΔP inside the microfluidic device, it was important to settle a ΔV at the inlet reservoirs, which generated to different ΔP inside the channels, thus determining also a transverse ΔP. Given that the outlets pressure $p_{out} = p_{atm}$, it is possible to choose to different volumes at inlet 1 and inlet 2 that translate in different ΔP inside channels. Inlet pressures depend on free surface height: by leveling up the cell medium volumes at different heights, transverse ΔP can be generated, as shown in Figure 2.3.6.1. Based on the literature studies, I conducted calculations and analysis in order to determine the needed flow rate with respect to the fluidic channels cross-section area, considering the physiological human capillary velocity that ECs can resist without losing adhesion on substrate [123]. As the capillary velocities range between 500 and 1500 µm/s, the calculations determined that the flow rates to be generated inside the channel with a cross-section area of 500 µm x 400 µm to obtain velocities of $v_1 = 1500$ µm/s and of $v_2 = 1000$ µm/s are $Q_1 = 1.8$ µL/min and $Q_2 = 1.2$ µL/min, respectively (from the flow rate formula $Q = v \cdot A$). In order to generate this flow rate with a pumpless system that can guarantee a continuous flow for at least 16 hours (time needed for an overnight culture before re-filling reservoirs), I designed a configuration – as a proof of principle – featuring two modified syringes presenting two valves for the independent control of the two flow lines: a difference in cell-media volumes inside the syringes translates in a difference in pressures in the two channels, thus generating an interstitial flow inside PVD ECM, mechanically stimulating cells and transporting the necessary nutrients for tissue and HUVECs to proliferate and remain viable. Figure 2.3.6.2 shows the experimental set-up used, which was also analyzed by means of CFD simulation, which that the culture conditions were sufficient for PVD and endothelial layers viability.

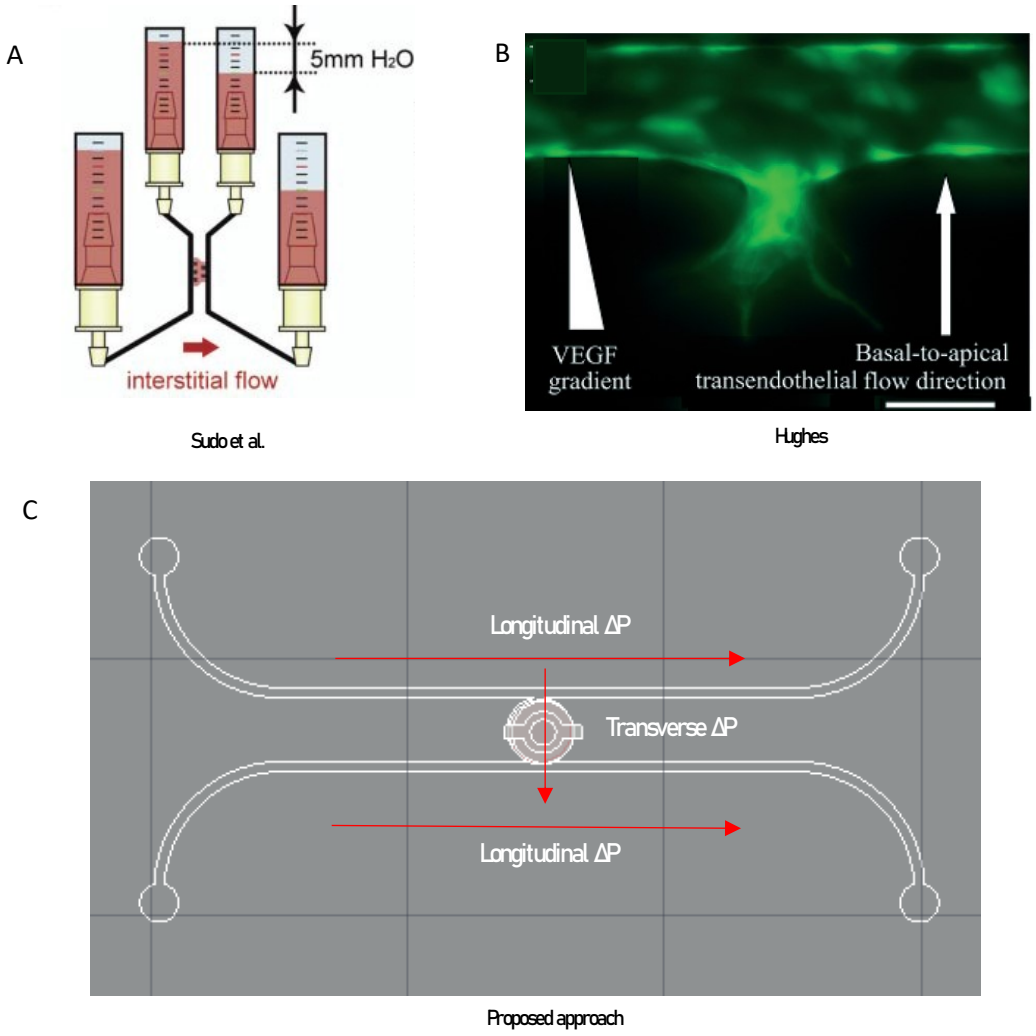

Figure 2.3.6.1: Schematization of principle for dynamic culture with pumpless system: hydrostatic pressure generates transverse and longitudinal ΔP. (A) Schematization of hydrostatic pressure for pumpless system dynamic culture (Sudo et al.) and (B) effect of ΔP on endothelial layer (Hughes et al.). (C) Schematization of hydrostatic pressure effects on designed microfluidic device.

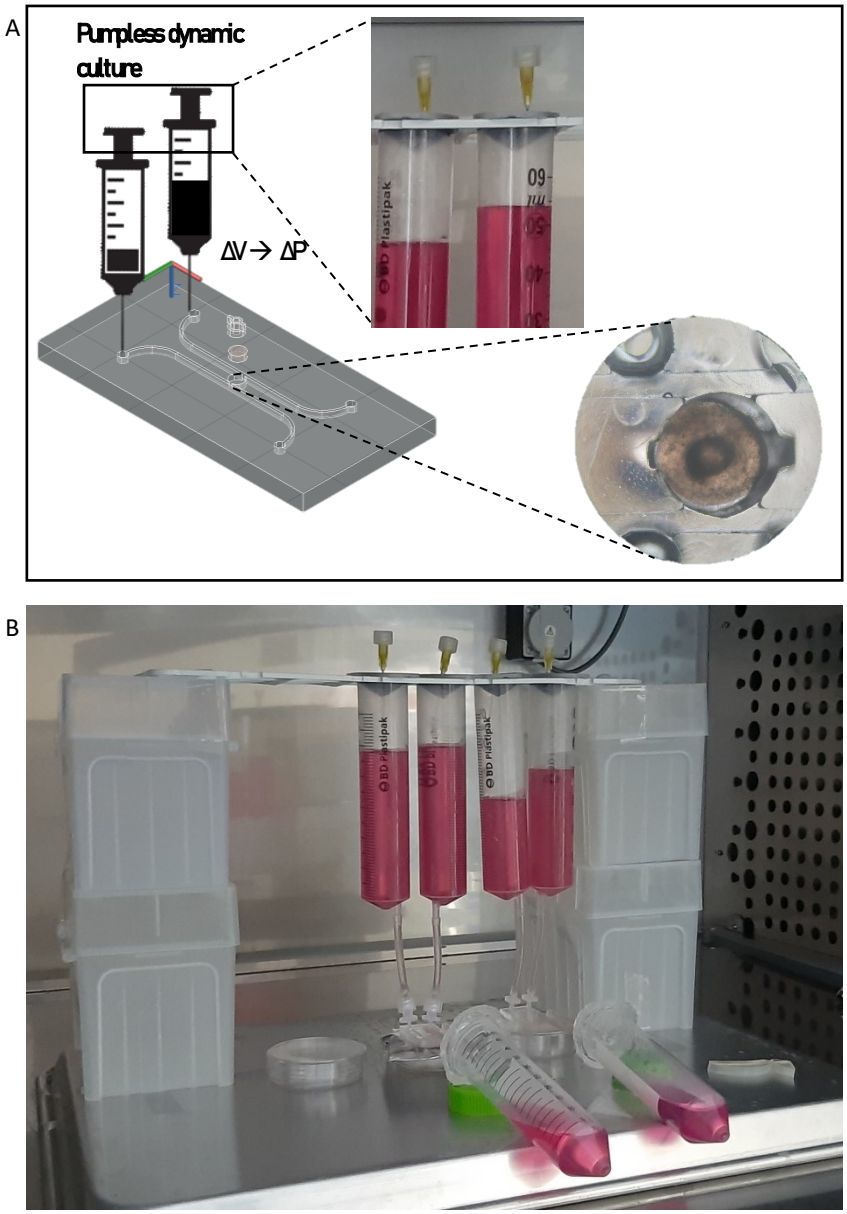

Figure 2.3.6.2: (A) Schematization of proof-of-principle pumpless system for dynamic culture: modified syringes contain different volumes of medium, determining a transverse ΔP inside the tissue chamber. (B) Image of the proof-of-principle pumpless system during dynamic culture experiment with living cells, inside an incubator for cell culture.

Several trials were performed with the designed pumpless system, that led to the final configuration:

- 60 mL modified syringes (2x) with removed plunger and with plunger-gasket used as a sealing cap;
- Needle inserted in the gasket with a Luer cap at the top, working as a valve;
- Tubes and connectors for inlets and outlets;
- Falcon tube for cell medium collection.

Several trials were also performed to fix the valve opening which corresponded to the volume reduction needed for the generation of velocities and flow rates described above: by measuring the volume reduction with time at different initial volumes at different valve opening, I was able to obtain the final experimental set-up. The obtained configuration allowed for a 14 days dynamic culture with no leakage, maintaining cell viability and without the use of automatized systems.

2.3.7 CFD simulation results

As described above, the CFD simulation allowed to determine if the device design and the dynamic culture conditions could guarantee cell viability inside the channels and 3D stromal tissue. The first parameter for viability is O_2 concentration: in order to maintain their functionality, cells must be cultured at 0.22 mol/m^3 O_2 concentration. Longitudinal and transverse pressure drops inside the microfluidic platform were obtained by literature [17], generated by values of pressure equal to 23 mmH_2O, 18 mmH_2O, 8 mmH_2O and 3 mmH_2O, to guarantee that velocities inside channels were in the range of physiological blood velocities inside human capillaries. To obtain such velocities inside the device with cross-section area A = 0.06 mm^2, nominal flow rates of 5.4 and 1.8 µL/min were needed in the two channels. By measuring volumes at the outlets with a given opening of the reservoirs valves, the flow rates were obtained and the culture condition was controlled to recapitulate the simulated conditions.

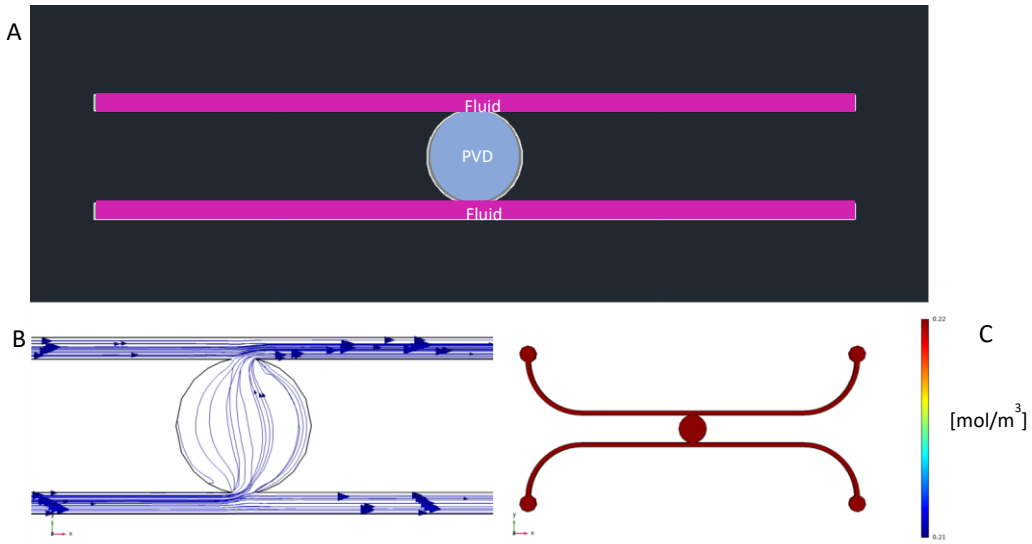

Figure 2.3.7.1: (A) Schematization of "fluid" and "PVD" domain inside the microfluidic platform. (B) Flux lines inside the device with imposed ΔP. (C) O_2 concentration [mol/m^3] inside the device: cell viability is guaranteed with the culture conditions imposed.

2.3.8 Dynamic culture effects on endothelium and 3D stromal tissue

The dynamic culture inside the microfluidic device allows for cell nutrition, thus determining their proliferation in a 3D, close to physiological environment. After producing the 3D stromal tissue equivalent in a disk-shape (2.5 mm diameter, 1 mm thickness), a pre-vascularization process was started as described above. After 11 days of pre-vascularization, a capillary-like structure (CLS) was formed with lumen inside tubular-assembled HUVECs. The obtained PVD was positioned inside the microfluidic device, and endothelialization of side channels was performed. It was possible to perform several experiments in order to obtain important information regarding vascularization:

- The effect of dynamic culture on endothelial cells in lateral channels;
- The role of pre-vascularization for the formation of an interconnected vascular network that anastomoses with both fluidic channels and anastomosis time;
- The role of transverse ΔP on angiogenic sprouts;
- Anastomosis time for 3D stromal tissue equivalent on-chip;
- HDFs localization outside the stromal tissue equivalent to support HUVECs inside the channels.

After 4 days of dynamic culture, confocal images were acquired to assess cell behaviour under dynamic culture. The pre-vascular network inside the PVD maintained its

structuration, as shown in Figure 2.3.8.1, A, and co-localized with collagen fibers, imaged by means of SHG. Endothelial layer in side channels proliferated and reached confluency (Figure 2.3.8.1, B), and PVD – channels interfaces were characterized by the presence of HUVECs in the channel and at PVD edge, with interaction starting between the two populations (Figure 2.3.8.1, C, at PVD edge highlighted with yellow dashed line) while no angiogenic sprouts were individuated yet (Figure 2.3.8.1, C and D). Endothelial layer at PVD-channel interface resulted not confluent as the side parts of channels, highlighting an issue in the formation of a continuous EC layer in the crucial part of the device, due to PVD positioning: PVD positioning inside the chamber strongly influences the precise control over the interfaces generation and the perfect adhesion to the bottom of the device, which is not always achieved due to micrometer-detachments for flow conditions. To solve this issue, a UV 3D printed ring was fabricated (the optimization will be described later in chapter 4) and positioned on top of the PVD, guaranteeing for a better adhesion of PVD to bottom part of the device.

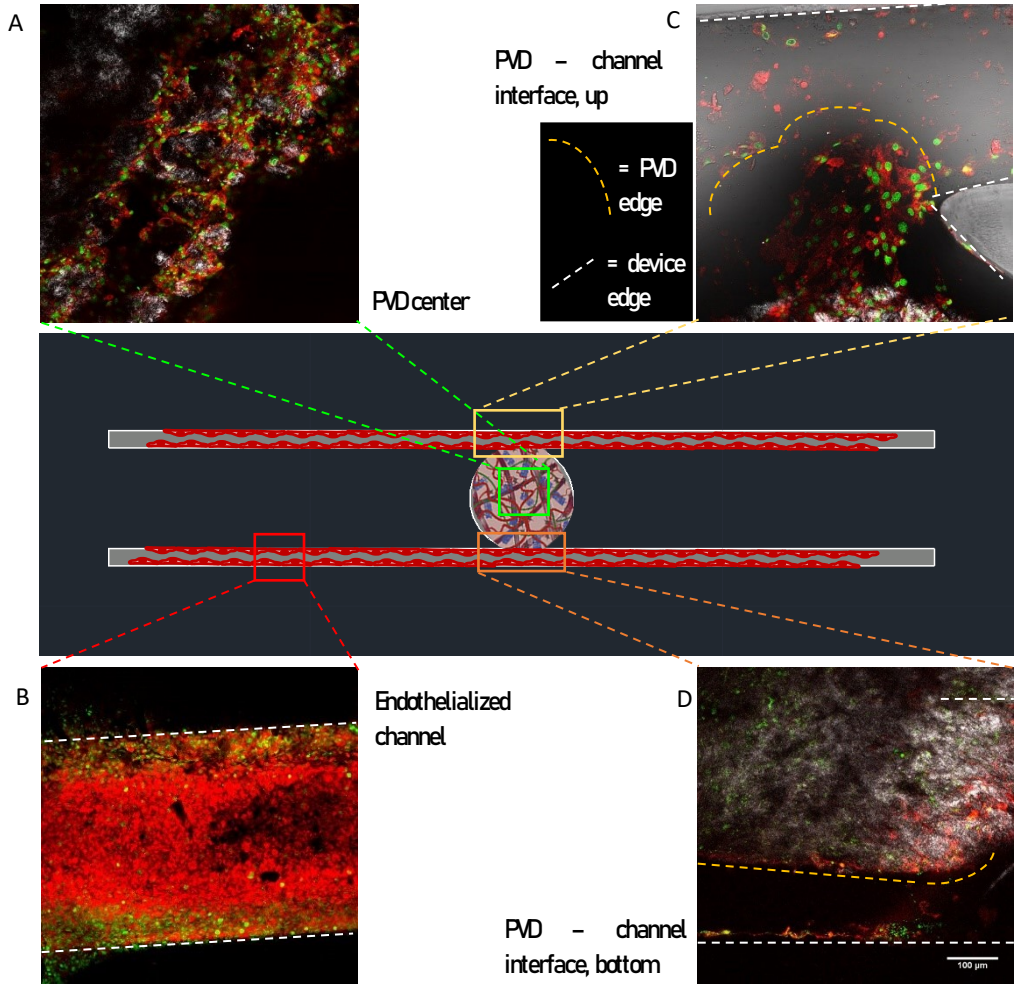

Figure 2.3.8.1: 3D stromal tissue of 7 weeks, pre-vascularized for 11 days, after 4 days of dynamic culture, thus presenting a capillary network after 15 days from HUVECs seeding inside 3D stromal tissue. Confocal images at day 4 of dynamic culture. (A) SHG for collagen fibers imaging, overlapped with fluorescent signals from HUVECs (red) and nuclei (green) show co-localization of pre-vascular network and collagen fibers, which act as support for the network. (B) Confocal image of a portion of endothelialized channel (red: HUVECs, green: nuclei), bottom part: a monolayer of ECs is visible, obtained by means of dynamic culture and flow, that together induced EC elongation and proliferation. (C, D) Confocal images of PVD – channel top (C) and bottom (D) interfaces: yellow dashed lines highlight PVD edge, while white dashed lines represent device edges. Endothelial cells from PVD and from channels start to interact (C, at PVD interface), but no angiogenic sprouts can be individuated yet.

Despite the mentioned issue, it was possible to investigate the key role of pre-vascularization for anastomosis of fluidic channels through the vascular network within the tissue with an experiment conducted with two configurations:

1) 14 days of pumpless dynamic culture of PVD (pre-vascularization of 7 days before on-chip positioning) and endothelialized channels;
2) 14 days of pumpless dynamic culture of dermis equivalent (without pre-vascularization) and endothelialized channels.

Results shown in Figure 2.3.8.2 and 2.3.8.3 allowed for an important information regarding anastomosis time: pre-vascularization processes inside a 3D stromal tissue drastically accelerate the phenomenon of anastomosis of fluidic channels through a vasculature inside the tissue. In particular, 14 days of pumpless dynamic culture of PVD (pre-vascularization of 7 days) with endothelialized channels were sufficient for anastomosis of fluidic channels, as shown in Figure TOT by the presence of angiogenic sprouts from both channels that are connected through the vasculature inside the tissue; on the other hand, 14 days of pumpless dynamic culture of dermis equivalent (without pre-vascularization) with endothelialized channels determined the formation of angiogenic sprouts departing from both endothelialized channels towards the tissue, but the lack of anastomosis between the two families of sprouts did not allow for the development of a complete, interconnected vasculature inside the tissue.

Another important information obtained by the above-described experiment regards the role of transverse ΔP on angiogenic sprouts: as literature studies underlined the fundamental role of transverse ΔP on the formation of tubular sprouts that depart from an endothelial layer [20], in particular focusing on the phenomenon by which angiogenic sprouts tend to better develop in the opposite direction of flow [20], the experimental set-up I designed – featuring a transverse ΔP in the up-down direction – determined the formation of angiogenic sprouts in both directions (Figure 2.3.8.3): this result opens the horizon of exploiting dynamic culture systems that do not rely on transverse ΔP, thus leading to the hypothesis that the endogenous ECM, with HDF-secreted growth factors, was sufficient in the development of angiogenic sprouts in both directions (towards and opposite to transverse ΔP).

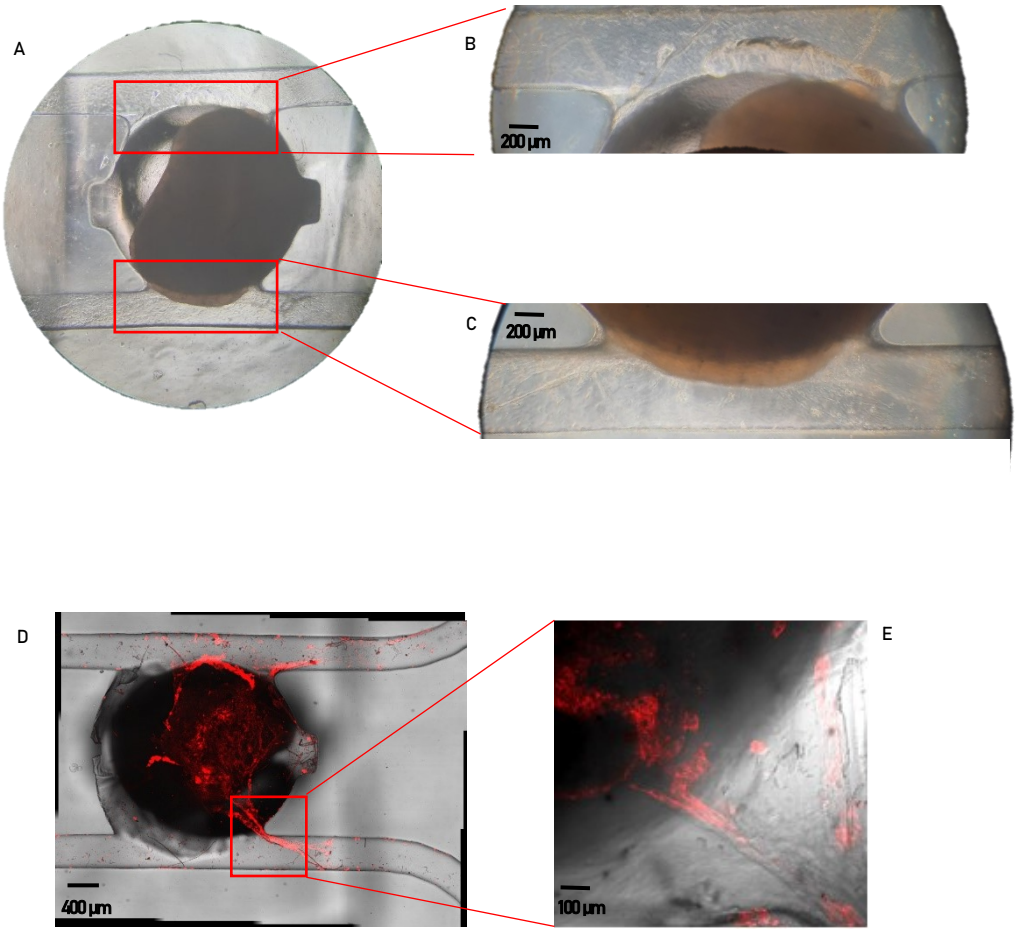

Figure 2.3.8.2: Results of configuration 1) experiment: 14 days of pumpless dynamic culture of PVD (pre-vascularization of 7 days) with endothelialized channels. (A) Optical microscope image of chamber with positioned PVD: magnifications (B) and (C) show the top and bottom interfaces, respectively. Top interface is not perfectly continuative with channel wall, while bottom interface is perfectly shaped to continue channel wall. Scale bars are 200 µm. (D) Confocal tile-scan of PVD chamber and PVD-channels interfaces: a continuous, interconnected vascular network (red) is visible from top interface to bottom interface. Both interfaces are present angiogenic sprouts from channel that anastomose to pre-vascular network inside the tissue, even if there was no switch of transverse ΔP direction, thus obtaining an important platform for angiogenesis model. Scale bar is 400 µm. (E) Confocal image of angiogenic sprout from bottom channel anastomosed with vascular network inside the tissue. Scale bar is 100 µm.

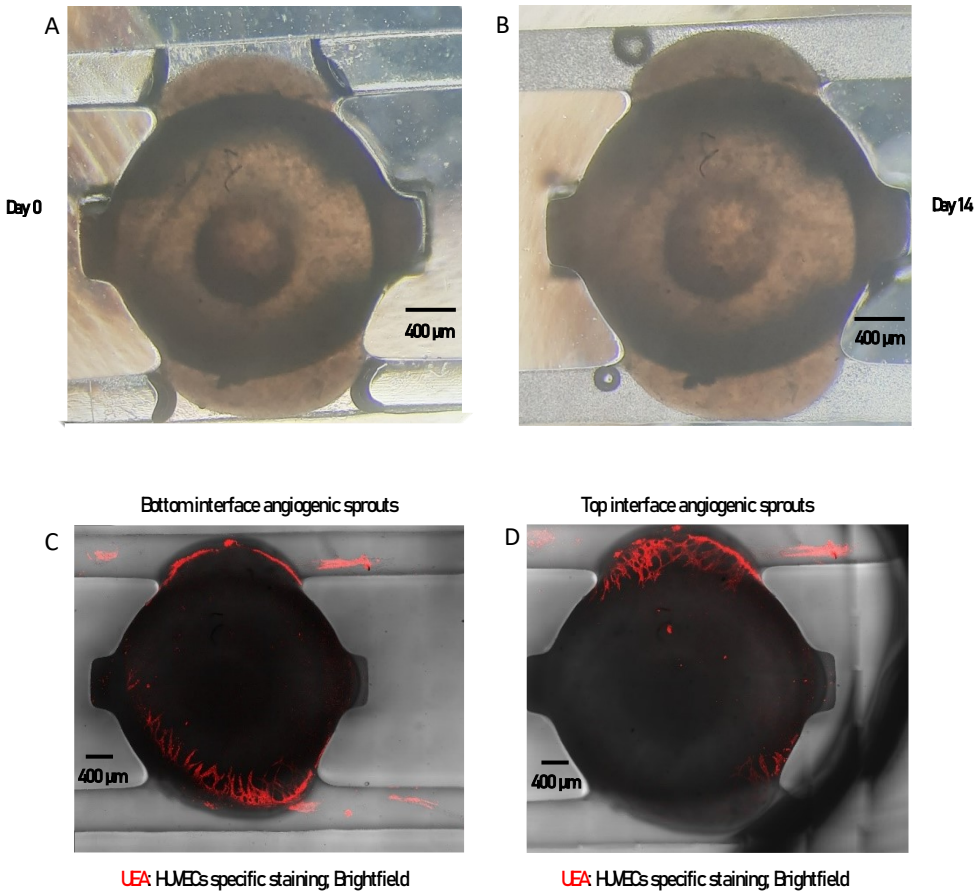

Figure 2.3.8.3: Results of configuration 2) experiment: 14 days of pumpless dynamic culture of dermis equivalent (not pre-vascularized) with endothelialized channels. Optical microscope images (A) and (B) show tissue chamber with loaded dermis equivalent before (A) and (B) after channels endothelialization, which represents the only source of ECs. (C) Confocal tile-scan of tissue chamber where bottom-interface angiogenic sprouts are visible (direction of development = opposite of direction of ΔP). (D) Confocal tile-scan of tissue chamber where top-interface angiogenic sprouts are visible (direction of development = direction of ΔP). Confocal images (C) and (D) show that no vascular network connects the top and bottom angiogenic sprouts inside the tissue, thus determining that the pre-vascularization of tissue is fundamental for the anastomosis time of fluidic channels through the vasculature inside the tissue. On the other hand, the development of angiogenic sprouts from both sides – towards and opposite to transverse ΔP – represents an important result, reconsidering the possibility of a dynamic culture system without transverse ΔP.

Another relevant result is presented in Figure 2.3.8.4: the co-localization of HUVECs and HDFs outside the 3D stromal tissue equivalent. In particular, HUVECs specific staining with UEA I and general staining of nuclei allowed for the individuation of HUVECs and HDFs localization: nuclei without red staining – labeling HDFs – can be spotted outside the tissue chamber, inside the channels, co-localized with HUVECs (red), acting as a support for angiogenic sprouts inside the channels.

The designed microfluidic platform allows for dynamic culture and anastomosis between a pre-vascularized 3D stromal equivalent and an external source of HUVECs after 14 days of pumpless dynamic culture, thus representing a tool for the study of interaction between endothelial cells from an external source and a tissue, even *an ex vivo* transplantation as PVD may represent.

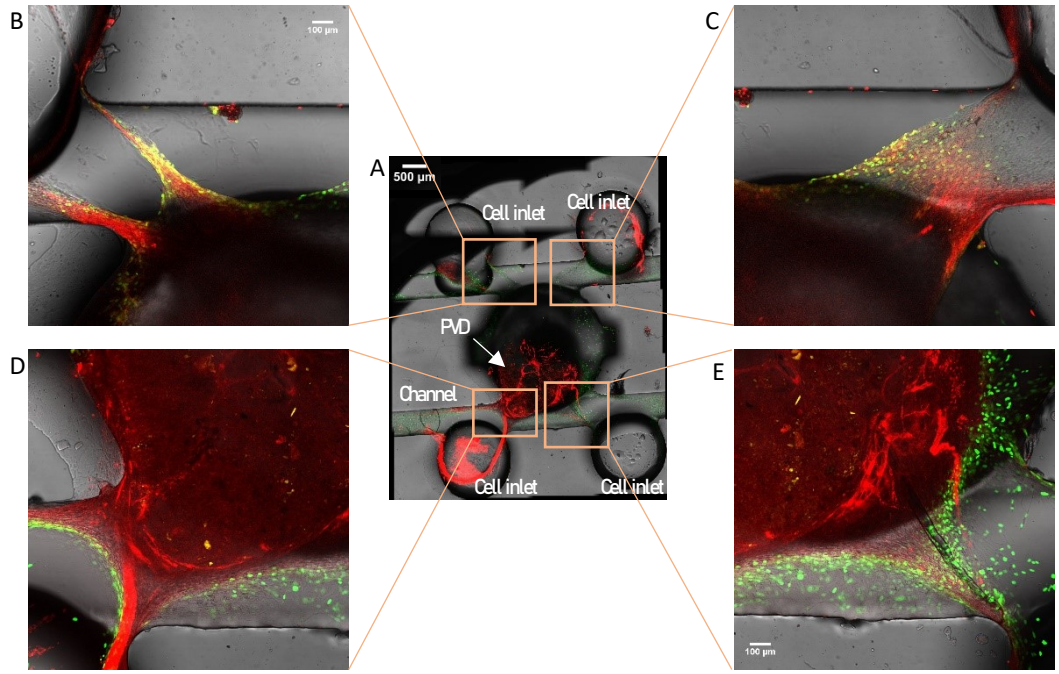

Figure 2.3.8.4: 3D stromal tissue of 7 weeks, pre-vascularized for 11 days, after 14 days of dynamic culture, thus presenting a capillary network after 25 days from HUVECs seeding inside 3D stromal tissue. Red signal highlights the presence of HUVECs, while green signal represents nuclei. (A) Tile-scan confocal image of central part of microfluidic device showing capillary structure inside PVD that anastomoses with tubular formation outside the tissue, inside the channel. Scale bar is 500 µm. (B-E) Magnifications of top-left (B), top – right (C), bottom – left (D), bottom – right (E) regions of chamber – channel interface showing angiogenic sprouts with tubular structuration. Bright field and nuclei staining also highlight the role of HDFs in supporting HUVECs tubular-like migration inside the channels. Image (B) and (D) show two bifurcations. with angiogenic sprouts connecting stromal tissue to cell inlets. Image (C) shows a wide migration of HUVECs of non-properly tubular shape. Image (E) shows a single tubular formation of HUVECs connecting 3D stromal tissue to cell inlet. Dynamic culture allows for long-lasting capillary-like structures, which anastomose to tubular formations inside lateral channels towards the four cell inlets.

2.4 Achievements, limitations and future perspectives

The reported results regarding the proposed *in vitro* vascularization model can be summarized in the following points:

- The designed microfluidic platform allowed for a 14 days dynamic culture of a 3D pre-vascularized stromal tissue and its characterization, which can be defined as a long-lasting vasculature considering a 7 day – pre-vascularization process;
- The combination of EC lining of side channels and a pre-vascularization strategy *via* vasculogenesis of 3D stromal tissue was able to determine anastomosis of angiogenic sprouts departing from channels to the vascular network inside the tissue at day 14 of culture;
- The role of transverse ΔP inside from the channels to chamber revealed less relevant than the above-mentioned studies probably due to the presence of a 3D stromal tissue with well-structured collagen fibers and endogenous growth factors that were sufficient for angiogenic sprouts to occur;
- The generation of a precise channel-tissue interface through a communication pore reveals as a crucial parameter to obtain a source of angiogenesis;

The dynamic culture conducted on the designed microfluidic platform for 14 days determined the development of vasculature – inside a 3D endogenous ECM – that already formed 7 days before on-chip positioning of the tissue equivalent, thus obtaining a long-lasting vasculature of 21 days. This result, compared to the above-mentioned studies by Hughes et al, Seiler et al., and others from chapter 1, determined a step forward in the lasting of vasculature in an *in vitro* 3D tissue model on-chip.

Nonetheless, some issues must be underlined and overcome with a strategy modification:

- PVD positioning – even with the introduction of a 3D printed ring as a support for PVD adhesion to the bottom of the device – presented a micrometer-range detachment from the bottom of the device that did not allow for the fine control of EC lining process of PVD lateral wall during channels endothelialization;
- The control over flow parameters, which revealed to be fundamental for an *in vitro* vascularization model, lacked of a precise, automatized system of the opening of the valves, thus determining a long transitory state before reaching the needed valve opening for pumpless system activation at the proper flow rate. Probably this transitory state determined high impulse forces on channel endothelium, translating in a non-continuous endothelium at PVD-channel interface;

- Time-consuming approach: 3D stromal tissue production as described above results in a 6 – 7 weeks procedure, which determines low chances of scalability and long-time before a result can be obtained, thus reconsidering the possibility to use the designed platform as a high-throughput *in vitro* model for the study of vasculature-related phenomena.

Given these achievements and limitations, a new strategy was proposed to overcome the above-mentioned issues, maintaining the positive results of the exposed experimental campaign. In particular, the PVD dermis equivalent was substituted with a collection of microtissue precursors (µTPs), which represent the building block of the dermis equivalent: they present the same composition (HDF, endogenous structured ECM) but their dimension is in the order of microns instead of millimeters and present an endogenous ECM produced in a shorter time. Nonetheless, the dynamic culture on µTPs inside a confined region may lead to their assembly into a single, 3D stromal tissue under controlled dynamic culture. Another modification to the above-described strategy regards the microfluidic platform design: a new geometry must be introduced in order to maintain the positive features of the previous chip, together with the new requirement of µTPs confinement. Finally, a dynamic culture system with fine control over flow rate – even at early stage of dynamic culture – must be taken into account for a microfluidic platform with the goal of developing long-lasting vasculature as a study model of vascularization phenomena.

3 µTPs for anastomosis-on-a-chip

Graphical abstract

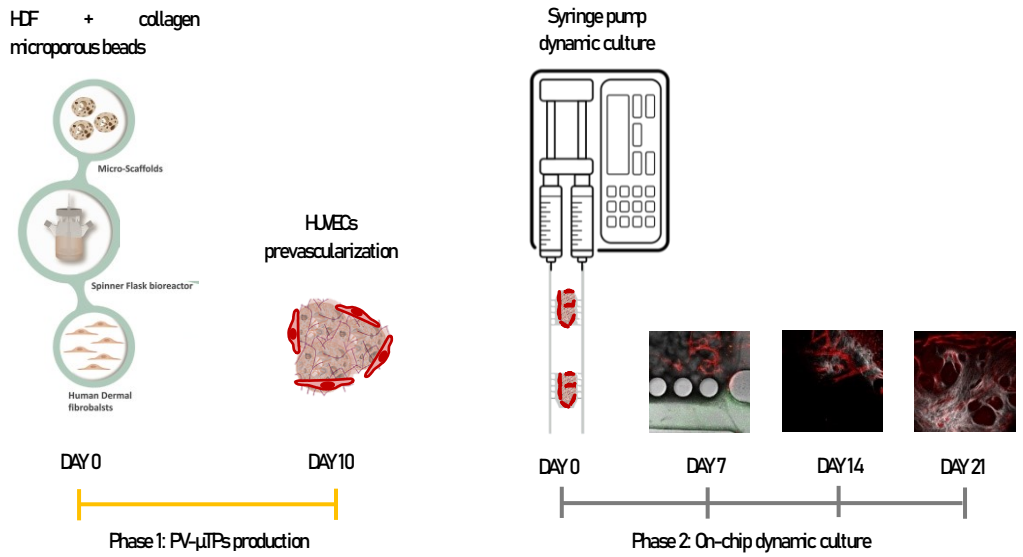

Vascularization on-chip strategy can be divided in two phases, the first being PV-µTPs production, the second consisting in dynamic culture on microfluidic device. Phase 1 consists in the production of µTPs from a previously described procedure – briefly consisting in spinner culture of microbeads and HDFs, HDF proliferation and aggregation of cell-laden beads – followed by pre-vascularization process by HUVECs seeding and adhesion. Phase 2 starts with PV-µTPs loading on the microfluidic platform, continues with the EC lining of channels walls, which is followed by syringe pump-driven dynamic culture for different time intervals for the development of angiogenic sprouts and anastomosis to tissue vasculature.

3.1 Introduction

As highlighted in the final section of previous chapter, a new strategy must be designed in order to obtain a more reliable microfluidic platform for *in vitro* study of long-lasting vascularization model. In order to obtain more detailed information regarding vasculature formation, to develop a more controllable interface between stromal tissue and channel for endothelialization inside microfluidic platforms and to perfuse vessel

lumens through fluidic channels, a different approach was proposed. The idea generated from one of the most important features of µTPs: their capability to remodel, continuously reorganize and secrete ECM molecules due to their composition – human cells (HDF) and endogenous matrix – which determines µTPs versatility as a 3D stromal model [108], [130]. The proposed strategy relied on the on-chip µTPs assembly in order to obtain a continuous, 3D tissue with a vascular pre-network that could anastomose with endothelial lined side channels. The device geometry was modified in order to allow for µTPs positioning and confinement inside two chambers by the introduction of pillar rows, which simultaneously confined µTPs and allowed for their communication with two adjacent channels for media flow and endothelialization. Another important modification in the device was the closed-design, which overcome the possibility of leakage from the upper part of the PVD chip configuration and the adhesion of tissue to the bottom of the device. Two inlets were introduced for µTPs positioning, and inlets for endothelialization and media flow were combined in a single solution.

Fabrication approach was also modified in order to obtain the desired geometrical cues. 3D printing was substituted with micro-milling for the production of the hard master in PMMA, while replica molding was maintained as the final fabrication step of PDMS devices. As the 3D stromal tissue was modified, two main modifications regarding chip dimensioning were performed:

- chip height: a reduction in device height could be introduced, as the limiting size to consider for device design changed from PVD (1 mm thickness) to µTPs (300 to 600 µTPs);
- introduction of pillars: two rows of pillars per tissue chamber perform a double function, with µTPs confinement in a certain volume, together with the generation of the needed channel-tissue interface through interpillar spaces – which result in a modification in the tissue interface from continuous (PVD) to fragmented (µTPs), with multiple windows for angiogenic sprouts.

Another modification with respect to the previous strategy regarded the dynamic culture system: as the pumpless system presented issues in the early stage of dynamic culture, an automatized, precise control over flow rate was needed, and syringe pumps revealed to be the most reliable systems for the control of low flow rates.

In the following sections I will present the optimization of the experimental strategy, and results will be shown and discussed.

3.2 Materials and methods

3.2.1 µTPs characterization

After µTPs production as described in chapter 2, characterization of µTPs was performed to assess the correct formation of collagen fibers within gelatin beads, at day 7 – 10 of spinner dynamic culture: the process determines the assembly of HDF-loaded gelatin beads and initial secretion of endogenous oriented molecules constituting stromal ECM. Characterization was performed by means of 2-photon confocal imaging for SHG, as described above.

3.2.2 Pre-vascularized µTPs (PV- µTPs) production

After µTPs characterization to highlight the presence of oriented collagen fibers secreted by HDFs, crucial for endothelium adhesion and growth inside the stromal tissue, pre-vascularization process was designed. In order to obtain the 3:1 HDFs – HUVECs ratio needed [120], a quantification of HDFs at day 10 of spinner dynamic culture was performed. A volume of 500 µL of highly-concentrated µTPs was withdrawn from spinner flask and µTPs were quantified using a custom-made petri dish with a grid on the bottom. To quantify the number of HDFs / µTP, 1 hour treatment with collagenase type A (Sigma Aldrich) was performed to break down peptidic bonds of collagen, resulting in widening ECM mesh. After centrifuging and discarding supernatant, trypsin was used to detach HDFs from ECM for counting. A number of 600000 HDFs was counted in 30 µTPs, which corresponds to a ratio of 20000 HDFs / µTP at day 10 of culture. A 3:1 ratio HDFs : HUVECs was obtained by seeding 100000 HUVECs / mL inside a 24-well low attach dish with an average of 30 µTPs / well and a total volume of 2 mL / well. Pre-vascularization occurred in alternate regime (5 minutes 60 rpm, 30 minutes static condition for at least 6 hours) to let HUVECs adhere at µTPs surface with VascuLife (Lonza) in the first day, and with a 2:1 MEM:VascuLife solution for the other days of culture. After 2-3 days of prevascularization process, PV-µTPs were fixe and stained as described above for the assessment of CLS.

3.2.3 PV-µTPs characterization

In order to study the capillary pre-network formation inside PV-µTPs a dynamic culture in multiwell was maintained for 3 weeks after HUVECs seeding on PV-µTPs surface, and different time point (1 week, 2 weeks and 3 weeks) were analyzed by means of immunofluorescence and confocal imaging. CLS area was also assessed in order to obtain CLS trend versus time.

3.2.4 Immunofluorescence on the whole sample

Samples were fixed in 4% Paraformaldehyde (P61148-500g Sigma Aldrich) for 30 minutes at RT and washed in PBS1X. They were permeabilized using 0,1% Triton (Triton® X-100 T9284-100ML Sigma) in PBS1X for 5minutes at RT, washed three times with PBS1X and blocked in 1% BSA (A9418-100G Sigma) for 1 hour at RT. Some samples were stained with coincubation of Rhodamine Ulex Europaeus Agglutinin I (UEA I Vector Laboratories RL-1062) and primary Anti-Laminin antibody produced in rabbit (Sigma-Aldrich) and secondary Cy5 for endothelium and laminin marking respectively, while other samples were stained only with UEA I at a final concentration of 20 µg/mL in blocking solution, in order to mark the endothelium, overnight (ON) at 4°C in the dark. Next morning, samples were washed with PBS1X. The nuclei of all the cells were stained with Sytox Green (Invitrogen S7020) for 20 minutes at RT.

3.2.5 Confocal imaging

Confocal acquisitions were performed with the following parameters:

- rhodamine (UEA I): λ_{ex} = 543 nm/ λ_{em} = 550-560 nm;
- Cy5 (Laminin): λ_{ex} = 633 nm/ λ_{em}= 650-680 nm;
- FITC (Sytox green and NPs for perfusion test): λ_{ex}= 488 nm/ λ_{em}=500-530 nm.

3.2.6 CLS area fraction

The capillary like structures (CLS) area fraction was calculated as percentage of the ratio between the thresholded red volume of the endothelium marked by Rhodamine-UEA I and the total surface of the sample acquired for different slice of a z-stack. The surface values were obtained applying the ImageJ plugin "Measure" to the red thresholded channel and to the total surface of tissue acquired.

The formula used for CLS area fraction was:

$$CLS\ Area\ Fraction\ (\%) = \frac{acquired\ CLS\ surface}{acquired\ sample\ surface} \times 100$$

AF and junctions/µm^2 are used as parameters to quantitative assess CLS features. Despite these parameters regard 2D features, it was previously demonstrated [60] that 2D features present the same trend as 3D features (Volume Fraction and junctions/µ m^3). For this reason, 2D parameters are presented. Nonetheless, the number of junctions were assessed on confocal images from z-stacks, with a section thickness of

4.611 µm. As the capillary diameters range from 9 to 25 µm – thus less than section thickness of confocal acquisition – , the totality of assessed junctions are not z-projection artifacts.

3.2.7 Statistics

Experiments were performed in triplicate. Data are expressed as mean ± SD. Differences between groups were determined using the statistic test ANOVA Tukey HSD test. Significance between groups was established for *p* value < 0.01 or *p* value < 0,05.

3.2.8 µTPs microfluidic device

The new configuration of microfluidic device needed several modifications in terms of design and fabrication, which will be described in the next paragraphs.

3.2.8.1 Chip design and fabrication

To investigate angiogenic sprouts formation and anastomosis, a miniaturized and optically accessible microfluidic platform was designed with computer aided design (CAD) software (AutoCAD 2022, Autodesk). The design modifications with respect to the PVD chip regard channel – chamber interface, channels width and chip height. The core of the design consists of two channels for media flow and endothelialization process, and two chambers for PV-µTPs positioning. Two rows of pillars in each tissue chamber separate µTPs space from adjacent channels.

Device configuration presents two µTPs chambers with a size of 2 (length) x 1.2 (width) x 0.6 (height) mm^3. Each chamber was delimited by two rows of four cylindrical pillars, which were 300 µm in diameter and 600 µm in height, and featured an inlet, which measured 4 x 0.8 x 0.6 mm^3, for µTPs injection. Spacing between pillars was 100 µm in some experiments, 50 µm in other experiments, and chambers were connected to two side channels which measured 14 x 0.4 x 0.6 mm^3 in some experiments, 14 x 0.1 x 0.6 mm^3 in other experiments, Channels function was to guarantee a cross-flow of nutrients supply to µTPs and to obtain endothelialization at the sides of chambers. Two inlets and two outlets were positioned at the edges of the channels (Figure 3.2.8.1.1). Microfluidic

device volume is 9.6 mm^3 (1.44 mm^3 each chamber + 3.36 mm^3 each channel), that correspond to 9.6 µL.

To fabricate the microfluidic device, the CAD file was converted into a Computer-Aided Machine (CAM) file using DESKAM software. Afterwards, a Poly (methyl methacrylate) (PMMA, Goodfellow) master was obtained using micromilling machine (Minitech CNC Mini-Mill). By replica molding, a polydimethylsiloxane (PDMS) (Sylgard 184, Mascherpa) device was fabricated. PDMS base and curing agent were mixed using a weight ratio 10:1 and were poured on the PMMA master. Then, the PMMA master with the blend was degassed under vacuum for 1 hour to remove the air bubbles and cured in an oven for 2 hours at 80°C. Then, the PDMS layer was softly detached from the PMMA master and inlets and outlet holes were obtained by inserting inside the fabricated cylindrical guides a biopsy punch (DifaCooper) with a 1.5 mm diameter for µTPs loading channels, inlets and outlets. After punching, the PDMS layer was bonded on a glass coverslip (Menzel-Glaser 24 x 60 mm # 1,5) by oxygen plasma treatment for 1 min at 50 W in an oxygen plasma oven (Plasma Femto, Diener). After the treatment, the device was placed in an oven and maintained at 80°C for 24 hours with the metal weights to ensure that the bonding was maintained.

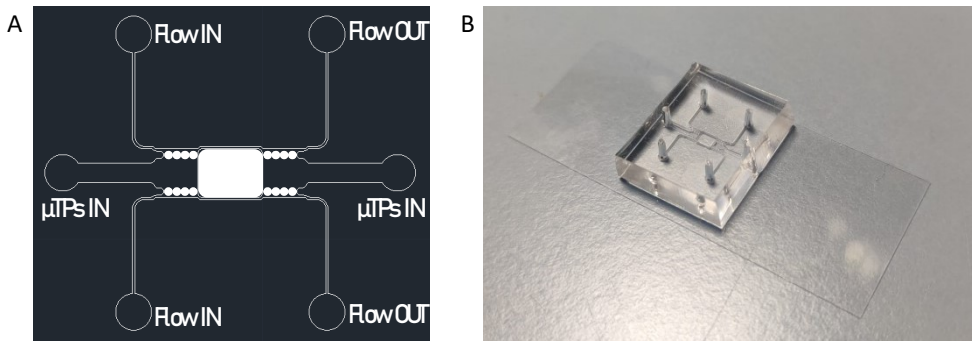

Figure 3.2.8.1.1: (A) Schematization of new design for µTPs microfluidic device, top-view: inlets and outlets for cell medium and inlets for µTPs loading are highlighted. Interpillar spacing allows for medium flow from channels to tissue chambers and angiogenic sprouts formation. (B) Image of a fabricated device, by means of micro-milling for negative hard master, replica molding for PDMS patterned slab fabrication and plasma bonding with coverslip glass for the final configuration.

3.2.8.2 CFD simulation

To define the experimental setup, COMSOL Multiphysics version 5.3a (build 280) was used to evaluate the three-dimensional velocity distribution, the oxygen profile, shear rate and shear stress on endothelial walls inside the channels, before *in vitro* experiments. The simulations were carried out as previously described [134] by

modifying several parameters. Briefly, the devices were divided into two different domains, a fluid domain inside the channels, which identified the regions filled with culture medium, and microtissue domains inside the tissue chambers, which identified the regions filled with PV-μTPs. μTPs properties were manually set up considering previous knowledge of the research group, while *Free and Porous Media Flow* and *Transport of Diluted Species in Porous Media* modules were coupled in steady state conditions; the first physics implements Navier-Stokes equation for the free fluid phase and Brinkman extended Darcy's equation for the porous matrix, while the second physics implements the mass balance equation:

- Navier-Stokes equation

$$\begin{cases} \rho \boldsymbol{u} \cdot \nabla \boldsymbol{u} = \nabla \cdot [-pI + \mu(\nabla \boldsymbol{u} + (\nabla \boldsymbol{u})^T)] + \boldsymbol{F} \\ \rho \cdot \nabla \boldsymbol{u} = 0 \end{cases}$$

- Brinkman equation

$$\begin{cases} \dfrac{\rho}{\varepsilon_p} \boldsymbol{u} \cdot \nabla \dfrac{\boldsymbol{u}}{\varepsilon_p} = \nabla \cdot \left[-pI + \dfrac{\mu}{\varepsilon_p} (\nabla \boldsymbol{u} + (\nabla \boldsymbol{u})^T) - \dfrac{2}{3} \dfrac{\mu}{\varepsilon_p} (\nabla \cdot \boldsymbol{u}) I \right] - \left(\mu \kappa^{-1} + \beta_F |\boldsymbol{u}| + \dfrac{Q_{br}}{\varepsilon_p^2} \right) \boldsymbol{u} + \boldsymbol{F} \\ \rho \nabla \cdot \boldsymbol{u} = Q_{br} \end{cases}$$

- Mass balance

$$\begin{cases} \nabla \cdot \boldsymbol{\Gamma_i} + \boldsymbol{u} \cdot \nabla c_i = R_i + S_i \\ \boldsymbol{N}_i = \boldsymbol{\Gamma_i} + \boldsymbol{u} c_i = -\mathcal{D}_{e,i} \nabla c_i + \boldsymbol{u} c_i \end{cases}$$

Concerning the boundary conditions, at the chip outlet atmospheric pressure was considered (p = 1 atm), no slip condition was adopted at the walls, equality for velocity and pressure was imposed at the Navier-Stokes (u, v, w, p)/ Brinkman (u_2, v_2, w_2, p_2) interfaces. Imposing for O_2 concentration in the culture medium (0.22 mol/m^3), the diffusion coefficient (D) (10^{-9} m^2/s), cell density (ρ) ($0.2 \cdot 10^{14}$ cell/m^3).

3.2.8.3 Device characterization

After devices fabrication by replica molding using PDMS, characterization of a sample was performed in order to determine the real size of the geometry details, which are crucial for experiments success. Scanning Electron Microscope (SEM) (Carl Zeiss Ultraplus Field Emission Scanning Electron Microscope) was used to analyze surface details and to measure pillars, channels and chambers size. After cutting a representative sample from the PDMS device, a metallization treatment was necessary

to enhance its electrical conductivity. Deposition of 7 nm layer of gold was performed and several images of the sample were acquired. Measures were obtained with the measuring function of ZEISS software, considering the tilting angle of the sample at the moment of acquisition, with the formula:

$$S = {}^{M}/_{\cos(\alpha)}$$

with S equal to the real size, M equal to the measured size, α equal to the sample tilting angle.

3.2.9 Anastomosis-on-chip experimental set-up assembly

Anastomosis-on-chip devices were autoclaved, and Tygon tubes (0.89mm ID) and connectors were sterilized by 70% (v/v) ethanol for 30 min, then rinsed in sterile PBS to remove residual ethanol and placed under UV light for 1 hour. Afterwards, tubes were inserted into the inlets and outlet of the channels using Polyethylene Tubing (0.58 ID x 0.97 OD mm) male and barbed female Luer lock connectors (Harvard Apparatus), previously sterilized. In some configurations, the tube of the inlet was split into two tubes using Y connectors (Harvard Apparatus) to guarantee the same medium supply in both channels, while in the other configurations every channel had an independent flow source. Before starting the µTPs loading phase, the devices were flushed with pre-heated medium to minimize bubble formation. In detail, the whole device volume was filled with medium, and the device was placed at 37°C in a humidified atmosphere with 5% CO_2 for 30 minutes.

The dynamic culture was performed using a double-syringe pump (Harvard Apparatus) for the control of the flow inside the two fluidic channels. Different flow rate (10 µL/min for chip featuring 400 µm wide channels; 5.4 µL/min and 1.8 µL/min for chip featuring 100 µm wide channels) – that guarantee to not overcome physiological velocities inside capillaries *in vivo* – were set and several time points were analyzed (7 days, 12 days, 18 days of dynamic culture).

3.2.10 PV- µTPs loading

The experimental phase inside the microfluidic device started with the PV- µTPs loading. µTPs were selected using p1000 pipette (Gilson) and a low-density suspension of tissues was injected in the loading inlet directly in the two chambers using a pipette-driven loading process. Optical microscope was used to control the correct loading, with fully-loaded chambers and µTPs contact with pillars, in order to obtain the needed interface for channels endothelialization step. µTPs inlets were then closed using 250 µm PDMS

membrane (realized with spin coater 500 rpm for 30 seconds) or PDMS cylinders obtained by punching a PDMS block.

3.2.11 Channels endothelialization

After µTPs loading, channels were coated with laminin (Laminin from Engelbreth-Holm-Swarm murine sarcoma basement membrane, Sigma-Aldrich) and devices were incubated at 37°C in a humidified atmosphere with 5% CO_2 for 30 minutes. After laminin removing by medium dilution, Human Umbilical Vein Endothelial Cells (HUVECs, Lonza) were seeded in both channels at a high density of 10000 – 15000 cells / mm^2. The devices were incubated for a minimum time of 3 hours, alternating vertical and horizontal positioning for cell adherence on each side of the channels, and avoiding channels drying by adding a drop of medium at the free inlets when necessary. Optical microscope was used to monitor HUVECs adhesion, and also a control of HUVECs in a petri dish was used to check cell adhesion. Once HUVECs adhered, devices were connected to syringe pumps (Harvard Apparatus) and flow was started at different flow rates (10, 5.4 and 1.8 µL/min) for 7, 10, 14 and 18 days of dynamic culture.

3.2.12 Vessel perfusion test

In order to assess vessel perfusability, a test was performed by using commercial FITC-fluorescent nanoparticles (NPs) with a nominal diameter of 0.52 µm (Fluoresbrite Carboxylate, Polysciences) from a stock solution with 2.6% of solid component. Confocal acquisitions at different concentrations revealed that the most suitable V/V concentration for acquisitions was 10 µL/mL. The microfluidic device, after PFA fixing and immunostaining for endothelium and laminin, was perfused with the NPs solution with a cross-flow (Figure 3.2.12.1): the bottom-left and up-right inlets were closed, and NPs flow was activated from up-left inlet, through the channels and tissue chambers towards the bottom-right outlet. Confocal acquisitions were performed after 15 minutes and 45 minutes, in order to assess the presence of NPs inside vessel lumina.

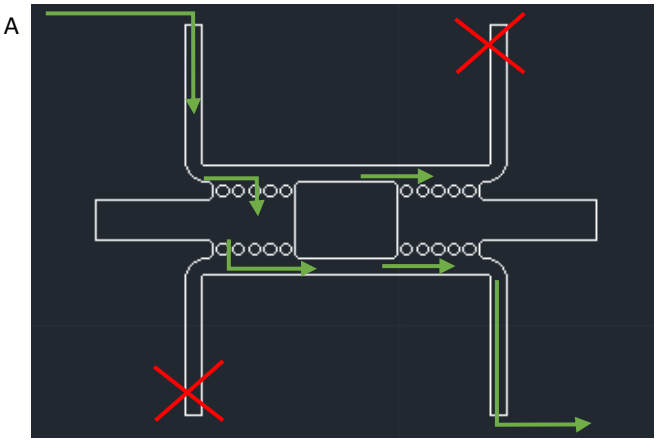

Figure 3.2.12.1: (A) Schematization of perfusion test performed with fluorescent NPs, whose flow – represented with green arrows – started from up-left inlet and ended at bottom-right outlet. Cross-flow was guaranteed by closing bottom-left and up-right inlets.

3.3 Results and discussion

3.3.1 µTPs characterization

In order to determine the best conditions for pre-vascularization process, assessment of collagen fibers inside µTPs was fundamental, as the presence of well structured, organized and endogenous collagen fibers act as a support for HUVECs to adhere, proliferate and, in the presence of co-cultured HDFs which secrete growth factors such as VEGF and bFGF, self-assembly in tubular-like formations. The presence of collagen fibers also translates in healthy environment and viable HDFs that can express their functionality. After fixing µTPs, SHG was obtained by means of 2-photon excitation. Figure 3.3.1.1 show the results of the acquisitions: both images assess the assembly of different HDF-loaded gelatin beads, but while image (A) shows collagen fibers at their initial step of formation, image (B) show more structured collagen fibers, which can determine a support for HUVECs seeding and adhesion. This analysis allowed for the determination of the best time conditions for pre-vascularization processes, which is at least day 10 of spinner dynamic culture.

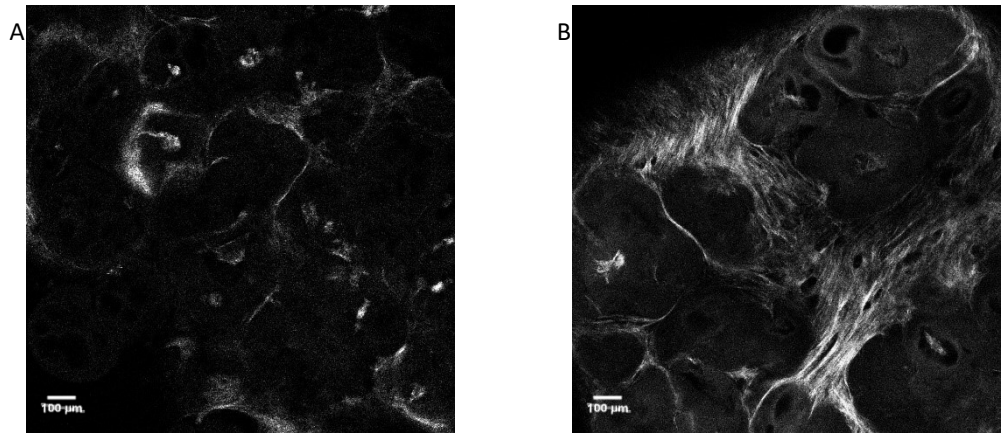

7 days uTPs

10 days uTPs

Figure 3.3.1.1: SHG for collagen fibers imaging inside µTPs at day 7 (A) and day 10 (B) of spinner dynamic culture. Both images show assembly of different HDF-loaded gelatin beads due to the formation of interstitial collagen fiber. Nonetheless, image (A) shows that collagen fibers are at their initial step of formation, thus more time is needed before HUVECs seeding for pre-vascularization process. On the other hand, image (B) shows more structured collagen fibers, which can act as a support for HUVECs adhesion during following pre-vascularization process. Scale bars are 100 µm.

3.3.2 PV-µTPs characterization

PV-µTPs characterization was performed by means of fixing, immunofluorescent staining and confocal imaging of pre-vascular network formed inside the ECM before PV-µTPs loading inside microfluidic devices. Figure 3.3.2.1 shows three different times (1 week, 2 weeks and 3 weeks) after HUVECs seeding on PV-µTPs surface and reports the assessed CLS area: HUVECs cultured in PV-µTPs in multiwell show a maximum of CLA area fraction after 1 week of culture, with a decrease in CLA area fraction after 2 and 3 weeks due to vessel pruning, probably caused by the absence of lumen perfusion, one of the fundamental physiological conditions of vessels *in vivo* [126].

After evaluating the long-term behaviour of HUVECs in PV-µTPs, shorter time intervals were assessed. Figure 3.3.2.2 shows that the proliferation of HUVECs and their initial assembly into tubular-like structures starts after 48 hours of dynamic culture inside a low-attachment multiwell. Due to the possibility of a dynamic culture on-chip, the idea was to proceed to PV-µTPs loading inside the devices after 48 hours from HUVECs seeding, in order to continue the process of capillary pre-network formation inside the chip; this strategy could synchronize the formation of a capillary pre-network via

vasculogenesis – with well-formed CLS at day 7 of dynamic culture – and the formation of angiogenic sprouts from endothelialized channels, which I demonstrated to occur after 7 days of culture in the previously described PVD on-chip model.

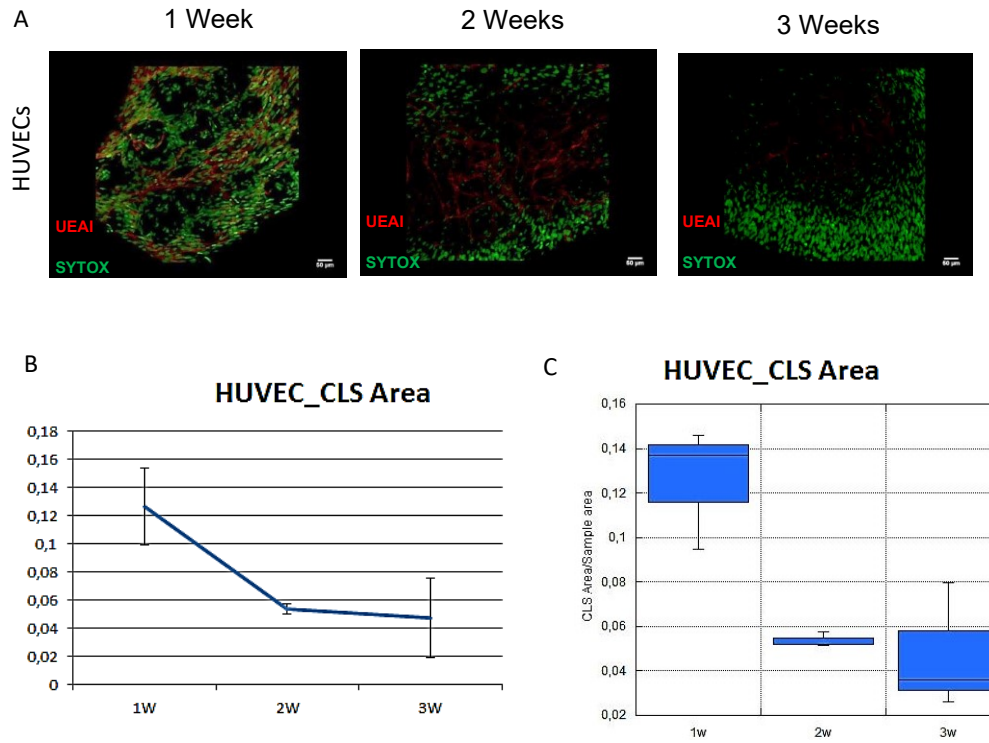

Figure 3.3.2.1: (A) Confocal images of CLS inside PV-µTPs at different time points (1 week, 2 weeks, 3 weeks) of multiwell dynamic culture [126]. Red signal shows HUVECs tubular formations, while green signal highlights HDF and HUVECs nuclei: it is possible to qualitatively evaluate a regression of CLS inside PV-µTPs, that has a pick at after 1 week of culture, and decreases as vessel tend to prune due to the absence of direct lumen perfusion.

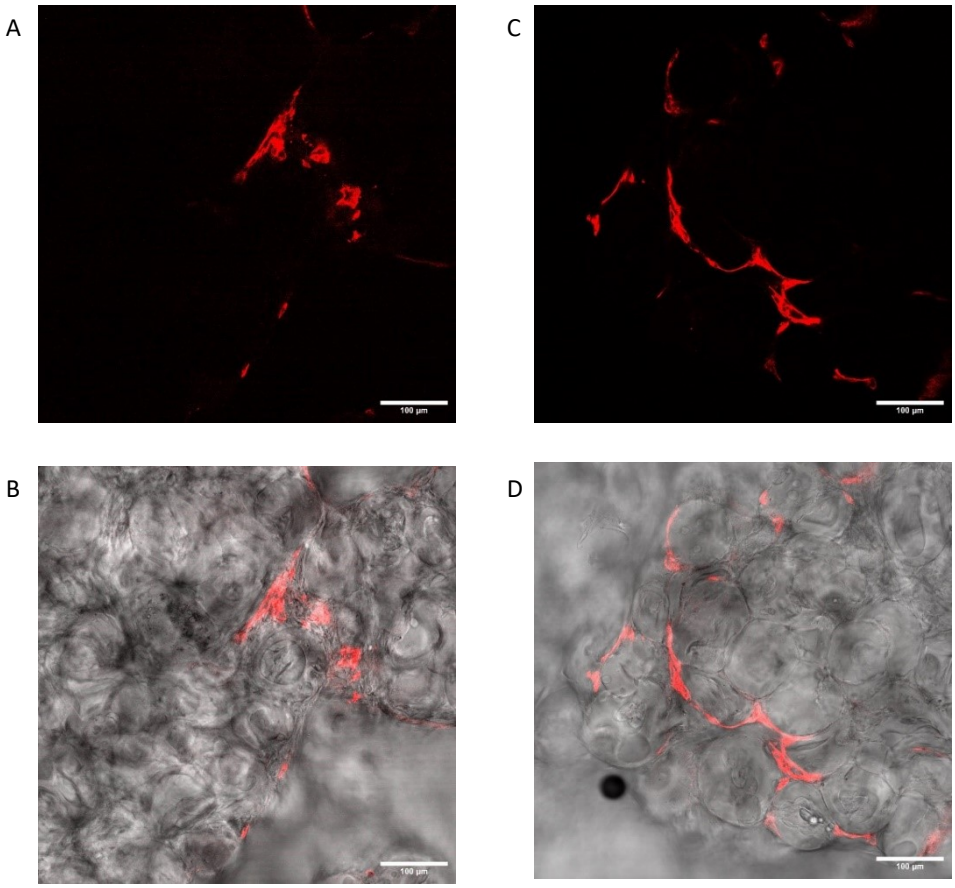

Figure 3.3.2.2: Confocal images of HUVECs (red) adhered on PV- µTPs surface (shown in bright-field images B and D). (A) Confocal image of HUVECs inside PV-µTPs 24 hours after seeding: HUVECs adhered, but no tubular formation can be individuated. (B) Confocal image of HUVECs (red) and bright-field of PV-µTPs. (C) Confocal image of HUVECs inside PV-µTPs 48 hours after seeding: HUVECs adhered and started to interact to form tubular structures. (D) Confocal image of HUVECs (red) and bright-field of PV- µTPs at 48 hours of dynamic culture inside multiwell. Scale bars are 100 µm.

3.3.3 Microfluidic device characterization

3.3.3.1 SEM characterization

In order to assess the quality of device fabrication and to measure the size of the designed pillars, chamber and channels, SEM imaging was performed. Quality of fabrication was evaluated by the difference between designed size and the measured size of channels width, chamber height, pillars diameter and interpillar distance,

reported in Table 3.3.3.1.1 SEM images show that the fabrication techniques allowed for a faithful replica of the designed device (Figures 3.3.3.1.1, 3.3.3.1.2 e 3.3.3.1.3).

Device feature	Designed size (µm) (D)	Measured size (standard deviation) (µm) (M)	[|D - M|/ D] (%)
Channel width	100	111.125 (2.916)	11.125
Chamber height	600	602.800 (9.899)	0.467
Pillars diameter	300	278.067 (4.197)	7.311
Interpillar distance	50	65.259 (4.964)	31.04

Table 3.3.3.1.1: Device features are reported: designed and measured features show slight differences due to fabrication technique resolution, which do not negatively affect the experiments.

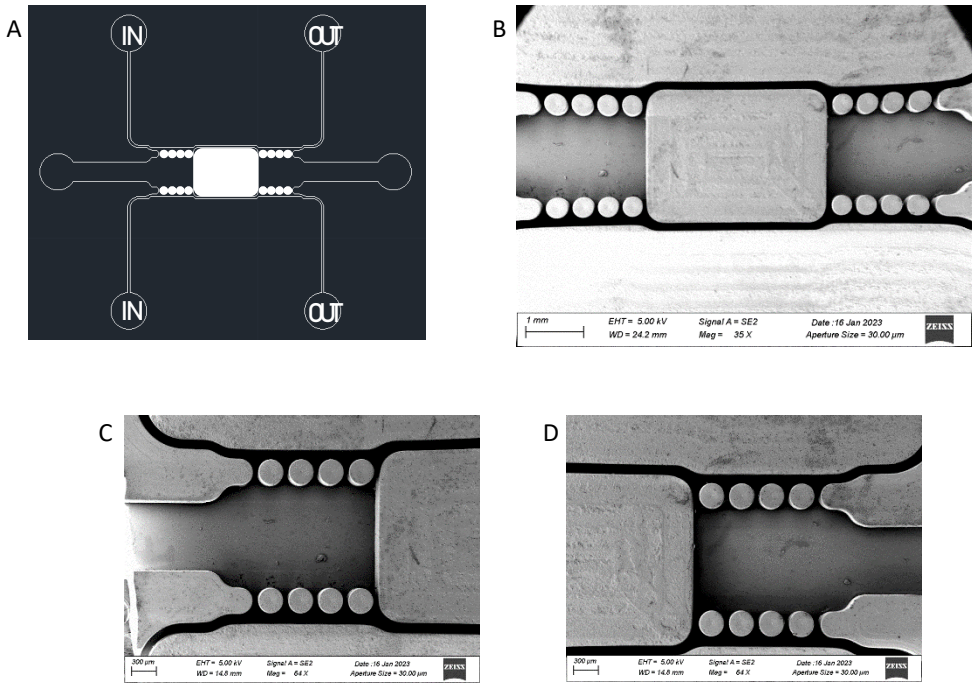

Figure 3.3.3.1.1: (A) Schematization of the designed device geometry. (B-D) SEM images of the fabricated PDMS device: image (B) shows the two tissue chambers with pillars for µTPs confinement, while images (C) and (D) show the left and right chambers, respectively.

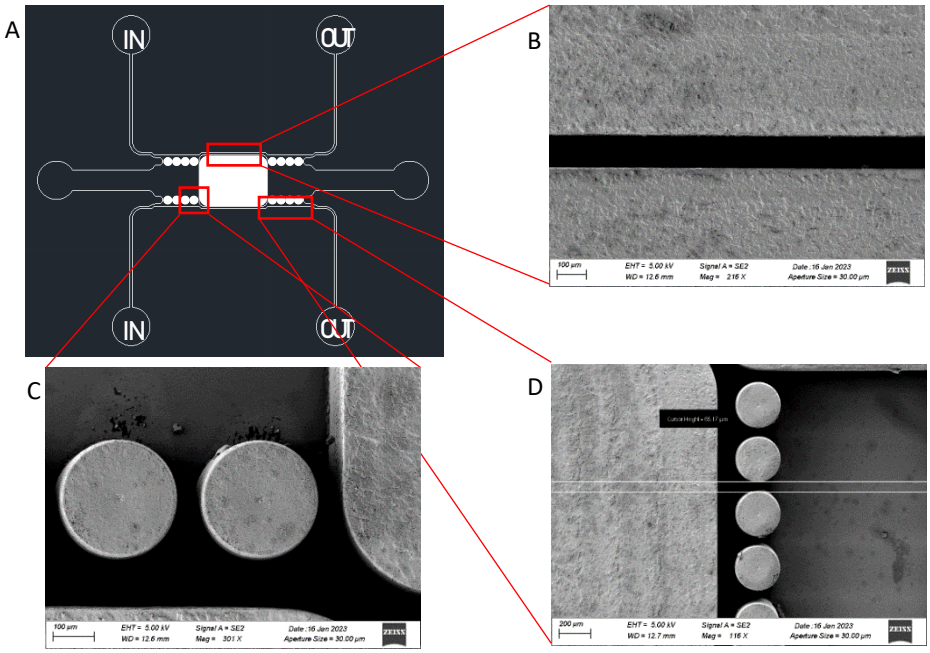

Figure 3.3.3.1.2: (A) Schematization of µTPs microfluidic device. (B) shows SEM image of fluidic channel. (C) shows a SEM image of interpillar space and the region between pillar and chamber bottom. (D) shows SEM image of a pillar row.

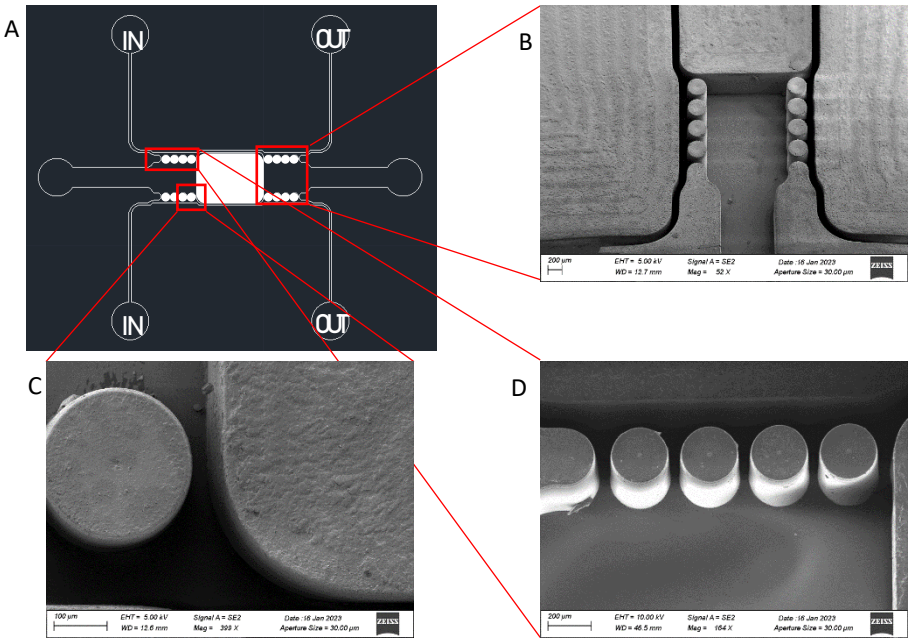

Figure 3.3.3.1.3: (A) Schematization of µTPs microfluidic device. (B) shows SEM image of µTPs chamber. (C) shows a SEM image of the region between pillar and chamber bottom. (D) shows SEM image of a pillar row.

3.3.3.2 CFD simulation

As described above, the CFD simulation allowed to determine if the device design and the dynamic culture conditions were able to guarantee viability of cells inside the channels and 3D stromal tissue. The first parameter for viability is O_2 concentration: in order to maintain their functionality, cells must be cultured at 0.22 mol/m^3 O_2 concentration. Physiological culture conditions need fluid velocity v below 1500 µm/s, which translates in a flow rate Q equal to or below 5.4 µL/min inside channels with cross-section area equal to 0.06 mm^2. Imposed the flow rate Q inside the two channels, CFD simulation determined flux lines, O_2 concentration and shear stress at channels walls. Figure 3.3.3.2.1 shows concentration inside the device: the lower concentration is equal to 0.203 mol/m^3, thus guaranteeing cell viability at steady state.

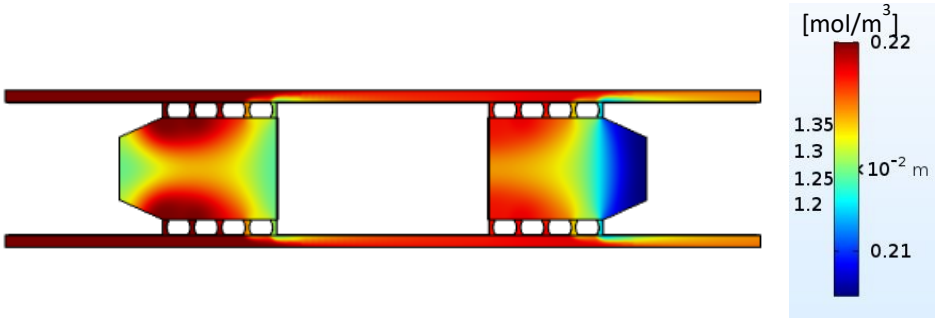

Figure 3.3.3.2.1: O_2 consumption (concentration [mol/m^3] by PV-µTPs inside tissue chambers with the physiological velocities imposed: concentration is maintained in a physiological range, thus guaranteeing cells viability during the anastomosis-on-chip experiments.

As described above, a single flow rate was maintained in the two channels, in order to maintain velocities inside fluidic channels below the limit of physiological capillary velocities. In particular, for the given cross-section area, a flow rate of 5.4 µL/min was necessary. CFD simulations were necessary to assess cell viability during dynamic culture with the parameters obtained by literature studies: CFD simulation confirmed that concentration was preserved in the totality of the chip volume, thus guaranteeing cell viability during the experiments at controlled velocities.

The velocity distribution with the given culture condition was assessed, determining values of velocities at the channel walls – thus on endothelial layer lining the channel walls – close to physiological velocities in human capillaries. Velocities on channel walls ranged between 452 and 525.8 µm/s (shown in Figure 3.3.3.2.2), guaranteeing cells adhesion preservation.

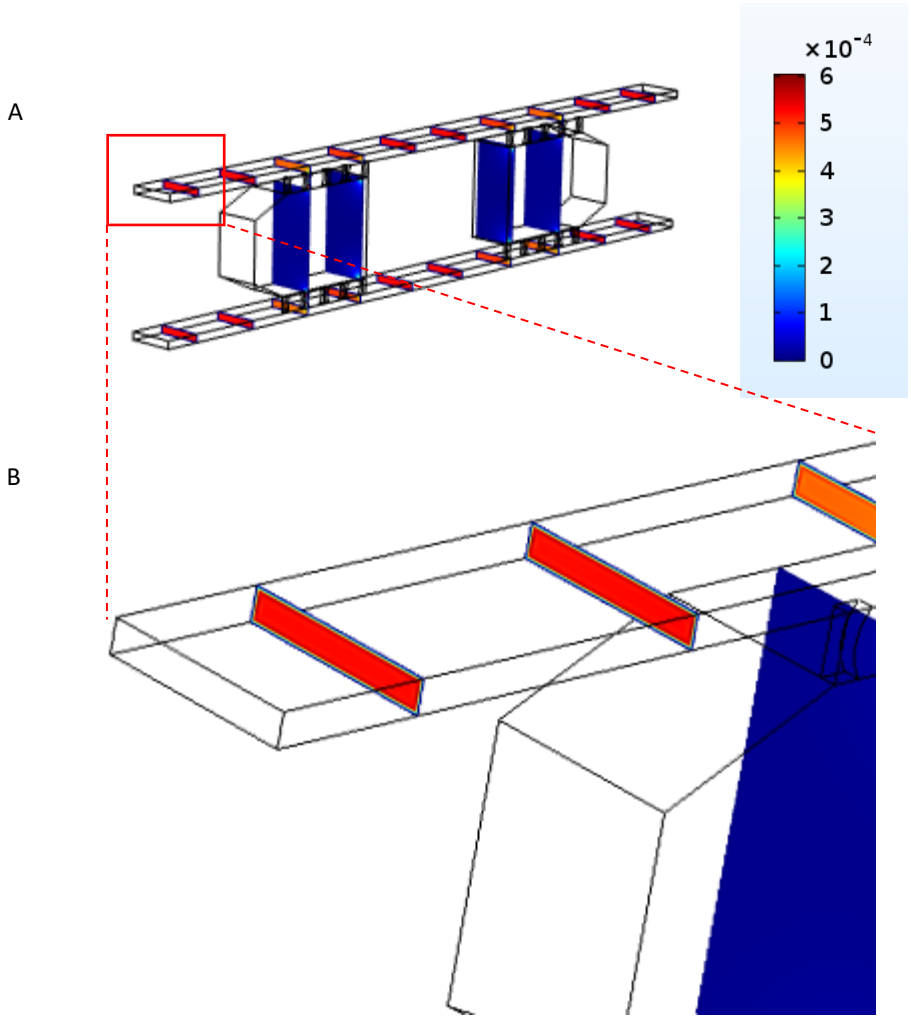

Figure 3.3.3.2.2: CFD simulation of velocity distribution inside the microfluidic device (A) and magnification of channels (B): velocity range between sub-physiological and physiological values.

The shear rate on endothelial walls was also assessed: as shown in Figures 3.3.3.2.3 and 3.3.3.2.4, shear rate at channels walls range between 60 and 70 s^{-1}, below the limit of physiological shear rate of 500 s^{-1}.

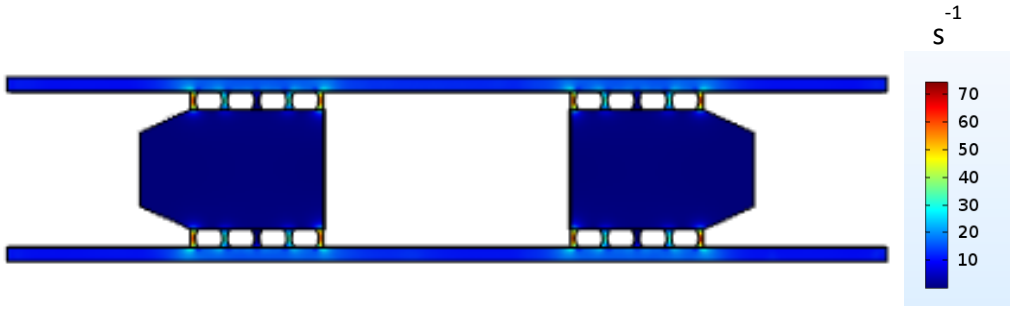

Figure 3.3.3.2.3: CFD simulation results of shear rate values inside the microfluidic device: numerical analysis shows that shear rate at endothelial walls inside channels range between 60 and 70 s^{-1}.

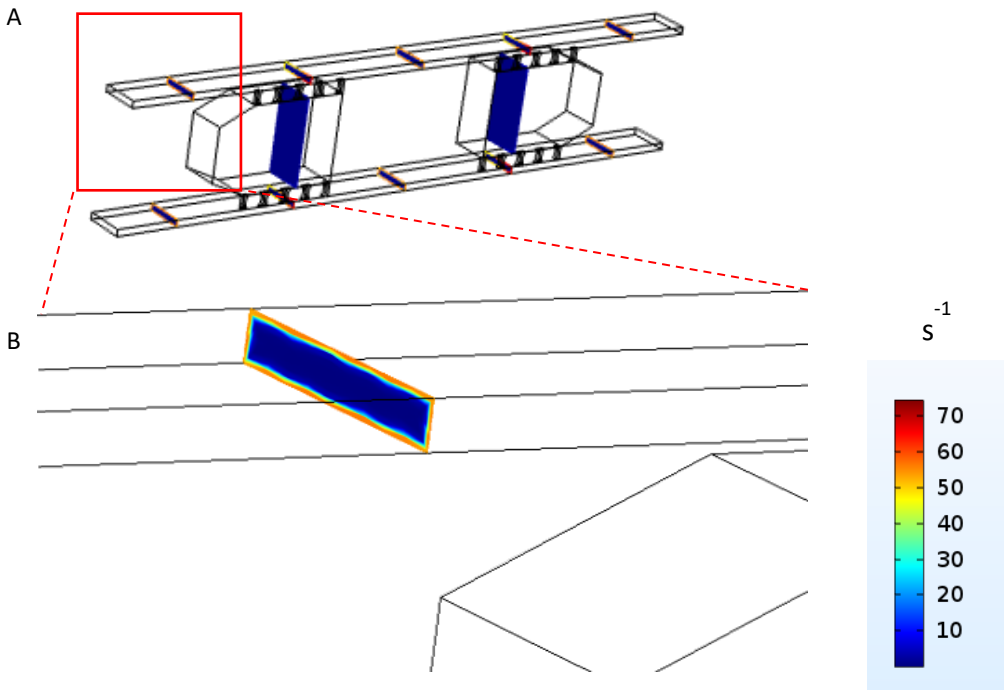

Figure 3.3.3.2.4: 45 degrees view of shear rate inside microfluidic device (A) and magnification of channel cross-section (B). Shear rate at endothelial walls inside channels range between 60 and 70 s^{-1}.

The shear stress on endothelial walls was also evaluated with CFD simulation, showing interesting results (Figure 3.3.3.2.5): endothelial walls inside channels undergo shear stress that range between 0.055 N/m^2 and 0.06 N/m^2, which is lower than physiological values assessed in literature [115]. As demonstrated in Seiler, sub-physiological range

of shear stress on endothelial walls influence the formation of angiogenic sprouts [20], which is the needed condition at tissue-channel interface.

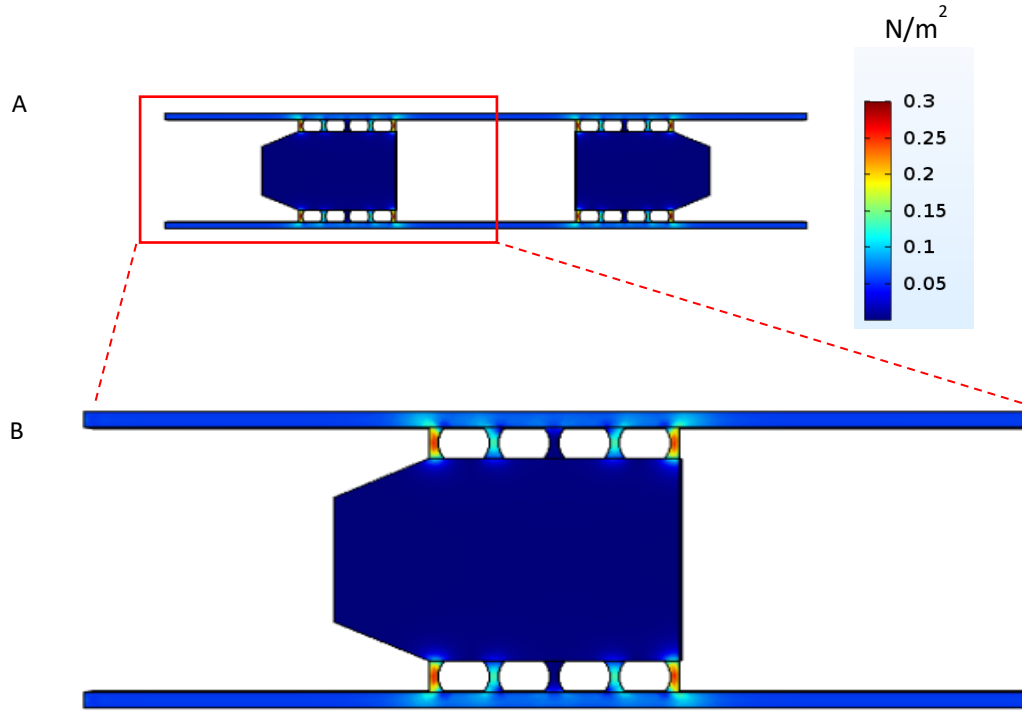

Figure 3.3.3.2.5: CFD simulation of shear stress inside microfluidic device (A) and magnification of left tissue chamber and channels (B). Numerical output showed that shear stress ranged between 0.055 N/m^2 and 0.06 N/m^2.

3.4 PV-µTPs loading

The experimental phase inside the microfluidic device started with the PV-µTPs loading, which represents the critical step regarding the formation of the correct interface to endothelialize: the idea of generating a tissue – channel interface constituted by PV-µTPs edges inside interpillar spaces determines the formation of a surface from which angiogenic sprouts can depart. By using a p1000 pipette (Gilson) it was possible to select the µTPs with diameter under 600 µm, which is the height of the device. A low-density suspension of tissues was injected in the loading inlet directly in the two chambers using a pipette-driven loading process and optical microscope was used to control the correct loading (Figure TOT), with fully-loaded chambers and µTPs contact with pillars, in order

to obtain the needed interface for channels endothelialization step. µTPs inlets were then closed using 250 µm PDMS membrane (realized with spin coater 500 rpm for 30 seconds) or PDMS cylinders obtained by punching a PDMS block.

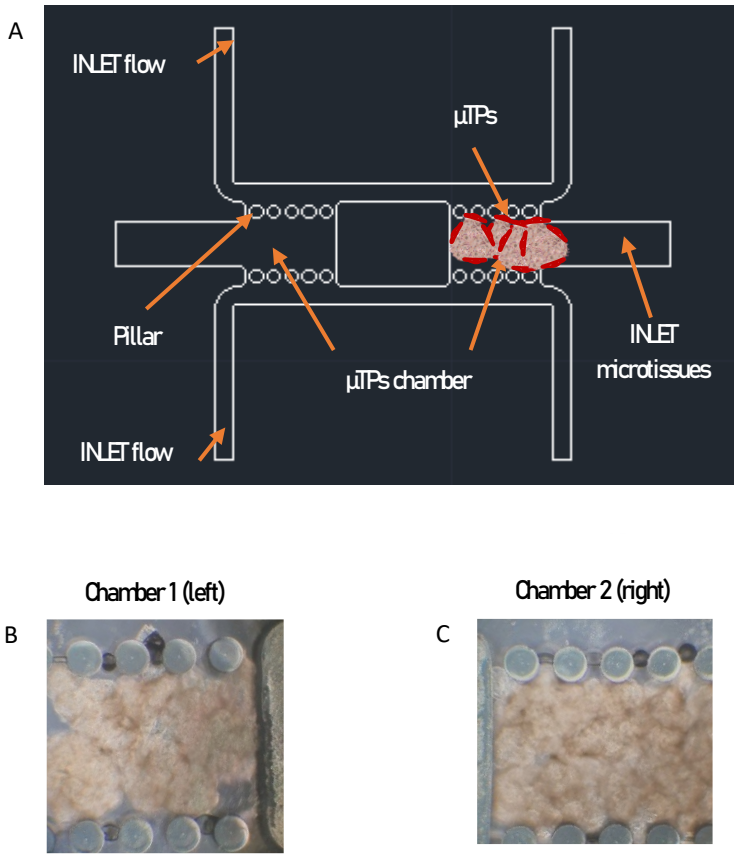

Figure 3.3.4.1: Process of PV-µTPs loading. (A) Schematization of pipette-driven loading. (B, C) 10x optical microscope image of left (B) and right (C) chamber showing correct loading. PV-µTPs fit in the chamber with no voids, and the interpillar space show a continuous interface constituted by PV-µTPs edges, which will undergo endothelialization process.

3.3.5 Channels endothelialization

Another important step for the anastomosis-on-chip strategy is channel endothelialization: endothelium seeding on lateral channels walls, under flow conditions and in the presence of a 3D stromal tissue equivalent (the PV-µTPs), represents the source of ECs for sprouting angiogenesis, thus determining anastomosis between fluidic channels and the pre-vascular network inside the PV-µTPs.

A

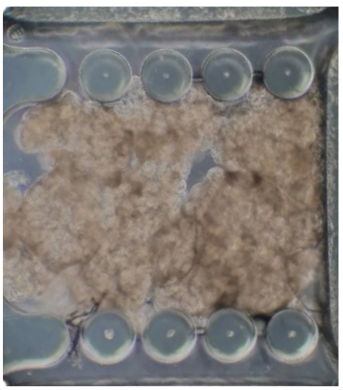

µTPs chip before channel endothelialization

B

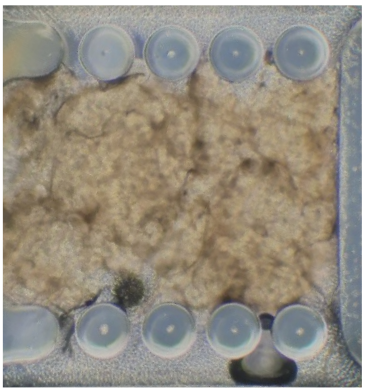

µTPs chip after channel endothelialization

Figure 3.3.5.1: Optical microscope images of PV-µTPs chip before (A) and after (B) channels endothelialization: it is possible to see HUVECs filling the channels in contact with PV-µTPs edges.

3.3.6 Dynamic culture system

The microfluidic approach relies on the control of parameters such as flow rate, velocities, shear stress and gradients. in order to fully control such parameters, a double-syringe pump was used for the dynamic culture of PV-µTPs chips. Dynamic culture of engineered 3D stromal tissues and endothelial layers inside a microfluidic device depend on several parameters: O_2 and nutrients must reach every region of the device in order to correctly resemble physiological conditions for cell viability, but the velocity, shear rate and shear stress exerted on endothelial cells layer must not overcome the physiologically "sensed" values inside capillaries (500 – 1500 µm/s for velocity, 100 – 500 s^{-1} for shear rate, 0.5 -1 N/m^2 for shear stress). As previously

described, a CFD simulation can determine if the needed flow rates are sufficient for nutrition of 3D stromal equivalent and HUVECs during dynamic culture. Given the crucial role of velocities, shear rate and shear stress for ECs elongation, maintenance in a long-lasting system and to preserve adhesion of cells to channels, syringe pumps revealed to be the most reliable system for controlled dynamic culture on the designed microfluidic platform (Figure 3.3.6.1).

As previously described, angiogenic sprouts inside the PVD microfluidic platform developed in both directions (towards and opposite to transverse ΔP): the same flow rate was imposed in both channels, in order to generate a channel velocity below 1500 µm/s – maximum of physiological range 500 – 1500 µm/s inside human capillaries *in vivo* – which allows for EC elongation for the formation of a confluent monolayer. Given that the cross-section area of fluidic channels is (0.1 x 0.6) mm^2, it is possible to obtain the flow rate to be imposed from the formula $Q = v \cdot A$, where Q is the flow rate, v the velocity and A the cross-section area. The obtained flow rate was 5.4 µL/min, which can be exerted by syringe pump system.

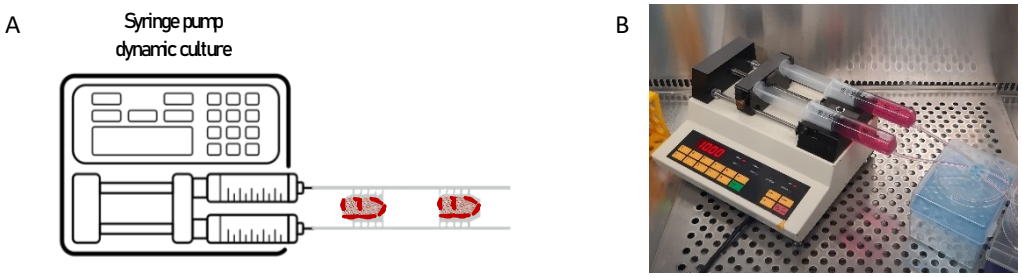

Figure 3.3.6.1: Schematization (A) and image (B) of double-syringe pump dynamic culture system: after PV-µTPs loading and channels endothelialization with HUVECs endothelial cells, each channel of microfluidic platform was connected a syringe with cell culture medium and a flow rate of 5.4 µL/min or 1.8 µL/min (corresponding to channel velocity of maximum and minimum of physiological velocity range inside human capillaries, respectively). The syringe pump system allows for fine control over flow rate, thus generating a reproducible mechanical stimulation on endothelial walls and on PV-µTPs.

3.3.7 Long-lasting dynamic culture of PV-µTPs devices for anastomosis investigation

The above-described experimental set-up led to several results:

- µTPs assembly on-chip;
- anastomosis between fluidic channels and capillary pre-network inside PV-µTPs;

- long-lasting capillary network inside a custom-designed microfluidic platform;
- Perfusability of capillary network through microfluidic channels.

The introduction of PV-µTPs instead of a pre-formed 3D stromal tissue equivalent could determine issues in the formation of an interconnected, perfusable network inside a microfluidic device: the pre-formed tissue described in chapter 2 already presented a pre-vascular network with interconnected vessels, while each PV-µTP present an independent incipient pre-vascular formation at the step of injection inside the device. Nonetheless, the syringe pump-based dynamic culture determined the assembly of PV-µTPs into a single tissue with interconnected vessels after 7 days of culture: this phenomenon was due to the dynamic culture conditions, which represent a stimulus both for HDFs – inside the 3D ECM for collagen and laminin secretion and remodeling – and for HUVECs communication that led to their assembly in tubular shapes and connection between the HUVECs populations of different PV-µTPs.

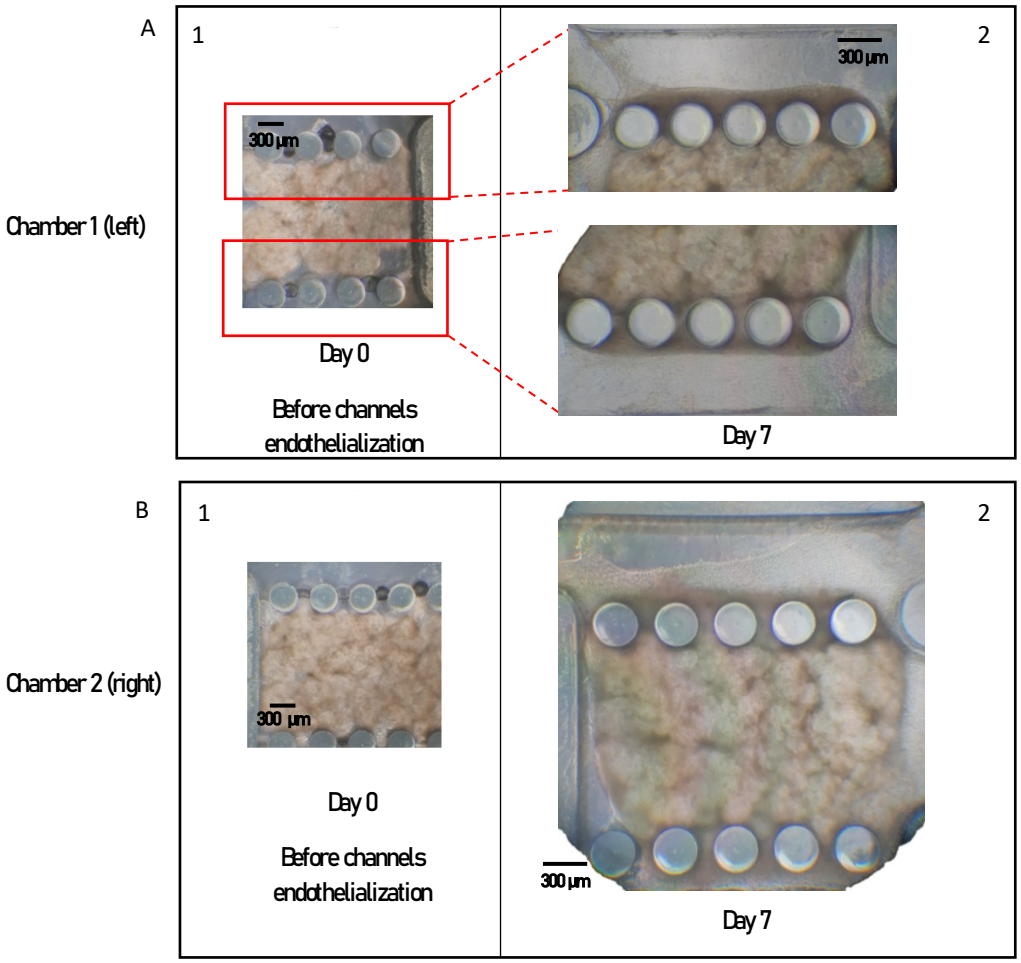

Figure 3.3.7.1: Optical microscope images at 10x magnification showing PV-µTPs assembly inside the designed microfluidic device. Image (A.1) and (B.1) showing the two PV-µTPs chambers at the loading step: separated PV-µTPs confined in the chambers by pillars can be individuated. Images (A.2) and (B.2) showing the same chambers after 7 days of culture: PV-µTPs assembly is clearly visible and, in addition, PV-µTPs interaction with HUVECs inside channels determined clutching of µTPs to the pillars, as a response to the dynamic culture, thus generating a perfect interface for endothelium adhesion and following sprouts formation. Endothelium can also be seen inside the channels. Scale bars are 300 µm.

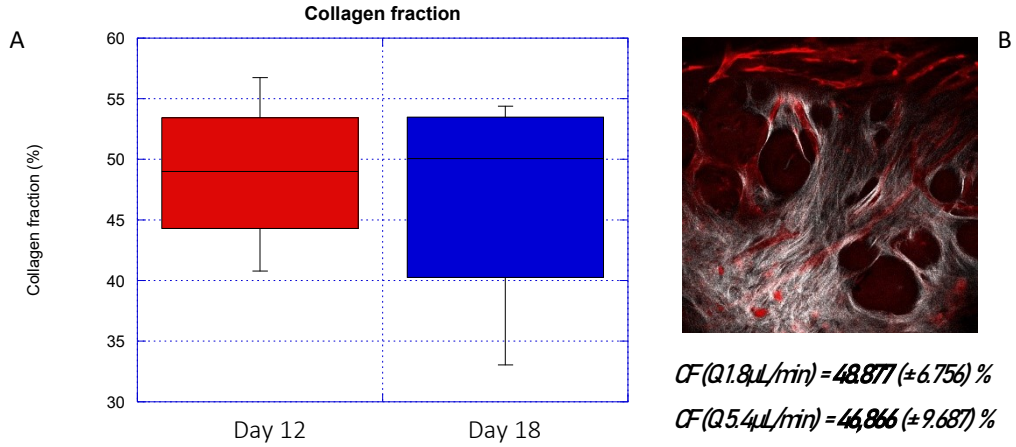

Figure 3.3.7.2: (A) Graph of measured collagen fraction (CF) inside the assembled PV-µTPs at day 12 and day 18 of dynamic culture: CF % values – also reported at bottom-right corner - are comparable, thus resulting in a stable ECM and no degradation of collagen, thus highlighting the 3D stromal tissue viability inside the designed device for at least 18 days. Confocal image (B) represents an example of endogenous collagen fibers inside the PV-µTPs, with well-structured ECM, imaged by means of 2-photon excitation for SHG.

In order to determine the role of dynamic flow on PV-µTPs assembly and capillary network formation inside the microfluidic device, control samples were maintained in static culture conditions, and stained as the dynamic culture sample to assess HUVECs configuration in the channels and inside the tissue. The results reported in Figure 3.3.7.3 show that static culture conditions only allowed for partial PV-µTPs assembly, and HUVECs did not develop an interconnected capillary network, but adhered at the periphery of each PV-µTP, thus anastomotic phenomena could not occur: this cellular and ECM configuration shows the important role of a dynamic culture for the development of endogenous ECM molecule and the formation of an interconnected capillary network with an accessible lumen. The design of the microfluidic platform, combined with the dynamic culture system, determined the perfect conditions for both PV-µTPs assembly and capillary network development.

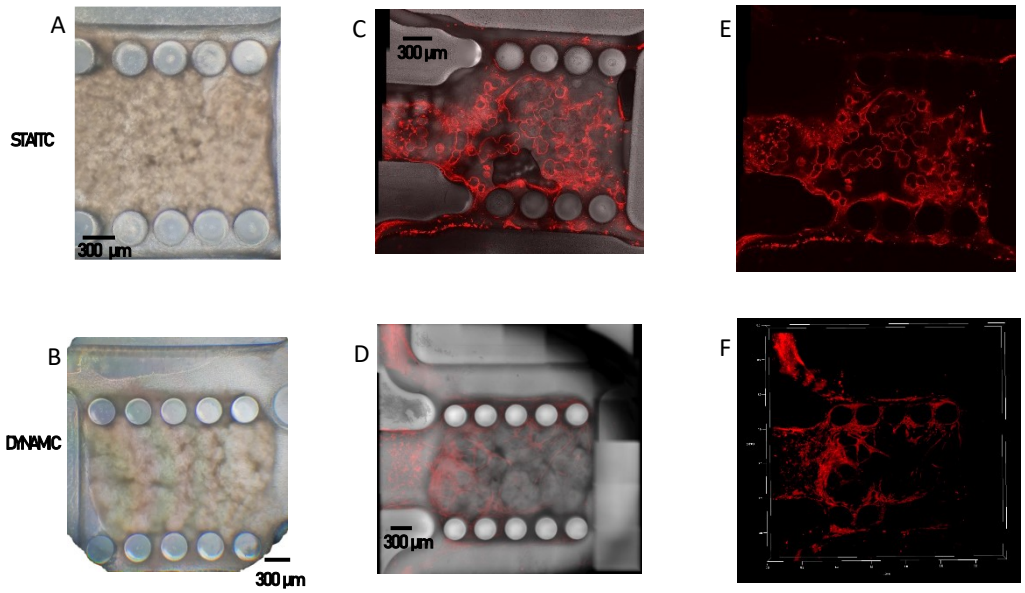

Figure 3.3.7.3: Optical microscope (A, B), confocal (C, D) and 3D reconstruction (E, F) images of microfluidic device with PV-µTPs and endothelialized channels at day 7 of chip culture. The first row of images shows the effect of static culture conditions, while second row of images shows the effect of dynamic culture conditions. Images (A, B) clearly show the assembly of PV-µTPs, which is only partial in the static culture condition chip, while it is complete and mature in the dynamic culture condition chip at day 7 of culture. Confocal images (C, D) show endothelial cells (red) and bright-field signal: image (C) highlights the localization of HUVECs at the peripheric part of PV-µTPs, with no capillary assembly formations; on the other hand, image (D) shows an interconnected capillary network and angiogenic sprouts inside the channels, thus highlighting the positive effect of dynamic culture on the 3D capillary network development in a stromal equivalent on-chip. Images (E, F) represent a 3D reconstruction of HUVECs organization in the 3D ECM, with no lumen in the static conditions, and interconnected capillary network shown in the dynamic culture conditions. Scale bars are 300 µm.

The second result regards anastomosis between fluidic channels and capillary pre-network inside PV-µTPs: this phenomenon occurred at day 7 of dynamic culture, as shown in Figures 3.3.7.4, 3.3.7.5 and 3.3.7.6. The combination of dynamic culture, the secretion of growth factors such as VEGF and bFGF by HDFs from µTPs and the designed geometrical cues of microfluidic platform (*i.e.*, pillars and interpillar spacing) allowed for the generation of a capillary network inside an engineered 3D stromal tissue that connected to fluidic channels through the presence of endothelial tubular formations inside the channels.

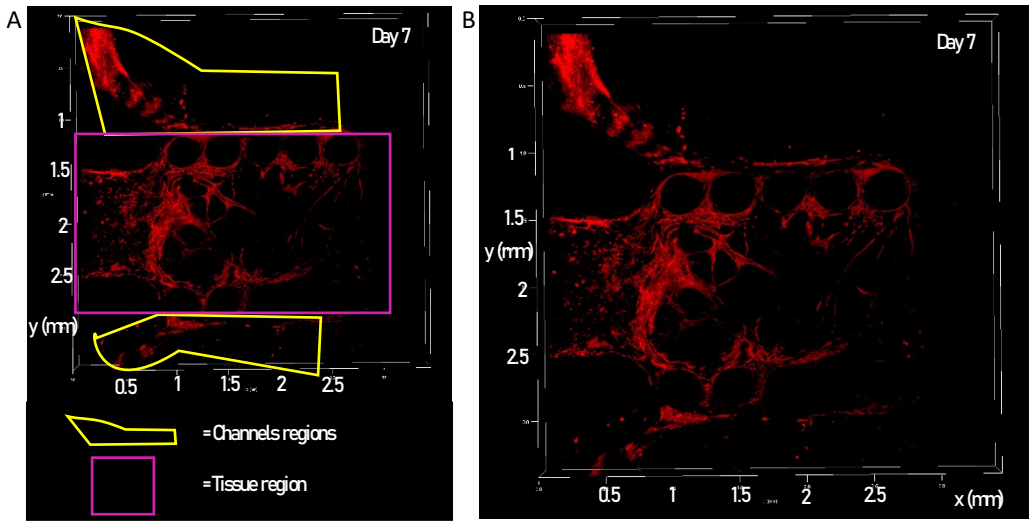

Figure 3.3.7.4: 3D reconstruction obtained with LAS X software tool from a confocal z-stack tile scan acquisition of the left chamber of a microfluidic platform after 7 days of dynamic culture. Red signal represents HUVECs endothelial cells. Anastomotic, interconnected capillary network inside the microfluidic device is clearly visible. Image (A) shows the channels region (yellow) with capillary structures formed by HUVECs, that anastomose with the capillary network inside the tissue region (magenta) at the interpillar spaces (pillars are represented by the black circular voids). Image (B) shows a magnification of the 3D reconstruction. Anastomosis between HUVECs tubular formations inside the channels and capillary network inside the tissue is visible at the interpillar spaces, and an interconnected capillary network is shown inside the 3D tissue between the two pillar rows.

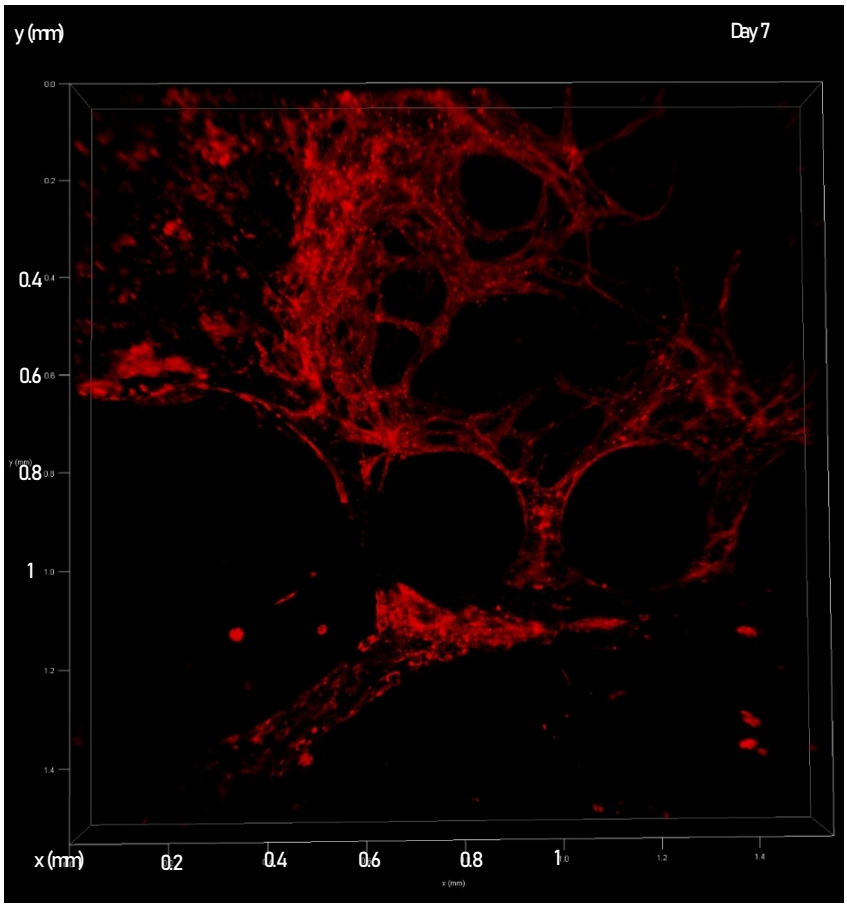

Figure 3.3.7.5: Magnification of the 3D reconstruction of capillary network inside the PV-µTPs on-chip after 7 days of dynamic culture: the network anastomoses to the angiogenic sprout inside the lower channel (bottom-left) through the interpillar spaces.

Further investigations were necessary to obtain information regarding anastomosis between the capillary network and the fluidic channels. The formation of angiogenic sprouts inside the channels determine a connection between the vasculature inside the 3D tissue and the channels. Angiogenic sprouts formed inside the channels present diameter that range from 22 µm to 58 µm: this configuration does not allow for complete endothelial lining of channel walls, thus determining the formation of an intra-channel sprout which, nonetheless, anastomose to the vasculature inside the 3D stromal tissue.

Endothelial layers are usually extremely fragile and tend to disrupt with high flow rates if no support is present [7]: the angiogenic sprouts formed inside the microfluidic channels present a laminin layer around the external part of endothelial layer (Figure

3.3.7.6) that acts as a mechanical support for angiogenic sprout, thus determining its stability along dynamic culture. Laminin support, which resembles physiological conditions of capillaries *in vivo*, is usually produced by fibroblasts: it is reasonable to hypothesize that HDFs inside PV-µTPs inside the tissue chambers "sense" HUVECs inside channels and, through cross-talk and communications, determine interactions that may lead to the secretion of laminin on endothelial layer by HDFs: this phenomenon determines stabilization of angiogenic sprouts inside channels, even for the part of endothelium that does not directly adhere at channels walls.

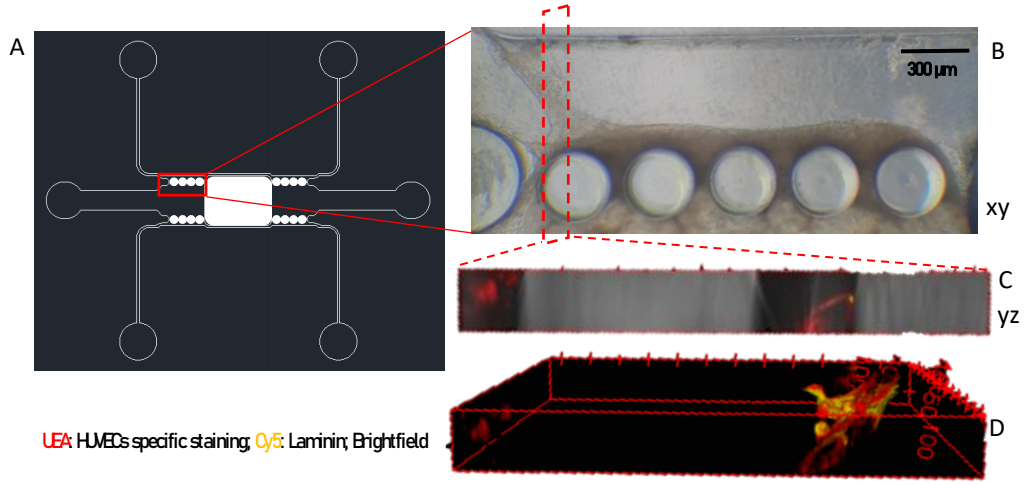

Figure 3.3.7.6: Angiogenic sprout formation inside up-channel, left side. (A) Schematization of microfluidic device. (B) Optical microscope magnification (10x) of upper part of left chamber with visible angiogenic sprout and tissue clutching pillars. Scale bar is 300 µm. (C) Confocal yz cross-section of up-channel – with angiogenic sprout – and tissue close to the pillar, obtained from a 3D reconstruction of a fine z-stack acquisition: HUVECs (red) co-localize with laminin (yellow) inside fluidic channel, and a perfusable lumen is clearly visible. (D) 3D reconstruction of angiogenic sprout with a slight rotation which allows to observe the co-localization of endothelial wall (red) and laminin (yellow).

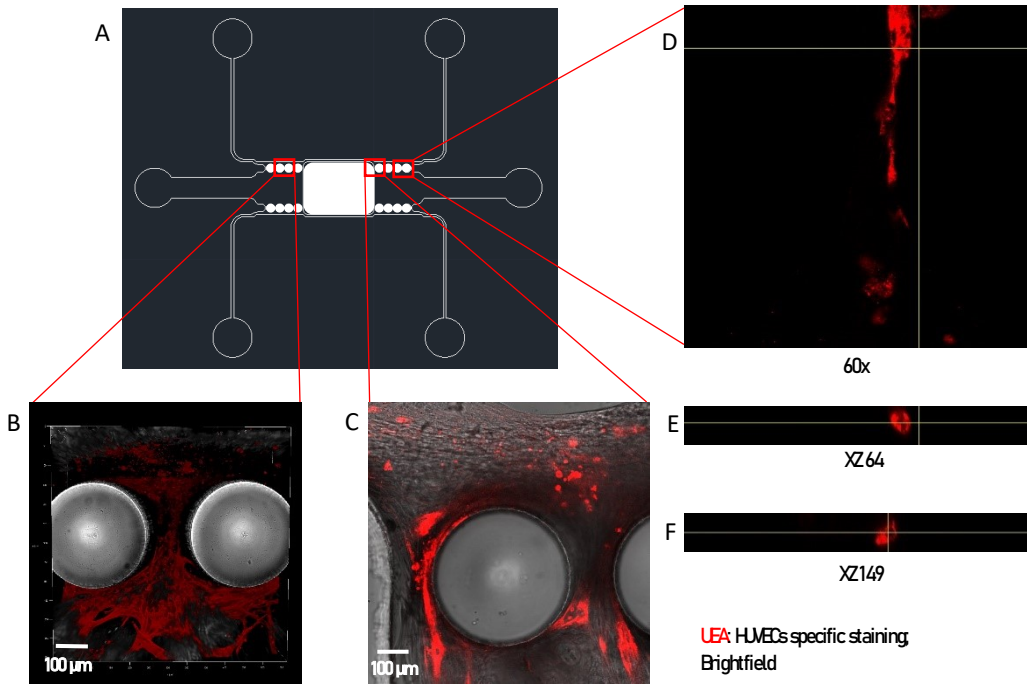

Figure 3.3.7.7: Different anastomotic points inside microfluidic device at day 7 (B, C) and day 14 (D) of dynamic culture. (A) Schematization of microfluidic device. (B) Confocal image of capillary formation (red) in the interpillar space in left chamber at day 7 of dynamic culture. Scale bar is 100 µm. (C) Confocal image at day 7 of dynamic culture of endothelial tubular formations around first pillar in right chamber, partially highlighted with red signal and partially shown by bright-field: the dotted pattern above the pillar – inside the channel – represents a combination of HDFs and HUVECs inside the channel, which interact with the capillary structures inside the chamber – below the pillar. Scale bar is 100 µm. (D) Confocal image at day 14 of dynamic culture showing HUVECs angiogenic sprout (red) in the interpillar region of right chamber (bright-field not shown). (E) and (F) images represent angiogenic sprout cross-sections at interpillar space, at different xz-plane (xz 64 is closer to channel; xz 149 is closer to tissue). Images (E, F) were obtained from a 3D reconstruction of a fine z-stack acquisition: HUVECs circular formations represent vessel cross-section at different distances from tissue, thus guaranteeing a continuous lumen from channel to tissue.

In order to determine if the angiogenic sprouts preserve the feature of long-lasting, dynamic culture on microfluidic device was maintained for 18 days, and angiogenic sprouts were investigated at different time points. Figure 3.3.7.8 highlights the presence of angiogenic sprouts at the tissue-channel interface at different time points (day 7, day 12 and day 18 of dynamic culture).

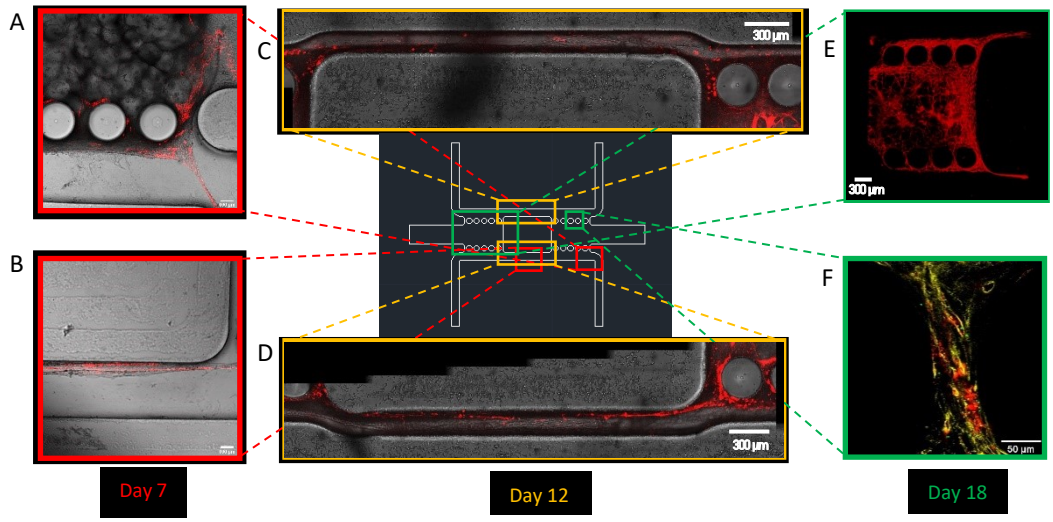

Figure 3.3.7.8: Angiogenic sprouts at different time of dynamic culture. (A, B) Confocal images at day 7 of dynamic culture of angiogenic sprouts at bottom-right tissue-channel interface at right chamber (A) and inside low-channel between the two tissue chambers (B): HUVECs (red) form capillary structures that connect the tissues. Scale bars are 100 µm. (C, D) Confocal tile-scan of up-channel (C) and low-channel (D) inside a microfluidic device cultured for 12 days: both channels present a tubular formation of HUVECs (red) that anastomose to both tissue chambers (visible also in bright-field). Scale bars are 300 µm. (E, F) Confocal images of angiogenic sprouts at day 18 of dynamic culture inside the device: HUVECs (red) inside up- and low-channels assembly into tubular formations – visible in the right part of image – and anastomose to vasculature inside the chamber (tile-scan of left chamber E, scale bar is 300 µm). Image (F) shows interpillar space with HUVECs (red) and laminin (yellow) forming tubular shapes at tissue-channel interface. Scale bar is 50 µm.

3.3.8 CLS quantitative assessment at different days (vessel lumen)

Once evaluated the formation of a capillary network inside the ECM of a 3D stromal equivalent on-chip and its anastomosis with the fluidic channels at day 7 of culture, the possibility to obtain a long-lasting capillary network with perfusable lumen on-chip was investigated, in order to obtain a reliable microfluidic platform for the study of vascularization phenomena and endothelial cells behaviour in a 3D endogenous ECM during long intervals of time, which involves ECM remodeling studies. The dynamic culture was maintained for 18 days, and the microfluidic devices were investigated by means of confocal imaging, with the following results: by analyzing as time points day 12 and day 18, it was possible to verify that:

- PV-µTPs presented highly-branched, interconnected capillary network inside ECM at different time points;
- Angiogenic sprouts from tissue to channels was detected at different time points;

- Lumen inside vessels was individuated with z-stack confocal acquisition with 1 µm slice thickness for high-resolution imaging.

Regarding the first point, Figure 3.3.8.1 shows the development of capillary network at different time points (day 7, day 12 and day 18 of on-chip dynamic culture). It is important to note that endothelial cells adhered on stromal ECM of PV-µTPs 3 days before on-chip loading, thus leading to a 21 days-vascularization at the last time point investigated. It is possible to highlight the important role of dynamic culture for long-lasting development of vascular networks inside a stromal ECM and its anastomosis to angiogenic sprouts in the fluidic channels, together with the presence of VEGF and bFGF [17], growth factors secreted by HDFs inside the tissue chambers.

it is interesting to observe vessel area fraction (AF) trend versus time, in order to determine how dynamic culture and growth factors inside the microfluidic device influenced HUVECs behaviour, growth and vascularization phenomena and whether the designed microfluidic device is suitable or not for a long-lasting vascularization model platform. A trend showing an increase in vessel AF with time can represent an indicator of the possibility of strongly prolonging vessel maturation and lasting for even more than the 21 days obtained. In particular, Figure 3.3.8.2 shows AF trend for the previously mentioned time points (day 7 – shown as week 1, day 12 – shown as week 2, and day 18 – shown as week 3): an increase in area fraction with time was detected, from a value of 12.117 % at week 1 of dynamic culture to a value of 16.496 % at week 3 of dynamic culture, with only a slight decrease from week 1 to week 2, maybe due to the angiogenic formations towards the channels, outside the tissue chamber. This result represents an important step for long-lasting vascularization on-chip studies, as the designed microfluidic platform can be considered as a reliable tool for the development of an *in vitro* vascularization model on a chip inside a 3D stromal tissue equivalent with endogenous ECM, and with angiogenic sprouts that anastomose the network to the fluidic channels, for at least 18 days of syringe pump dynamic culture – 21 days since vascularization process started in PV-µTPs.

A

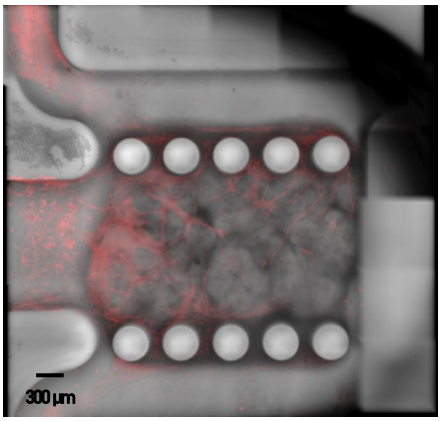

B

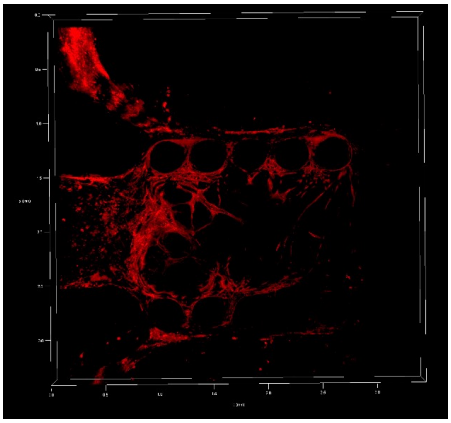

Day 7

UEA: HUVECs; Brightfield

C

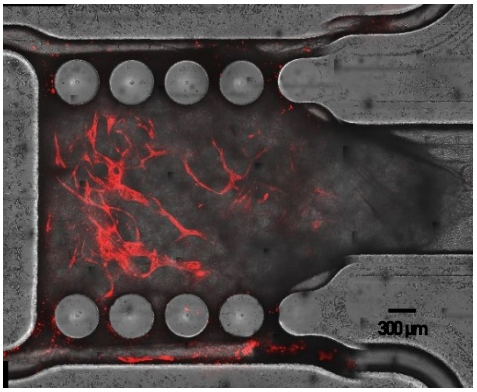

D

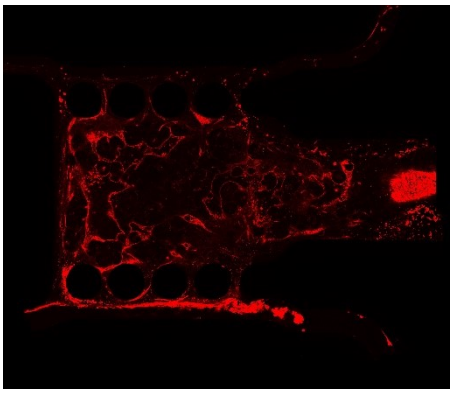

Day 12

UEA: HUVECs; Brightfield

E

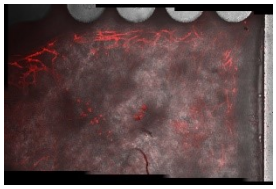

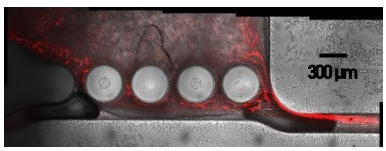

F

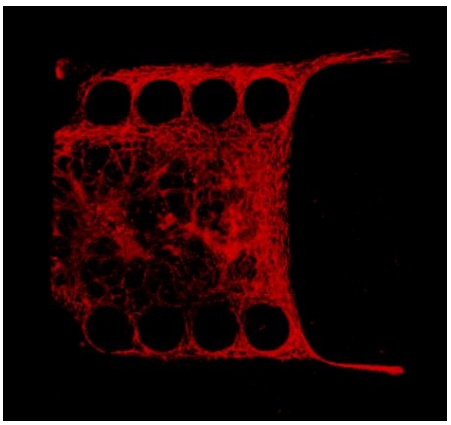

Day 18

UEA: HUVECs; Brightfield

Figure 3.3.8.1: Confocal images (A, C, E) and 3D reconstructions (B, D, F) of interconnected capillary networks and endothelial formations in channels that anastomose to capillaries inside stromal tissue on microfluidic devices at different time points (day 7, day 12, day 18) of dynamic culture at 5.4 µL/min (which guarantees velocity below the maximum of physiological velocity range of 1500 µm/s inside the fluidic channels). It is important to note that endothelial adhesion to stromal ECM was obtained 3 days before introduction of PV-µTPs inside the device, thus translating in a vascularization of 21 days at the last time point investigated. Scale bars are 300 µm.

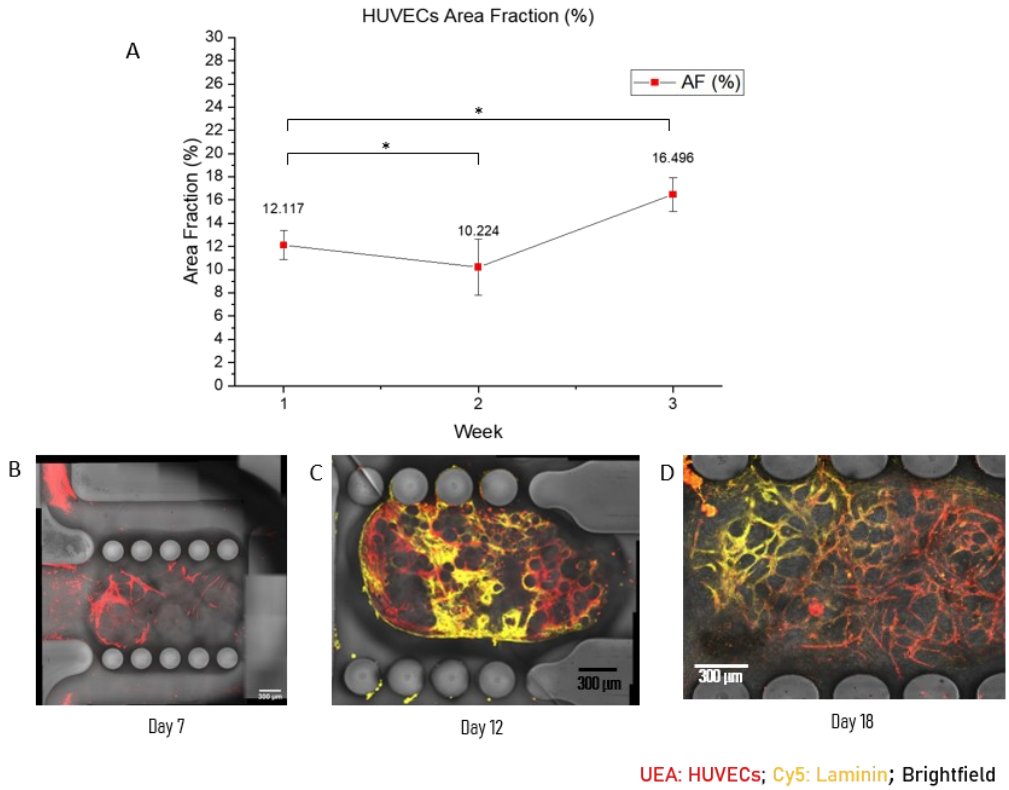

Figure 3.3.8.2: HUVECs Area fraction (AF) trend versus time. (A) Graph or AF (%) values at day 7, day 12 and day 18 of dynamic culture on-chip: AF shows a slight decrease at day 12, probably due to HUVECs migration towards fluidic channels, and an increase at day 18, that highlights cell viability and the key role of dynamic flow and growth factors secreted by HDFs for HUVECs proliferation with tubular assembly in an interconnected network. *$p < 0.05$. Confocal images (B, C, D) show capillary networks inside the 3D stromal tissue inside the microfluidic device at day 7 (B), day 12 (C) and day 18 (D).

After the assessment of vessel area fraction inside the microfluidic platform, CLS can be characterized for capillary diameter size and junction density in order to determine the

interconnectedness rate of the network as a parameter of CLS development. As shown in Figure 3.3.8.3, the number of junctions per μm^2 (as area fraction, junctions/μm^2 present the same trend as junctions/μm^3) increases with time under dynamic culture on-chip. Junctions represent the interconnectedness rate, thus capillary network development inside the tissue, as formation of new vessels usually occurs by splitting from a single vessel to two or three vessels [136]: an increase in junctions density translates in capillary network maturation and development with time.

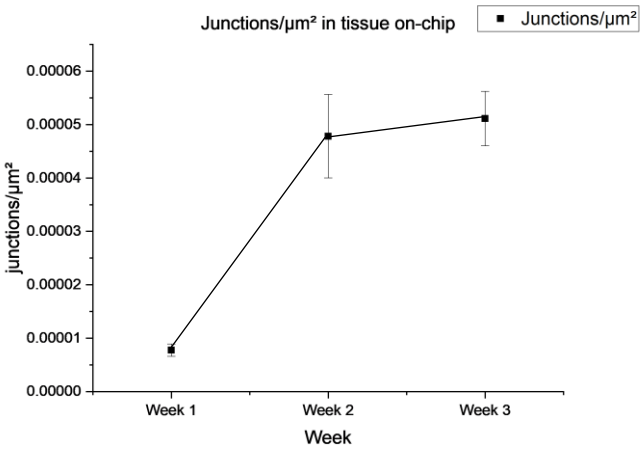

Figure 3.3.8.3: Graph of junction density trend with time: increase in number of junctions translates in capillary structure physiological development by splitting angiogenesis.

Capillary diameters were measured in different samples, and ranged between 9.830 µm to 25.350 µm, which belong to the range of physiological human capillaries *in vivo*.

3.3.9 Vessel maturity: co-localization of laminin and collagen fibers with vascular network as a key element for long-lasting capillary structures

Once the capillary network inside the PV-µTPs was characterized and analyzed in its features, it was important to observe the reasons why the capillary network developed inside the microfluidic device for a long interval of time: maturity of vessels is fundamental, together with perfusability, for the maintenance of a vascular network without vessel pruning. In order to assess vessel maturity, the co-localization of endothelium with collagen fibers and laminin represents a valuable parameter: laminin is the major constituent of basement membrane, the substrate on which endothelial layer stabilizes as the vessel develops; collagen fibers act as a structural component for

mechanical support of vascular vessels, thus generating the conditions for vessel maturity and, as a result, long-lasting network. Figure 3.3.9.1 shows laminin – HUVECs co-localization at day 18 of dynamic culture, in comparison with a static culture chip with low laminin signal and no tubular formations by HUVECs: dynamic culture represents an important parameter for vessel maturity. Figures 3.3.9.2 and 3.3.9.3 present a comparison between day 12 and day 18 of dynamic culture for laminin formation: the presence of co-localization of HUVECs vessels with laminin at both time points underlines the maturity of the network, without regression and pruning of vessels. Figure 3.3.9.4 shows the results of immunostaining following standard confocal acquisitions and 2-photon excitation for SHG – for collagen imaging – which allowed for the assessment of co-localization of capillaries, laminin and collagen fibers inside microfluidic devices at different time points of dynamic culture (day 12 and day 18).

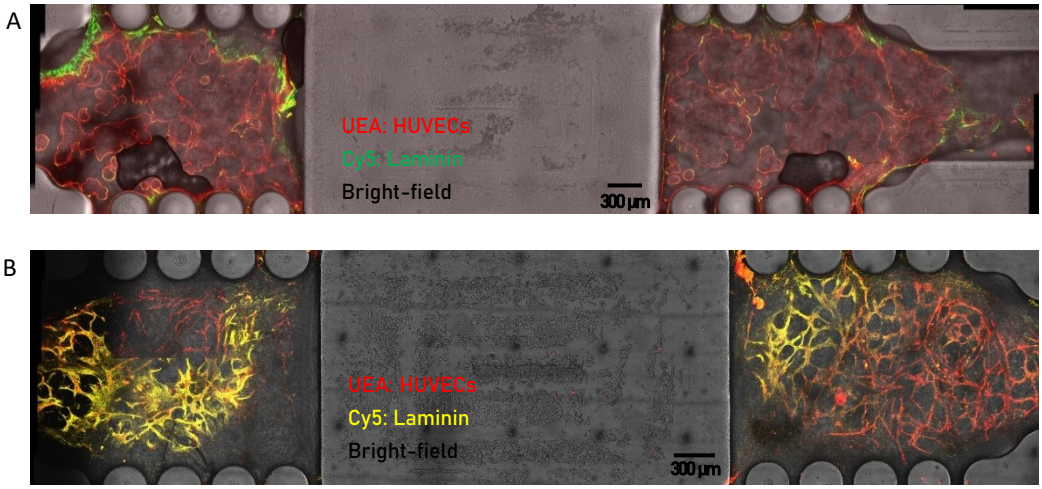

Figure 3.3.9.1: Tile scan confocal images of PV-µTPs-laden microfluidic device with staining of HUVECs and laminin under static (A) and dynamic (B) culture conditions: confocal image (A) shows endothelial cells at periphery of PV-µTPs, without tubular formations, and low laminin signal; confocal image (B), on the other hand, shows a highly interconnected capillary network that develops throughout the total volume of PV-µTPs at day 18 of dynamic culture. Co-localization of vessel-forming HUVECs (red) and HDF-secreted laminin (yellow) is clearly visible, thus highlighting the maturity of the obtained *in vitro* vasculature on-chip. Both images were acquired with wide pinhole (400 µm) in order to highlight the signal from different z-planes, thus obtaining a 2D projection of a 3D vasculature. Scale bars are 300 µm.

A

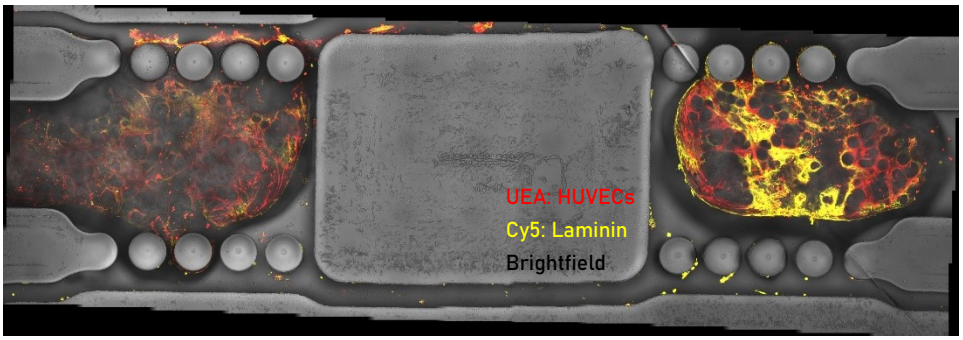

B

Figure 3.3.9.2: Tile scan confocal images of PV-µTPs-laden microfluidic device with staining of HUVECs and laminin after 7 days (A) and 18 days (B) of dynamic culture conditions: the designed microfluidic platform allowed for laminin (yellow) and HUVECs capillary structures (red) co-localization at different time points, thus resulting in a reliable tool for the formation of a long-lasting mature vessel network inside a 3D stromal tissue with endogenous ECM. Both images were acquired with wide pinhole (400 µm) in order to highlight the signal from different z-planes, thus obtaining a 2D projection of a 3D vasculature. Scale bars are 300 µm.

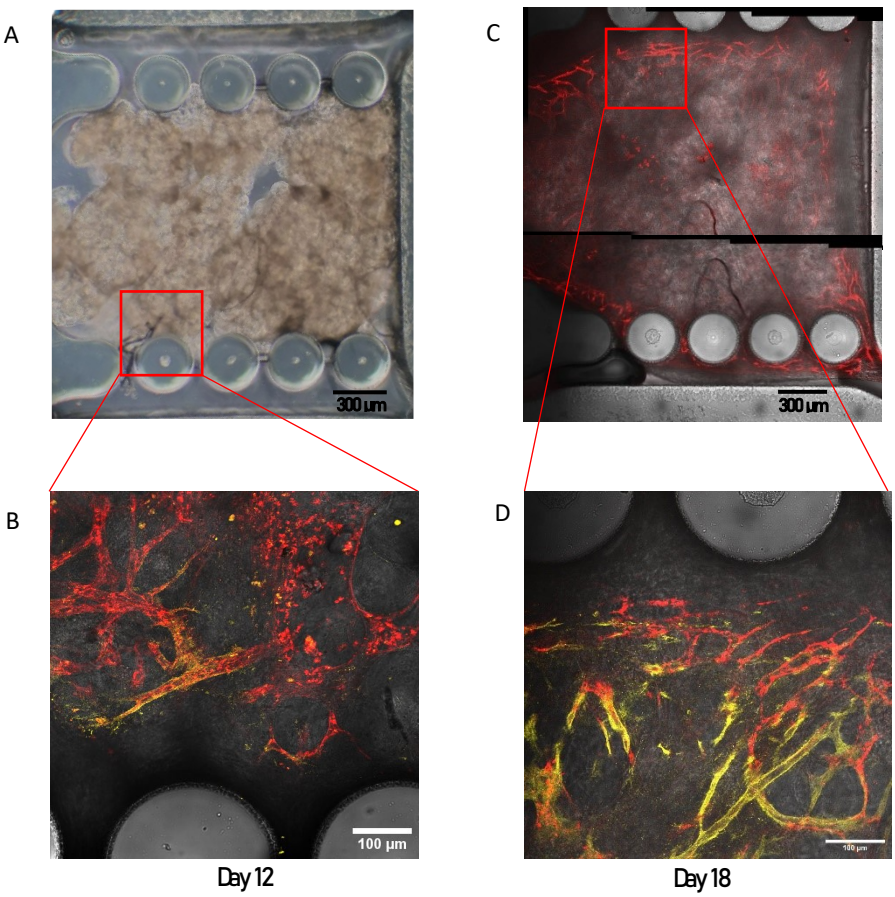

Figure 3.3.9.3: Confocal images of capillary network inside microfluidic device after day 12 (B) and day 18 (D) of dynamic culture showing HUVECs (red) and laminin (yellow) co-localization: maturation of vessels is highlighted in the magnification images (B) and (D). Images (A) and (C) represent the left chamber of devices at day 12 and day 18, respectively, with scale bar of 300 µm. Confocal images (B) and (D) present scale bar of 100 µm.

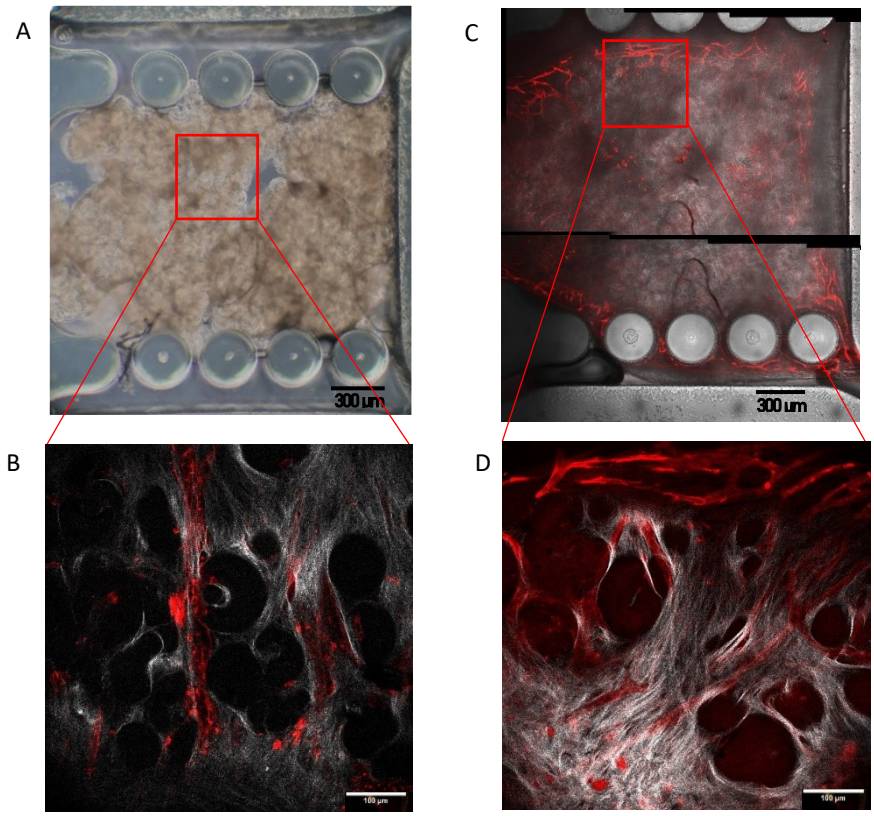

Figure 3.3.9.4: Images of microfluidic device left chamber after day 12 (A, B) and day 18 (C, D) of dynamic culture. Optical microscope image (A) and confocal (2-photon and standard) image (B) show left chamber and a magnification, respectively, of day 12 microfluidic device: co-localization of collagen fibers (imaged by means of 2-photon SHG) and HUVECs vessels (red) is clearly visible. Confocal images (C) and (D) show left chamber and a magnification, respectively, of microfluidic device at day 18 of dynamic culture: a qualitative analysis can highlight the more compact collagen fibers with respect to day 12, and collagen – HUVECs co-localization is still present, thus guaranteeing maturity of long-lasting vessel network. Scale bars are 300 µm for images (A) and (C), and 100 µm for images (B) and (D).

In order to determine if the obtained vascular network is perfusable, an investigation of existing lumina was performed. Figure 3.3.9.5 shows an example of the conducted analysis, which started from the acquisition of a fine (slice thickness = 1 µm) confocal z-stack, and a 3D reconstruction allowed for the imaging of vessel lumina (Figure 3.3.9.5). Vessel lumen is fundamental for vascular perfusability: the obtained vasculature on-chip

is suitable for perfusion after 18 days of dynamic culture inside the designed microfluidic platform.

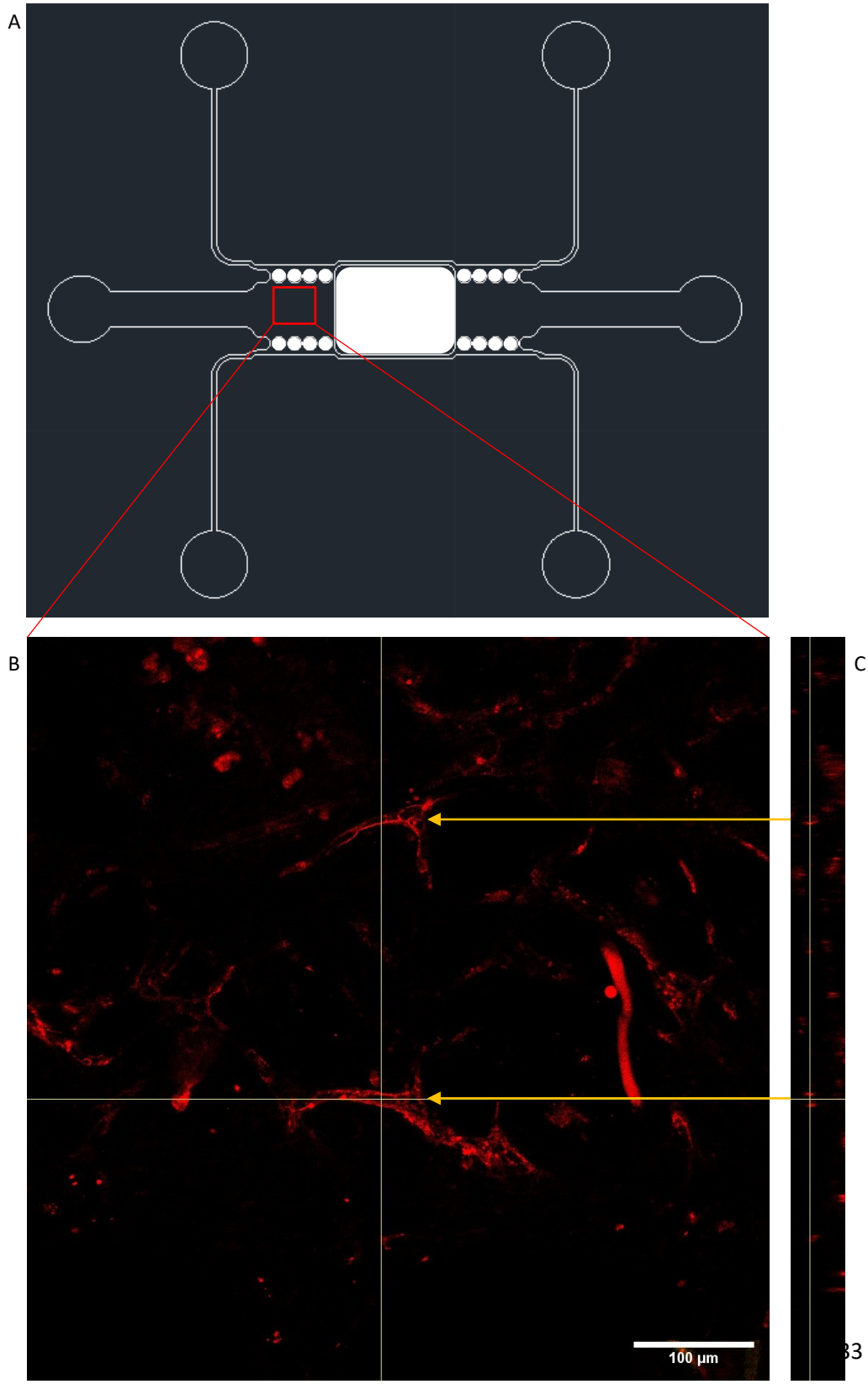
A
B
C
100 µm

Figure 3.3.9.5: Schematization of microfluidic device (A) and 3D reconstruction (B, C) from fine confocal z-stack acquisition of vessel lumina: confocal image (B) shows a single z-plane, in particular representing the z-slice (showing xy-plane) where the highlighted vessels (yellow arrows) present the maximum distance between the endothelial walls, thus determining the imaging of the entire lumen in yz-projection plane (C). The highlighted vessels in image (B) present an orientation of circa 90° with respect to yz-plane, thus presenting a circular-shaped cross section. Scale bar is 100 µm.

3.3.10 Perfusion test with nanoparticles (NPs)

In order to assess vessel perfusability inside the designed microfluidic device, a perfusion test was performed: FITC-fluorescent NPs with a diameter of 500 nm were chosen for the test and diluted for a final V/V concentration of 10 µL/mL from a stock solution of with 2.6% of solid component. As previously described, flow was activated from the up-left inlet and cross-flow was obtained by closing up-right and bottom-left inlets, thus determining flow outcome from bottom-right outlet and allowing NPs flow inside channels and tissue chambers (Figure 3.3.10.1, A). In order to investigate the presence of NPs inside vessel lumina, fine z-stack confocal acquisitions were performed. Results show that NPs enter the capillary network inside left and right chamber through angiogenic sprouts present inside the up-channel and exit the tissue from the angiogenic sprout present in low-channel, close to bottom-right outlet (Figures 3.3.10.1, 3.3.10.2 and 3.3.10.3). The path also involves the endothelial tubular formation in the low channel between left and right channels and that connects 3D stomal tissues of the two chambers (Figure 3.3.10.2). Co-localization of NPs signal (green) and HUVECs signal (red) also allows for the detection of NPs inside a vessel formation in the central part of 3D stromal tissue (Figure 3.3.10.1), thus highlighting the perfusability of the obtained mature vasculature on-chip.

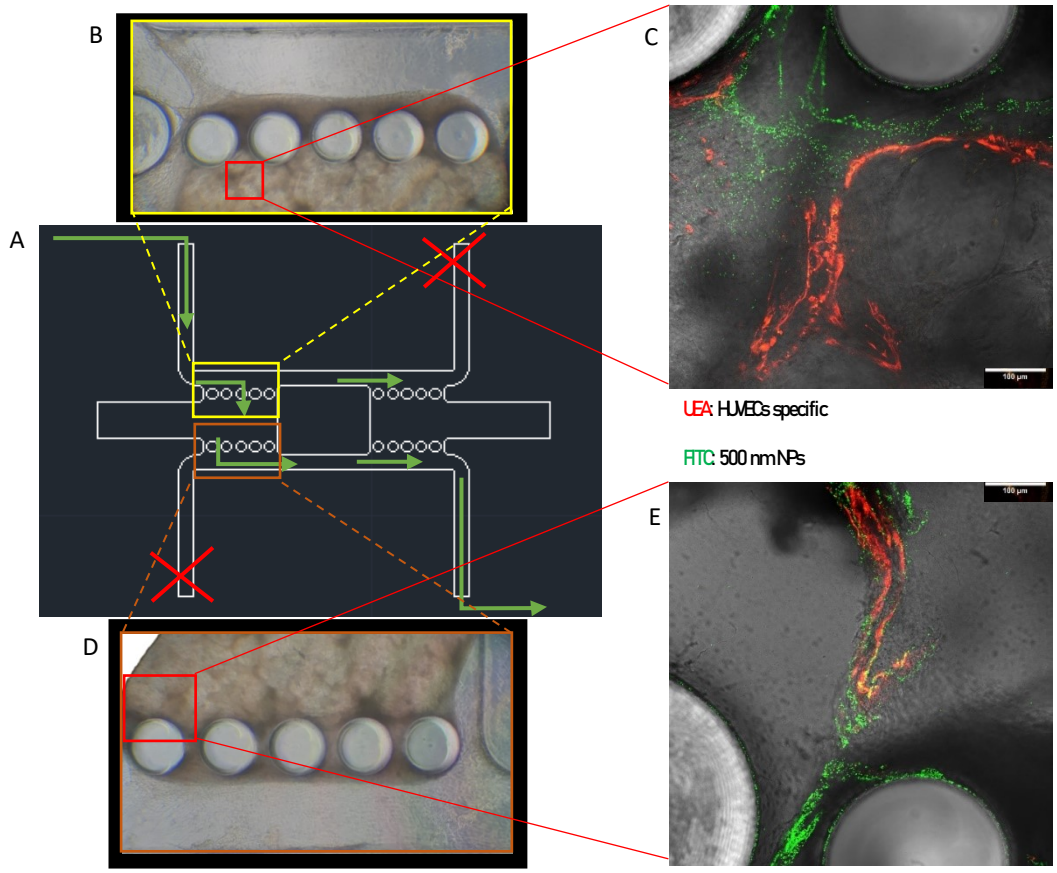

Figure 3.3.10.1: Perfusion test images after 7 days of dynamic culture: (A) Schematization of performed perfusion test inside microfluidic platform at day 7 of dynamic culture: NPs enter the chip at up-left inlet and exit at bottom-right outlet, with cross-flow guaranteed by closing up-right and bottom-left inlets. (B) Optical microscope magnification (10x) of upper part of left chamber with visible angiogenic sprouts inside up-channel. (C) Confocal image of interpillar space, up-left. Vessel is clearly visible (red) and NPs are focused in a capillary shape, thus guaranteeing intraluminal flow. (D) Optical microscope magnification (10x) of lower part of left chamber with visible clutching of PV-µTPs to pillars. (E) Confocal image of interpillar space, bottom-left. Vessel is clearly visible (red) and NPs are focused in a capillary shape, thus guaranteeing intraluminal flow through the interpillar space. Scale bars are 100 µm.

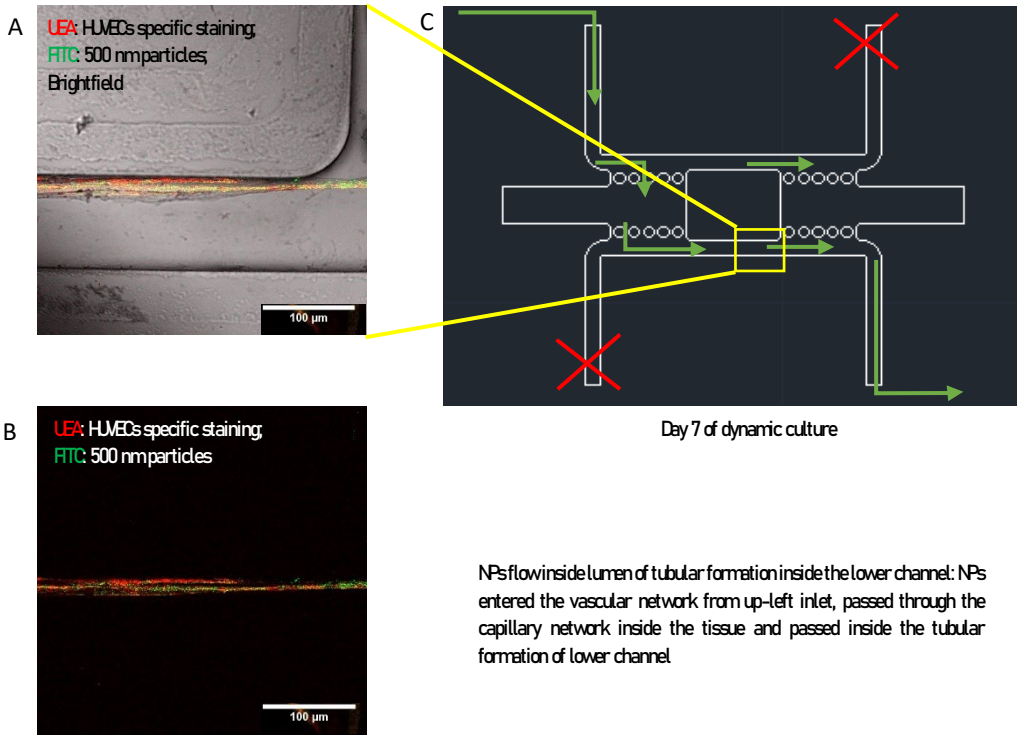

Figure 3.3.10.2: Perfusion test images after 7 days of dynamic culture: (A) Confocal image (red: HUVECs; green: NPs; gray: bright-field) of vessel structure inside lower channel, perfused by NPs entered from left tissue chamber. (B) Confocal image as (A), without bright-field. Vessel is clearly visible (red) and NPs are focused in vessel lumen, showing intraluminal flow. Scale bars are 100 µm.

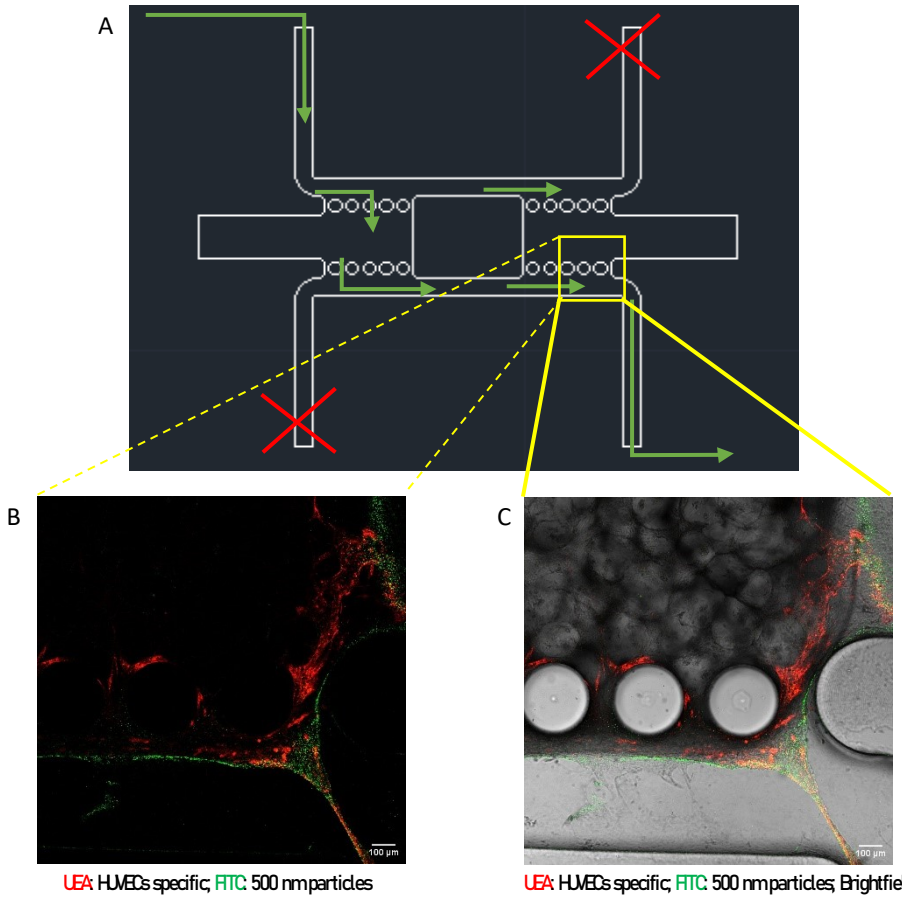

Figure 3.3.10.3: Perfusion test images after 7 days of dynamic culture: (A) Schematization of Schematization of performed perfusion test inside microfluidic platform at day 7 of dynamic culture: NPs enter the chip at up-left inlet and exit at bottom-right outlet, with cross-flow guaranteed by closing up-right and bottom-left inlets. (B) Confocal image (red: HUVECs; green: NPs) of bottom-right part of right chamber and low-channel: the angiogenic sprout lumen visible inside the channel is perfused with NPs, which entered the sprout from the capillary network inside 3D stromal tissue filling right chamber. (C) Confocal image (red: HUVECs; green: NPs; gray: bright-field) with bright-field overlapped on image (B) in order to better appreciate the role of the designed pillars inside the microfluidic device. Scale bars are 100 µm.

Figures (3.3.10.1, 3.3.10.2 and 3.3.10.3) show NPs walk inside capillary lumina formed inside the 3D stromal tissue on the microfluidic device after 7 days of dynamic culture, assuring that the designed platform allows for the formation of a perfusable capillary network on-chip after 7 days of culture. As a result, an important step forward in the field of vasculature model studies can be highlighted: the combination of a microfluidic approach – with fine control over flow rates and small volumes – and a 3D stromal tissue equivalent with endogenous ECM, strongly allowed for vascularization phenomena to

occur, thus recapitulating the mechanisms involved – vasculogenesis, angiogenesis and anastomosis – in 7 days of dynamic culture.

After investigating the perfusability of the network, the idea was to guarantee a long-lasting perfusability of capillary network: perfusion tests were performed after 18 days of dynamic culture to assess lumina perfusability of a long-lasting vasculature *in vitro*. Results of the test show that vessel lumina inside the 18 days device were perfusable, as Figure 3.3.10.4 highlights.

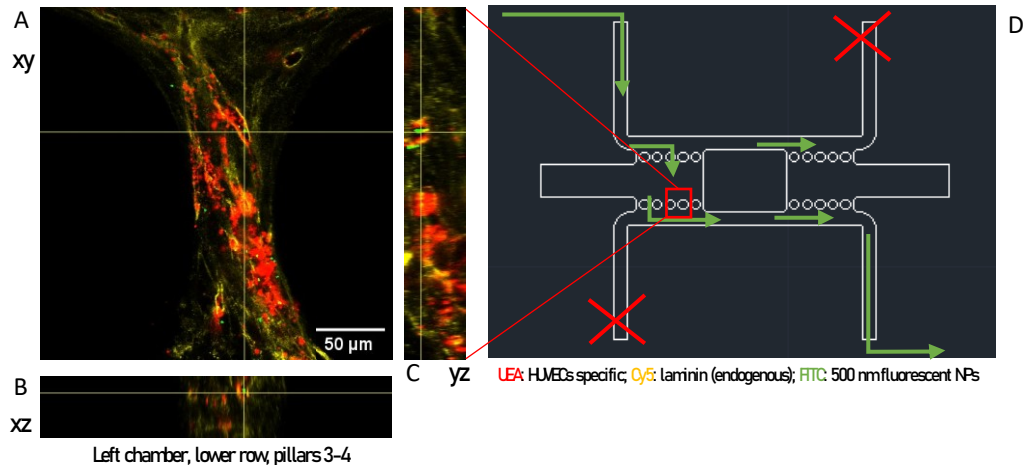

Figure 3.3.10.4: Perfusion test images after 18 days of dynamic culture: after introducing NPs from up-left inlet and obtaining cross-flow by closing up-right and bottom-left inlet, NP was spotted inside a lumen of a capillary, which formed between pillar 3 and 4 of lower row at left chamber, showing co-localization of HUVECs and laminin (A): laminin co-localization and perfusability represent important parameters of mature vessels, features characterizing the vessel after 18 days of culture, thus obtaining a long-lasting vessel culture on-chip. (B) xz orthogonal view obtained by fine z-stack acquisition: the circular HUVECs formation (red) surrounded by laminin (yellow) represents mature capillary cross-section, where one NP was spotted. (C) yz orthogonal view obtained by fine z-stack acquisition: the circular HUVECs formation (red) surrounded by laminin (yellow) represents mature capillary cross-section, where one NP was spotted. Scale bar is 50 µm.

Figure 3.3.10.4 shows NPs inside the lumen of a capillary formed at tissue – channel interface after 18 days of dynamic culture on the microfluidic platform. As a result, long-lasting perfusability of capillaries on-chip, due to the presence of and endogenous ECM, represents a step forward in the field of tissue engineering and *in vitro* vascularization models: previously existing on-chip models do not achieve long-lasting perfusion in an endogenous ECM, but only up to 4 days of perfusion inside a hydrogel, which does not recapitulate the complex structure of physiological ECM.

3.4 Conclusion and future perspectives

The proposed strategy for *in vitro* vascularization on-chip inside a 3D stromal tissue equivalent led to several interesting results:

- Long-lasting *in vitro* 3D developed vasculature on a microfluidic platform with capability of inflow control for 18 days (reported) – 21 days from vascularization processes started;
- Anastomosis of tissue vasculature with fluidic channels through angiogenic sprouts;
- Perfusion of vessel lumina detectable with optically accessible microfluidic platform and fluorescent imaging, overcoming the time of perfusion of existing literature models described above.

It is important to highlight the key role of 3D stromal tissue for long-lasting of vasculature inside the platform: as described in the state-of-the-art section, vasculature physiological environment is represented by stromal tissue, which is recognized as the scaffold and the mechanical support of all organs, included vascular system. Nonetheless, stromal tissue does not only exert a mechanical function, but also contributes in cell-cell signaling, biochemical stimulation to cells, presenting a spatio-temporal gradient of growth factors that strongly influence cell behaviour *in vivo*. As a result, an *in vitro* long-lasting vascularization model must take into account the fundamental role played by stromal tissue. As a step forward with respect to the above-mentioned works on vascularization on-chip, it is important to underline that the long-lasting vasculature obtained on-chip relies on the presence of a stromal tissue, which, together with perfusion, guarantees vessels maturity, fundamental parameter for long-lasting. In particular, the highlighted collagen fibers and laminin surrounding capillaries in the microfluidic platform determine vascular maturity, thus validating the platform as a reliable *in vitro* model for long-term vascularization study.

Another achievement to be considered is the perfusion of capillary network inside the tissue from fluidic channels, through angiogenic sprouts: intraluminal flow generates a tensional state inside the capillary that allows for vessel maturity; as a result, the perfusion obtained guaranteed a prolonged 3D dynamic culture with capillaries developing and preserving a tubular conformation – that closely replicates physiological vascular architecture – for a long interval of time (18 days), and the maturity of vessels

lasts for 3 weeks, with respect to the tissues cultured in multiwell, whose vasculature undergo a regression after 2 weeks.

The proposed strategy – that relies on the combination of microfluidic approach and bottom-up tissue engineering – consists in a reliable model for the investigation of such interactions – vascularization processes, angiogenesis, vasculogenesis, anastomosis and vessel perfusion in a long interval of time, thus representing an important tool for vascularization research field.

Despite the promising features of the designed microfluidic device, limitations can be underlined and modifications may be proposed for the enhancement of the platform. In particular, only partial perfusion of capillary network was obtained: flow split between channels and capillary lumen. Quantification of splitting could be assessed considering the total fluorescence intensity of injected NPs, and the fluorescence intensity of NPs inside the lumen of vessels: the ratio between the lumen NPs fluorescence and the total injected NPs fluorescence could represent an index of vascular perfusion inside the platform. Further studies will be performed in this direction.

Regarding the splitting of flow, the reason regards channels endothelialization process. Endothelial lining of channels wall can be optimized: the angiogenic sprouts form within channels lumen, thus generating a non-properly stable configuration at the tissue-channel interface. The ideal configuration may present endothelial cells that completely line channels walls, forming a uniform, stable vessel with endothelial cells adhered to channel, thus guaranteeing that the entire volume of liquid that enters the device is conveyed inside vasculature lumen. In order to achieve this configuration, a strategy is proposed for potential improvement of the platform: the reduction of channels height from 600 µm to 50 µm. Channel cross-section could be comparable with capillary structures formed within channels in the existing microfluidic platform, thus guaranteeing a correct endothelialization of channels walls. In this way, the flow would be completely inoculated inside the capillary structure, which anastomose to vessels inside the tissue. As tissue chamber must feature a 600 µm height for µTPs injection, the strategy for device fabrication could be the following: micro-milling for the fabrication of a 600 µm-height negative master, followed by the removal of material from the negative of channels to obtain a 50 µm height, which could be performed with a second step of micro-milling.

As a future perspective, optimization of intraluminal flow could be achieved by reducing channels cross-section area to values comparable with capillary size (10 to 20 µm in diameter, or to introduce a progressive reduction of section from channels to tissue interface at the interpillar space. Another important improvement may be obtained using transfected HUVECs for permanent fluorescence, for live-monitoring of vascular

sprouts formation and maturation using confocal imaging, and not only optical microscope for live monitoring of HUVECs inside the channels.

As a conclusion, vessel maturity and perfusion – together – in a 3D stromal tissue with endogenous ECM within a microfluidic platform for control over intraluminal flow can be suitable for different applications: systemic drug-testing can be obtained in a miniaturized, high-throughput platform; different stromal tissue – physiological or pathological – models could be obtained using different cell types (*i.e.*, lung (hLF) or intestine fibroblasts, cancer-associated fibroblasts (CAF) or others) in order to analyze differences in vascular development in different districts of human body, and to study tumor angiogenesis and vascular development in cancer [137][138][139].

4 Supplementary: optimization of UV 3D printing for hard master rapid prototyping and biocompatible components fabrication

4.1 Introduction

UV 3D printing represents a versatile, precise and fast fabrication technique with high resolution, suitable for rapid prototyping due to its short time of fabrication. The operating principle is based on a layer-by-layer photopolymerization – by means of UV excitation – of a liquid resin to obtain a component from a CAD file: this configuration allows for the fabrication of complex geometries and architectures in a precise manner.

For these reasons, I chose UV 3D printing for different applications:

- the printing of a negative hard master for microfluidic device fabrication with critical geometrical cues;
- the design and fabrication of a component to integrate in a 3D cell culture inside the microfluidic platform;
- the design and fabrication of a 4-reservoir mask to be directly connected to the device for preliminary studies of pumpless dynamic culture and for the static culture samples.

As previously described, in order to correctly generate the chamber-channels interfaces for a round-shape 3D stromal tissue equivalent, the designed geometry featured 4 cusps at the communication pores from chamber to channels (Figure 4.1.1): due to high resolution of UV 3D printing technique and the possibility – not shared by, for example, micro-milling – to obtain patterns with acute angles, UV 3D printing was chosen as the fabrication technique.

Regarding the design of a component to integrate in a 3D cell culture inside the microfluidic platform, the idea generated from the need for PVD adhesion to the bottom of the device (mentioned in chapter 2): a round ring with two guides was designed to be positioned at the top of the PVD inside the tissue chamber, and tracks at the periphery of tissue chamber guaranteed ring correct positioning and locking (Figure 4.1.2). Following the component design, it was important to produce high number of pieces (Figure 4.1.3) for the experimental campaign in a short interval of time, and to guarantee their biocompatibility: optimization of UV 3D printing of commercial resin could allow to comply with these conditions.

Finally, a 4-reservoir mask was designed for the study of pumpless dynamic culture and to guarantee a static culture platform with sufficient amount of cell medium volumes (Figure 4.1.4): geometrical complexities, the presence of 4 nozzles with small diameters and the need for a high number of components made again UV 3D printing suitable for this application.

On one hand, UV 3D printing represents a reliable technique for the fabrication of the needed components due to its features – high-resolution, time-saving and possibility of biocompatibility [68]; on the other hand, in order to reach high precision of printing and biocompatibility, the optimization of photopolymerization must be performed. In particular, it is important to focus on the principle of polymer curing: UV excitation activates photoinitiators – molecules that form free radicals if excited at a precise wavelength – that rapidly react in order to form polymer chains, resulting in a macroscopic passage from a liquid to a solid state. This chemical reaction results extremely fast, thus leading to the possibility to obtain complex components in short interval of time. As a counterpart, the possible presence of residual unreacted monomers could determine the loss of biocompatibility. For this reason, polymerization of resin must be controlled.

UV 3D printing of biocompatible components was optimized in terms of printing parameters – one being exposure time of each layer – and post-processing – ultrasonication in IPA time interval and UV post-curing - in order to assure the absence of unreacted monomer, and biocompatibility was assessed by means of cell viability assays in different conditions of cell-culture.

First step for the production of the needed components was the design. As described above, the microfluidic device design was chosen and modifications were introduced in order to insert the ring. The round ring was designed to feature two male guides for the precise insertion on top of PVD inside the tissue chamber (Figure 4.1.2). The 4-reservoir mask was designed to feature nozzles similar to Luer connectors, in order to perfectly fit into the punched inlets of the device (Figure 4.1.3).

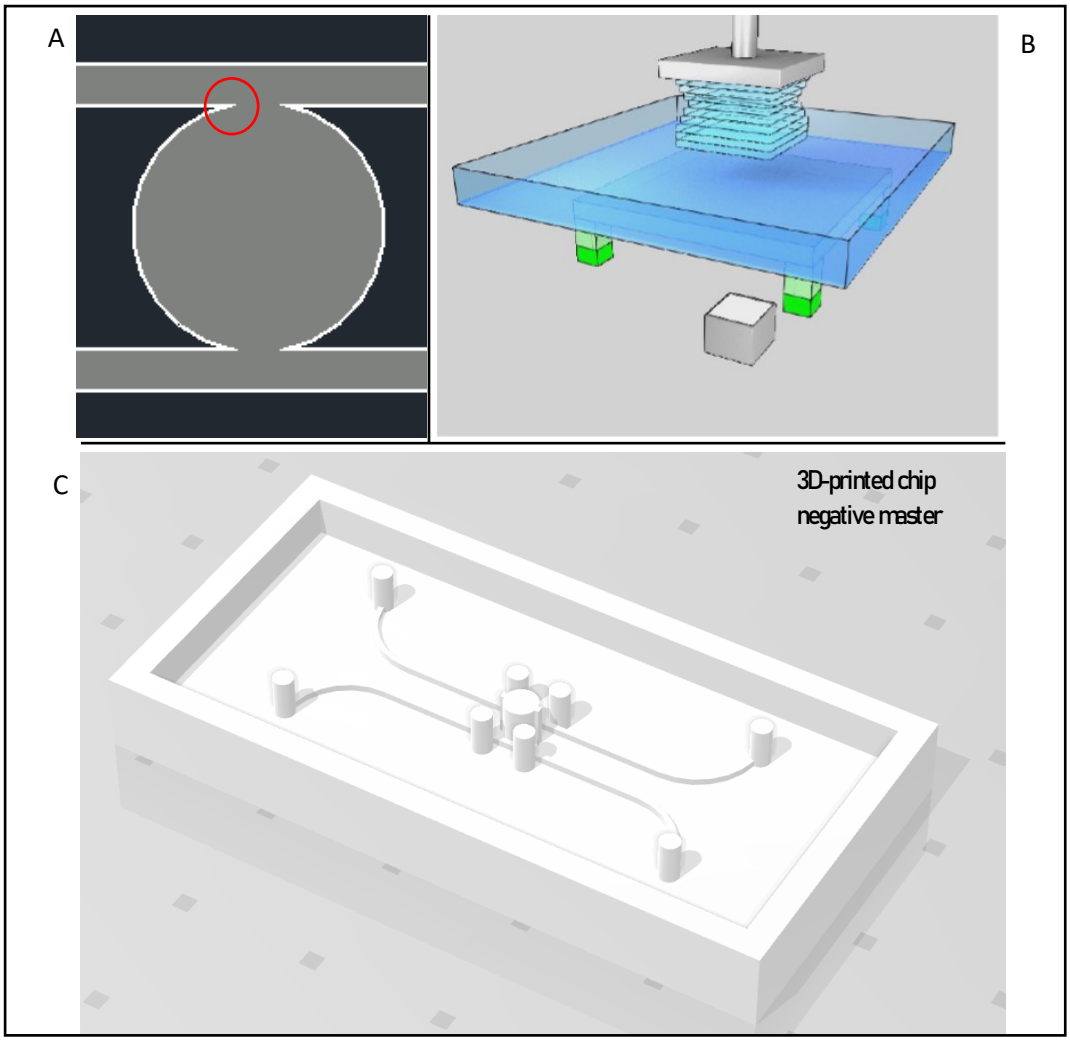

Figure 4.1.1: (A) Schematic representation of geometrical cusps (red circle). (B) Graphical representation of UV 3D printing operating principle: a UV light source (grey cube in the bottom) can start photopolymerization of the liquid polymer inside a vat with transparent bottom. Each layer presents a pattern of illuminated and non-illuminated dots, and the stacking of different layers (deriving from a .stl file) results in the final printed component, attached to a stage. (C) Designed vat for microfluidic device fabrication by replica molding. The negative pattern of the device presents: a central part for tissue chamber (featuring the tracks for ring insertion); two channels for cell medium flow and EC lining; eight cylinders that represent the guides for inlets and outlets punching in PDMS slab; a frame to confine PDMS in order to use the minimum amount of PDMS for replica molding of the device.

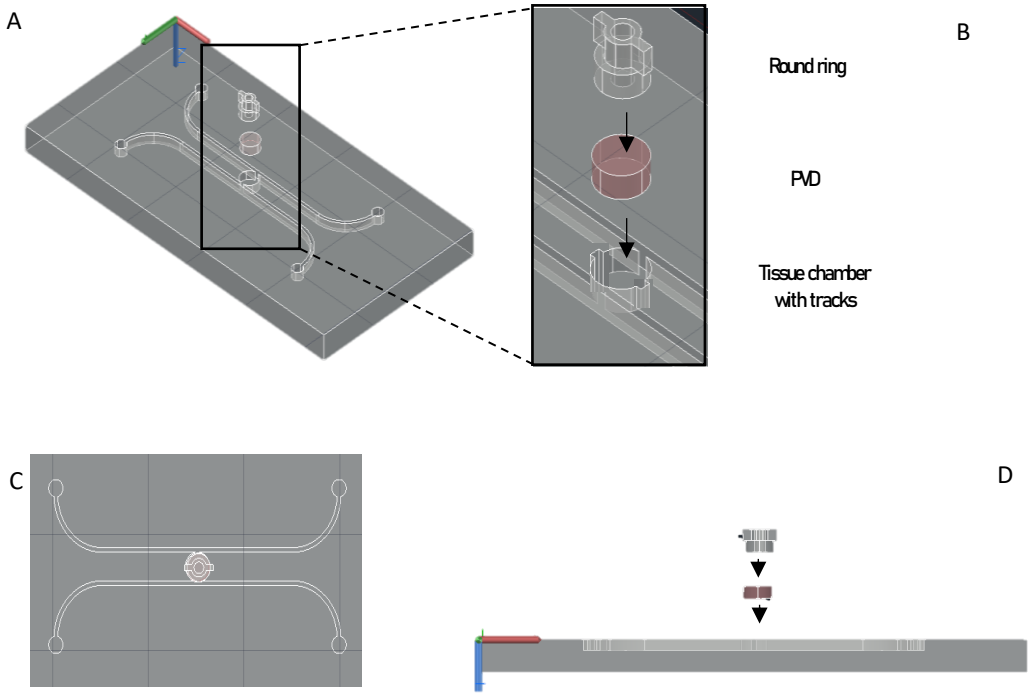

Figure 4.1.2: Schematization of the proposed strategy for PVD positioning enhancement and design of round ring. (A) 45 degrees-view of PVD positioning strategy. (B) Magnification of (A) showing the round ring positioning on top of the PVD and the tracks added to tissue chamber. (C) Top-view of positioning configuration. (D) Lateral view of positioning strategy.

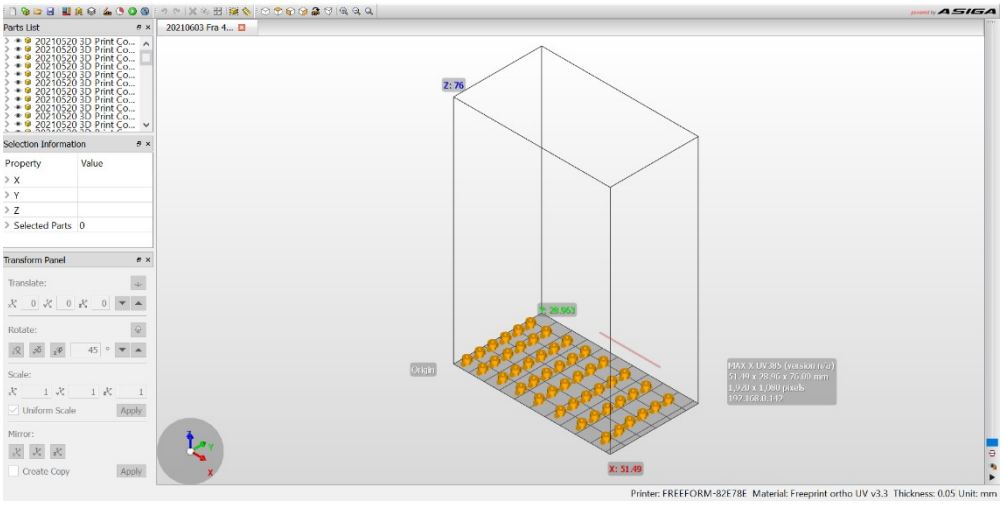

Figure 4.1.3: Asiga Composer software interface. Yellow components represent the round rings to be printed: 48 pieces can be printed in a single print of 10 minutes, determining he possibility of rapid prototyping.

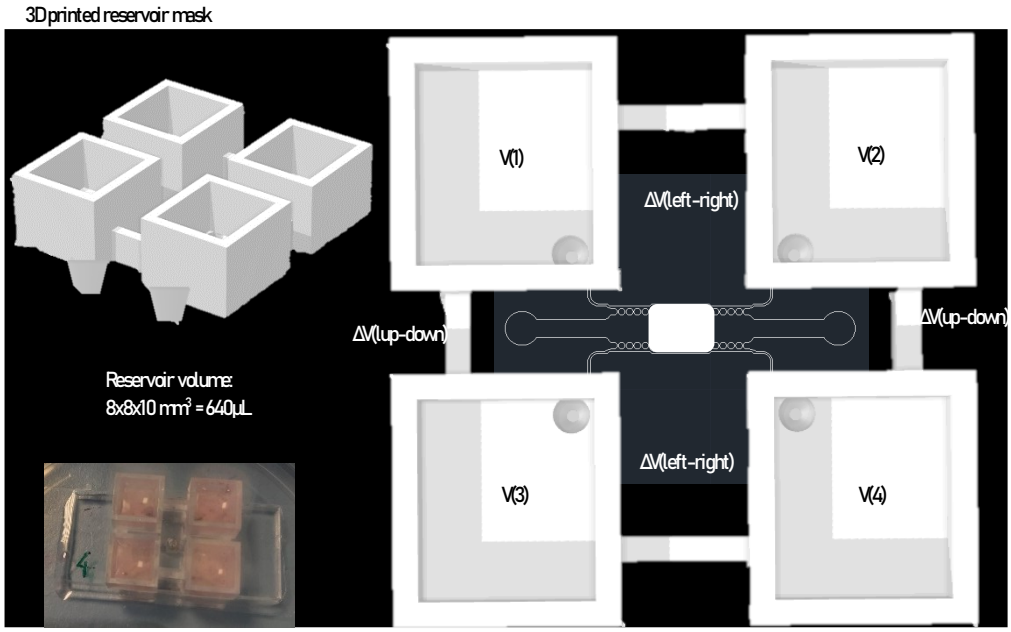

Figure 4.1.4: Schematization of strategy for pumpless optimization, showing the design parameter for the production of a 4-reservoir mask: 4 reservoirs with small volumes, independently connected to 4 inlets of a microfluidic device.

4.2 Materials and methods

4.2.1 UV 3D printer

The printing of 3D components was performed using a Max UV (Asiga) 3D printer model featuring a 385 nm UV light source (Figure 4.2.1.1). The printable (x, y, z) volume is 119 x 67 x 75 mm^3 and the file inputs are .stl, .slc and .stm. The printer features, from top to bottom: a motorized system with a removable stage; a vat with transparent bottom containing the resin; a light source for polymerization. Asiga Composer software allows for control of printing parameter and machine. Printed components can present supports for geometrical complexities that can be removed after printing. CAD file in the proper extension can be loaded on Asiga Composer software and modifications can be applied in order to optimize printing time and components positioning.

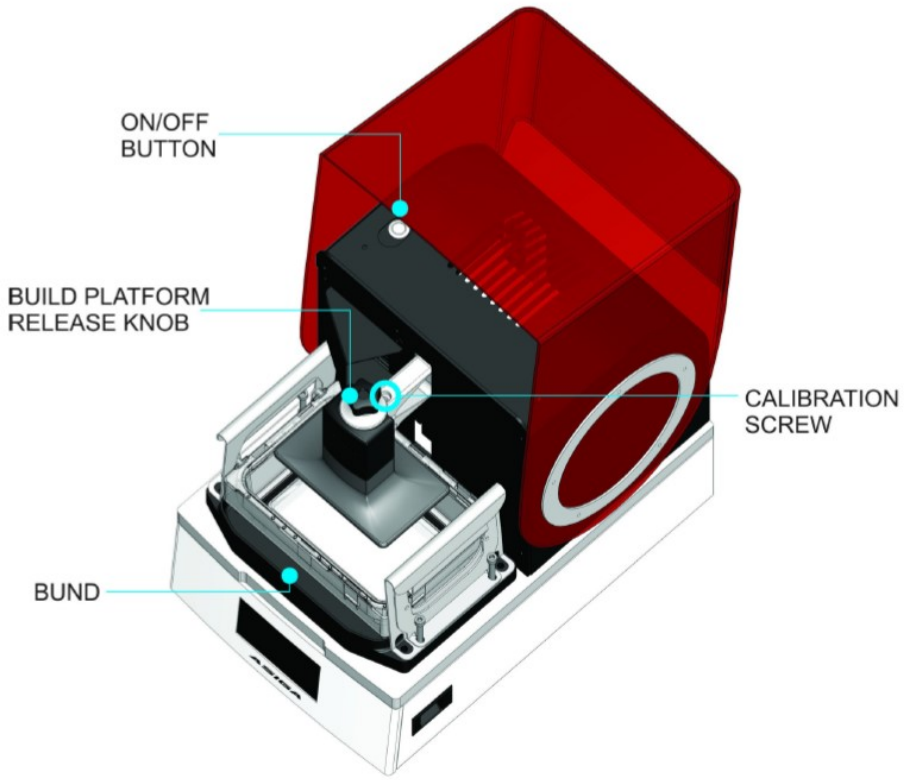

Figure 4.2.1.1: Asiga Max UV 3D printer with 385 nm light source. Technical features are highlighted.

4.2.2 Resin

The resin used for components printing is the commercial photopolymerizable Freeprint Ortho (Detax), a transparent resin that polymerizes with excitation at 385 nm. The purchased resin featured a .ini file with suggested printing parameters, but several modifications were necessary to guarantee biocompatibility.

4.2.3 Design and printing procedure

CAD software (Autodesk) was used for components design and generation of .stl file. Designed components were printed by opening .stl file in Asiga Composer software, which presents a window for component positioning in x-y plane and orientation (angle). Positioning reveals to be crucial for the correct printing of components, in order to avoid unpolymerized resin to be entrapped in component's cavities. Once correctly positioned in the software, supports can be automatically or manually added to the component to avoid eventual failure or collapsing of pieces. The component can be printed by deciding slice thickness (50 or 100 µm), exposure time (modifiable from

suggested value, in the order of seconds per slice), burn-up layer (possibility to print a first layer with higher exposure time to avoid component detachment from stage). The printed components were post-processed with two ultrasonication steps (3 minutes each) in propan-2-ol (isopropyl alcohol, IPA) (Ultrasonicator bath DW-50, Indiamart), drying and with a 30 minutes UV step for further polymerization.

4.3 Viability test

In order to assess cytotoxicity of printed components, lactate dehydrogenase (LDH) assay and 3-(4,5-Dimethylthiazol-2-yl)-2,5-Diphenyltetrazolium Bromide (MTT) assay were performed in different conditions (cell types and contact with resin). LDH assay was performed on HUVECs cells in the following contact conditions with resin:

- indirect contact: a piece of printed resin was maintained in cell medium for 24 hours (conditioned medium) and used to culture HUVECs in multiwell in order to assess release of toxic molecules (unpolymerized resin) by resin;
- direct contact: HUVECs were seeded in multiwell and co-cultured with a printed component;
- adhesion: HUVECs were seeded on top of a thin disk of printed resin (after coating with 1% gelatin as protocol for HUVECs 2D culture).
- Control: HUVECs seeded in multiwell.

Performed viability tests are described below:

- LDH assay: The LDH assay, also known as LDH release assay, is a cell death / cytotoxicity assay used to assess the level of plasma membrane damage in a cell population. Lactate dehydrogenase (LDH) is a stable enzyme, present in all cell types, which is rapidly released into the cell culture medium upon damage of the plasma membrane. LDH is the most widely used marker used to run a cytotoxicity assay. The LDH assay protocol is based on an enzymatic coupling reaction: LDH released from the cell oxidizes lactate to generate nicotinamide adenine dinucleotide (NADH), which then reacts with a commercial tetrazolium salt WST to formazan (yellow colour). The intensity of the generated color correlates directly with the number of lyzed cells. 10 µL of culture medium is required for the assay, and thus the background from serum and culture medium is significantly reduced.
  LDH activity was quantified by spectrophotometer at 450 nm after LDH reaction mix was added and incubated for 30 minutes at room temperature.

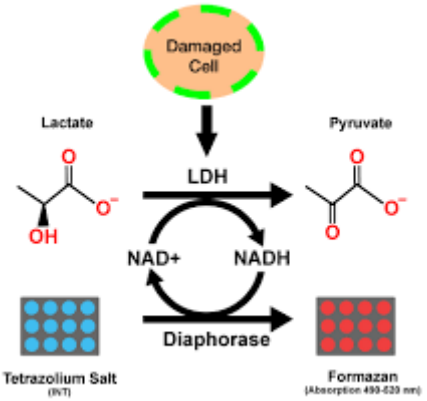

Figure 4.3.1: Schematization of LDH assay functioning principle: LDH from death cells is released and reacts to obtain formazan.

- MTT assay: To evaluate the cell viability after 7 days and 14 days of HDFs co-culture with printed component, 3-(4,5-dimethylthiazol-2-yl)-2,5-diphenyltetrazolium bromide (MTT) assay was used according to the manufacturer's instructions (Sigma). Briefly, after 7 days and 14 days of cell-resin co-culture in multiwell, HDFs were washed twice with PBS, 200 µL of the MTT solution (5 mg/mL) was added in each well incubating at 37°C in a humidified 5% CO2 for 3 h in the dark. Then, MTT solution was removed from each well and the remaining crystals (formazan precipitates) were solubilized with 200 µl of DMSO, and the cells were incubated for an additional time interval of 30 min at 37 °C with gentle shaking. After 30 minutes, the optical density (OD) of each well sample was measured with a microplate spectrophotometer reader at 570 nm, and the cell viability (%) was calculated by the following equation:

$$Cell\ viability\ (\%) = \frac{OD\ coculture}{OD\ control} x\ 100$$

All statistical comparisons were performed with the ANOVA test followed by the Tukey HSD test. P-values of < 0.05 denote statistically significant differences. For all data sets, experiments were repeated in independent studies.

Confocal microscopy after immunofluorescence allowed for imaging of HUVECs adhered on top of the resin and control in order to determine differences in cells adhesion.

4.3 Results and discussion

The results of the printing process optimization will be presented in the next sections, with a focus on the design of the needed components, their features and the importance of time exposure of each slice for the correct polymerization of the resin to guarantee biocompatibility.

4.3.1 Design

The design of the three components (negative master for PVD chip fabrication, round ring and 4-reservoir mask) was performed with a CAD approach. Briefly, it is possible to describe the parameters considered for the design:

- Master for PVD chip: two channels communicating with a chamber (with tracks for round ring positioning); inlets and outlets for medium flow and inlets for cell seeding;

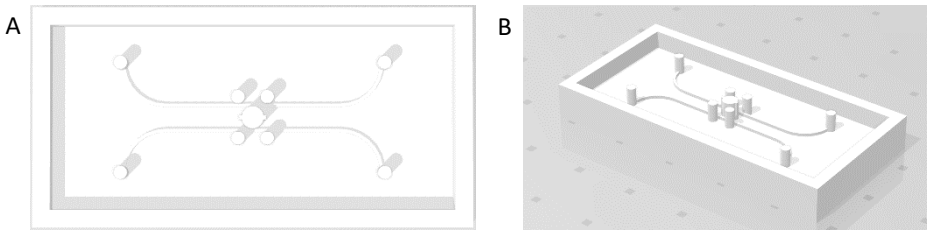

Figure 4.3.1.1: PVD chip master, top-view (A) and 45° view (B): design details are visible (central chamber with tracks, inlets for cells seeding at the periphery of the chamber, inlets and outlets at the extreme parts of the master). The design considered the negative master as a vat to contain a precise volume of PDMS, with no use of exceeding polymer.

- Round ring: a bottom flat disk of 2.5 mm diameter and 1 mm height; a cylinder 1.5 mm diameter and 2 mm height on top of the disk; a central passing hollow for cell medium collection; two lateral guides for correct fitting in tissue chamber (Figure 4.3.1.2);

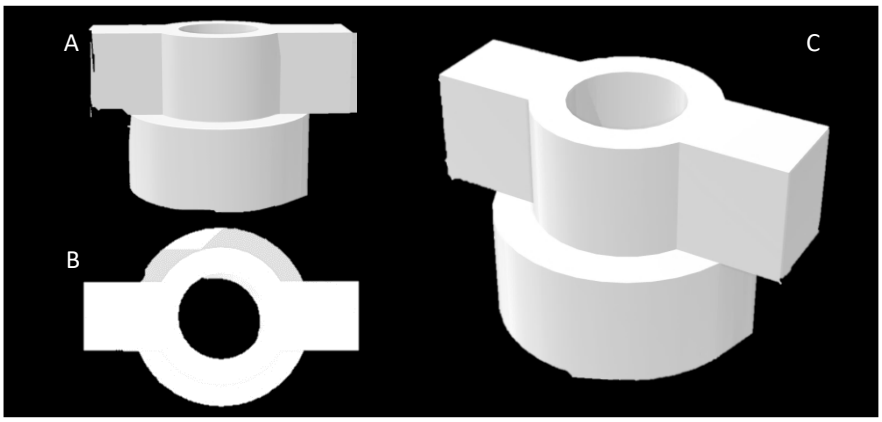

Figure 4.3.1.2: Schematization of round ring component. Lateral view (A), top-view (B) and 45° view (C). The cavity allows for cell medium collection inside the chamber, and the lateral guides determine correct fitting of the component inside the tissue chamber.

- 4-reservoir mask: four reservoirs (8 x 8 x 10 mm^3); a structure to connect the reservoirs; four nozzles with a maximum diameter of 1.5 mm to be inserted in device inlets (Figure 4.3.1.3).

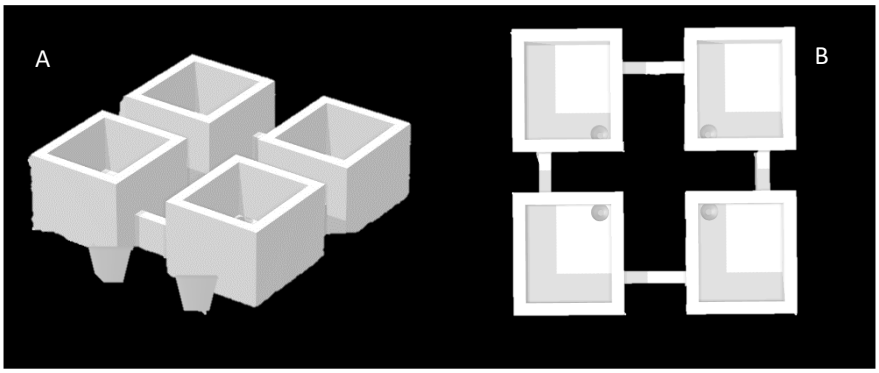

Figure 4.3.1.3: Schematization of 4-reservoir mask design: 45° degrees view (A) shows the presence of nozzles at the bottom part; top-view (B) shows the four reservoirs, the inlets and the frame that guarantees reservoirs leveling during insertion.

4.3.2 3D printing procedure optimization for biocompatibility

The optimization of 3D printing procedure was performed with the aim of obtaining components with complete absence of unpolymerized resin, which could represent an

issue when co-cultured with living cells due to its cytotoxicity. The optimization strategy was addressed to strike a balance between the absence of unreacted resin, the need for stiff components and the fabrication time.

The first step was to print components with geometrical complexities and thin parts (Figure 4.3.2.1) with the suggested parameters and post-processing procedure described above: this protocol determines the presence of visible unreacted resin on top of the components and the corrosion of thin parts due to IPA action during ultrasonication process (Figure 4.3.2.1, A). The presented issue regards the lack of stiffness by the thin parts, which do not undergo perfect polymerization with the exposure time suggested by the .ini file of the resin material. Different exposure times were chosen in order to obtain stiffer material, but a balance between printing time and stiffness was necessary: initial time exposure of 1.234 s was modified to 3.14 s and better results were obtained in terms of surface finishing and material stiffness (Figure 4.3.2.1, B). Further modifications to printing procedure regarded post-processing UV: in order to assure that no unreacted polymer was present, post UV step was performed for 30 minutes instead of 5 minutes. As a result, the printed components preserved their shape after IPA ultrasonication and no unreacted resin was visible (Figure 4.3.2.2). Table 4.3.2.1 shows final parameters for optimized 3D printing.

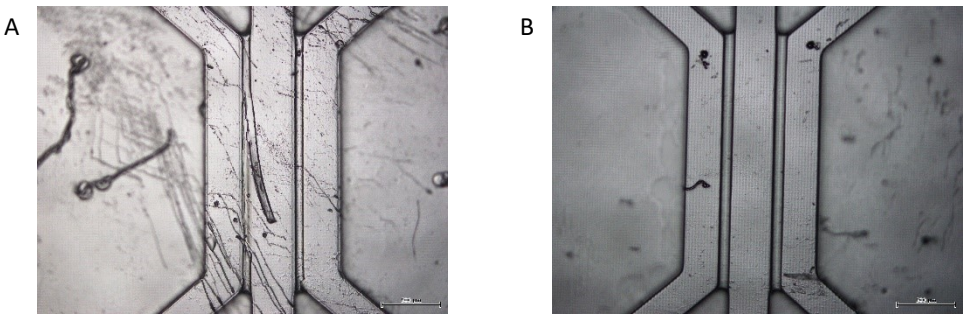

Figure 4.3.2.1: Optical microscope images of UV 3D printed samples. Image (A) shows the effects of IPA ultrasonication on a printed component with a time exposure equal to 1.234 s per slice (suggested by producer): detachment of thin parts was due to non-completely polymerized resin. Image (B) shows a printed component with exposure time equal to 3.14 s per slice: thin parts are preserved and surface finishing is maintained.

Figure 4.3.2.2: Image of UV 3D printed disks (up) for cell adhesion tests and multiwell with UV 3D printed spherical components (down) for cell viability tests. No unpolymerized resin is visible.

Printing parameters (385 nm UV 3D printer)	Exposure time (time/slice)	Slice thickness	Post-processing	UV post-treatment
Device PVD (negative master)	3.14 s	50 µm	3 min ultrasonication in IPA (2x)	30 minutes

Table 4.3.2.1: Printing parameters of for the fabrication of negative masters for PVD device.

4.3.3 Cell viability tests

In order to certify the absence of unpolymerized resin, cell viability tests were performed with two different cell lines (HUVECs and HDFs) and with different conditions. Next two sections show the results of the performed tests.

4.3.3.1 LDH assay

Results of LDH assay are shown in Figure 4.3.3.1.1: no toxic effect can be detected in all the conditions of resin-cell contact, guaranteeing biocompatibility of printed components with optimization of printing parameters.

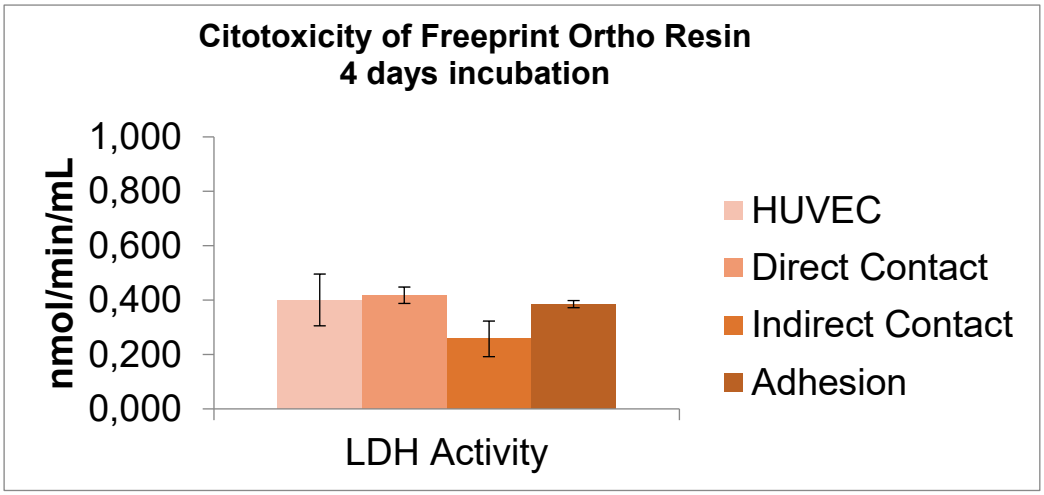

Figure 4.3.3.1.1: LDH activity of HUVEC control, direct contact, indirect contact and adhered on resin: the cytotoxicity level of resin is non-relevant if compared to control sample.

4.3.3.2 MTT assay

As described above, MTT test was conducted using HDF cells seeded in multiwell in contact with the printed resin for 7 days and 14 days of culture. The measured optical density (OD) of the solubilized crystals of different time points and conditions were correlated with the formula:

$$Viability = \frac{Resin\ OD}{Control\ OD}\ x\ 100$$

Viability values of HDFs with respect to control at day 7 of culture was equal to 94,469 %, while viability after day 14 was of 84.857 %, as a confirm of cell viability and non-toxicity of resin (Figure 4.3.3.2.1).

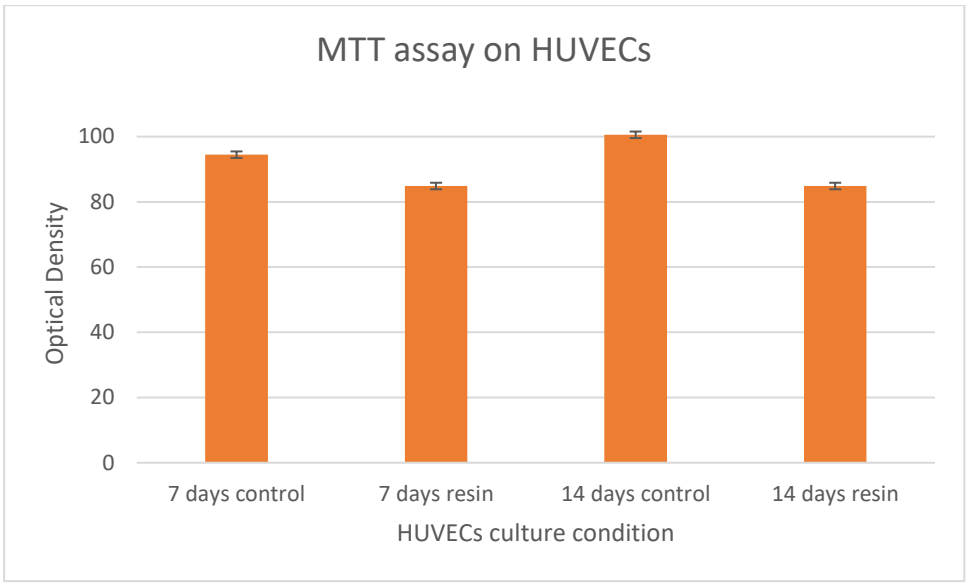

Figure 4.3.3.2.1: MTT assay results show that optical densities are comparable for all the samples (contact with resin) compared with controls, thus it is possible to assess that resin is biocompatible.

4.3.3.3 Confocal imaging

As a proof of cell viability, adhesion tests were performed using HUVECs cells. After gelatin 1% coating – as protocol procedure – cells were seeded on top of thin resin disks inside multiwell, and control wells without resin were cultured together with the samples. As a result, immunofluorescence and confocal imaging assessed HUVECs adherence on top of the resin without suffering. Figure 4.3.3.3.1 shows HUVECs seeded on resin and on standard well bottom, with no differences in cell morphology.

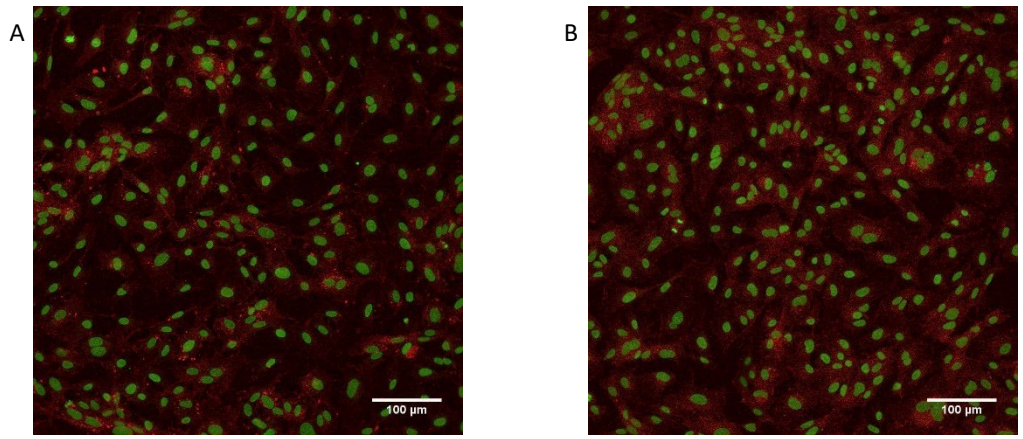

Figure 4.3.3.3.1: Confocal images of HUVECs (red for specific staining of HUVECs, green for nuclei) seeded on top of resin (A) and on standard well bottom (B): no differences in cell morphology can be assessed.

4.4 Conclusions and future perspective

The optimization of UV 3D printing procedure allowed for the fabrication of biocompatible components that can be used in 3D cell cultures inside microfluidic devices. In particular, the possibility to produce geometrically complex 3D elements with a rapid prototyping approach is combined with the biocompatibility of the material, thus generating an important perspective for on-chip 3D cell culture. Custom-designed reservoirs for pumpless system culture, components for the correct positioning of 3D biological constructs and specific elements for generating geometrical complexities inside a microfluidic device represent an interesting advantage in the design of microfluidic platforms for cell culture.

The fast design-to-manufacture process can be fundamental for the implementation of modifications in previously designed systems: a 3D printing, followed by sterilization of the component, can represent the solution to issues regarding leaking of microfluidic platform, positioning of 3D biological constructs, complex geometries needed. The custom-design of reservoirs, connectors and other components can facilitate the experimental set-up and guarantee a precise control over flow conditions.

5 Bibliography

[1] M. Radisic *et al.*, "Medium perfusion enables engineering of compact and contractile cardiac tissue," *Am. J. Physiol. - Hear. Circ. Physiol.*, vol. 286, no. 2 55-2, 2004, doi: 10.1152/ajpheart.00171.2003.

[2] H. H. G. Song *et al.*, "Transient Support from Fibroblasts is Sufficient to Drive Functional Vascularization in Engineered Tissues," *Adv. Funct. Mater.*, vol. 30, no. 48, Nov. 2020, doi: 10.1002/adfm.202003777.

[3] J. B. Tefft, C. S. Chen, and J. Eyckmans, "Reconstituting the dynamics of endothelial cells and fibroblasts in wound closure," *APL Bioeng.*, vol. 5, no. 1,

Mar. 2021, doi: 10.1063/5.0028651.

[4] L. A. Kunz-Schughart *et al.*, “Potential of fibroblasts to regulate the formation of three-dimensional vessel-like structures from endothelial cells in vitro,” *Am J Physiol Cell Physiol*, vol. 290, pp. 1385–1398, 2006, doi: 10.1152/ajpcell.00248.2005.-The.

[5] H. Azizgolshani *et al.*, “High-throughput organ-on-chip platform with integrated programmable fluid flow and real-time sensing for complex tissue models in drug development workflows,” *Lab Chip*, vol. 21, no. 8, pp. 1454–1474, Apr. 2021, doi: 10.1039/d1lc00067e.

[6] P. L. Tremblay, V. Hudon, F. Berthod, L. Germain, and F. A. Auger, “Inosculation of tissue-engineered capillaries with the host’s vasculature in a reconstructed skin transplanted on mice,” *Am. J. Transplant.*, vol. 5, no. 5, pp. 1002–1010, May 2005, doi: 10.1111/j.1600-6143.2005.00790.x.

[7] M. K. Pugsley and R. Tabrizchi, “The vascular system An overview of structure and function.”

[8] M. J. Adair TH, *Angiogenesis*. San Rafael (CA).

[9] “131 Risau - Mechanisms of Angiogenesis 1997”.

[10] D. H. T. Nguyen *et al.*, “Biomimetic model to reconstitute angiogenic sprouting morphogenesis in vitro,” *Proc. Natl. Acad. Sci. U. S. A.*, vol. 110, no. 17, pp. 6712–6717, Apr. 2013, doi: 10.1073/pnas.1221526110.

[11] A. Niemistö, V. Dunmire, O. Yli-Harja, W. Zhang, and I. Shmulevich, “Robust quantification of in vitro angiogenesis through image analysis,” *IEEE Trans. Med. Imaging*, vol. 24, no. 4, pp. 549–553, Apr. 2005, doi: 10.1109/TMI.2004.837339.

[12] A. Uccelli *et al.*, “Vascular endothelial growth factor biology for regenerative angiogenesis,” *Swiss medical weekly*, vol. 149. NLM (Medline), p. w20011, Jan. 14, 2019. doi: 10.4414/smw.2019.20011.

[13] U. Utzinger, B. Baggett, J. A. Weiss, J. B. Hoying, and L. T. Edgar, “Large-scale time series microscopy of neovessel growth during angiogenesis,” *Angiogenesis*, vol. 18, no. 3, pp. 219–232, Jul. 2015, doi: 10.1007/s10456-015-9461-x.

[14] J. S. Schechner *et al.*, “In vivo formation of complex microvessels lined by human endothelial cells in an immunodeficient mouse.” [Online]. Available: www.pnas.orgcgidoi10.1073pnas.150242297

[15] Z. Tahergorabi and M. Khazaei, “A Review on Angiogenesis and Its Assays.” [Online]. Available: www.mums.ac.ir

[16] S. P. Herbert and D. Y. R. Stainier, “Molecular control of endothelial cell behaviour during blood vessel morphogenesis,” *Nature Reviews Molecular Cell Biology*, vol. 12, no. 9. pp. 551–564, Sep. 2011. doi: 10.1038/nrm3176.

[17] X. Wang, D. T. T. Phan, A. Sobrino, S. C. George, C. C. W. Hughes, and A. P. Lee, “Engineering anastomosis between living capillary networks and endothelial cell-lined microfluidic channels,” *Lab Chip*, vol. 16, no. 2, pp. 282–290, 2016, doi: 10.1039/c5lc01050k.

[18] J. Pauty *et al.*, “A Vascular Endothelial Growth Factor-Dependent Sprouting Angiogenesis Assay Based on an In Vitro Human Blood Vessel Model for the Study of Anti-Angiogenic Drugs,” *EBioMedicine*, vol. 27, pp. 225–236, Jan. 2018, doi: 10.1016/j.ebiom.2017.12.014.

[19] Y. Shin *et al.*, “In vitro 3D collective sprouting angiogenesis under orchestrated ANG-1 and VEGF gradients,” *Lab Chip*, vol. 11, no. 13, pp. 2175–2181, Jul. 2011, doi: 10.1039/c1lc20039a.

[20] J. W. Song and L. L. Munn, “Fluid forces control endothelial sprouting,” *Proc. Natl. Acad. Sci. U. S. A.*, vol. 108, no. 37, pp. 15342–15347, Sep. 2011, doi: 10.1073/pnas.1105316108.

[21] C. W. Chi *et al.*, “High-Throughput Tumor-on-a-Chip Platform to Study Tumor–Stroma Interactions and Drug Pharmacokinetics,” *Adv. Healthc. Mater.*, vol. 9, no. 21, Nov. 2020, doi: 10.1002/adhm.202000880.

[22] O. De Wever and M. Mareel, “Role of tissue stroma in cancer cell invasion,” *Journal of Pathology*, vol. 200, no. 4. pp. 429–447, Jul. 01, 2003. doi: 10.1002/path.1398.

[23] S. Alkmin *et al.*, “Role of collagen fiber morphology on ovarian cancer cell migration using image-based models of the extracellular matrix,” *Cancers (Basel).*, vol. 12, no. 6, Jun. 2020, doi: 10.3390/cancers12061390.

[24] S. Grebenyuk and A. Ranga, “Engineering organoid vascularization,” *Frontiers in Bioengineering and Biotechnology*, vol. 7, no. MAR. Frontiers Media S.A., 2019. doi: 10.3389/fbioe.2019.00039.

[25] T. P. Richardson, M. C. Peters, A. B. Ennett, and D. J. Mooney, “Polymeric system for dual growth factor delivery,” 2001. [Online]. Available: http://biotech.nature.com

[26] A. P. Mcguigan and M. V Sefton, “Vascularized organoid engineered by modular assembly enables blood perfusion,” 2006. [Online]. Available: www.pnas.orgcgidoi10.1073pnas.0602740103

[27] J. Bai *et al.*, “A novel 3D vascular assay for evaluating angiogenesis across porous membranes,” *Biomaterials*, vol. 268, Jan. 2021, doi:

10.1016/j.biomaterials.2020.120592.

[28] K. M. Chrobak, D. R. Potter, and J. Tien, “Formation of perfused, functional microvascular tubes in vitro,” *Microvasc. Res.*, vol. 71, no. 3, pp. 185–196, May 2006, doi: 10.1016/j.mvr.2006.02.005.

[29] L. C. Roudsari, S. E. Jeffs, A. S. Witt, B. J. Gill, and J. L. West, “A 3D Poly(ethylene glycol)-based Tumor Angiogenesis Model to Study the Influence of Vascular Cells on Lung Tumor Cell Behavior,” *Sci. Rep.*, vol. 6, Sep. 2016, doi: 10.1038/srep32726.

[30] D. M. Hoganson, H. I. Pryor Ii, and J. P. Vacanti, “Tissue Engineering and Organ Structure: A Vascularized Approach to Liver and Lung,” 2008.

[31] H. Sekine *et al.*, “In vitro fabrication of functional three-dimensional tissues with perfusable blood vessels,” *Nat. Commun.*, vol. 4, 2013, doi: 10.1038/ncomms2406.

[32] K. Schimek *et al.*, “Integrating skin and vasculature in a Multi-Organ-Chip Platform,” *BMC Proc.*, vol. 9, no. S9, Dec. 2015, doi: 10.1186/1753-6561-9-s9-p20.

[33] A. Tourovskaia, M. Fauver, G. Kramer, S. Simonson, and T. Neumann, “Tissue-engineered microenvironment systems for modeling human vasculature,” *Exp. Biol. Med.*, vol. 239, no. 9, pp. 1264–1271, Sep. 2014, doi: 10.1177/1535370214539228.

[34] W. G. Chang and L. E. Niklason, “A short discourse on vascular tissue engineering,” *npj Regen. Med.*, vol. 2, no. 1, Mar. 2017, doi: 10.1038/s41536-017-0011-6.

[35] E. C. Novosel, C. Kleinhans, and P. J. Kluger, “Vascularization is the key challenge in tissue engineering,” *Advanced Drug Delivery Reviews*, vol. 63, no. 4. pp. 300–311, Apr. 30, 2011. doi: 10.1016/j.addr.2011.03.004.

[36] H. Eslami Amirabadi *et al.*, “Intestinal explant barrier chip: Long-term intestinal absorption screening in a novel microphysiological system using tissue explants,” *Lab Chip*, vol. 22, no. 2, pp. 326–342, Jan. 2022, doi: 10.1039/d1lc00669j.

[37] B. Trappmann, B. M. Baker, W. J. Polacheck, C. K. Choi, J. A. Burdick, and C. S. Chen, “Matrix degradability controls multicellularity of 3D cell migration,” *Nat. Commun.*, vol. 8, no. 1, Dec. 2017, doi: 10.1038/s41467-017-00418-6.

[38] A. Diaz-Santana, M. Shan, and A. D. Stroock, “Endothelial cell dynamics during anastomosis in vitro,” *Integr. Biol. (United Kingdom)*, vol. 7, no. 4, pp. 454–466, Apr. 2015, doi: 10.1039/c5ib00052a.

[39] S. Kim, W. Kim, S. Lim, and J. S. Jeon, “Vasculature-on-a-chip for in vitro disease

models," *Bioengineering*, vol. 4, no. 1. MDPI AG, Mar. 01, 2017. doi: 10.3390/bioengineering4010008.

[40] M. Inamori, M. Eng, H. Mizumoto, and T. Kajiwara, "An Approach for Formation of Vascularized Liver Tissue by Endothelial Cell-Covered Hepatocyte Spheroid Integration." [Online]. Available: www.liebertonline.com=ten.

[41] J. Rouwkema, J. De Boer, and C. A. Van Blitterswijk, "Endothelial Cells Assemble into a 3-Dimensional Prevascular Network in a Bone Tissue Engineering Construct."

[42] S. Chung, R. Sudo, I. K. Zervantonakis, T. Rimchala, and R. D. Kamm, "Surface-Treatment-Induced Three-Dimensional Capillary Morphogenesis in a Microfluidic Platform," *Adv. Mater.*, vol. 21, no. 47, pp. 4863–4867, Dec. 2009, doi: 10.1002/adma.200901727.

[43] E. A. Phelps and A. J. García, "Engineering more than a cell: Vascularization strategies in tissue engineering," *Current Opinion in Biotechnology*, vol. 21, no. 5. pp. 704–709, Oct. 2010. doi: 10.1016/j.copbio.2010.06.005.

[44] X. Li, S. Xu, P. He, and Y. Liu, "In vitro recapitulation of functional microvessels for the study of endothelial shear response, nitric oxide and [Ca2+]i," *PLoS One*, vol. 10, no. 5, May 2015, doi: 10.1371/journal.pone.0126797.

[45] I. S. Kinstlinger and J. S. Miller, "3D-printed fluidic networks as vasculature for engineered tissue," *Lab on a Chip*, vol. 16, no. 11. Royal Society of Chemistry, pp. 2025–2043, 2016. doi: 10.1039/c6lc00193a.

[46] G. Silvani *et al.*, "A 3D-Bioprinted Vascularized Glioblastoma-on-a-Chip for Studying the Impact of Simulated Microgravity as a Novel Pre-Clinical Approach in Brain Tumor Therapy," *Adv. Ther.*, vol. 4, no. 11, Nov. 2021, doi: 10.1002/adtp.202100106.

[47] T. Baltazar *et al.*, "Three Dimensional Bioprinting of a Vascularized and Perfusable Skin Graft Using Human Keratinocytes, Fibroblasts, Pericytes, and Endothelial Cells," *Tissue Eng. - Part A*, vol. 26, no. 5–6, pp. 227–238, Mar. 2020, doi: 10.1089/ten.tea.2019.0201.

[48] K. Kinoshita, M. Iwase, M. Yamada, Y. Yajima, and M. Seki, "Fabrication of multilayered vascular tissues using microfluidic agarose hydrogel platforms," *Biotechnol. J.*, vol. 11, no. 11, pp. 1415–1423, Nov. 2016, doi: 10.1002/biot.201600083.

[49] M. F. Leong *et al.*, "Patterned prevascularised tissue constructs by assembly of polyelectrolyte hydrogel fibres," *Nat. Commun.*, vol. 4, 2013, doi: 10.1038/ncomms3353.

[50] A. Dobos *et al.*, "On-chip high-definition bioprinting of microvascular

structures," *Biofabrication*, vol. 13, no. 1, Dec. 2020, doi: 10.1088/1758-5090/abb063.

[51] J. S. Miller *et al.*, "Rapid casting of patterned vascular networks for perfusable engineered three-dimensional tissues," *Nat. Mater.*, vol. 11, no. 9, pp. 768–774, 2012, doi: 10.1038/nmat3357.

[52] M. B. Applegate *et al.*, "Laser-based three-dimensional multiscale micropatterning of biocompatible hydrogels for customized tissue engineering scaffolds," *Proc. Natl. Acad. Sci. U. S. A.*, vol. 112, no. 39, pp. 12052–12057, Sep. 2015, doi: 10.1073/pnas.1509405112.

[53] Y. Nashimoto *et al.*, "Vascularized cancer on a chip: The effect of perfusion on growth and drug delivery of tumor spheroid," *Biomaterials*, vol. 229, Jan. 2020, doi: 10.1016/j.biomaterials.2019.119547.

[54] R. E. Unger *et al.*, "The rapid anastomosis between prevascularized networks on silk fibroin scaffolds generated in vitro with cocultures of human microvascular endothelial and osteoblast cells and the host vasculature," *Biomaterials*, vol. 31, no. 27, pp. 6959–6967, Sep. 2010, doi: 10.1016/j.biomaterials.2010.05.057.

[55] A. Sobrino *et al.*, "3D microtumors in vitro supported by perfused vascular networks," *Sci. Rep.*, vol. 6, Aug. 2016, doi: 10.1038/srep31589.

[56] J. Kim, M. Chung, S. Kim, D. H. Jo, J. H. Kim, and N. L. Jeon, "Engineering of a biomimetic pericyte-covered 3D microvascular network," *PLoS One*, vol. 10, no. 7, Jul. 2015, doi: 10.1371/journal.pone.0133880.

[57] H. C. Ott *et al.*, "Perfusion-decellularized matrix: Using nature's platform to engineer a bioartificial heart," *Nat. Med.*, vol. 14, no. 2, pp. 213–221, Feb. 2008, doi: 10.1038/nm1684.

[58] T. Neumann, B. S. Nicholson, and J. E. Sanders, "Tissue engineering of perfused microvessels," *Microvasc. Res.*, vol. 66, no. 1, pp. 59–67, 2003, doi: 10.1016/S0026-2862(03)00040-2.

[59] S. Kaihara *et al.*, "Original Articles Silicon Micromachining to Tissue Engineer Branched Vascular Channels for Liver Fabrication," Mary Ann Liebert, Inc, 2000.

[60] F. Gioiella, F. Urciuolo, G. Imparato, V. Brancato, and P. A. Netti, "An Engineered Breast Cancer Model on a Chip to Replicate ECM-Activation In Vitro during Tumor Progression," *Adv. Healthc. Mater.*, vol. 5, no. 23, pp. 3074–3084, Dec. 2016, doi: 10.1002/adhm.201600772.

[61] Y. S. Zhang *et al.*, "Bioprinting 3D microfibrous scaffolds for engineering endothelialized myocardium and heart-on-a-chip," *Biomaterials*, vol. 110, pp. 45–59, Dec. 2016, doi: 10.1016/j.biomaterials.2016.09.003.

[62] G. M. Whitesides, “The origins and the future of microfluidics,” *Nature*, vol. 442, no. 7101. pp. 368–373, Jul. 27, 2006. doi: 10.1038/nature05058.

[63] G. S. Offeddu *et al.*, “An on-chip model of protein paracellular and transcellular permeability in the microcirculation,” *Biomaterials*, vol. 212, pp. 115–125, Aug. 2019, doi: 10.1016/j.biomaterials.2019.05.022.

[64] A. Sontheimer-Phelps, B. A. Hassell, and D. E. Ingber, “Modelling cancer in microfluidic human organs-on-chips,” *Nature Reviews Cancer*, vol. 19, no. 2. Nature Publishing Group, pp. 65–81, Feb. 01, 2019. doi: 10.1038/s41568-018-0104-6.

[65] J. Kim *et al.*, “Implantable microfluidic device for the formation of three-dimensional vasculature by human endothelial progenitor cells,” *Biotechnol. Bioprocess Eng.*, vol. 19, no. 3, pp. 379–385, 2014, doi: 10.1007/s12257-014-0021-9.

[66] R. Wang, J. Ozsvar, B. Aghaei-Ghareh-Bolagh, M. A. Hiob, S. M. Mithieux, and A. S. Weiss, “Freestanding hierarchical vascular structures engineered from ice,” *Biomaterials*, vol. 192, pp. 334–345, Feb. 2019, doi: 10.1016/j.biomaterials.2018.11.011.

[67] V. Narayanamurthy *et al.*, “Advances in passively driven microfluidics and lab-on-chip devices: A comprehensive literature review and patent analysis,” *RSC Adv.*, vol. 10, no. 20, pp. 11652–11680, Mar. 2020, doi: 10.1039/d0ra00263a.

[68] A. G. Niculescu, C. Chircov, A. C. Bîrcă, and A. M. Grumezescu, “Fabrication and applications of microfluidic devices: A review,” *International Journal of Molecular Sciences*, vol. 22, no. 4. MDPI AG, pp. 1–26, Feb. 02, 2021. doi: 10.3390/ijms22042011.

[69] F. Bally *et al.*, “Improved size-tunable preparation of polymeric nanoparticles by microfluidic nanoprecipitation,” *Polymer (Guildf).*, vol. 53, no. 22, pp. 5045–5051, Oct. 2012, doi: 10.1016/j.polymer.2012.08.039.

[70] D. Y. Park, J. Lee, J. J. Chung, Y. Jung, and S. H. Kim, “Integrating Organs-on-Chips: Multiplexing, Scaling, Vascularization, and Innervation,” *Trends in Biotechnology*, vol. 38, no. 1. Elsevier Ltd, pp. 99–112, Jan. 01, 2020. doi: 10.1016/j.tibtech.2019.06.006.

[71] A. Chandrasekaran *et al.*, “Hybrid Integrated Silicon Microfluidic Platform for Fluorescence Based Biodetection,” *Sensors*, vol. 7, pp. 1901–1915, 2007, [Online]. Available: www.mdpi.org/sensors

[72] A. Singh, C. K. Malek, and S. K. Kulkarni, “Development in microreactor technology for nanoparticle synthesis,” *Int. J. Nanosci.*, vol. 9, no. 1–2, pp. 93–112, Feb. 2010, doi: 10.1142/S0219581X10006557.

[73] Y. Liao *et al.*, “Direct laser writing of sub-50 nm nanofluidic channels buried in glass for three-dimensional micro-nanofluidic integration,” *Lab Chip*, vol. 13, no. 8, pp. 1626–1631, 2013, doi: 10.1039/c3lc41171k.

[74] K. Malecha, L. Jasińska, A. Grytsko, K. Drzozga, P. Slobodzian, and J. Cabaj, “Monolithic microwave-microfluidic sensors made with Low Temperature Co-Fired Ceramic (LTCC) technology,” *Sensors (Switzerland)*, vol. 19, no. 3, Feb. 2019, doi: 10.3390/s19030577.

[75] D. Huh, G. A. Hamilton, and D. E. Ingber, “From 3D cell culture to organs-on-chips,” *Trends in Cell Biology*, vol. 21, no. 12. pp. 745–754, Dec. 2011. doi: 10.1016/j.tcb.2011.09.005.

[76] K. Zhou *et al.*, “Fabrication of PDMS microfluidic devices using nanoclay-reinforced Pluronic F-127 as a sacrificial ink,” *Biomed. Mater.*, vol. 16, no. 4, Jul. 2021, doi: 10.1088/1748-605X/abe55e.

[77] M. S. Kim, J. H. Yeon, and J. K. Park, “A microfluidic platform for 3-dimensional cell culture and cell-based assays,” *Biomed. Microdevices*, vol. 9, no. 1, pp. 25–34, Feb. 2007, doi: 10.1007/s10544-006-9016-4.

[78] O. F. Khan and M. V. Sefton, “Endothelial cell behaviour within a microfluidic mimic of the flow channels of a modular tissue engineered construct,” *Biomed. Microdevices*, vol. 13, no. 1, pp. 69–87, Feb. 2011, doi: 10.1007/s10544-010-9472-8.

[79] L. L. Bischel, E. W. K. Young, B. R. Mader, and D. J. Beebe, “Tubeless microfluidic angiogenesis assay with three-dimensional endothelial-lined microvessels,” *Biomaterials*, vol. 34, no. 5, pp. 1471–1477, Feb. 2013, doi: 10.1016/j.biomaterials.2012.11.005.

[80] A. Ovsianikov, V. Mironov, J. Stampf, and R. Liska, “Engineering 3D cell-culture matrices: Multiphoton processing technologies for biological and tissue engineering applications,” *Expert Review of Medical Devices*, vol. 9, no. 6. pp. 613–633, Nov. 2012. doi: 10.1586/erd.12.48.

[81] V. Vickerman, J. Blundo, S. Chung, and R. Kamm, “Design, fabrication and implementation of a novel multi-parameter control microfluidic platform for three-dimensional cell culture and real-time imaging,” *Lab Chip*, vol. 8, no. 9, pp. 1468–1477, 2008, doi: 10.1039/b802395f.

[82] J. A. Whisler, M. B. Chen, and R. D. Kamm, “Control of perfusable microvascular network morphology using a multiculture microfluidic system,” *Tissue Eng. - Part C Methods*, vol. 20, no. 7, pp. 543–552, Jul. 2014, doi: 10.1089/ten.tec.2013.0370.

[83] J. B. Nielsen, R. L. Hanson, H. M. Almughamsi, C. Pang, T. R. Fish, and A. T. Woolley, “Microfluidics: innovations in materials and their fabrication and

functionalization," *Analytical Chemistry*, vol. 92, no. 1. American Chemical Society, pp. 150–168, Jan. 07, 2020. doi: 10.1021/acs.analchem.9b04986.

[84] C. Rivet, H. Lee, A. Hirsch, S. Hamilton, and H. Lu, "Microfluidics for medical diagnostics and biosensors," *Chem. Eng. Sci.*, vol. 66, no. 7, pp. 1490–1507, Apr. 2011, doi: 10.1016/j.ces.2010.08.015.

[85] Y. Zhang, J. Liu, H. Wang, and Y. Fan, "Laser-induced selective wax reflow for paper-based microfluidics," *RSC Adv.*, vol. 9, no. 20, pp. 11460–11464, 2019, doi: 10.1039/C9RA00610A.

[86] E. B. Strong, S. A. Schultz, A. W. Martinez, and N. W. Martinez, "Fabrication of Miniaturized Paper-Based Microfluidic Devices (MicroPADs)," *Sci. Rep.*, vol. 9, no. 1, Dec. 2019, doi: 10.1038/s41598-018-37029-0.

[87] V. Soum, S. Park, A. I. Brilian, O. S. Kwon, and K. Shin, "Programmable paper-based microfluidic devices for biomarker detections," *Micromachines*, vol. 10, no. 8. MDPI AG, Aug. 01, 2019. doi: 10.3390/mi10080516.

[88] S. Bhatia *et al.*, "Hybrid Bio/Artificial Microdevices: Endothelialized Networks with a Vascular Geometry in Microfabricated Poly(dimethyl siloxane)," Kluwer Academic Publishers, 2004.

[89] S. P. Kojic, G. M. Stojanovic, and V. Radonic, "Novel cost-effective microfluidic chip based on hybrid fabrication and its comprehensive characterization," *Sensors (Switzerland)*, vol. 19, no. 7, Apr. 2019, doi: 10.3390/s19071719.

[90] Y. Gao, G. Stybayeva, and A. Revzin, "Fabrication of composite microfluidic devices for local control of oxygen tension in cell cultures," *Lab Chip*, vol. 19, no. 2, pp. 306–315, Jan. 2019, doi: 10.1039/C8LC00825F.

[91] Q. Chen, G. Li, Y. Nie, S. Yao, and J. Zhao, "Investigation and improvement of reversible microfluidic devices based on glass-PDMS-glass sandwich configuration," *Microfluid. Nanofluidics*, vol. 16, no. 1–2, pp. 83–90, 2014, doi: 10.1007/s10404-013-1222-9.

[92] C. Xu, W. Chai, Y. Huang, and R. R. Markwald, "Scaffold-free inkjet printing of three-dimensional zigzag cellular tubes," *Biotechnol. Bioeng.*, vol. 109, no. 12, pp. 3152–3160, Dec. 2012, doi: 10.1002/bit.24591.

[93] S. R. Oh, "Thick single-layer positive photoresist mold and poly(dimethylsiloxane) (PDMS) dry etching for the fabrication of a glass-PDMS-glass microfluidic device," *J. Micromechanics Microengineering*, vol. 18, no. 11, Nov. 2008, doi: 10.1088/0960-1317/18/11/115025.

[94] J. Hwang, Y. H. Cho, M. S. Park, and B. H. Kim, "Microchannel Fabrication on Glass Materials for Microfluidic Devices," *International Journal of Precision Engineering and Manufacturing*, vol. 20, no. 3. SpringerOpen, pp. 479–495,

Mar. 01, 2019. doi: 10.1007/s12541-019-00103-2.

[95] L. Tang and N. Y. Lee, “A facile route for irreversible bonding of plastic-PDMS hybrid microdevices at room temperature,” *Lab Chip*, vol. 10, no. 10, pp. 1274–1280, 2010, doi: 10.1039/b924753j.

[96] E. Brinksmeier, R. Gläbe, O. Riemer, and S. Twardy, “Potentials of precision machining processes for the manufacture of micro forming molds,” *Microsyst. Technol.*, vol. 14, no. 12, pp. 1983–1987, Nov. 2008, doi: 10.1007/s00542-008-0656-6.

[97] D. J. Guckenberger, T. E. De Groot, A. M. D. Wan, D. J. Beebe, and E. W. K. Young, “Micromilling: A method for ultra-rapid prototyping of plastic microfluidic devices,” *Lab Chip*, vol. 15, no. 11, pp. 2364–2378, Jun. 2015, doi: 10.1039/c5lc00234f.

[98] Z. Dereli-Korkut, H. D. Akaydin, A. H. R. Ahmed, X. Jiang, and S. Wang, “Three dimensional microfluidic cell arrays for ex vivo drug screening with mimicked vascular flow,” *Anal. Chem.*, vol. 86, no. 6, pp. 2997–3004, Mar. 2014, doi: 10.1021/ac403899j.

[99] C. W. Chi, A. R. Ahmed, Z. Dereli-Korkut, and S. Wang, “Microfluidic cell chips for high-throughput drug screening,” *Bioanalysis*, vol. 8, no. 9. Future Science Ltd, pp. 921–937, May 01, 2016. doi: 10.4155/bio-2016-0028.

[100] F. Sommonte, E. Weaver, E. Mathew, N. Denora, and D. A. Lamprou, “In-House Innovative ‘Diamond Shaped’ 3D Printed Microfluidic Devices for Lysozyme-Loaded Liposomes,” *Pharmaceutics*, vol. 14, no. 11, p. 2484, Nov. 2022, doi: 10.3390/pharmaceutics14112484.

[101] A. L. Beckwith, J. T. Borenstein, and L. F. Velasquez-Garcia, “Monolithic, 3D-Printed microfluidic platform for recapitulation of dynamic tumor microenvironments,” *J. Microelectromechanical Syst.*, vol. 27, no. 6, pp. 1009–1022, Dec. 2018, doi: 10.1109/JMEMS.2018.2869327.

[102] Y. Alapan, M. N. Hasan, R. Shen, and U. A. Gurkan, “Three-Dimensional Printing Based Hybrid Manufacturing of Microfluidic Devices,” *J. Nanotechnol. Eng. Med.*, vol. 6, no. 2, May 2015, doi: 10.1115/1.4031231.

[103] I. Maschmeyer *et al.*, “A four-organ-chip for interconnected long-term co-culture of human intestine, liver, skin and kidney equivalents,” *Lab Chip*, vol. 15, no. 12, pp. 2688–2699, Jun. 2015, doi: 10.1039/c5lc00392j.

[104] N. Mori, Y. Morimoto, and S. Takeuchi, “Skin integrated with perfusable vascular channels on a chip,” *Biomaterials*, vol. 116, pp. 48–56, Feb. 2017, doi: 10.1016/j.biomaterials.2016.11.031.

[105] X. Wang, Q. Sun, and J. Pei, “Microfluidic-based 3D engineered microvascular

networks and their applications in vascularized microtumor models," *Micromachines*, vol. 9, no. 10. MDPI AG, 2018. doi: 10.3390/mi9100493.

[106] C. A. Staton, S. M. Stribbling, S. Tazzyman, R. Hughes, N. J. Brown, and C. E. Lewis, "CURRENT STATUS REVIEW Current methods for assaying angiogenesis in vitro and in vivo I N T E R N AT I O N A L JOURNAL OF E X P E R I M E N TA L PAT H O L O G Y."

[107] L. F. Alonzo, M. L. Moya, V. S. Shirure, and S. C. George, "Microfluidic device to control interstitial flow-mediated homotypic and heterotypic cellular communication," *Lab Chip*, vol. 15, no. 17, pp. 3521–3529, Jun. 2015, doi: 10.1039/c5lc00507h.

[108] A. Garziano, F. Urciuolo, G. Imparato, F. Martorina, B. Corrado, and P. Netti, "A micro-perfusion bioreactor for on line investigation of ECM remodeling under hydrodynamic and biochemical stimulation," *Lab Chip*, vol. 16, no. 5, pp. 855–867, 2016, doi: 10.1039/c5lc01481f.

[109] A. Albanese, A. K. Lam, E. A. Sykes, J. V. Rocheleau, and W. C. W. Chan, "Tumour-on-a-chip provides an optical window into nanoparticle tissue transport," *Nat. Commun.*, vol. 4, 2013, doi: 10.1038/ncomms3718.

[110] E. W. K. Young, "Advances in Microfluidic Cell Culture Systems for Studying Angiogenesis," *Journal of Laboratory Automation*, vol. 18, no. 6. pp. 427–436, Dec. 2013. doi: 10.1177/2211068213495206.

[111] R. K. Jain, P. Au, J. Tam, D. G. Duda, and D. Fukumura, "Engineering vascularized tissue," 2005. [Online]. Available: http://www.nature.com/naturebiotechnology

[112] W. Saadi, S. W. Rhee, F. Lin, B. Vahidi, B. G. Chung, and N. L. Jeon, "Generation of stable concentration gradients in 2D and 3D environments using a microfluidic ladder chamber," *Biomed. Microdevices*, vol. 9, no. 5, pp. 627–635, Oct. 2007, doi: 10.1007/s10544-007-9051-9.

[113] J. J. Kim, L. Hou, and N. F. Huang, "Vascularization of three-dimensional engineered tissues for regenerative medicine applications," *Acta Biomaterialia*, vol. 41. Elsevier Ltd, pp. 17–26, Sep. 01, 2016. doi: 10.1016/j.actbio.2016.06.001.

[114] S. Chung, R. Sudo, P. J. MacK, C. R. Wan, V. Vickerman, and R. D. Kamm, "Cell migration into scaffolds under co-culture conditions in a microfluidic platform," *Lab Chip*, vol. 9, no. 2, pp. 269–275, 2009, doi: 10.1039/b807585a.

[115] A. G. Koutsiaris, S. V. Tachmitzi, and N. Batis, "Wall shear stress quantification in the human conjunctival pre-capillary arterioles in vivo," *Microvasc. Res.*, vol. 85, no. 1, pp. 34–39, Jan. 2013, doi: 10.1016/j.mvr.2012.11.003.

[116] R. Sudo *et al.*, “Transport-mediated angiogenesis in 3D epithelial coculture,” *FASEB J.*, vol. 23, no. 7, pp. 2155–2164, Jul. 2009, doi: 10.1096/fj.08-122820.

[117] A. Dellaquila, C. Le Bao, D. Letourneur, and T. Simon-Yarza, “In Vitro Strategies to Vascularize 3D Physiologically Relevant Models,” *Advanced Science*, vol. 8, no. 19. John Wiley and Sons Inc, Oct. 01, 2021. doi: 10.1002/advs.202100798.

[118] M. L. Moya, Y. H. Hsu, A. P. Lee, C. W. H. Christopher, and S. C. George, “In vitro perfused human capillary networks,” *Tissue Eng. - Part C Methods*, vol. 19, no. 9, pp. 730–737, Sep. 2013, doi: 10.1089/ten.tec.2012.0430.

[119] V. van Duinen, D. Zhu, C. Ramakers, A. J. van Zonneveld, P. Vulto, and T. Hankemeier, “Perfused 3D angiogenic sprouting in a high-throughput in vitro platform,” *Angiogenesis*, vol. 22, no. 1, pp. 157–165, Feb. 2019, doi: 10.1007/s10456-018-9647-0.

[120] K. M. Seiler *et al.*, “Patient-derived small intestinal myofibroblasts direct perfused, physiologically responsive capillary development in a microfluidic Gut-on-a-Chip Model,” *Sci. Rep.*, vol. 10, no. 1, Dec. 2020, doi: 10.1038/s41598-020-60672-5.

[121] Y. Nashimoto *et al.*, “Integrating perfusable vascular networks with a three-dimensional tissue in a microfluidic device,” *Integr. Biol. (United Kingdom)*, vol. 9, no. 6, pp. 506–518, Jun. 2017, doi: 10.1039/c7ib00024c.

[122] “029 Davies How Do Vascular Endothelial Cells Respond to Flow”.

[123] B. Fagrell, M. Intaglietta, and J. Stergren, “Relative Hematocrit in Human Skin Capillaries and Its Relation to Capillary Blood Flow Velocity 1,” 1980.

[124] C. L. E. Helm, A. Zisch, and M. A. Swartz, “Engineered blood and lymphatic capillaries in 3-D VEGF-fibrin-collagen matrices with interstitial flow,” *Biotechnol. Bioeng.*, vol. 96, no. 1, pp. 167–176, Jan. 2007, doi: 10.1002/bit.21185.

[125] E. I. Chang *et al.*, “Tissue engineering using autologous microcirculatory beds as vascularized bioscaffolds,” *FASEB J.*, vol. 23, no. 3, pp. 906–915, Mar. 2009, doi: 10.1096/fj.08-114868.

[126] C. Mazio, C. Casale, G. Imparato, F. Urciuolo, and P. A. Netti, “Recapitulating spatiotemporal tumor heterogeneity in vitro through engineered breast cancer microtissues,” *Acta Biomater.*, vol. 73, pp. 236–249, Jun. 2018, doi: 10.1016/j.actbio.2018.04.028.

[127] “126 Nilsson - Growth of anchorage-dependent cells on macroporous microbeads (Biglie)”.

[128] F. Urciuolo, G. Imparato, A. Totaro, and P. A. Netti, “BuildinG a tissue in vitro FroM the BottoM uP: iMPliCations in reGenerative MediCine,” 2013.

[129] C. Palmiero, G. Imparato, F. Urciuolo, and P. Netti, “Engineered dermal equivalent tissue in vitro by assembly of microtissue precursors,” *Acta Biomater.*, vol. 6, no. 7, pp. 2548–2553, 2010, doi: 10.1016/j.actbio.2010.01.026.

[130] F. Urciuolo *et al.*, “Biophysical properties of dermal building-blocks affect extra cellular matrix assembly in 3D endogenous macrotissue,” *Biofabrication*, vol. 8, no. 1, Jan. 2016, doi: 10.1088/1758-5090/8/1/015010.

[131] E. Metzen, M. Wolff, J. Fandrey, and W. Jelkmann, “Pericellular Po2 and 0 2 consumption in monolayer cell cultures,” 1995.

[132] A. H. Rezwanuddin Ahmed, Z. Dereli Korkut, H. Dogus Akaydin, and S. Wang, “Simulation and Analysis of a Flow Profile and Reaction Rate Within a 3D Microfluidic Cell Culture Array,” 2013. [Online]. Available: http://asme.org/terms

[133] S. Mitragotri *et al.*, “Mathematical models of skin permeability: An overview,” *International Journal of Pharmaceutics*, vol. 418, no. 1. pp. 115–129, Oct. 10, 2011. doi: 10.1016/j.ijpharm.2011.02.023.

[134] B. Corrado, V. De Gregorio, G. Imparato, C. Attanasio, F. Urciuolo, and P. A. Netti, “A three-dimensional microfluidized liver system to assess hepatic drug metabolism and hepatotoxicity,” *Biotechnol. Bioeng.*, vol. 116, no. 5, pp. 1152–1163, May 2019, doi: 10.1002/bit.26902.

[135] F. Martorina, C. Casale, F. Urciuolo, P. A. Netti, and G. Imparato, “In vitro activation of the neuro-transduction mechanism in sensitive organotypic human skin model,” *Biomaterials*, vol. 113, pp. 217–229, Jan. 2017, doi: 10.1016/j.biomaterials.2016.10.051.

[136] C. Mazio *et al.*, “Pre-vascularized dermis model for fast and functional anastomosis with host vasculature,” *Biomaterials*, vol. 192, pp. 159–170, Feb. 2019, doi: 10.1016/j.biomaterials.2018.11.018.

[137] T. Donnem *et al.*, “Vessel co-option in primary human tumors and metastases: An obstacle to effective anti-angiogenic treatment?,” *Cancer Medicine*, vol. 2, no. 4. pp. 427–436, 2013. doi: 10.1002/cam4.105.

[138] R. Lugano, M. Ramachandran, and A. Dimberg, “Tumor angiogenesis: causes, consequences, challenges and opportunities,” *Cellular and Molecular Life Sciences*, vol. 77, no. 9. Springer, pp. 1745–1770, May 01, 2020. doi: 10.1007/s00018-019-03351-7.

[139] S. Lee *et al.*, “3D Microfluidic Platform and Tumor Vascular Mapping for Evaluating Anti-Angiogenic RNAi-Based Nanomedicine,” *ACS Nano*, vol. 15, no. 1, pp. 338–350, Jan. 2021, doi: 10.1021/acsnano.0c05110.